INTERACTIONS BETWEEN CHROMODOMAINS AND TRIMETHYLLYSINE MARKS ON HISTONE H3 PEPTIDES

Robyn Jessica Eisert

A dissertation submitted to the faculty of the University of North Carolina at Chapel Hill in partial fulfillment of the requirements for the degree of Doctor of Philosophy in the Department of Chemistry.

Chapel Hill
2011

Approved by:

Professor Marcey Waters

Professor Gary Pielak

Professor Matthew Redinbo

Professor Linda Spremulli

Professor Brian Strahl

ABSTRACT

Robyn J. Eisert: Interactions Between Chromodomains and Trimethyllysine Marks on Histone H3 Peptides
(Under the Direction of Professor Marcey L. Waters)

Recent findings suggest that a variety of post-translational modifications (PTMs) found on N-terminal tails of histones are intricately involved in DNA packaging and directly control levels of gene expression. These modifications include methyllysine, methylarginine, phosposerine, phosphothreonine, and acetyllysine. Methyllysine marks on the N-terminal tail histone H3 are known to recruit effector proteins that can modify chromatin structure and regulate gene expression. Trimethyllysine 4 of histone H3 recruits CHD1 (chromo-ATPase/helicase-DNA binding domain 1), which is part of a chromatin-remodeling complex associated with active transcription. Additionally, trimethyllysine 9 of histone H3 recruits heterochromatin protein 1α (HP1α), which stabilizes heterochromatin, which is typically associated with repressed gene expression. I investigated the protein-protein interactions in each of these complexes to explore the driving force and the selectivity of recognition.

The tandem chromodomain of CHD1 binds H3 K4Me_3 with an aromatic cage consisting of two tryptophan residues (Trp64 and Trp67) forming cation-π interactions with the trimethyllysine. Arginine 2 of histone H3 is involved in an H-bond with the backbone of Gly66 of the tandem chromodomain and a cation-π interaction with Trp67. The effect of incorporating methylarginine and citrulline at position 2 in H3 K4Me_3 on

CHD1 binding affinity was explored. The results show that symmetric dimethylarginine and citrulline weakened binding affinity while asymmetric dimethylarginine enhanced binding affinity. This study demonstrates the significance of these three modifications and how they may play a role in regulating gene expression by affecting protein-protein interactions.

The HP1α chromodomain binds to H3 K9Me$_2$ with a K_D of 20 μM H3 K9Me$_3$ with a K_D of 17 μM. The chromodomain contains a three-membered aromatic cage and a glutamate (Glu52) around di- and trimethyllysine. The aromatic residues are involved in a cation-π interaction with methyllysine and Glu52 forms a water-mediated H-bond to dimethyllysine. The histone tail is also inserted between two β-strands of the chromodomain to form a 3-stranded β-sheet.

First, Glu52 was modified to enhance selectivity for H3 K9Me$_3$ over H3 K9Me$_2$. The E52Q mutant had a 2.5 fold weaker binding affinity to H3 K9Me$_2$ (K_D=52 μM) and maintained the same binding affinity to H3 K9Me$_3$ (K_D=15 μM) most likely because glutamine is a weak H-bond acceptor compared to glutamate.

Second, β-sheet interactions between HP1α chromodomain and H3 K9Me$_3$ were investigated. Residue Thr6 of the histone tail forms cross-strand interactions with Ala25 and Asp62 of the chromodomain. Each of these three residues was systematically substituted for amino acids known to have high β-sheet propensity and form favorable sidechain-sidechain interactions. These studies demonstrated the applicability of information gleaned from model systems and statistical studies to protein-protein recognition.

Lastly, two PTM-recognition domains, derived from naturally occurring effector proteins were coupled together to create a coupled-receptor construct to visualize dual modifications on a single histone tail. Two HP1α chromodomains were coupled to determine if they were functional for detecting a synthetic peptide with two H3 K9Me_2 sequences as proof that coupled receptors can have cooperative binding for a peptide with two dimethyllysine marks.

Taken together, these studies provide a new mechanistic insight into the protein-protein interactions between chromodomains and methyllysine marks on N-terminal histone H3 tails, which are important for sequence selectivity and binding affinity.

Acknowledgements

First and foremost, I would like to acknowledge Professor Marcey Waters for giving me the opportunity to join her lab and pursue my project. I would also like to thank her for her patience, guidance, and understanding. I would also like to thank my committee members and the other faculty and staff members of the Chemistry Department for the advice that they have given me.

I would like to thank all of the past and present members of the Waters lab for their insight and knowledge. I would especially like to thank Dr. Amanda Stewart who assisted me when I first joined the lab. I would also like to acknowledge the members of the Redinbo lab in for their assistance.

I would also like to acknowledge all of my chemistry professors from my undergraduate institution, Goucher College. Professor Lesley Brown introduced me to my first research experience in a chemistry lab. Without her and the other faculty members to give me their constant guidance and support, I may not have pursued my PhD.

All of my friends outside of the department have been a blessing. They have been like a family to me and have given me their unconditional love and support these past five years. They have kept me grounded, provided me with spiritual guidance, and have shown me what is truly important in life. No words can convey how much they have meant to me.

I would like to thank my family who are the most important people in my life. My brother, Michael, and my parents Bill and Susan, have supported me through the good and bad times. Also, my grandparents, Dr. Otto and Ruth Eisert, have always wanted the best for me. My late Grandpa Otto had the sort of genuine passion for science and medicine that does not come naturally to most people. I know how much my family loves and supports me just as I love them. I am truly grateful to have them in my life.

TABLE OF CONTENTS

LIST OF TABLES

Tables Page

LIST OF FIGURES

Figures Page

LIST OF SYMBOLS AND ABBREVIATIONS

5(6)-FAM	5(6)-Carboxyfluorescein
5(6)-TAMRA	5-(6)-Carboxytetramethylrhodamine
Ala, A	Alanine
Arg, R	Arginine
Asn, N	Asparagine
Asp, D	Aspartic acid
BPTF	Bromodomain PHD transcription factor
Boc	t-Butoxycarbonyl
CD	Circular dichroism
CHD1	chromo-ATPase/helicase-DNA binding domain 1
Cit	Citrulline
Cys, C	Cysteine
DIPEA	Disopropylethyl amine
DMAa	asymmetric dimethylarginine
DMAs	symmetric dimethylarginine
DMF	Dimethylformamide
DMSO	Dimethyl sulfoxide
DNA	Deoxyribonucleic acid
dNTP	Deoxyribonucleotide triphosphate
DTT	Dithiothreitol
ESI-TOF	Electro Spray Ionization Time of Flight
FMOC	N-9-Fluorenylmethyloxycarbonyl
FPLC	Fast protein liquid chromatography
ΔG	Gibbs' free energy
Gln, Q	Glutamine
Glu, E	Glutamic acid
Gly, G	Glycine
HB site	Hydrogen bonded site
H-bond	Hydrogen-bond

HBTU	2-(1H-Benzotriazole-1-yl)-1,1,3,3-tetramethyluronium hexafluorophosphate
His, H	Histidine
HOBt	N-hydroxybenzotriazole
HP1	Heterochromatin protein 1
HPLC	High pressure liquid chromatography
Hrs	Hours
Ile, I	Isoleucine
ivDde	1-(4,4-Dimethyl-2,6-dioxo-cyclohexylidene)-3-methyl-butyl
kcal	Kilocalories
$K(Me)_2$	Dimethyllysine
$K(Me)_3$	Trimethyllysine
LC/MS	Liquid chromatography-mass spectrometry
Leu, L	Leucine
Lys, K	Lysine
MeOH	Methanol
Met, M	Methionine
Mins	Minutes
M	Molar
mM	Millimolar
μM	Micromolar
MTBD	1,3,4,6,7,8-Hexahydro-1-methyl-2*H*-pyrimido[1,2-a]pyrimidine
NHB site	Non-hydrogen bonded site
NMR	Nuclear magnetic resonance
PDB	Protein data bank
PHD	Plant homeodomain
Phe, F	Phenylalanine
Pro, P	Proline
PTM	Post-translational modification
SDS-PAGE	Sodium Dodecyl Sulfate-polyacrilamide gel electrophoresis
Ser, S	Serine

tBu	t-Butyl
TCEP	tris(2-carboxyethyl)phosphine
TFA	Trifluoroacetic acid
Thr, T	Threonine
TIPS	Triisopropyl silane
Trp, W	Tryptophan
trt	Trityl
Tyr, Y	Tyrosine
Val, V	Valine

Chapter I

INTRODUCTION

A. Significance of This Research

Recent findings have suggested that a variety of post-translational modifications (PTMs) on N-terminal tails of histones are intricately involved in DNA packaging and may directly control levels of gene expression. In fact, multiple modifications have been shown to occur simultaneously, resulting in different levels of expression, which have led to the "Histone Code" hypothesis.[1] With this information in hand, there has been an effort to understand how recognition domains within effector proteins read these modifications. This research will provide insight into how molecular recognition and protein-protein interactions modulate selectivity of these domains for their intended targets**.** Additionally, a set of coupled PTM receptors have been developed which will be able to detect the presence of two modifications on a single histone tail.

B. DNA Packaging

The DNA within the nucleus of a eukaryotic cell is billions of base-pairs in length and several orders of magnitude longer than the nucleus in which the DNA is packaged.[2,3] Despite the length of the eukaryotic genome, DNA is remarkably packaged into well-organized higher structures while maintaining appropriate accessibility for replication and transcription. Extensive research dating as far back as the 1940's and pioneered by

Watson, Felsenfeld, Roger Kornberg and others has been performed to understand how appropriate packaging is maintained and regulated.

The first order of DNA packaging is the nucleosome, which consists of approximately 147 base pairs of DNA, which are wrapped around a basic octameric protein complex referred as a histone. Two of each of the histones, H2A, H2B, H3, and H4 subunits comprises the nucleosome core particle (Fig. 1.1). Histone H1 keeps the DNA in place and interacts with the "linker" DNA, which is the DNA that connects two nucleosome.[4, 5] The entire particle, including the DNA and histone subunits, was determined to take a disk-like shape with a approximate diameter of 100 Å, which was measured by X-ray diffraction.[6]

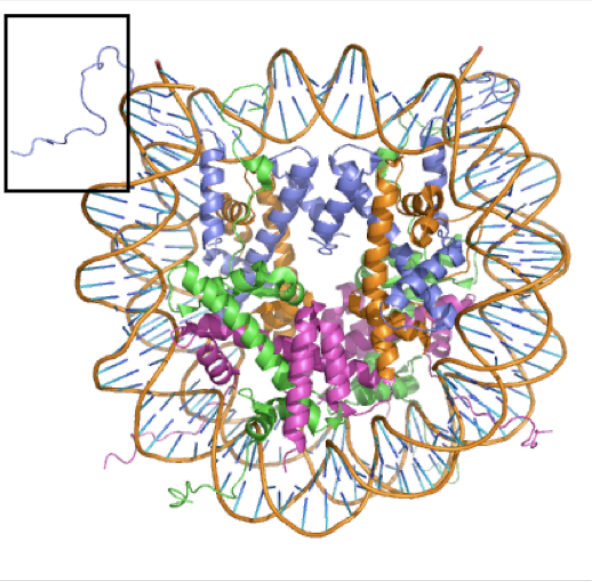

Figure 1.1. Nucleosome structure with DNA wrapped around the histone. The different colors represent the four different histone subunits. An example of a histone tail is boxed in.[4]

Nucleosomes are further packaged into higher orders of chromatin structure (Fig. 1.2). Euchromatin is loosely packaged similar to beads on a string and is typically

associated with activated transcription and replication. Distinct from euchromatin is heterochromatin, which takes a more compact structure with genes that are typically not expressed.[7] Regulating these structures properly is critical for proper transcription, replication, and cell division.

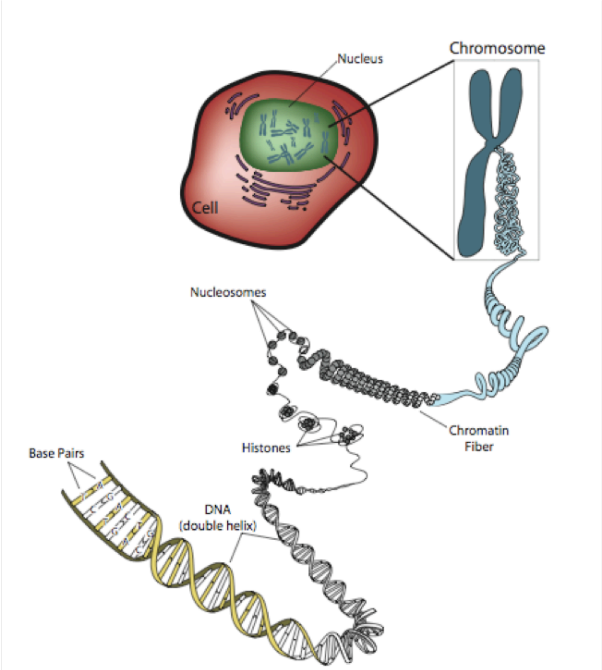

Figure 1.2. DNA packaging within a nucleus. Adapted from a National Genome Research Institute image.[8]

C. Epigenetics and Gene Expression

The term "epigenetics" refers to changes in gene expression that are not controlled by DNA sequences.[9] Condrad Waddington is credited with coining the term "epigenome" and proposing epigenetics as the means by which cells are able to obtain large diversity as they evolve from a stem cell despite having identical genomes. Waddington published a scheme demonstrating how a cell, which is depicted by the ball, starts with the same genotype, but can still develop different phenotypes depending on epigenetic markers, which are represented by the valleys (Fig. 1.3).[10] Epigenetic modes of regulation include DNA methylation, which silences gene expression. These marks

occur in 60% of promotor sites in the human genome.[11] A second mode of regulation is RNA-associated silencing or RNA interference.[12] The third mechanism of epigenetic gene regulation involves covalent post-translational modifications (PTMs) of proteins including histones, chromatin remodeling proteins, and transcriptional regulators.[13] Only recently has it become clear that each of these three regulatory mechanisms are interconnected resulting in additional levels of complexity. For example, certain PTMs have been known to recruit DNA methyltransferases while DNA methyl marks can recruit histone modifying enzymes.[14] Any aberrant regulation of these mechanisms can lead to a variety of diseases such as Rett syndrome, autoimmune diseases, and cancer.[15] Therefore, understanding how these epigenetic regulators work is necessary to fully understand cellular growth, development, and disease. The focus of this research will be on histone modifications, specifically H3 methylation.

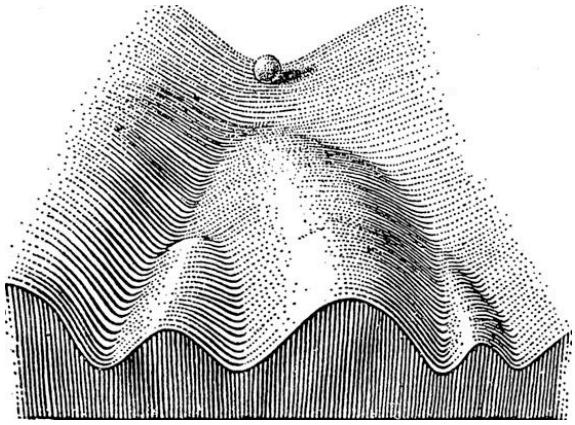

Figure 1.3. Waddington's depiction of how the epigenetic landscape can lay out different paths leading to cellular diversity.[16]

D. Significance of Histone Modifications

Histone proteins have N-terminal tails, which are defined as unstructured regions of histones that protrude outwards from the nucleosome particle and are extended by

regions that can make contacts with DNA. Histone tails constitute 28% of the mass of the histone proteins (Fig. 1.1). These regions are highly conserved in eukaryotes and are composed primarily of basic residues, which are ideal for making salt-bridges with the sugar-phosphate backbone of DNA.[4, 17, 18] There have been extensive documented occurrences of a wide variety of covalent modifications on histone tails. These modifications include serine and threonine phosphorylation, lysine and arginine methylation, lysine acetylation, and several others (Fig. 1.4).[19-23]

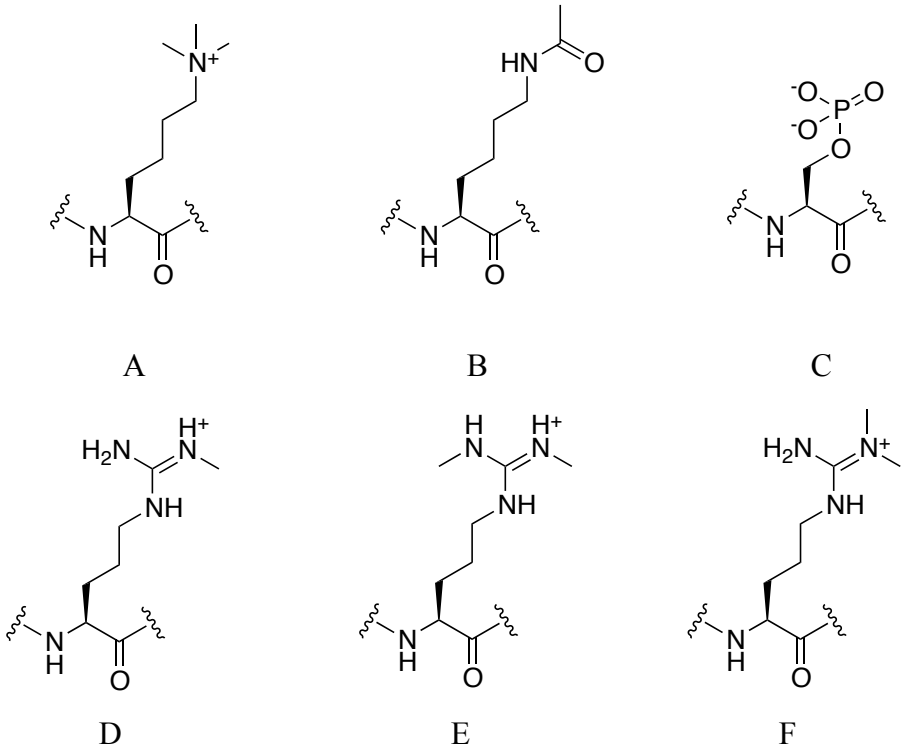

Figure 1.4. Examples of post-translational modifications. (A) Trimethyllysine, (B) acetyllysine, (C) phosphoserine, (D) monomethylarginine, (E) symmetric dimethylarginine (DMAs), (F) asymmetric dimethylarginine (DMAa).

For a long time PTMs on histone tails, namely lysine acetylation and methylation, have been known to play a role in regulating genetic processes such as replication, transcription, and DNA repair.[18, 22] These modifications were initially believed to manipulate the electrostatic interactions between histones and DNA thereby loosening or

compacting chromatin. For example, acetylation on lysine has been shown to sufficiently neutralize the positive charge of the basic side-chain and weaken protein-DNA interactions.[24-26] Phosphorylation also places a negative charge on serines and threonines, which also disrupts interactions between histones and DNA.[27, 28]

Wile PTMs do have an effect on the electrostatic properties of histones that can directly affect chromatin structure, evidence has shown that PTMs can also manipulate gene expression through more complex mechanisms. For instance, lysine acetylation does not only function by reducing protein-DNA interactons, but it is also capable of recruiting transcriptional activators such as TFIID.[29] Phosphorylation of serine 10 on the Histone H3 tail has also been linked to both chromatin condensation and gene silencing in addition to loosening chromatin and gene activation, implying that this mark also recruits effector proteins to elicit a variety of cellular responses.[28, 30, 31] Table 1.2 lists some of the most well-characterized PTMs and their effects on regulation gene expression.

Table 1.1. Examples of histone H3 modifications and their effect on gene expression.[32-39]

H3 Modifications	Residue	Expression
Lysine Methylation	K4, K36, K79	Active
	K9, K27	Inactive
Phosphorylation	S10	Active
Lysine Acetylation	K9, K14, K18, K23, K27	Active

i. "Cross-Talk" Between Histone Modifications

The idea that PTMs can be read as a "code" has arisen in the past decade to explain how modifications are able to regulate gene expression.[1] Site-specific modifications act as docking sites for recruiting effector proteins that are components of chromatin-remodeling complexes and transcriptional regulators.[40] The "code" is further

complicated by the presence of multiple modifications that occur in a combinatorial fashion, which is often referred to as cross-talk, to illicit specific biological responses.[41]

There are different ways in which modifications can affect one another. Certain PTMs can either promote or reverse other modifications. There are many examples of histone-modifying enzymes that contain recognition domains. Inhibitor growth protein 2 (ING2) is part of a tumor suppressor protein that responds to DNA damage. ING2 contains a domain that recognizes trimethyllysine 4 of Histone H3 (H3 $K4Me_3$) and once bound to the histone, an HDAC (histone deacetylase) is stabilized and removes acetyl groups from neighboring acetylated lysine to turn off gene expression.[33]

Another example of how one modification can inhibit other modifications is the cross-talk between lysine-4 and lysine-9 of Histone H3. Chromatin immunoprecipitation experiments (ChIP) demonstrated that these two modifications have an inverted relationship with one another, which means that if one lysine is methylated then the other cannot be methylated. This phenomenon is important for maintaining heterochromatin boundaries and for properly regulating gene expression.[42] Another study demonstrated that JARID1C, which is encoded by an X-linked mental retardation gene, contains both a lysine recognition domain that targets H3 $K9Me_3$ and a lysine demethylase domain (JmjC) that targets H3 $K4Me_3$. In patients with X-linked mental retardation there is a point mutation in JARID1C that causes a loss in demethylase activity, which causes a breakdown in the proper cross-talk between these two modifications.[43]

Another method of cross-regulation between multiple modifications is through the use of multivalent effector proteins. Dozens of proteins have been reported as multivalent, meaning that they are composed of multiple domains that recognize multiple

modifications. These effectors can either bind to two different histone tails in the same nucleosome (*trans*) or to the same histone tail (*cis*). The *trans* binding allows for one protein to make contacts with different promoters located near the same nucleosome. One example is the Bromodomain PHD Transcription Factor (BPTF), which contains an acetyllysine recognition domain (bromodomain) and a methyllysine recognition domain (PHD finger) on H4 and H3 respectively.[44] The *trans* binding allows tighter, cooperative binding between the effector protein and histone tail.[45] This mode of recognition also promotes enhanced selectivity because both modifications must be present for efficient binding. The TATA-binding protein-associated factor ($TAFII_{250}$) is a subunit of the TFII transcription facter and is an example of a *cis* binder. $TAFII_{250}$ contains two bromodomains that recognize acetyllysine on H4 histones and binding is enhanced by two orders of magnitude when two acetyl marks are present as opposed to only one.[29]

Effector proteins complexed with two different nucleosomes can also be crosslinked with one another. Heterochromatin protein 1 (HP1) contains a methyllysine reading domain that targets H3 $K9Me_3$. Cross-linking between two HP1 proteins can condense euchromatin into genetically silent heterochromatin, which will be further discussed below.[46, 47]

A third mechanism of cross-talk between modifications is by a binary "switch" system. Phosphorylation of the hydroxyl side-chains of serine and threonine is a highly transient mark, especially compared to the more stably methyl mark. When HP1 is bound to H3 $K9Me_3$, chromatin is condensed into heterochromatin. However, serine 10 of Histone H3 is more readily susceptible to phosphorylation compared to lysine demethylation. During M phase serine 10 is phosphorylation and as a result HP1 is

ejected from H3 $K9Me_3$, which may be important for properly regulating condensation of chromosomes.[48, 49]

Though many combinations of modifications and their means of cross-talk have been identified (Table 1.2), many PTMs that have the potential for cross-regulation remain unidentified. Other concurrent modifications that have been identified still are not well understood.[50]

Table 1.2. Examples of histone modifications that have been shown to co-localize and their effect on genetic expression.[39, 48, 51, 52]

Modification 1 (H3)	Modification 2 (H3)	Effect on Expression
$K9Me_3$	$S10PO_4^-$	Active
$K4Me_3$	$K27Me_3$	Inactive
$S10PO_4^-$	K14Ac	Active
$K9Me_3$	$K27Me_3$	Inactive

ii. Lysine Methylation on Histones

Of the various covalent histone modifications reported, methylation is among the most ubiquitous, complex, and least understood of the covalent modifications and is the focus of this research. This complexity is in part due to the different levels of lysine and arginine methylation including mono-, di-, or trimethyllysine (Fig. 1.3). Unlike acetylation, which is generally associated with active expression, methylation is site-specific and is associated with both active and suppressed gene expression.[53] Therefore, understanding how methyl marks regulate gene expression has been complicated.

Lysine is methylated by histone methyltransferases (HMTs), almost all of which contain an exymatic SET-domain. These enzymes can act as exclusively as mono-, di-, or trimethyltrasferases or they can act as all three with S-adenosylmethionine (AdoMet)

as the methyl-donating cofactor (Fig. 1.5). State-specific methylation is dependent on the size of the binding cleft and sequence specificity relies on specific H-bonds to amino acids surrounding the lysine substrate with a (K/R)-(STA) motif preceding the lysine substrate.[54, 55] This sequence and methylation specificity further demonstrates the intricacy involved in lysine methylation.

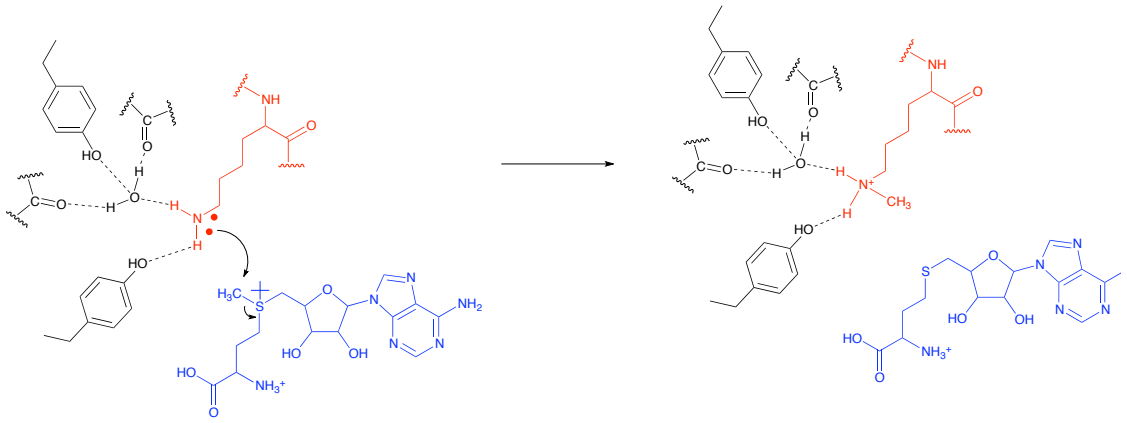

Figure 1.5 Scheme of lysine 9 methylation carried out by SET7/9, which is a monomethyltransferase. This histone lysine is in red, AdoMet is in blue, which is converted to S-adenosyl homocysteine (AdoHcy), and SET7/9 residues are in black.[54]

Less is known about lysine demethylation. Until recently, methyllysine was thought to be an irreversible modification, which required phosphorylation of a neighboring amino acid to reverse the effects of the methyl mark. While phosphorylation does act as a switch as previously described, two classes of lysine demethylases have been recently identified. Lysine-specific demethylase-1 (LSD1) was the first demethylase to be identified and is specifically targets mono- and dimethyllysine.[56] LSD1 is a flavin-containing enzyme that relies on FAD for amine oxidation (Fig. 1.6A). This enzyme requires that the amine be protonated and therefore is unable to target trimethyllysine.[56, 57] Jumonji histone demethylases (JHDM) were identified as

demethylases that specifically target di- and trimethyllysine. This class of enzymes relies on the Fe(II) for catalysis via a iron-oxo intermediate (Fig. 1.6B).[58, 59]

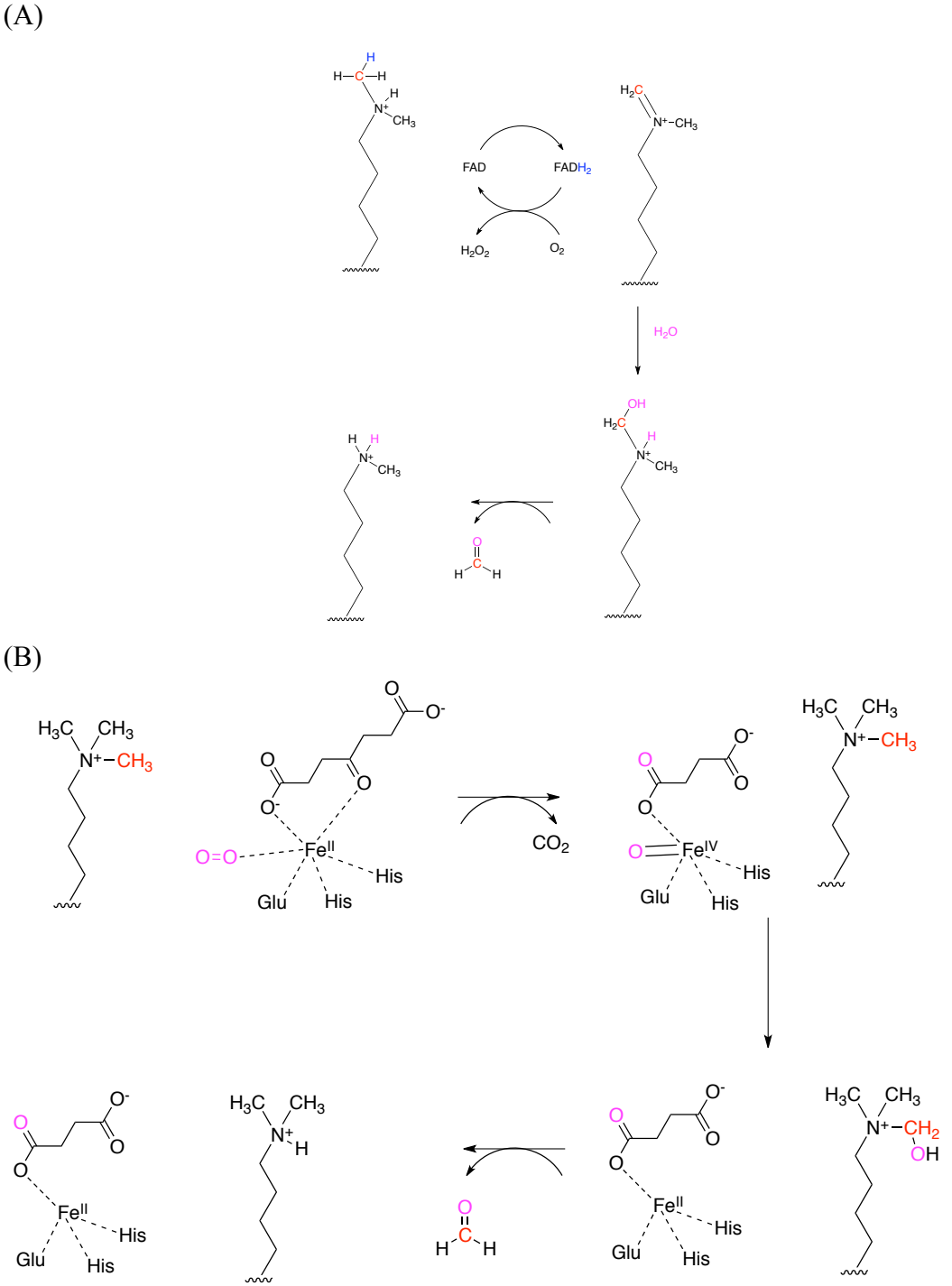

Figure 1.6. (A) Scheme of LSD1-catalyzed demethylation of dimethyllysine.[56] (B) Scheme of JHDM-catalyzed demethylation of trimethyllysine.[59]

Various types of "reader" domains interpret methyllysine. These domains are selective for methylation states and for the amino acid sequence (Table 1.3). There are two general families of reader domains that recognize methyllysine, the Royal and PHD families. The members of the Royal family are composed of four β-strands, three form a β-sheet while the forth only becomes part of the β-sheet once the histone peptide is inserted between the forth strand and another strand for form a 5-stranded β-barrel. The methyllysine typically interacts with loop regions of the domain (Fig. 1.7).[60] Unlike the Royal family, the PHD finger family only has two β-strands connecting two zinc-fingers (Fig. 1.8).[44, 61]

Table 1.3. Families of reader domains and examples of methyl marks that they target.[61]

	Reader Domain	**PTM Mark**
Royal	Chromodomain	H3 K9$Me_{2/3}$, H3 K27$Me_{2/3}$
	Double Chromodomain	H3 K4$Me_{1/2/3}$
	Chromo barrel	H3 K36$Me_{2/3}$
	Tudor	H3 K79Me_3, H4K20Me_3
	Double/tandem tudor	H3 K4Me_3, H4 K20$Me_{1/2/3}$
	MBT	H4 K20$Me_{1/2,}$ H1 K26$Me_{1/2,}$ H3 K4Me_1, H4 K9$Me_{1/2}$
PHD finger		H3 K4Me_3, H3 K9Me_3, H3 K36Me_3

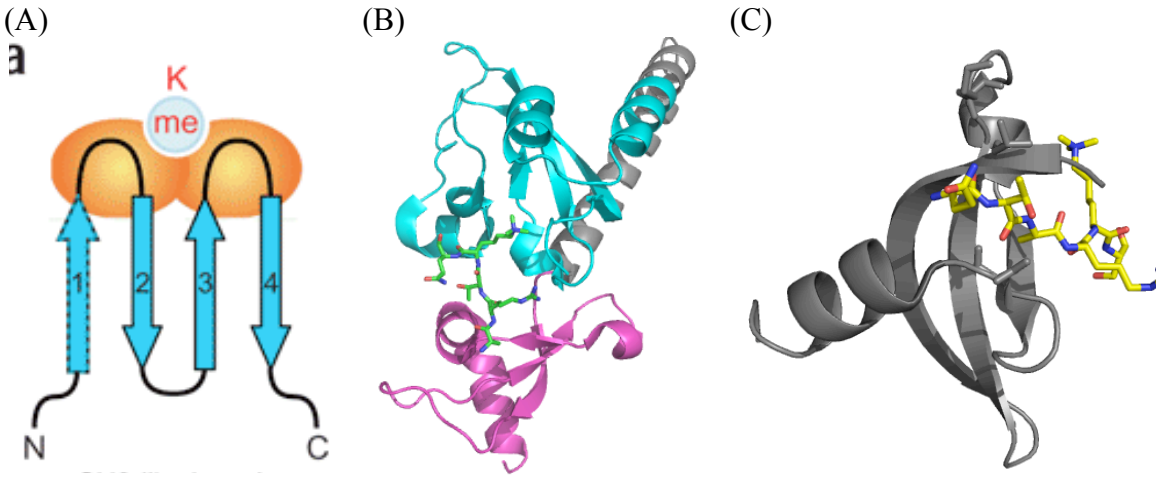

Figure 1.7. (A) Topology of Royal family domains.[61] (B) Crystal structure of H3 K4Me$_3$ peptide bound to CHD1 tandem chromodomains. Chromo1 (cyan), chromo2 (magenta), linker (grey), histone tail (green). (PDB 2B2W). (C) Crystal structure of H3 K9Me$_3$ peptide (yellow), bound to HP1 chromodomain (grey). (PDB 1KNE)

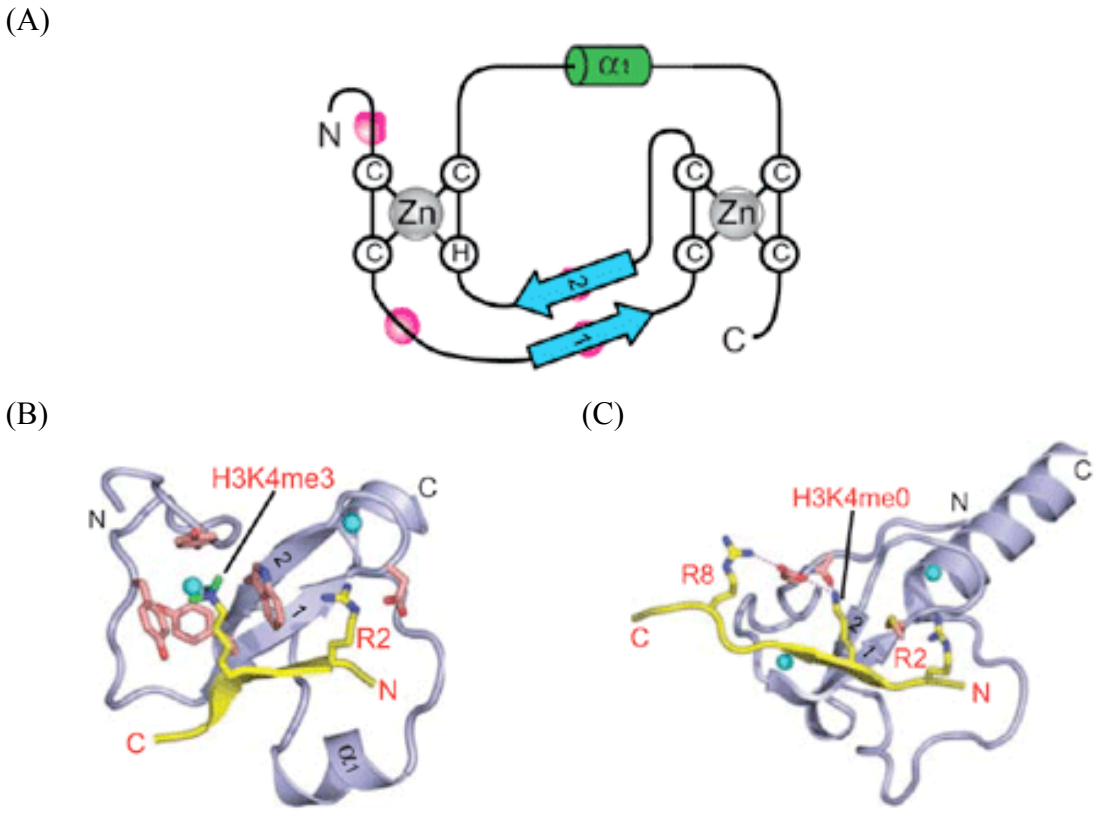

Figure 1.8. (A) Topology of the PHD family domains (pink indicates were members of the aromatic cage are located). (B) Crystal structure of H3K4me3 peptide with BPTF PHD finger (PDB 2F6J). (C) Crystal structure of H3K4 peptide with BHC80 PHD finger (PDB 2PUY). [61]

Though these two families are topologically different, the modes of recognition have striking similarities. They all involve the use of an aromatic cage for recognizing methyllysine, which is stabilized by a cation-π interaction.[62] The state specific readout of methyllysine will be addressed in further detail in Chapter III.[61, 63] They also mediate sequence selectivity through similar means. In solution histone tails have no structure. Once in complex with recognition domain, they form an antiparallel β-sheet motif with the domain, which will also be addressed in further detail in Chapter IV.[44, 61, 64] There has been significant progress in understanding how these reader domains maintain selectivity because different methyl-marks are linked very different biological responses.

iii. Lysine 4 of Histone H3 Tail

Methylation used to be associated primarily with silent chromatin, however methylation of lysine 4 on the Histone H3 (H3 K4$Me_{2/3}$) is typically associated with active chromatin while dimethylation is present on both active and silent euchromatin.[65] This methylation is catalyzed several methyltransferases including SET1 and SET7/9.[66, 67] Several proteins have been identified that interact specifically with H3 K4$Me_{2/3}$ including BPTF, CHD1 and WDR5. As will be addressed in Chapter II, CHD1 (chromo-ATPase/helicase-DNA binding domain 1) is part of a chromatin-remodeling complex is recruited by H3 K4Me_3. This complex contains HAT activity, which provides another example of a PTM that is responsible for perpetuating further histone modifications. WDR5 only binds H3 K4Me_2 when R2 is also methylated. WDR5 is believed to recruit SET1 to add a third methyl group to H3 K4Me_2, which can then activate gene expression by recruiting chromatin-remodeling proteins.

iv. Lysine 9 of Histone H3 Tail

Trimethyllation of lysine 9 on H3 (H3 K9Me_3) is typically associated with genetically silent heterochromatin.[68] Methylation of H3 K9 is catalyzed by a number of different enzymes in humans including Suv39h1, G9a, ESET, GLP, and RIZ, which have been linked to silenced gene expression.[53]

HP1 contains an N-terminal chromodomain (CD) and a C-terminal chromo shadow domain (CSD). The two domains of HP1 are separated by a hinge region (Fig. 1.9A). The chromodomain, which is a member of the Royal family of methyllysine readers, is highly selective for H3 K9Me_3 over other methylated lysine marks, such as H3 K4Me_3. Point mutations to the chromodomain not only disrupt binding to H3 K9Me_3, but it also inhibits the localization of HP1 to heterochromatin, stabilization of heterochromatin, and gene-silencing. Therefore proper targeting of HP1 via the chromodomain is necessary for maintaining proper chromatin function.[69, 70]

There has been some debate over how HP1 regulates gene expression once bound to H3 K9Me_3. Phage display libraries demonstrated that CSD can mediate protein-protein interactions. The experiments showed that CSD binds a specific pentapeptide consensus sequence, PxVxL. This study was incredibly revealing because this consensus sequence is present in human, mouse, and fly HP1 homologs resulting in dimerization.[46] A more current study additionally suggested that chromodomains of two HP1 proteins can also cross-link, which permits further oligomerization of HP1. A current proposed mechanism by which HP1 can condense euchromatin into heterochromatin is by oligomerization between HP1 thereby cross-linking two separate nucleosomes (Fig. 1.9B).[47] Once cross-linked, chromatin is condensed preventing replication and transcription machinery from

reaching promoter sites. The CSD has also been shown to interact with other proteins such as SUV39H1, which can perpetuate H3 K9Me$_3$ methylation and result in the spreading of heterochromatin.[70]

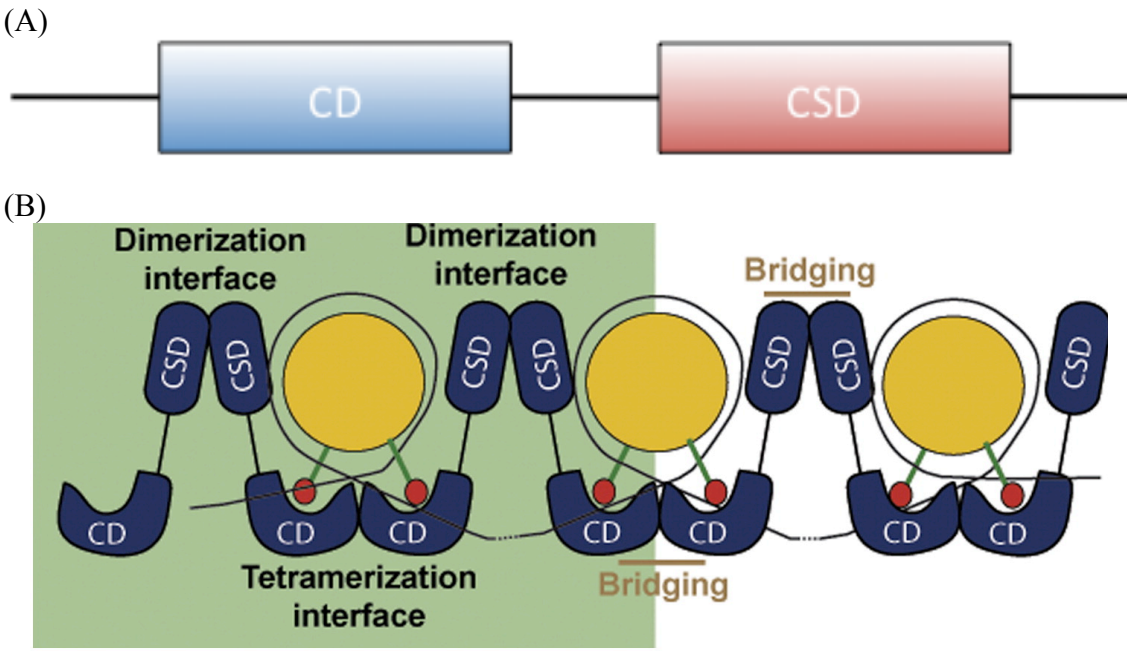

Figure 1.9. (A) Scheme of HP1 with the chromodomain shown in blue, the chromo shadow domain in red, and an unstructured hinged region between them. (B) A model depicting possible HP1 CD-CD and CSD-CSD interactions leading to oligomerization of histones.[47]

There is a need to understand interactions between lysine 9 methylation of Histone H3 and HP1 because these two proteins critical for controlling genetic expression and maintaining a stable genome during key points of development and the cell cycle.[71] Aberrant methylation of H3 K9 due to deregulation of SUV39H1 drastically affects recruitment of HP1 and heterochromatin maintenance. For example, both upregulation and down regulation of SUV39H1 and histone H3 methylation have been linked to

cancer states.[72, 73] These conflicting roles of lysine 9 methylation and HP1 makes understanding their roles in growth, development, and disease elusive.

E. Project Goals

Though a number of effector proteins such as HP1 and CHD1 have been identified, there is a need to establish a clear understanding of how these proteins interact with PTMs. In this work we had two general goals. The first was to investigate interactions between the chromodomains of CHD1 and HP1α and H3 K4Me_3 and H3 K9Me_3, respectively. Specifically, we set out to investigate how H3 R2 modifications (DMAa, DMAs, and citrullination) influence binding of CHD1 tandem chromodomain to H3 K4Me_3. We also investigated interactions between the aromatic cage of the HP1 chromodomain to di- and trimethyllysine 9 of H3. Third, we studied how sequence selectivity of HP1 chromodomain for H3 K9Me_3 can be manipulated by making point mutations to both the chromodomain and histone tail. These studies have implications for the cross-regulation between arginine 2 and lysine 4 of the Histone H3. They also give insight into the molecular recognition of chromodomains for histone tails. The second goal of this work is to develop a technique to study PTMs that occur in conjunction with one another.

References

1. Strahl, B. D.; Allis, C. D., The Language of Covalent Histone Modifications. *Nature* **2000,** *403*, 41-45.

2. Venter, J. C.; *al, e.*, The Sequence of the Human Genome. *Science* **2001,** *291*, 1304-1351.

3. Widom, J., Toward a Unified Model of Chromatin Folding. *Annu Rev Biophys Bio* **1989,** *18*, 365-395.

4. Luger, K.; Mäder, A. W.; Richmond, R. K.; Sargent, D. F.; Richmond, T. R., Crystal Structure of the Nucleosome Core Particle at 2.8Å Resolution. *Nature* **1997,** *389*, 251-160.

5. Thoma, F.; Koller, T. H.; Klug, A., Involvement of Histone H1 in the Organization of the Nucleosome and of the salt-Dependent Superstructures of Chromatin. *J Cell Biol* **1979,** *83*, 403-427.

6. Pardon, J. F.; WIlkins, M. H. F.; Richards, B. M., Super-Helical Model for Nucleohistone. *Nature* **1967,** *215*, 508-509.

7. Frenster, J. H.; Allfrey, V. G.; Mirsky, A. E., Repressed and Active Chromatin Isolated from Interphase Lymphocytes. *Biochemistry* **1963,** *50*, 1026-1032.

8. Amato, I., To Save Space, Genomic DNA is Packaged Into Chromatin. *Chem Eng News* **2006,** *84*,18.

9. Egger, G.; Liang, G.; Aparicio, A.; Jones, P. A., Epigenetics in Human Disease and Prospects for Epigenetic Therapy. *Nature* **2004,** *429*, 457-463.

10. Waddington, C. H., The Epigenotype. *Endeavour* **1942,** *1*, 18-20.

11. Tate, P. H.; Bird, A. P., Effects of DNA Methylation on DNA-BOnding Proteins and Gene Expression. *Curr Opin Genet Dev* **1993**, 226-231.

12. Mello, C. C.; Conte, D., Revealing the World of RNA Interference. *Nature* **2004,** *431*, 338-342.

13. Kouzarides, T., Chromatin Modifications and Their Function. *Cell* **2007,** *128*, 693-705.

14. Fuks, F.; Hurd, P. J.; Wolf, D.; Nan, X.; Bird, A. P.; Kouzarides, T., The Methyl-CpG-binding Protein MeCP2 Links DNA Methylation to Histone Methylation. *J Biol Chem* **2003,** *278*, 4035-4040.

15. Lu, Q.; Qiu, X.; Hu, N.; Wen, H.; Su, Y.; Richardson, B. C., Epigenetics, Disease, and Therapeutic Interventions. *Ageing Res Rev* **2006,** *5*, 449-467.

16. Waddington, C. H., *The Strategy of the Genes*. Allen and Unwin: London, 1957.

17. Luger, K.; Richmond, T. J., The Histone Tails of the Nucleosome. *Curr Opin Genet Dev* **1998,** *8*, 140-146.

18. Hansen, J. C.; Tse, C.; Wolffe, A. P., Structure and Function of the Core Histone N-Termini: More Than Meets the Eye. *Biochemistry* **1998,** *37*, 17637-17641.

19. vanHolde, K. E., (ed. Rich, A.) 111-148 (Springer, NewYork, 1988). **1988**.

20. Langan, T. A., Histone Phosphorylation: Stimulation by Adenosine 3',5'-Monophosphate. *Science* **1968,** *162*, 579-580.

21. Langan, T. A., Cyclic AMP and Histone Phosphorylation. *Ann NY Acad Sci* **1971,** *185*, 166-180.

22. Allfrey, V. G.; Faulkner, R.; Mirsky, A. E., Acetylation and Methylation of Histones and Their Possible Role in the Regulation of RNA Synthesis. *Biochemistry* **1964,** *51*, 786-794.

23. Mahadevan, L. C.; Willis, A. C.; Barratt, M. J., Rapid Hisonte H3 Phosphorylation in Response to Growth Factors, Phorbol Ester, Okadaic Acid, and Protein Synthesis Inhibitors. *Cell* **1991,** *65*, 775-783.

24. Shahbazian, M. D.; Grunstein, M., Functions of Site-Specific Histone Acetylation and Deacetylation. *Annu Rev Biochem* **2007,** *76*, 75-100.

25. Ren, Q.; Gorovsky, M. A., Histone H2A.Z Acetylation Modulates and Essential Charge Patch. *Mol Cell* **2001,** *7*, 1329-1335.

26. Shogren-Knaak, M.; Ishii, H.; Sun, J.-M.; Pazin, M. J.; Davie, J. R.; Peterson, C. L., Histone H4-K16 Acetylation Controls Chromatin Structure and Protein Interactions. *Science* **2006,** *311*, 844-847.

27. Wolffe, A. P.; Hayes, J. J., Chromatin Disruption and Modification. *Nucl Acids Res* **1999,** *27*, 711-720.

28. Dou, Y.; Gorovsky, M. A., Phosphorylation of Linker Histone H1 Regulates Gene Expression In Vivo by Creating a Charge Patch. *Mol Cell* **2000,** *6*, 225-231.

29. Jacobson, R. H.; Ladurner, A. G.; King, D. S.; Tjian, R., Structure and FUnciton of Human $TAF_{II}250$ Double Bromodomain Module. *Science* **2000,** *288*, 1422-1425.

30. Wei, Y.; Yu, L.; Bowen, J.; Gorovsky, M. A.; Allis, C. D., Phosphorylation of Hisonte H3 is Required for Proper Chromosome Condensation and Segregation. *Cell* **1999,** *91*, 99-109.

31. Strelkov, S. V.; Davie, J. R., Ser-10 Phosphorylation of Histone H3 and Immediate Early Gene Expression in Oncogene-Transformed Mouse Fibroblasts. *Cancer Res* **2002,** *62*, 75-78.

32. Cheung, P.; Tanner, K. G.; Cheung, W. L.; Sassone-Cori, P.; Denu, J. M.; Allis, C. D., Synergistic Coupling of Histone H3 Phosphorylation and Acetylation in Response to Epidermal Growth Factor Stimulation. *Mol Cell* **2000,** *5*, 905-915.

33. Shi, X.; *al, e.*, ING2 PHD Domain Links Histone H3 Lysine 4 Methylation to Active Gene Repression. *Nature* **2006,** *442*, 96-99.

34. Keogh, M.-C.; Kurdistani, S. K.; Morris, S. A.; Ahn, S. H.; Podolny, V.; Collins, S. R.; Schuldiner, M.; Chin, K.; Punna, T.; Thompson, N. J.; Boone, C.; Emili, A.; Weissman, J. S.; Hughes, T. R.; Strahl, B. D.; Grunstein, M.; Greenblatt, J. F.; Buratowski, S.; Krogan, N. J., Cotranscriptional Set2 Methylation of Histone H3 Lysine 36 Recruits a Repressive Rpd3 Complex. *Cell* **2005,** *123*, 593-605.

35. Ng, H. H.; Ciccone, D. N.; Morshead, K. B.; Oettinger, M. A.; Struhl, K., Lysine-79 of Histone H3 is Hypomethylated at Silenced Loci in Yeast and Mammalian Cells: A Potential Mechanism for Position-Effect Variegation. *Proc Natl Acad Sci* **2003,** *100*, 1820-1825.

36. Cao, R.; Wang, L.; Wang, H.; Xia, L.; Erdjument-Bromage, H.; Tempst, P.; Jones, R. S.; Zhang, Y., Role of Histone H3 Lysine 27 Methylation in Polycomb-Group Silencing. *Science* **2002,** *298*, 1039-1043.

37. Liang, G.; Lin, J. C. Y.; Wei, V.; Yoo, C.; Cheng, J. C.; Nguyen, C. T.; Weisenberger, D. J.; Egger, G.; Takai, D.; Gonzales, F. A.; Jones, P. A., Distinct Localization of Hisotne H3 Acetylation and H3-K4 Methylation to the Transcriptional Start Sites in the Human Genome. *Proc Natl Acad Sci* **2004,** *101*, 7357-7362.

38. Marvin, K. W.; Yau, P.; Bradbury, E. M., Isolation and Characterization of Acetylated Histones H3 and H4 and
Their Assembly into Nucleosomes. *J Biol Chem* **1990,** *265*, 19839-19847.

39. Lo, W.-S.; Trievel, R. C.; Rojas, J. R.; Duggan, L.; Hsu, J.-Y.; Allis, C. D.; Marmorstein, R.; Berger, S. L., Phosphorylation of Serine 10 in Histone H3 Is Functionally Linked In Vitro and In Vivo to Gcn5-Mediated Acetylation at Lysine 14 *Mol Cell* **2000,** *5*, 917-926.

40. Berger, S. L., The Complex Language of Chromatin Regulation During Transcription. *Nature* **2007,** *447*, 407-412.

41. Latham, J. A.; Dent, S. Y. R., Cross-Regulation of Histone Modifications. *Nat Struct Mol Biol* **2007,** *14*, 1017-1024.

42. Noma, K.-i.; Allis, C. D.; Grewal, S. I. S., Transitions in Distinct Histone H3 Methylation Patterns at the Heterochromatin Domain Boundaries. *Science* **2001,** *293*, 1150-1155.

43. Iwase, S.; Lan, F.; Bayliss, P.; Torr-Ubieta, L.; Huarte, M.; Qi, H. H.; Whetstine, J. R.; Bonni, A.; Roberts, T. M.; Shi, Y., The X-Linked Mental Retardation Gene SMCX/JARID1C Defines a Family of HIstone H3 Lysine 4 Demethylases. *Cell* **2007,** *128*, 1077-1088.

44. Li, H.; Llin, S.; Wang, W.; Duncan, E. M.; Wysocka, J.; Allis, C. D.; Patel, D. J., Molecular Basis for Site-Specific Read-Out of Histone H3K4me3 by the BPTF PHD Finger of NURF. *Nature* **2006,** *442*, 91-95.

45. Ruthenburg, A. J.; Li, H.; Milne, T. A.; Dewell, S.; McHinty, R. K.; Yuen, M.; Ueberheide, B. M.; Dou, Y.; Muir, T. W.; Patel, D. J.; Allis, C. D., Recognition of a Mononucleosomal Histone Modification Pattern by BPTF via Multivalent Interactions. *Cell* **2011,** *145*, 692-706.

46. Smothers, J. F.; Henikoff, S., The HP1 Chromo Shadow Domain Binds a Consensus Peptide Pentamer. *Curr Biol* **2000,** *10*, 27-30.

47. Canzio, D.; Chang, E.; Shankar, S.; Kuchenbecker, K. M.; Simon, M. D.; Madhani, H. D.; Narlikar, G. J.; Al-Sady, B., Chromodomain-Mediated Oligomerization of HP1 Suggests a Nucleosome-Bridging Mechanism for Heterochromatin Assembly. *Mol Cell* **2011,** *41*, 67-81.

48. Fischle, W.; Tseng, B. S.; Dormann, H. L.; Ueberheide, B. M.; Garcia, B. A.; Shabanowitz, J.; Hunt, D. F.; Funabiki, H.; Allis, C. D., Regulation of HP1-Chromatin Binding by Histone H3 Methylation and Phosphorylation. *Nature* **2005,** *438*, 1116-1122.

49. Hirota, T.; Lipp, J. J.; Toh, B.-H.; Peters, J.-M., Histone H3 Serine 10 Phosphorylation by Aurora B Causes HP1 Dissociation from Heterochromatin. *Nature* **2005,** *438*, 1176-1180.

50. Johnson, L.; Mollah, S.; Garcia, B. A.; Muratore, T. L.; Shabanowites, J.; Hunt, D. F.; Jacobsen, S. E., Mass Spectrometry Analysis of *Arabidopsis* Histone H3 Reveals Distinct Combinations of Post-Translational Modifications. *Nucl Acids Res* **2004,** *32*, 6511-6518.

51. Lindroth, A. M.; Shultis, D.; Jasencakova, Z.; Fuchs, J.; Johnson, L.; Schubert, D.; Patnaik, D.; Pradhan, S.; Goodrich, J.; Schubert, I.; Jenuwein, T.; Khorasanizadeh, S.; Jacobson, S. E., Dual Histone H3 Methylation Marks at Lysines 9 and 27 Required for Interaction with Chromomethylase3. *EMBO J* **004,** *23*, 4286-4296.

52. Zhao, X. D.; Han, X.; Chew, J. L.; Liu, J.; Chiu, K. P.; Choo, A.; Orlov, Y. L.; Sung, W.-K.; Shahab, A.; Kuznetsov, V. A.; Bourque, G.; Oh, S.; Ruan, Y.; JNg, H.-H.; Wei, C.-L., Whole-Genome Mapping of Histone H3 Lys4 and 27 Trimethylations Reveals Distinct Genomic Compartments in Human Embryonic Stem Cells. *Cell Stem Cell* **2007,** *1*, 286-298.

53. Martin, C.; Zhang, Y., The Diverse Functions of HIstone Lysine Methylation. *Nat Rev Mol Cell BIol* **2005,** *6*, 838-849.

54. Xiao, B.; Jing, C.; Wilson, J. R.; Walker, P. A.; Vasisht, N.; Kelly, G.; Howell, S.; Taylor, I. A.; Blackburn, M.; Gamblin, S. J., Structure and Catalytic Mechanism of the Human Histone Methyltransferase SET7/9. *Nature* **2003,** *421*, 652-656.

55. Cheng, X.; Zhang, Y., Structural Dynamics of Protein Lysine Methylation and Demethylation. *Mutat Res* **2007,** *618*, 102-115.

56. Shi, Y.; Lan, F.; Matson, C.; Mulligan, P.; Whetstine, J. R.; Cole, P. A.; Casero, R. A.; Shi, Y., Histone Demethylation Mediated by the Nuclear Amine Oxidase Homolog LSD1. *Cell* **2004,** *119*, 941-953.

57. Stravropoulos, P.; Blobel, G.; Hoelz, A., Crystal Structure and Mechanism of Human Lysine-Specific Demethylase-1. *Nat Struct Mol Biol* **2006,** *13*, 626-632.

58. Whetstine, J. R.; Nottke, A.; Lan, F.; Smolikov, S.; Chen, Z.; Spooner, E.; Li, E.; Zhang, G.; Colaiacovo, M.; Shi, Y., Reversal of Histone Lysine Trimethylation by the JMJD2 Family of Histone Demethylases. *Cell* **2006,** *125*, 467-481.

59. Tsukada, Y.-i.; Fang, J.; Erdjument-Bromage, H.; Warren, M. E.; Borchers, C. H.; Tempst, P.; Zhang, Y., Histone Demethylation by a Family of JmjC Domain-Containing Proteins. *Nature* **2006,** *439*, 811-816.

60. Nielson, R. R.; Nietlispach, D.; Mott, H. R.; Callaghan, J.; Bannister, A.; Kousarides, T.; Murzin, A. G.; Murzina, N. V.; Laue, E. D., Stucture of the HP1 Chromodomain Bound to Histone H3 Methylated at Lysine9. *Nature* **2002,** *416*, 103-107.

61. Taverna, S. D.; Li, H.; Ruthenburg, A. J.; Allis, C. D.; Patel, D. J., How Chromatin-Binding Modules Interpret Histone Modifications: Lessons from Professional Pocket Pickers. *Nat Struct Mol Biol* **2007,** *14*, 1025-1040.

62. Ma, J. C.; Dougherty, D. A., The Cation-π Interaction. *Chem Rev* **1997,** *97*, 1303.

63. Hughes, R. M.; Wiggins, K. R.; Khorasanizadeh, S.; Waters, M. L., Recognition of Trimethyllysine by a Chromodomain is not Driven by the Hydrophobic Effect. *Proc Natl Acad Sci* **2007,** *104*, 11184-11188.

64. Jacobs, S. A.; Khorasanizadeh, S., Structure of HP1 Chromodomain Bound to a Lysine 9-Methylated Histone H3 Tail. *Science* **2002,** *295*, 2080-2083.

65. Santon-Rosa, H.; Schneider, R.; Bannister, A. J.; Sherriff, J.; Berstein, B. E.; Tolga Emre, N. C.; Schreiber, S. L.; Mellow, J.; Kouzarides, T., Active Genes are Tri-methylated at K4 of Histone H3. *Nature* **2002,** *419*, 407-411.

66. Chin, H. G.; Patnaik, D.; Estève, P.-O.; Jacobsen, S. E.; Pradhan, S., Catalytic Properties and Kinetic Mechanism of Human Recombinant Lys-9 Histone H3 Methyltransferase SUV39H1: Participation of the Chromodomain in Enzymatic Catalysis. *BIochemistry* **2006,** *45*, 3272-3284.

67. Briggs, S. D.; Bryk, M.; Strahl, B. D.; Cheung, W. L.; Davie, J. R.; Dent, S. Y. R.; Winston, F.; Allis, C. D., Histone H3 Lysine 4 Methylation is Mediated by Set1 and Required for Cell Growth and rDNA Silencing in *Saccharomyces cerevisiae*. *Genes Dev* **2001,** *15*, 3286-3295.

68. Schotta, G.; Ebbert, A.; Krauss, V.; Fischer, A.; Hoffmann, J.; Rea, S.; Jenuwein, T.; Dorn, R.; Reuter, G., Central Role of *Drosophila* SU(VAR)3-9 in Histone H3-K9 Methylation and Heterochromatic Gene Silencing. *EMBO J* **2002,** *21*, 1121-1131.

69. Platero, J. S.; Hartnett, T.; Eissenberg, J. C., Functional Analysis of the Chromo Domain of HP1. *EMBO J* **1999,** *14*, 3977-3986.

70. Bannister, A. J.; Zegerman, P.; Partidge, J. F.; Miska, E. A.; Thomas, J. O.; Allshire, R. C.; Kouzarides, T., Selective Recognition of Methylated Lysine 9 on Histone H3 by the HP1 Chromo Domain. *Nature* **2001,** *410*, 120-124.

71. Bernard, P.; Maur, J.-F.; Partidge, J. F.; Genier, S.; Javerzat, J.-P.; Allshire, R. C., Requirement of Heterochromatin for Cohesion at Centromeres. *Science* **2001,** *294*, 2539-2542.

72. Peters, A. H.; O'Carroll, D.; Scherthan, H.; Mechtler, K.; Sauer, S.; Schöfer, C.; Weipoltshammer, K.; Pagani, M.; Lachner, M.; Kohlmaier, A.; Opravil, S.; Doyle, M.; Sibilia, M.; Jenuwein, T., Loss of the Suv39h Histone Methyltransferases Impairs Mammalian Heterochromatin and Genome Stability. *Cell* **2001,** *107*, 323-337.

73. Czvitkovish, S.; Sauer, S.; Antoine, H. F. M.; Deiner, E.; Wolf, A.; Laible, G.; Opravil, S.; Beug, H.; Jenuwein, T., Over-Expression of the SUV39H1 Histone Methyltransferase Induces Altered Proliferation and Differentiation in Transgenic Mice. *Mech Dev* **2001,** *107*, 141-153.

Chapter II

EFFECTS OF ARGININE MODIFICATIONS ON CHD1 TANDEM CHROMODOMAIN RECOGNITION

A. Background

i. Arginine Modifications

Four distinct modified arginine residues on histone tails have been reported, which include monomethylarginine, asymmetric dimethylarginine (DMAa), symmetric dimethylarginine (DMAs), and citrulline (Cit). Each of these modifications has a drastic effect on the electronics and chemical properties of arginine, which will be discussed, and, therefore, influence effector protein recognition. In this research, I sought to understand how these modifications regulate recognition of the tandem chromodomains from the effector protein, CHD1.

ii. Arginine Methylation

Arginine methylation is a modification ubiquitous to N-terminal histone tails. The two forms of dimethylation are each catalyzed by a different family of protein arginine methylation transferases (PRMTs). Type I enzymes catalyze asymmetric dimethylation while type II enzymes catalyze symmetric dimethylation.[1] These types of enzymes are thought to have opposing effects on gene expression. PRMT1 is a type I enzyme that methylates H4 R3.[2] The acetyltransferase, p300, is subsequently activated and acetylates lysine residues on H4. The result is an up-regulation of gene expression.[3]

Less is known about type II enzymes. However, PRMT5 has been identified and are known to place symmetric dimethyl marks on histone tails *in vito*, which are correlated with gene silencing.[4-6]

Methylarginine can regulate gene expression through several possible mechanisms. First, dimethylargine has been shown to act as a "switch" and block the binding of effector proteins.[7] Proteins that contain methyllysine-specific domains such as PHD fingers, chromo, Tudor, and WD40 domains can be affected by methylation of a neighboring arginine. Specifically, WDR5 is a transcriptional activator with a WD40 domain that selectively recognizes H3 $K4Me_3$.[8] Serine and cysteine residues in WDR5 make important H-bonds with unmethylated Arg2. However, upon methylation of arginine those contacts are disrupted and WDR5 can no longer dock onto the histone tail and gene transcription is silenced.[8]

Effector proteins can also be recruited to dimethylarginine and can act as transcription repressors or activators. For example, the DNA methyltransferase DNMT3A contains a PHD finger, which binds DMAs marks at the Arg3 site of H4. Once bound, DNM3A can methylated DNA, which silences expression.[9] Alternatively, a DMAa mark on Arg3 of H4 can act as a docking site for the Tudor domain of TDRD3. Though the mechanism of TDRD3 is unclear, it is a known transcriptional cooactivator.[10] A number of other DMAa marks have also been reported as docking sites for transcriptional activators while DMAs marks recruit repressors.[11]

iii. Arginine Citrullination

The arginine deimination reaction, also commonly referred to as citrullination, is a modification known for its role in disease states such as multiple sclerosis and rheumatoid arthritis.[12, 13] Citrullination of arginine is a modification that regulates a multitude of biological functions including regulations of the cytoskeleton, the myelin basic protein important for the central nervous system, and gene expression.[14]

Arginine deimination in histone proteins is an epigenetic modification catalyzed by the enzymes arginine deiminase 4 (PAD4) (Fig. 2.1A, B).[15, 16] Recent evidence from *in vivo* and *in vitro* experiments has also suggested that PAD4 reverses the effects CARM1-catalyzed arginine methylation by performing arginine demethylimination. In fact, ChIP assays have shown that arginine methylation and citrullination are inversely correlated on histone proteins.[17] While the role of citrullination is largely unknown, this modification is known to act as a transcriptional repression mark that prevents the transcriptional machinery from binding to chromatin (Fig. 2.1C).[18]

(A)

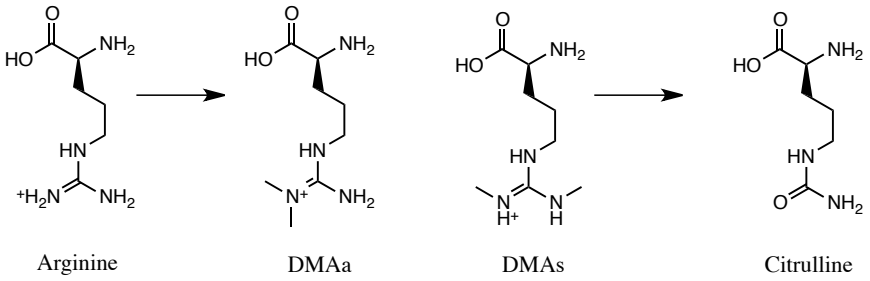

(B)

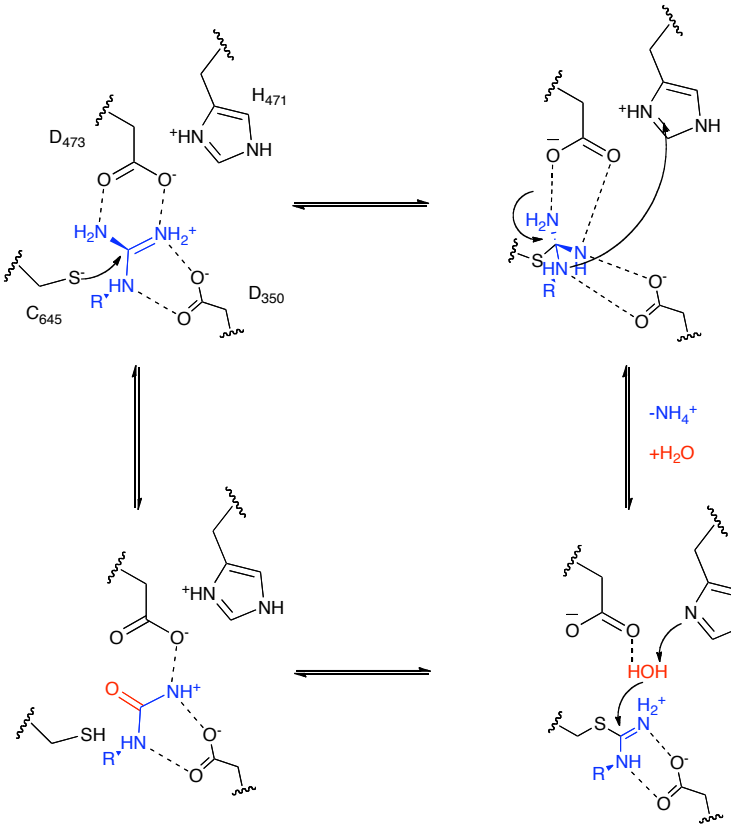

(C)

Figure 2.1. (A) Comparison of arginine asymmetric dimethylarginine (DMAa) and citrulline (Cit). (B) Proposed deimination mechanism by PAD4.[15] (C) Instances of citrullination observed *in vivo* and *in vitro*. Red indicates gene repression, green is gene activation, and yellow is unknown.[18]

iv. Citrulline and Methylarginine Interactions with Tryptophan

To understand how arginine methylation and deimination affects the cation-π interaction with aromatic binding pockets, an interaction critical in the read-out of PTMs, Hughes compared the cation-π and citrulline-π interactions using β-hairpins as model systems (Fig. 2.2).[19] NMR analysis revealed dimethylarginine (both symmetric and asymmetric) and tryptophan have an interaction energy of -1.0 kcal/mol, which is two-fold more favorable than the unmodified arginine with an interaction of -0.5 kcal/mol. The increased surface area of the dimethylarginine permitted a more favorable van der Waals interaction with tryptophan, which improved the interaction energy and folding. Citrulline and tryptophan have an interaction energy of -0.2 kcal/mol, which is approximately a two-fold weaker interaction energy than arginine with tryptophan. Citrulline is a neutral amino acid and therefore any favorable cation-π interaction with tryptophan is lost, resulting in a decrease in folding (data not published).

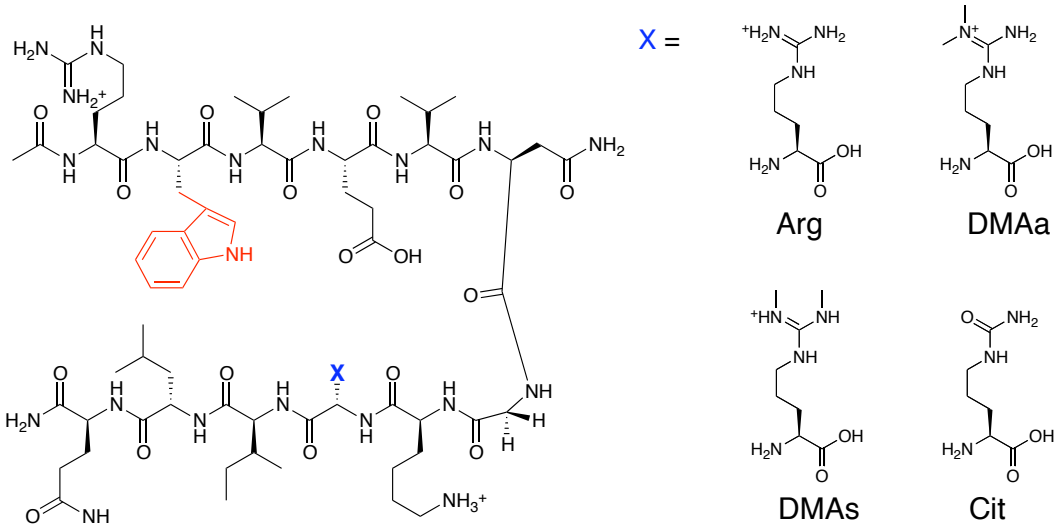

Figure 2.2. Cation-π and citrulline-π interactions with tryptophan in a β-hairpin.

v. Function of CHD1

CHD1 (chromo-ATPase/helicase-DNA binding domain 1) is a known ATP-dependent chromatin remodeling factor that regulates gene transcription.[20] CHD1 contains a set of N-terminal tandem chromodomains. Previously, effector proteins containing chromodomains were implicated in transcriptional repression. However, CHD1 also contains a helicase/ATPase domain, which has been implicated in DNA repair, replication, and transcriptional activation. The third motif within CHD1 is a DNA binding domain (Figure 2.3A).[21] In yeast, this protein occurs as part of the larger SAGA/SLIK histone acetyl transferase complex. It was also demonstrated that one of two chromodomains within CHD1 is responsible for the recognition of methylated Lys4 of the Histone H3 tail. This methyl-binding chromodomain activity is critical for acetyltransferase activity and has been linked to transcriptional activation.[22]

Several studies demonstrated that the human CHD1 tandem chromodomain in recognize trimethyllysine 4 of the Histone H3 tail (H3 $K4Me_3$) several orders of magnitude weaker than tandem chromodomains in budding yeast CHD1. While the function of CHD1 in various species is unclear, it is understood that methyllysine recognition of CHD1 is critical for proper transcriptional activity.[23, 24] To further understand the interactions between the tandem chromodomains of human CHD1 and trimethyllysine 4 of the H3 tail, the chromodomains and histone tail peptide were co-crystallized (Fig. 2.3B).

From the crystal structure, it is evident that the histone tail binds at an acidic surface, which forms an interface between Chromo1 and Chromo2 (Fig. 2.3C). Most chromodomains that recognize trimethyllysine require an aromatic cage consisting of

three aromatic residues.[25, 26] However, recognition of H3 K4Me$_3$ by CHD1 is mediated by a two-membered aromatic cage consisting of Trp64 and Trp67. While the lack of a third electron-rich aromatic cage ring may disfavor binding, the crystal structure indicates that Arg2 of the H3 tail is involved in a cation-π interaction with Trp67. Additionally Arg2 is able to form a hydrogen-bond (H-bond) to the carbonyl backbone of Gly66 (Figure 2.4).

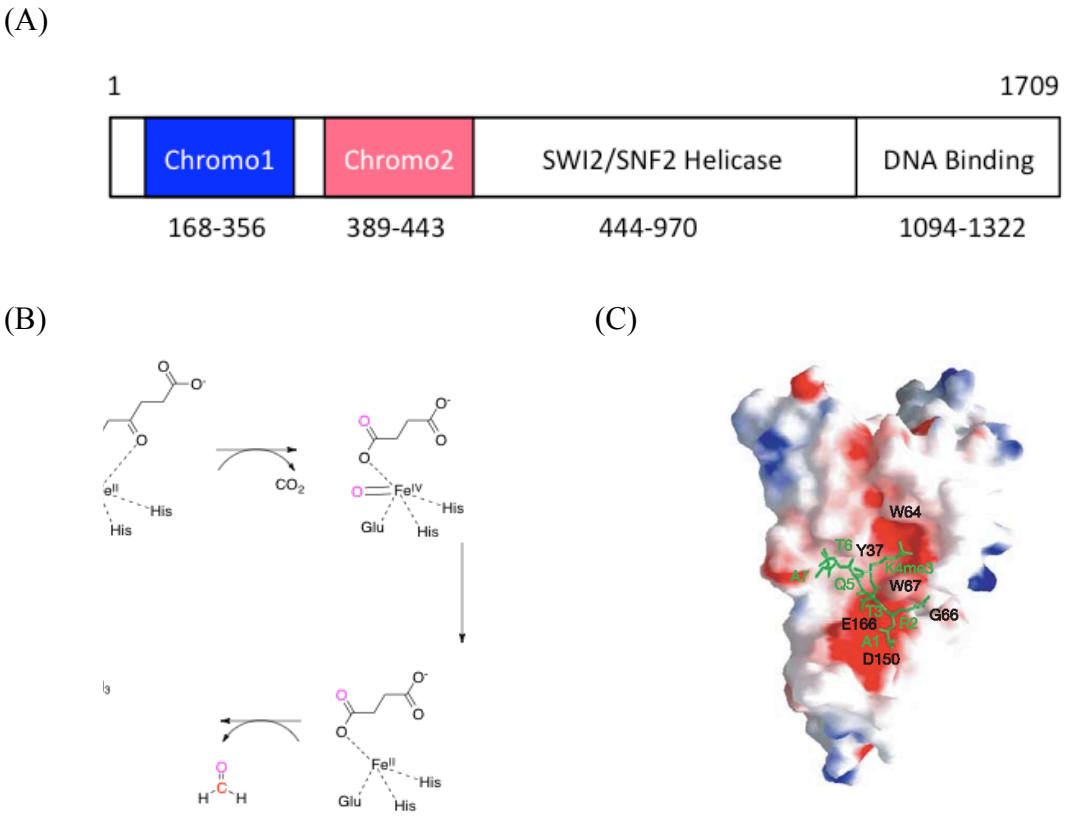

Figure 2.3. (A) The conserved domains in human CHD1. (B) The H3 K4Me$_3$ peptide bound to CHD1 tandem chromodomains. Chromo1 (cyan), chromo2 (magenta), linker (grey), histone tail (green). (C) Electrostatic potential map of CHD1 bound to H3 K4Me$_3$ peptide. Acidic regions are indicated with red and the basic regions are blue.[23]

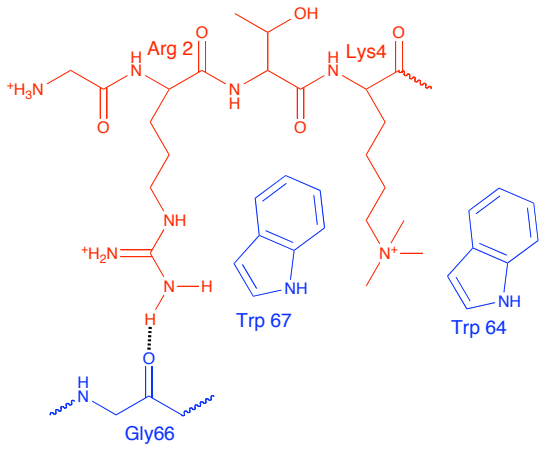

Figure 2.4 The aromatic cage of CHD1 with the H3 K4Me$_3$ peptide. The histone tail is in red and the residues from the chromodomain are in blue.[23]

Interestingly, no other lysine methyl mark has an arginine at the n-2 position, making Arg2 unique for this system and an important residue for selectivity. Enzymatic studies have shown that Arg2 is also subject to asymmetric dimethylation catalyzed by CARM1 (coactivator-associated arginine methyltransferase 1) and this activity has been linked to the transcriptional coactivator machinery.[27, 28] This enzymatic activity prompted further research to determine how Arg2 methylation affects CHD1 binding. Anisotropy experiments confirmed that the chromodomains have a four-fold stronger K_D for H3 K4Me$_3$ over the peptide containing both trimethyllysine and DMAa (5 μM and 24 μM respectively). The structure of the tandem chromodomains with the doubly modified peptide indicated that the dimethyl mark on Arg2 inhibit the H-bond to Gly66. It was therefore suggested that Arg2 methylation silences the Lys4 methyl mark.[23]

B. Goal

From past research is it clear that recognition of H3 K4Me$_3$ by the tandem chromodomains of CHD1 is critical for the proper regulation of gene expression.[22] It is

also evident that Arg2 is important for selectivity and binding affinity. In this work we aimed to further understand how arginine methylation and citrullination affect CHD1 selectivity and determine how these results compare to the β-hairpin model system.

C. Results

i. Peptide Design and Synthesis

In previous studies examining the binding of H3 K4Me_3 histone tails to the CHD1 tandem chromodomain, peptides were labeled on the N-terminus with fluorescein for the purpose of measuring binding by fluorescence anisotropy (Fig. 2.5A).[23, 29] However, Asp150 of the tandem chromodomain is known to form a H-bond to the N-terminal amine of the histone tail. It was a concern that the placement of a large aromatic fluorophore such as fluorescein may have influenced the previously measured dissociation constant. This concern was supported by the isothermal titration calorimetry measurements reported in the same article, which provided a K_D of 38 μM between CHD1 chromodomains and H3 K4Me_3.[23] Additionally, reports have suggested that placing a fluorophore a minimum of four amino acids from the binding site is necessary for accurate measurements.[29]

Therefore, a histone tail was redesigned to incorporate a fluorophore on the C-terminus of the histone tail linked by an amide bond to a non-native lysine. Lysine with the orthogonal protecting group, iVDde (1-(4,4-dimethyl-2,6-dioxocyclohex-1-ylidne)-3-methylbutyl), was incorporated at the C-terminus allowing for 5(6)-carboxyfluorescein (5(6)-FAM) to be conjugated to the peptide after synthesis and prior to the final cleavage by TFA. (Fig. 2.5B). Originally, I used Wang resin was used as the solid support for peptide synthesis because it yields a free C-terminal carboxylic acid. However, after

repeated failed attempts at synthesizing the peptide using various activators, it was clear that deprotection of Lys(iVDde) with 2% hydrazine was not compatible with Wang resin. Therefore Wang resin was substituted for clear amide resin, which yields a C-terminal amide as opposed to a carboxylic acid. Amide resins are known to be more stable than carboxylic acid resins and, therefore, it was hypothesized that the new resin would be compatible with the Lys(ivDde). Additionally, N-Hydroxybenzotriazole (HOBt) and O-Benzotriazole-N,N,N',N'-tetramethyl-uronium (HBTU), which are the standard activation agents used in solid phase peptide synthesis (SPPS), were ineffective in coupling 5(6)-FAM to the C-terminal lysine of the peptide. Therefore, diisopropylcarbodiimide (DIC) and HOBt were used instead. Despite low yields, the synthesis shown in Fig. 2.6 was successful.

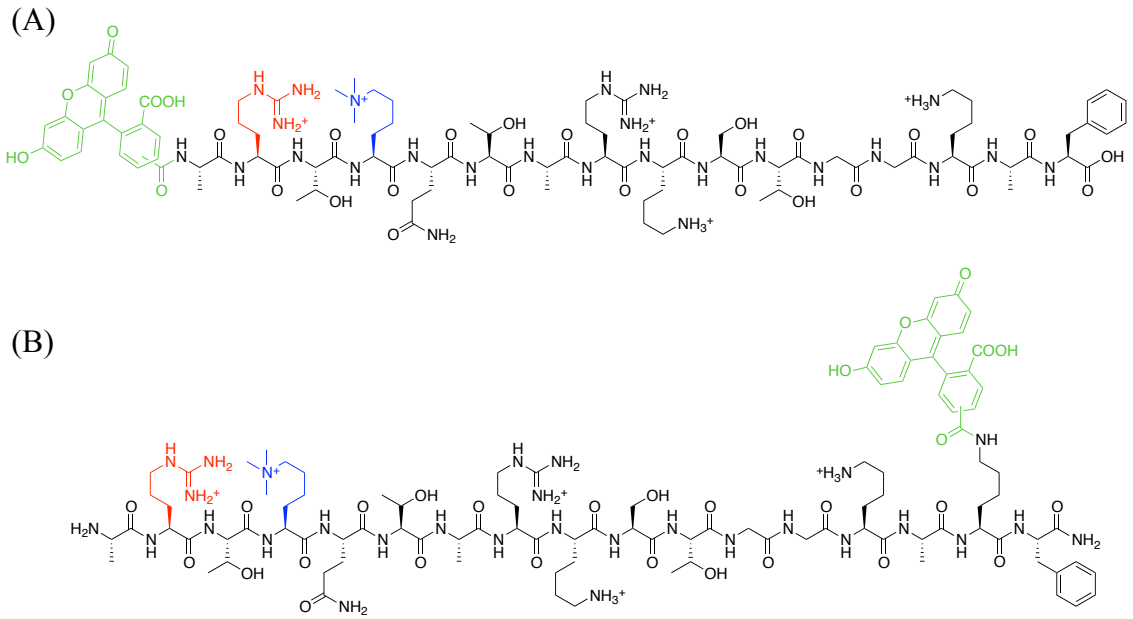

Figure 2.5. Structures of 5(6)-FAM-labelled H3 K4Me$_3$ histone tail peptides with fluorescein shown in green, K4Me$_3$ in blue, and Arg2 in red. (A) Peptide used by Flanagan and coworkers,[23] (B) peptide used in this research.

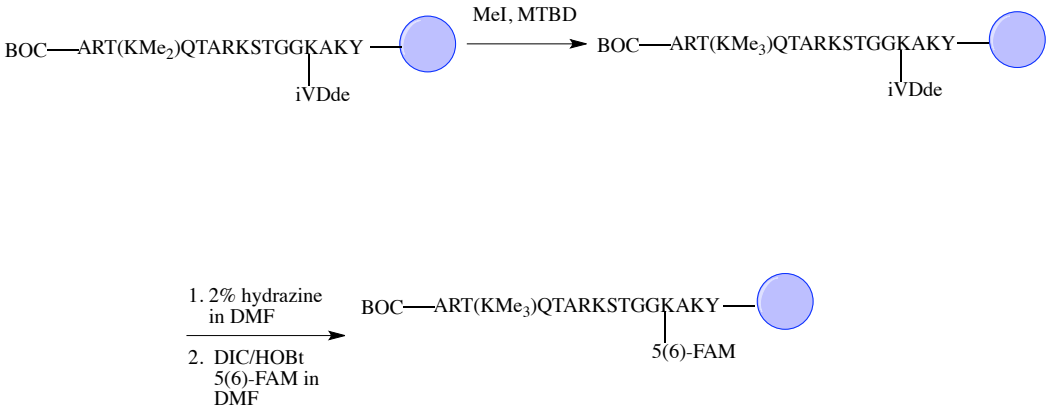

Figure 2.6. Synthetic scheme of H3 K4Me$_3$ peptides. (MTBD is 7-methyl-1,5,7-triazabicyclo[4.4.0]dec-5-ene and DMF is dimethylformamide)

ii. Structural Characterization

The CHD1 tandem chromodomain was expressed and purified from BL21 DE3 *E. coli* using a plasmid provided by the Khorasanizadeh group at the University of Virginia.[23] The structural integrity of the CHD1 tandem chromodomain was confirmed using circular dichroism. Much like HP1 chromodomains, which will be discussed later, CHD1 tandem chromodomains are composed primarily of α-helices. Therefore the CD spectra of the protein consisted of two strong minima at 208 nm and 222 nm as shown in Fig. 2.7, which confirmed the global structure of the protein.

The thermal stability of the tandem chromodomain was also evaluated by thermal denaturation, which was monitored by circular dichroism at 222 nm. The purpose was to confirm the stability of the protein at 25 ^{o}C because all previously published binding data were only performed at 15 ^{o}C. As shown in Fig. 2.8, the sigmoidal curve indicates that the protein remains fully folded up to 30 ^{o}C and has a melting temperature of approximately 33 ^{o}C. For this reason all samples were initially incubated at only 4 ^{o}C for thirty minutes to prevent denaturation and then allowed to incubate for ten minutes at room temperature prior to binding experiments.

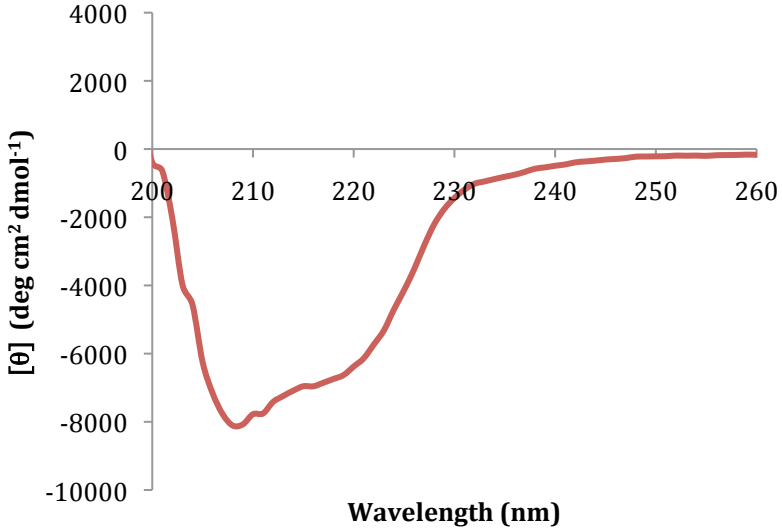

Figure 2.7. Circular dichroism spectra of CHD1 tandem chromodomains (25 μM) at 25 ^{o}C in 10 mM sodium phosphate pH 7.4 with 2 mM DTT. This curve is the average of three runs.

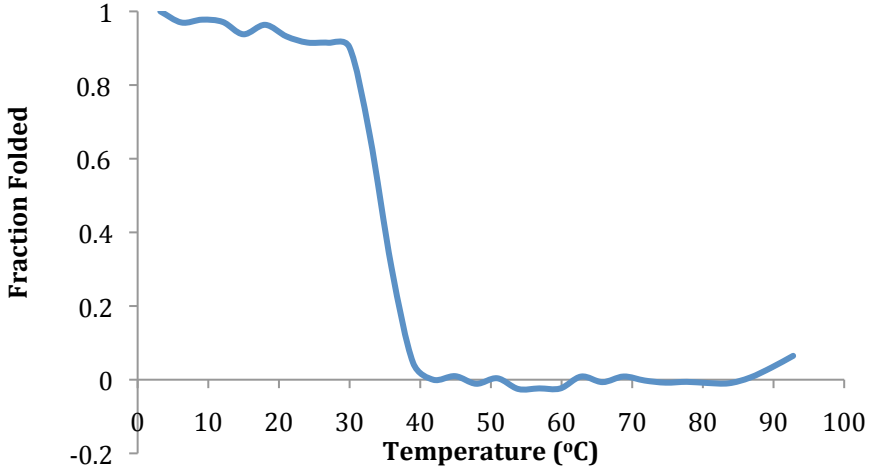

Figure 2.8. Thermal denaturation monitored by circular dichroism at 222 nm of CHD1 tandem in 10 mM sodium phosphate, pH 7.4, and 2 mM DTT.

iii. Binding Studies

Fluorescence anisotropy was used to measure the dissociation constants of the CHD1 tandem chromodomain with H3 K4Me$_3$ parent peptide, as well as, the with the

Arg2 variant peptides. Anisotropy revealed non-specific binding of the parent and DMAa peptides at chromodomain concentrations above approximately 125 μM.[30] Therefore, those data points were omitted from the final binding curves with a negligible effect on the dissociation constants. The final binding curves are shown in Fig. 2.9 and the dissociation constants and ΔG values are summarized in Table 2.1.

As shown in Table 2.1, the binding affinity of CHD1 chromodomains for the parent peptide containing KMe_3 was found to have a K_D of 21 μM as compared to 5.2 μM as previously published in the literature.[23] The 4-fold decrease in binding affinity with the parent histone tail compared to the literature value may be the result of differences in experimental conditions or from placing the fluorophore on the C-terminus as opposed to the N-terminus. At the N-terminus, fluorescein may interact directly with the aromatic pocket of the tandem chromodomains or intramolecularly with neighboring amino acid side-chains that would have otherwise been involved in molecular recognition with the chromodomains. Previous data had also been measured at 15 ^{o}C while the data shown here was measured at 25 ^{o}C, which can have an effect on measured binding constants. While speculative, these possibilities are likely to be the cause of the different binding affinities.

Also of note is the tighter binding affinity of H3 K4Me_3 DMAa (K_D=15±2 μM) compared to the literature value (K_D=24±4 μM). The difference in these values may also be contributed to different experimental conditions. The results reported here are further supported by the work of Strahl and coworkers who used peptide microarrays to demonstrate that asymmetric dimethylation of Arg2 in conjunction with trimethylation of Lys4 on the Histone H3 tail peptide enhances binding affinity of CHD1.[31] Alternatively,

incorporating DMAs weakened binding by more than 3-fold compared to the DMAa variant (K_D=42 μM).

The incorporation of citrulline in the H3 K4Me$_3$ peptide significantly disrupted binding by nearly an order of magnitude compared to the parent and DMAa-containing peptides (Fig. 2.8). As with the DMAa studies, these results are also consistent with those published by Strahl and coworkers who demonstrated that incorporation of citrulline in the 2-position of H3 K4Me$_3$ weakened binding of CHD1.[31]

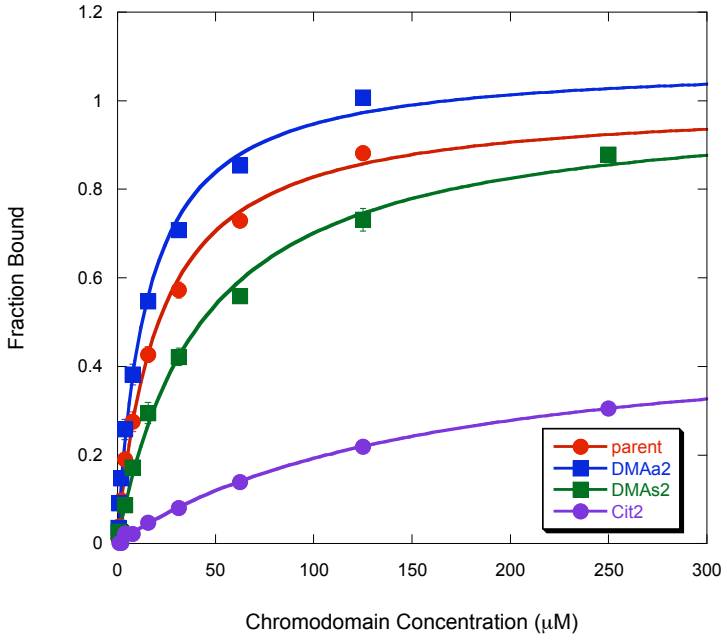

Figure 2.9. Final fluorescence anisotropy binding experiments of CHD1 tandem chromodomains with 0.5 μM H3 K4Me$_3$ (parent), H3 K4Me$_3$ DMAa, H3 K4Me$_3$ DMAs, and H3 K4Me$_3$ Cit2. Experiments were performed in 50 mM potassium phosphate buffer pH 8.0, 25 mM NaCl, and 5 mM TCEP at 25 °C. Each curve is an average of 3 runs.

Table 2.1. Dissociation constants (μM) of human CHD1 tandem chomodomain and H3 K4Me_3 and the mutants. The R^2 values were calculated using Kaleidagraph and are given in parenthesis. The ΔG^o values (kcal/mol) were calculated using the following equation: $\Delta G^o = RTln(K_D)$. The data was measured in 50 mM potassium phosphate buffer (pH 8), 25 mM NaCl, with 5 mM TCEP at 25°C. Error is determined from 3 replicates.

H3 K4 Me_3	Literature K_D[23]	Experimental K_D (μM)	Experimental ΔG^o (kcal/mol)
Parent	5.2±0.6	21 ± 2 (0.996)	-6.4 ± 0.1
DMAa	24±4	15 ± 2 (0.995)	-6.6 ± 0.1
DMAs	n.a.	43 ± 5 (0.996)	-6.0 ± 0.1
Cit2	n.a.	160 ± 14 (0.999)	-5.2 ± 0.1

D. Discussion

It is evident from studies involving the H3 K4Me_3 histone tail and the three Arg2 variants that the residue incorporated into the Arg2 position is important for controlling recognition of the CHD1 tandem chromodomains *in vitro*. Each modified arginine side-chain influences the binding affinity between the chromodomain and the N-terminal histone tail.

Interestingly, asymmetric and symmetric dimethylarginine have opposing effects on chromodomain recognition with the H3 K4Me_3 DMAs peptide binding 4-fold weaker than the DMAa containing-peptide. Previous studies using hairpin models showed that the interaction energies between both dimethylarginine and tryptophan are equivalent. However, in the context of a larger protein, the two different dimethylarginine marks are important for selectivity and have distinct roles in the regulation of gene expression, which has been demonstrated in the case of H4 R8.[11]

i. Effects of DMAa

The improved binding affinity of the DMAa-containing peptide and CHD1 chromodomain (15 μM) relative to unmethylated Arg contradicts the data previously

reported by Khorasanizadeh *et al*.[23] Asymmetric dimethylation Arg2 was reported to interfere with a H-bond to the backbone carbonyl of Gly66 of the tandem chromodomain and therefore weaken binding from 5 μM to 24 μM.[23] Additionally, methyl groups are known to be electron donating, which would weaken the ability of arginine to act as a H-bond donor.[23] However, in the case of DMAa, one nitrogen within the guanidinium group remains unmethylated, which still makes it a possible H-bond donor and capable of forming a H-bond to the carbonyl backbone of Gly66.

The slightly improved binding affinity of the DMAa-containing H3 peptide relative to the parent peptide is most likely the result of improved van der Waals contacts with Trp67. Upon examination of the electrostatic potential map (Fig. 2.9), it is apparent that the addition of two methyl groups on arginine significantly increases the surface area of the guanidinium group and results in the distribution of the positive charge across the side-chain (Fig. 2.10).[19] This charge distribution permits stronger van der Waals contacts with Trp67. The methyl groups allow for interactions with the indole ring of tryptophan to be entropically more favorable due to an added hydrophobic component.[19] It appears that any effects on the H-bond between Gly66 and DMAa are negated by the cation-π interaction and van der Waals contacts between DMAa and Trp67.

Interestingly, methylation of Arg2 by CARM1 has been implicated in transcriptional activation.[28] Therefore enhanced recognition of CHD1, a known transcriptional activator, for the DMAa variant histone peptide may further explain the biological significance of asymmetric arginine methylation.

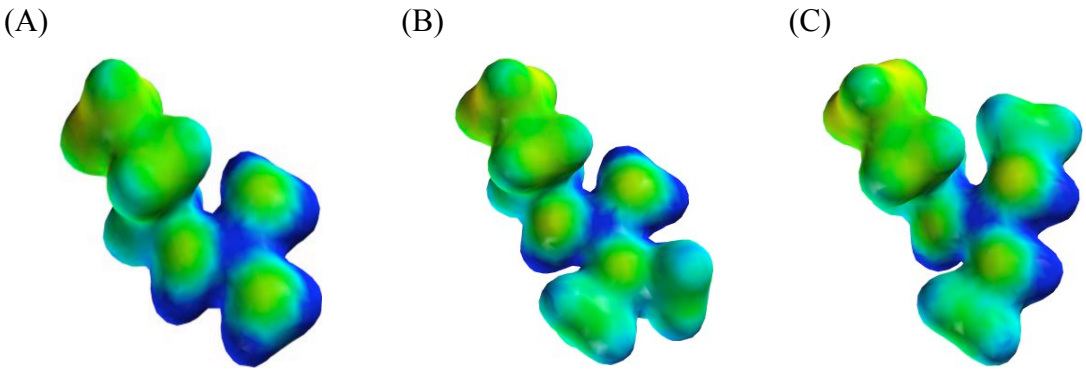

Figure 2.10. Electrostatic potential maps depicting (A) arginine, (B) DMAa and (C) DMAa. Electrostatic potential maps were generated with MacSpartan: HF/6-31g*; isodensity value = 0.02; range = 50 (red, electron rich) to 200 kcal/mol (blue, electron poor).

ii. Effects of DMAs

The DMAs variant had a weakened affinity of 42 μM and a ΔΔG of 0.4 kcal/mol compared to the parent peptide and 0.6 kcal/mol compared to the DMAa counterpart. Previous NMR studies using β-hairpin models to investigate cross-strand cation-π interactions demonstrated that peptides with either DMAa or DMAs had similar interaction energies with tryptophan (data not published). However, the β-hairpin is a simplified model that does not take into account the importance of neighboring residues in the chromodomain, orientation, and charge distribution as seen within the more complex histone tail-chromodomain complex. CHD1 also H-bonds to arginine, which varies in strength depending on what modifications are present on the side chain. The H-bond between Arg2 and the carbonyl of Gly66 is also important for CHD1 recognition. The presence of one methyl group on each nitrogen within the guanidinium of DMAs may weaken or inhibit H-bonding to Gly66 due to steric crowding, which can contribute to weakened binding affinity.

The DMAs modification is not catalyzed by CARM1. Symmetric dimethylation is carried out by type II protein arginine methyltransferases (PRMTs) while CARM1 is a type I PRMT. The most well characterized type II PRMT is PRMT5. Though very little is known about the effects of the DMAs mark, PRMT5 does associate with the SWI/SNF complex, which is a chromatin remodeling complex that suppresses expression of tumor suppressor proteins and is associated with cell proliferation.[32] The weakened binding affinity that CHD1 has for the DMAs variant is consistent with the repressed gene expression associated with type II PRMTs.[33] However, the effects of symmetric dimethylation and the identification of the type II PRMTs responsible remain largely unknown.

iii. Effects of Citrulline

Deimination has been suggested as nature's method for reversing the effects of arginine methylation. Therefore, we wanted to determine how incorporation of Cit2 influences the binding affinity of the H3 $K4Me_3$ peptide to the CHD1 tandem chromodomains. Citrullination of Arg2 in the histone tail significantly disrupts binding by a factor of eight with a $\Delta\Delta G$ of 1.2 kcal/mol. There are two possible explanations for the decrease in binding affinity. The first is a loss in cation-π interactions and the second is a loss of an H-bond.

Citrulline is capable of participating in polar-π interactions. However, citrulline does not have the cationic character found in arginine and methylarginine, which results in the loss of the favorable cation-π interaction with Trp67. In the β-hairpin model system employed by Hughes (data not published), the difference between arginine and citrulline was approximately 0.3 kcal/mol. The larger effect that deimination has on

binding to CHD1 may be attributed to the loss of the H-bond with Gly66 because citrulline is a significantly weaker H-bond donor compared to arginine, DMAa, or DMAs. These two factors both contribute to the clear disruption of binding to the CHD1 tandem chromodomains.

iv. Conclusions

Asymmetric and symmetric methylation and deimination are three modifications that are known to occur within nature and notably on N-terminal histone tails. Each of these arginine modifications has a distinct impact on the recognition of CHD1 chromodomains for histone peptides. What is clear from these studies is that DMAa and DMAs are not equivalent modifications and are capable of having opposite outcomes on the read-out of PTMs. Evidence has even demonstrated that DMAa and DMAs have opposing effects on gene expression with DMAa acting as a transcriptional activating mark and DMAs acting as a suppressing mark.[2, 6] Furthermore, deimination does not simply reverse the effects of arginine methylation. Rather the loss of the positive charge is a change that is significant enough to disrupt binding of effector proteins such as CHD1 and perhaps silence gene expression. While the effects of H3 K4Me_3 variants on CHD1 recognition have been substantiated here and by Strahl and coworkers, much can still be learned about how these three modifications affect the Histone Code.

E. Experimental

i. Protein Expression and Purification

The Khorasanizadeh Group at the University of Virginia supplied the PET11a plasmid containing the coding region of human CHD1 Chromodomain with an N-terminal 6-Histidine tag. *E. coli* BL21 (DE3) gold cells were transformed with the

plasmid and were grown as 1.5 L cultures in LB media with 50 mg/L ampicillin at 37^{o}C. At A_{600}=0.5-0.7, the cultures were induced with 0.1 mM isopropyl β-D-1-thiogalactopyranoside (IPTG). The temperature of the shaker was reduced to 18 ^{o}C and the cultures are allowed to incubate overnight. The cells were harvested by centrifugation for 20 mins at 4500 rpm using a Sorvall RC-3B refrigerated centrifuge with a H6000A swinging bucket rotor. The supernatant was discarded and the cells were resuspended in approximately 30 mL NiA buffer (5 mM imidazole, 50 mM potassium phosphate, pH 7.4, 150 mM NaCl, 0.01% sodium azide) and stored at -80^{o}C for a later time.

The cells (40 mL) were thawed and subsequently lysed by sonication (Branson 102C CE, 1 min 30 sec with a 0.5 sec pulse and 1.5 sec off) in the presence of DNase, cOmplete, EDTA-free Protease Inhibitor Cocktail Tablets (Roche Applied Sciences) and a final concentration of 1 mM phenylmethanesulfonylfluoride (PMSF). The lysate was centrifuged at 17000 rmp for 60 mins to yield a clear supernatant using a Sorvall RC-3B refrigerated superspeed centrifuge with an SS-34 rotor. The supernatant was filtered through a sterile 2 μM filter. The protein was purified using Nickel affinity chromatography using a gravity column with 10 mL Nickel-NTA agarose resin slurry from Qiagen. NiB buffer (250 mM imidazole, 50 mM potassium phosphate, pH 7.4, 150 mM NaCl, 0.01% sodium azide) was used to elute the protein. After the flowthrough was collected, the column was washed with 150 mL NiA then 50 mL of 95:5 NiA:NiB and 50 mL of 90:10 NiA:NiB. The protein was eluted in 5-10 mL fractions using NiB. The purity was confirmed using SDS-PAGE (Fig. 2.11). The protein was then dialyzed in 1L 50 mM potassium phosphate pH 8.0, 25 mM NaCl.

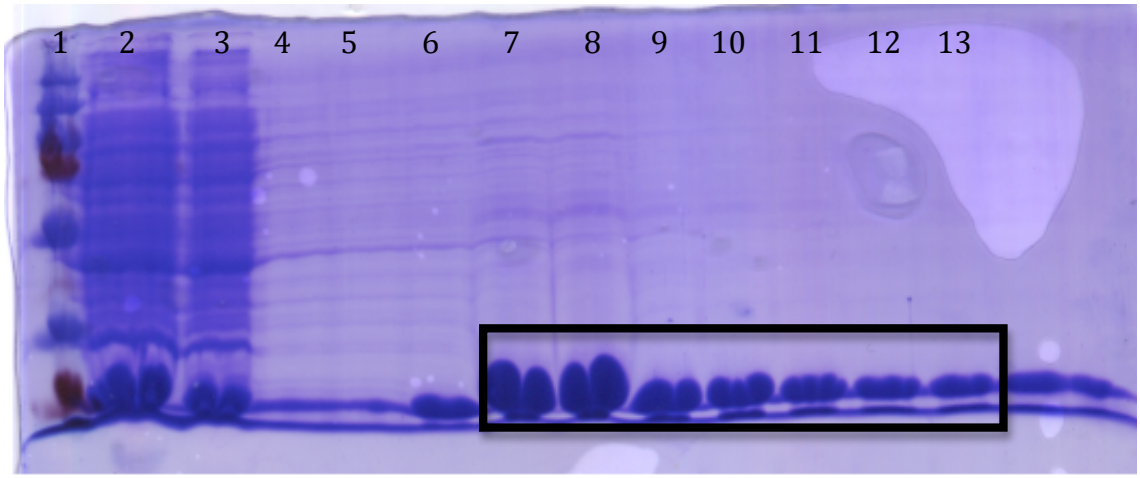

Figure 2.11. Purity of CHD1 Chromodomain by 15% SDS-PAGE. (1) Ladder, (2) Supernatant, (3) Flowthrough and NiA wash, (4) 5% B wash, (5) 10% B wash, (6-15) 100% B wash. Fractions from lanes 6-10 were pooled.

ii. Peptide Synthesis and Purification

Histone tails (residues 1-15 of the H3 tail with a C-terminal tyrosine) were synthesized using automated solid phase peptide synthesis with a Thuramed Tetras synthesizer on a 0.06 mmol scale. Fmoc protected amino acids were used with Clear-Amide resin from Peptides International, Inc. Amino acid residues were activated with HBTU (O-benzotriazole-N,N,N',N',-tetramethyluronium hexafluorophosphate) and HOBT (N-hydroxybenzotriazole) with DIPEA (diisopropylethylamine) in DMF (N,N-dimethylformamide) using four equivalents of amino acid, activator, and DIPEA. Amino acids were deprotected twice with 2% DBU (1,8-diazabicyclo[5.4.0]undec-7-ene) and 2% piperidine in DMF for 15 mins each step. Each amino acid was coupled on double cycles of 30 mins each to improve coupling. Fmoc-Lys(ivDde)-OH was the second amino acid to be coupled for a total of 5 hrs using two molar equivalents. Fmoc-Cit-OH, Fmoc-SDMA$(Boc)_2$-OH, or Fmoc-ADMA(Pbf)-OH were coupled at position 2 using two molar

equivalents. Boc-Ala-OH was used as the final residue the C-terminus so Lys(ivDde) could be deprotected with hydrazine. Fmoc-Lys(Me)$_2$-OH was coupled at position 9 for 10 hrs methylated at the end of the peptide synthesis with the N-terminal amine still Boc-protected. Methylation was performed with 10.8 mL MTBD and 37.4 μL iodomethane in 5mL DMF and bubbled with N_2 for 4-5 hrs with a vented septum. The iVDde protecting group was deprotected from lysine by washing with 10 mL of 2% hydrazine in DMF 3 times for 3 mins each time. The 5(6)-carboxyfluorescein (5(6)-FAM) was coupled to the free amine as follows. First 34 mg 5(6)-FAM (1.5 eq) and 12.2 mg HOBt (1.5 eq) were combined in 5 mL DMF then 15.8 mL diisopropylcarbodiimide (1.7 eq) were added and the solution was allowed to react for ten mins at room temperature. The solution was then added to the resin, which was bubbled overnight with nitrogen gas. Cleavage of the peptides from the resin was performed in 95% trifluoroacetic acid (TFA), 2.5% H_2O, 2.5% triisopropylsilane (TIPS) for three hrs. TFA was evaporated by blowing the peptide with nitrogen, and cold diethyl ether was used to precipitate the product. The product was extracted with deionized MilliQ water and lyophilized to a powder.

Peptides were purified by reversed-phase HPLC. A Waters semi-preparative HPLC system with an Atlantis Prep OBD dC-18 semi-preparative column was used for separation with a gradient of 0% to 100% solvent B over 60 mins with solvent A (95:5 water:acetonitrile, 0.1% TFA) and solvent B (95:5 acetonitrile:water, 0.1% TFA). This purification process was repeated twice to remove impurities. Peptides were lyophilized and the molecular weight was confirmed by ESI-TOF mass spectrometry (Table 2.2).

iii. Circular Dichroism

CD measurements were performed on an Aviv 62DS Circular Dichroism Spectrometer. CD data was obtained for the chromodomain at 33.3 μM concentration in 10 mM Na_2HPO_4, pH 7.4, 2 mM DTT. Wavelength scans were performed in triplicate and averaged. Scans were performed at 25° C from 260-185 nm. All scans were corrected by subtracting the spectrum of the buffer used in the experiment and the signal was converted to Mean Residue Ellipticity (MRE) using Eq. 2.1. Where signal refers to circular dichroism signal, ℓ is path length in cm, c is conentration in M, and r is the number of amino acid residues.

$$\Theta = \frac{signal}{10 \cdot \ell \cdot c} \cdot \frac{1}{r} \qquad \text{Eq. 2.1}$$

Thermal denaturation experiments were preformed using the same buffer and concentrations as described above and measurements were taken between 275 and 366 K. The melting curves were normalized to show the fraction folded using Eq. 2.2 where Θ_O is MRE, Θ_D is the MRE for the fully denatured protein, and Θ_F is MRE for initially folded protein.

$$Fraction\ Folded = \frac{\Theta_O - \Theta_D}{\Theta_F - \Theta_D} \qquad \text{Eq. 2.2}$$

iv. Anisotropy

Binding assays were performed using a POLARstar Omega microplate reader with untreated 96 half area flat bottom plates. CHD1 chromodomain was prepared using 1:2 serial dilutions (0 μM to 500 μM) in 50 mM potassium phosphate buffer, pH 8, 25 mM NaCl that CHD1 chromodomain was dialyzed in and 5 mM TCEP was added to it. The protein was centrifuged for 1 min at 4000 rpm to draw down any air bubbles. A 1

μM stock of H3 K4Me$_3$ was prepared (ε_{492}=78,000 cm$^{=1}$M^{-1}) in 50 mM potassium phosphate buffer, pH 8, 25 mM NaCl. The chromodomain and peptide were mixed in the microplate with 50 μL of chromodomain and 50 μL of peptide. This reduced the concentration of peptide, TCEP, and chromodomain by half (0.5 μM peptide, 2.5 mM TCEP , 0 μM to 250 μM chromodomain). The samples were mixed by pipetting them ten times while introducing as few air bubbles as possible and centrifuged at 3000 rpm for 1 min using a Sorvall T1 centrifuged with a T20 microplate rotor to remove any additional air bubbles. All samples were allowed to reach equilibrium for 30 mins at 4^{o}C then at ambient temperature for 10 mins prior to analysis. Measurements were taken with an excitation wavelength of 485 nm and an emission wavelength at 520 nm. The data was fitted using Eq. 2.3 in Kaleidagraph where r is anisotropy, r_0 is the initial anisotropy, r_∞ is the maximum anisotropy, p is the total concentration of fluorescein-labeled peptide, [c] is the total chromodomain concentration added, and K_D is the dissociation constant. The values for r_0, r_∞, and K_D were treated as floating variables.

$$r = \left(\left(\frac{-(-p-[c]-K_D) \pm \sqrt{(-p-[c]-K_D)^2 - 4(p\cdot[c])}}{2\cdot p} \right) \cdot (r_\infty - r_0) \right) + r \qquad \text{Eq. 2.3}$$

Once the values for r_∞ and r_0 were determined from the curve fit, the fraction of bound chromodomain was calculated using Equation 2.4. The data was re-plotted as fraction bound as a function of chromodomain concentration to give the final data as shown in Fig. 2.6.

$$fraction\ bound = \frac{r - r_0}{r_\infty - r_0} \qquad \text{Eq. 2.4}$$

Table 2.2. Mass spectrometry data for the peptides synthesized for this study.

Peptide	Expected Mass (Da)	Observed Mass (Da)
H3 K4Me$_3$	2251.6	2251.2
H3 K4Me$_3$ Cit	2252.2	2252.8
H3 K4Me$_3$ DMAa	2279.2	2279.8
H3 K4Me$_3$ DMAs	2279.2	2279.3

References

1. Zhang, Y.; Reinberg, D., Transcription Regulation by Histone Methylation: Interplay Between Different Covalent Modifications of the Core Histone Tails. *Genes Dev* **2001,** *15*, 2343-2360.

2. Strahl, B. D.; Briggs, S. D.; Brame, C. J.; Caldwell, J. A.; Koh, S. S.; Ma, H.; Cook, R. G.; Shabanowites, J.; Hunt, D. F.; Stallcup, M. R.; Allis, C. D., Methylation of Histone H4 at Arginine 3 Occurs In Vivo and is Mediated by the Nuclear Receptor Coactivator PRMT1. *Curr Biol* **2001,** *11*, 996-1000.

3. Wang, H.; Huang, Z.-Q.; Xia, L.; Feng, Q.; Erdjument-Bromage, H.; Strahl, B. D.; Briggs, S. D.; Allis, C. D.; Wong, J.; Tempst, P.; Zhang, Y., Methylation of Hisotne H4 at Arginine 3 Facilitating Transcriptional Activation by Nuclear Hormone Recptor. *Science* **2001,** *293*, 853-857.

4. Branscombe, T. L.; Frankel, A.; Lee, J.-H.; Cook, J. R.; Yang, Z.-H.; Pestka, S.; Clarke, S., PRMT5 (Janus Kinase-binding Protein 1) Catalyzes the Formation of Symmetric Dimethylarginine Residues in Proteins. *J Biol Chem* **2001,** *276*, 32971-32976.

5. Lee, J.-H.; Cook, J. R.; Yang, Z.-H.; Mirochnitchenko, O.; I., G. S.; Felix, A. M.; Herth, N.; Hoffman, R.; Peska, S., PRMT7, a New Protein Arginine Methyltransferase that Synthesizes Symmetric Dimethylarginine. *J Biol Chem* **2005,** *280*, 3656-3664.

6. Fabbrizio, E.; Messaoudi, S. E.; Polanowka, J.; Paul, C.; Cook, J. R.; Lee, J.-H.; Nègre, V.; Rousset, M.; Pestka, S.; Cam, A. L.; Sardet, C., Negative Regulation of Transcription by the Type II Arginine Methyltransferase PRMT5. *EMBO Rep* **2002,** *3*, 641-645.

7. Iberg, A. N.; Espejo, A.; Cheng, D.; Kim, D.; Michaud-Levesque, J.; Richard, S.; Bedford, M. T., Arginine Methylation of the Histone H3 Tail Impedes Effector Binding. *J Biol Chem* **2008,** *283*, 3006-3010.

8. Couture, J.-F.; Collazo, E.; Trievel, R. C., Molecular Recognition of Histone H3 by the WD40 Protein WDR5. *Nat Struct Mol Biol* **2006,** *13*, 698-703.

9. Zhao, Q.; Rank, G.; Tan, Y. T.; Li, H.; Moritz, R. L.; Simpson, R. J.; Cerruti, L.; Curtis, D. J.; Patel, D. J.; Allis, C. D.; Cunningham, J. M.; Jane, S. M., PRMT5-Mediated Methylation of Histone H4R3 Recruits DNMT3A, Coupling Histone and DNA Methylation in Gene Silencing. *Nat Struct Mol Biol* **2009,** *16*, 304-311.

10. Yang, Y.; Lu, Y.; Espejo, A.; Wu, J.; Xu, W.; Liang, S.; Bedford, M. T., TDRD3 is an Effector Molecule for Arginine-Methylated Histone Marks. *Mol Cell* **2010,** *40*, 1016-1023.

11. Lorenzo, A. D.; Bedford, M. T., Histone Arginine Methylation. *FEBS Lett* [Online early access]. doi:10.1016/j.febslet.2010.11.010. Published Online: November 2010.

12. Moscarello, M. A.; Mastronardi, F. G.; Wood, D. D., The Role of Citrullinated Proteins Suggests a Novel Mechanism in the Pathogenesis of Multiple Sclerosis. *Neurochem Res* **2007,** *32*, 251-256.

13. Chang, X.; Yamada, R.; Suzuki, A.; Sawada, T.; Yoshino, S.; Tokuhiro, S.; Yamamoto, K., Localization of Peptidylarginine Deiminase 4 (PADI4) and Citrullinated Protein in Synovial Tissue of Rheumatoid Arthritis. *Rheumatology* **2004,** *44*, 40-50.

14. György, B.; Tóth, E.; Tarcsa, E.; Falus, A.; Buzás, E., Citrullination: A Posttranslational Modification in Health and Disease. *Int J Biochem Cell Biol* **2006,** *38*, 1662-1677.

15. Kearney, P. L.; Bhatia, M.; Jones, N. G.; Yuan, L.; Glascock, M. C.; Catchings, K. L.; Yamada, M.; Thompson, P. R., Kinetics Characterization of Protein Arginine Deiminase 4: A Transcriptional Corepressor Implicated in the Onset and Progression of Rheumatoid Arthritis. *Biochemistry* **2005,** *44*, 10570-10582.

16. Hagiwara, T.; Nakashima, K.; Hirano, H.; Senshu, T.; Yamada, M., Demination of Arginine Residues in Neucleophosmin/B23 and Histones in HL-60 Granulocytes. *Biochem Biophys Res Commun* **2002,** *290*, 979-983.

17. Wang, Y.; Wysocka, J.; Syegh, J.; Lee, Y. H.; Perlin, J. R.; Leonelli, L.; Sonbuchner, L. S.; McDonald, C. H.; Cook, R. G.; Dou, Y.; Roeder, R. G.; Clarke, S.; Stallcup, M. R.; Allis, C. D.; Coonrod, S. A., Human PAD4 Regulates Histone Arginine Methylation Levels via Demethylimination. *Science* **2004,** *306*, 279-283.

18. Wysocka, J.; Allis, C. D.; Coonrod, S., Histone Arginine Methylation and its Dynamic Regulation. *Font Biosci* **2006,** *11*, 344-355.

19. Hughes, R. M.; Waters, M. L., Arginine Methylation in a β-Hairpin Peptide: Implications for Arg-π Interactions, ΔC_p^o, and the Cold Denatured State. *J Am Chem Soc* **2006,** *128*, 12735-12742.

20. Tran, H. G.; Steger, D. J.; Lyer, V. R.; Johnson, A. D., The Chromo Domain Protein Chd1p from Budding Yeast is an ATP-Dependent Chromatin-Modifying Factor. *EMBO J* **2000,** *19*, 2323-2331.

21. Stokes, D. G.; Perry, R. P., DNA-Binding and Chromatin Localization Properties of CHD1. *Mol Cell Biol* **1995,** *15*, 2745-2753.

22. Pray-Grant, M. G.; Daniul, J. A.; Schieltz, D.; Yates, J. F.; Grant, P. A., Chd1 Chromodomain Links Histone H3 Methylation with SAGA-and SLIK-Dependent Acetylation. *Nature* **2005,** *433*, 434-438.

23. Flanagan, J. F.; Mi, L. Z.; Chruszcz, M.; Cymborowski, M.; Clines, K. L.; Kim, Y.; Minor, W.; Rastinejad, F.; Khorasanizadeh, S., Double Chromodomains Cooperate to Recognize the Methylated Histone H3 Tail. *Nature* **2005,** *438*, 1181-1185.

24. Sims, R. J.; F., C. C.; Santos-Rosa, H.; Kouzarides, T.; Patel, S. S.; Reinberg, D., Human but Not Yeast CHD1 Binds Directly and Selectively to Histone H3 Methylated at Lysine 4 via Its Tandem Chromodomains. *J Biol Chem* **2005,** *280*, 41789-41792.

25. Jacobs, S. A.; Khorasanizadeh, S., Structure of HP1 Chromodomain Bound to a Lysine 9-Methylated Histone H3 Tail. *Science* **2002,** *295*, 2080-2083.

26. Fischle, W.; Wang, Y.; Jacobs, S. A.; Kim, Y.; Allis, C. D.; Khorasanizadeh, S., Molecular Basis for the Discrimination of Repressive Methyl-Lysine Marks in Histone H3 by Polycomb and HP1 Chromodomains. *Genes Dev* **2003,** *17*, 1870-1881.

27. Chen, D.; Ma, H.; Hong, H.; Koh, S. S.; Huang, S. M.; Schurter, B. T.; Aswad, D. W.; Stallcup, M. R., Regulation of Transcription by a Protein Methyltransferase. *Science* **1999,** *240*, 2174-2177.

28. Schurter, B. T.; Koh, S. S.; Chen, D.; Bunick, G. J.; Harp, J. M.; Hanson, B. L.; Henschen-Edman, A.; Mackay, D. R.; Stallcup, M. R.; Aswad, D. W., Methylation of Histone H3 by Coactivator-Associated Arginine Methyltransferase 1. *Biochemistry* **2001,** *40*, 5747-5756.

29. Jacobs, S. A.; Fischle, W.; Khorasanizadeh, S., Assays for the Determination of Structure and Dynamics of the Interaction of the Chromodomain with Histone Peptides. *Methods Enzymol* **2004,** *376*, 131-148.

30. Schalch, T.; Job, G.; Noffsinger, V. J.; Shanker, S.; Kuscu, C.; Joshua-Tor, L.; Partridge, J. F., High-Affinity Binding of Chp1 Chromodomaini to K9 Methylated Histone H3 Is Required to Establish Centromeric Heterochromatin. *Mol Cell* **2009,** *34*, 36-46.

31. Fuchs, S. M.; Krajewski, K.; Baker, R. W.; Miller, V. L.; Strahl, B. D., Influence of Combinatorial Histone Modifications of Antibody and Effector Protein Recognition. *Curr Biol* **2010,** *21*, 53-58.

32. Pal, S.; Vishwanath, S. N.; Erdjument-Bromage, H.; Tempst, P.; Sif, S., Human SWI/SNF-Associated PRMT5 Methylates Histone H3 Arginine 8 and Negatively Regulates Expression of ST7 and NM23 Tumor Suppressor Genes. *Mol Cell BIol* **2004,** *24*, 9630-9645.

33. Bedford, M. T., Clarke, S. G., Protein Arginine Methylation in Mammals: Who, What, and Why. *Mol Cell* **2009,** *33*, 1-13.

Chapter III

ENHANCING THE SELECTIVITY OF THE AROMATIC CAGE OF HP1α CHROMODOMAIN FOR TRIMETHYLLYSINE 9 OF HISTONE H3

A. Background

Lysine methylation is a post-translational modification that is pervasive throughout the entire proteome, including histones.[1-3] Lysine can have up to three different methylation states including mono-, di-, or tri-methylation. Each methylation state affects DNA expression differently. For example, trimethyllysine 9 of the Histone H3 (H3 K9Me_3) is localized at heterochromatin and associated with silencing expression while H3 K9Me_1 is localized at active euchromatin.[4-6] Therefore, the proper read-out of the different methyl states by effector proteins is critical for proper gene expression.

The recognition of lysine methyl marks by effector proteins is mediated by contacts made between the methylammonium of methyllysine and an aromatic cage.[7, 8] The aromatic cage is a motif that is prevalent in all methyllysine reader domains. Importantly, this motif is not present in domains that target un-modified lysine such as the PHD (plant homeodomain) finger found in BHC80.[9] The aromatic cage is composed of two to four aromatic amino acid residues that are involved in cation-π interactions with methyllysine.[7] The cation-π interaction is due to the presence of a negative quadrapole moment resulting in negative electrostatic potential on the faces of the preorganized aromatic rings within the cage. The negative quadrupoles can, therefore, be involved in

favorable electrostatic interactions with cationic residues such as lysine.[8] N-methylated lysine also has additional polarized methyl groups, which can be involved in favorable cation-π interactions with the aromatic cage (Fig. 3.1). As a result, interactions with the aromatic cage are further stabilized with only a modest hydrophobic contribution.[7, 10]

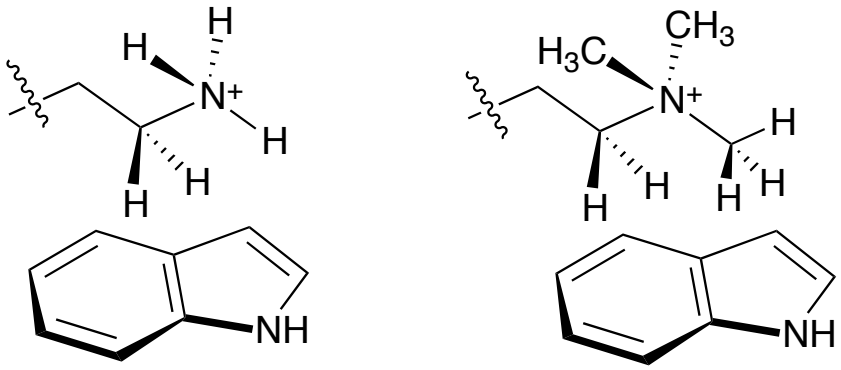

Figure 3.1. Possible interaction geometries between Trp-Lys and Trp-Lys(Me_3).[4]

Though aromatic cages are found in all methyllysine "readers", many of them vary in composition and structure to obtain the desired selectivity for mono-, di-, or trimethyllysine. For example, readers have two modes of selection for lysines with lower methylation states. First, some cages that are found in malignant brain tumor (MBT) modules form a deep groove, which binds mono- and dimethyllysine, but excludes bulkier trimethyllysine.[11, 12] Other cages such as those found in HP1 or CHD1 chromodomains[10, 13] form surface grooves, which are shallow, but wide enough to accommodate higher methylation states such di- or trimethyllysine.[14]

Additionally, many aromatic cages are supplemented with a neighboring acidic residue such as aspartate or glutamate, which is capable of forming either a direct or water-mediated H-bond to methyllysines other than KMe_3 via an NH from the methyl

lysine. [10-12, 14, 15] Li and coworkers manipulated the composition of the BPTF PHD finger aromatic cage to reverse its selectivity for di- and tri-methyllysine.[16] The wild-type PHD finger binds H3K4Me$_3$ and H3 K4Me$_2$ with K_D values of 3 μM and 6 μM respectively. However, by substituting Tyr17 of the aromatic cage for glutamate, the selectivity of the PHD finger was reversed to favor H3 K4Me$_2$ (K_D = 7 μM) over H3 K4Me$_3$ (K_D = 15 μM). Comparing the crystal structures of the wild-type and Y17E PHD finger confirmed that the change in selectivity is the result of the incorporation of a direct H-bond between Y17E and dimethyllysine 4 (Fig. 3.2). The re-engineering of the BPTF PHD finger highlighted the significant role of the H-bond in the recognition of lower methylation states of lysine.[16]

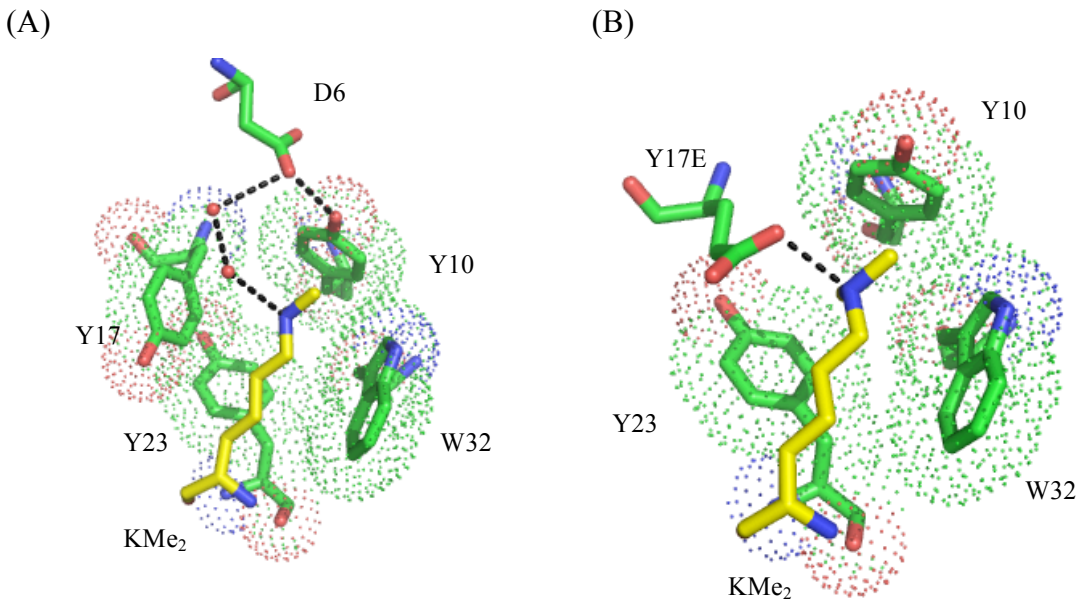

Figure 3.2. The aromatic cage of the BPTF PHD finger (green) with the dimethyllysine of H3 K4Me$_2$ (yellow). (A) shows the wild-type aromatic cage with water-mediated H-bonds to KMe$_2$ shown in red (PDB 2FSA) and (B) shows the Y17E mutant with the direct H-bond to KMe$_2$ in red (PDB 2RI7).[16] This image was generated using PyMol.

Unlike the BPTF PHD finger, the chromodomain is a surface-groove binding domain with an aromatic cage composed of two tyrosine residues, a tryptophan, and a glutamate (Fig. 3.3). This particular chromodomain shows a slight preference for H3 $K9Me_3$ over H3 $K9Me_2$.[10] In the structure containing dimethyllysine, the glutamate is involved in a water-mediated H-bond to the dimethyllysine. However, when in complex with the trimethyllysine, the water molecule is slightly displaced from the cage. Since trimethyllysine has no lone pair of electrons, it cannot be involved in a H-bond. Additionally, upon mutation of glutamate to alanine, a minimal change in binding affinity to H3 $K9Me_3$ is observed while mutating the aromatic residues to alanine disrupts binding. These results indicate that glutamate is not important for binding to trimethyllysine.[10] However, these experiments were not repeated with H3 $K9Me_2$ and it is possible that the H-bond to dimethyllysine is important for binding in addition to the cation-π interaction.

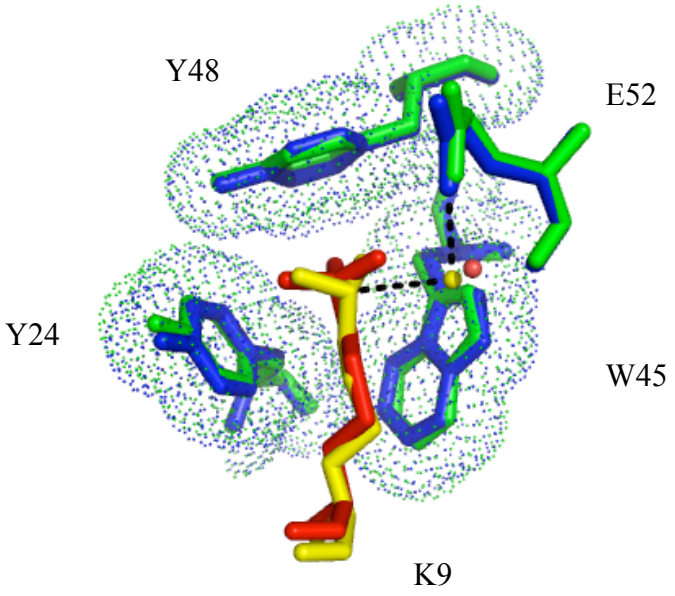

Figure 3.3. Structure of H3 K9Me$_2$ (yellow) and H3 K9Me$_3$ (red) in the aromatic cage of HP1 chromodomain (blue and green respectively) The water-mediated H-bond between Glu52 and K9Me$_2$ is depicted in black. PDB numbers for chromodomain bound to H3 K9Me$_2$ and H3 K9Me$_3$ are 1KNA and 1KNE respectively.[10] This image was generated using PyMol.

B. Significance

The purpose of this research was to further investigate the significance of Glu52 of HP1α chromodomain to understand if and how Glu52 enhances binding to H3K9Me$_2$. The glutamate was mutated to residues incapable of forming a favorable H-bond to dimethyllysine, but still able to maintain favorable interactions with trimethyllysine. By making mutations to Glu52 we gained a better understanding of how aromatic cages are selective for various lysine methylation states and we were able to enhance the selectivity of chromodomain for H3 K9Me$_3$ over H3 K9Me$_2$.

C. Results

i. System Design

The importance of the water-mediated H-bond between Glu52 and the N-H group on dimethyllysine has previously been implicated in stabilizing the binding event between HP1α chromodomain and H3 $K9Me_2$.[10] Substitution of Glu52 for residues unable to form a water mediated H-bond to lysine should weaken interactions with dimethyllysine while having a positive or limited effect on interactions with the H3 $K9Me_3$ peptide.

The first set of mutations incorporated the aromatic residues, phenylalanine and tryptophan, at position 52. Supplementing the aromatic cage with a fourth aromatic amino acid adds an additional cation-π interaction with trimethyllysine 9. Phenylalanine was also selected because it is the smallest of the aromatic residues, which reduces steric hindrance within the binding pocket of the chromodomain. Tryptophan was chosen because it is known to have the most favorable cation-π interaction with trimethyllysine compared to the smaller aromatic residues due to the larger aromatic face.[17]

The second set of mutations to Glu52 that were explored included the hydrophobic amino acids, isoleucine and valine. It was postulated that these two residues can maintain favorable van der Waals contacts with the methyl groups on trimethyllysine 9. Since these residues lack a H-bond donor or acceptor, they are unable to form the water-mediated H-bond to dimethyllysine and therefore should reduce binding to H3 $K9Me_2$ and improve selectivity for H3 $K9Me_3$.

The third set of mutations included the polar residues, aspartate and glutamine. Though aspartate is capable of forming a H-bond to water, the alkyl chain is shorter by

one methylene group as compared to glutamate. By shortening the distance between E52D and lysine 9, the H-bond network responsible for stabilizing the HP1 chromodomain-H3 $K9Me_2$ complex will be disrupted, which in turn will disfavor binding to dimethyllysine. Glutamine is structurally similar to glutamate. However, an amide is a considerably weaker H-bond acceptor than a carboxylic acid and should therefore be favored within the aromatic cage without interacting with dimethyllysine 9.

ii. Structural Characterization

The structural integrity of the six chromodomain Glu52 mutants was examined by circular dichroism. The two minima at 208 nm and 222 nm are characteristic of α-helical structure and are known to mask the weaker signal at 210 nm, which is characteristic of β-sheet structure. The maximum peak coincides with an exciton coupling peak, which is related to the orientation of aromatic sidechains such as those in the aromatic cage.[18]

The CD spectra indicate that the E52W mutant chromodomain had an overall destabilizing effect on the global structure of chromodomain and therefore no further studies were performed using this mutant (Fig. 3.4). However, the phenylalanine mutation did not perturb on the global structure of the chromodomain indicating that any observed changes in binding affinity to the E52F mutant are not due to a variation in the global structure of the protein.

The CD spectra of E52V and E52I mutants (Fig. 3.5) indicate that these point mutations had no effect on the minima at 208 nm and 222 nm, which indicates no change to the α-helix within the chromodomain and most likely a minimal change if any to the global structure of the protein. There is a loss of signal at 232 nm, which suggests a small perturbation in the aromatic cage which can be expected due to the mutation.

The final set of mutations including E52D and E52Q had the least effect on the global structure of chromodomains (Fig. 3.6). The minima at 208 nm and 222 nm are within error of the minima for the wild-type chromodomain. The exciton coupling peak at 232 nm is also consistent with the wild-type protein.

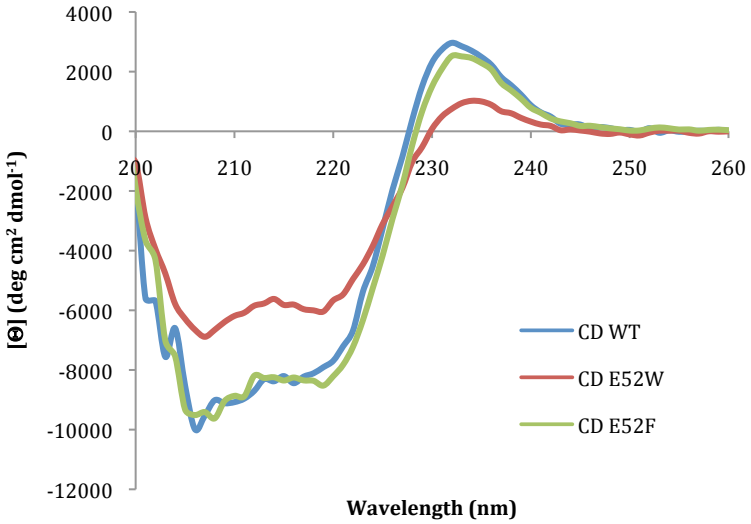

Figure 3.4. Circular dichroism spectra comparison of HP1α chromodomain to the mutants, E52W and E52F at 25 °C in 10 mM sodium phosphate pH 7.4 with 2 mM DTT. These are the averages of three runs.

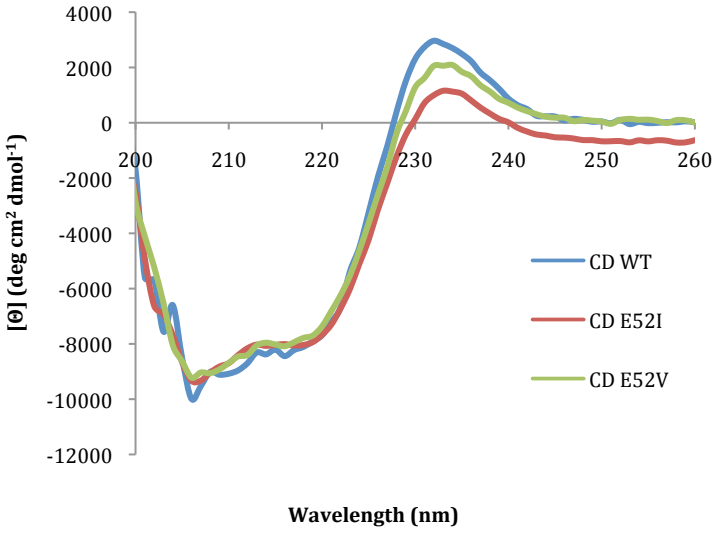

Figure 3.5. Circular dichroism spectra comparison of HP1α chromodomain (blue) to the mutants, E52I (red) and E52V (green) at 25 °C in 10 mM sodium phosphate pH 7.4 with 2 mM DTT. These are the averages of three runs.

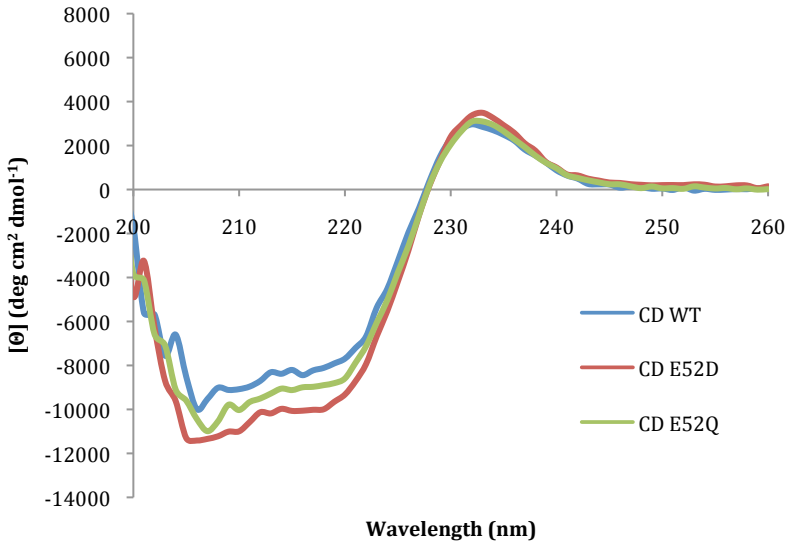

Figure 3.6. Circular dichroism spectra comparison of HP1α chromodomain (blue) to the mutants, E52D (red) and E52Q (green) at 25 °C in 10 mM sodium phosphate pH 7.4 with 2 mM DTT. These are the averages of three runs.

Wile the five chromodomain E52 mutants have a minimal effect on the protein structure, thermal denaturation experiments were nevertheless conducted to determine whether substituting Glu52 for Phe, Ile, Val, Asp, or Gln affected the stability of the protein (Fig. 3.7 through Fig. 3.9). The melting temperature was estimated by examining the inflection point of each curve (Table 3.1). Though there is some deviation from the melting temperature of the native chromodomain (47 ^{o}C), all chromodomain mutants are stable at 25 ^{o}C, which is the temperature at which all subsequent binding experiments were conducted.

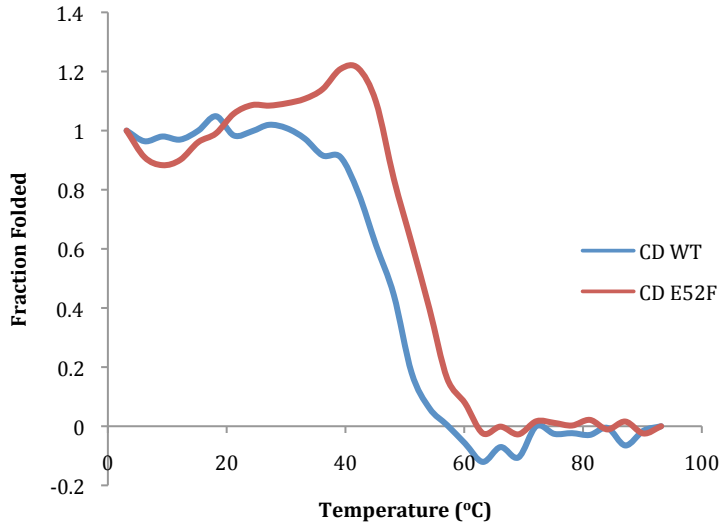

Figure 3.7. Thermal denaturation monitored by circular dichroism at 222 nm of HP1α chromodomain WT (blue) and E52F (red) in 10 mM sodium phosphate pH 7.4 and 2 mM DTT.

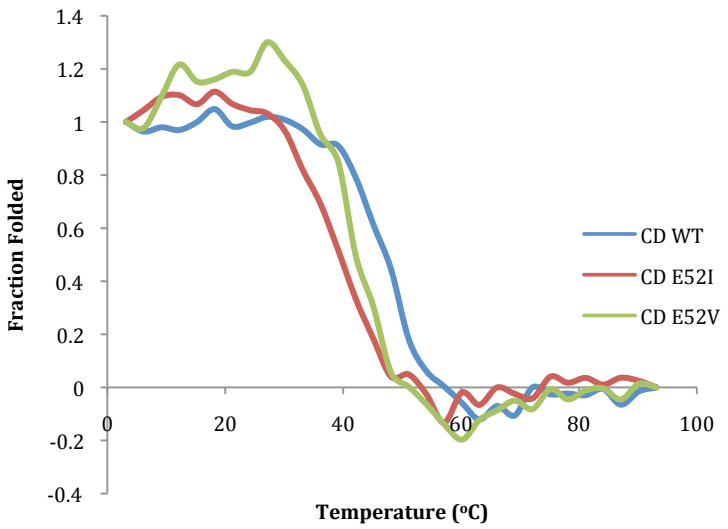

Figure 3.8. Thermal denaturation monitored by circular dichroism at 222 nm of HP1α chromodomain WT (blue), E52I (red), and E52V (green) in 10 mM sodium phosphate pH 7.4 and 2 mM DTT.

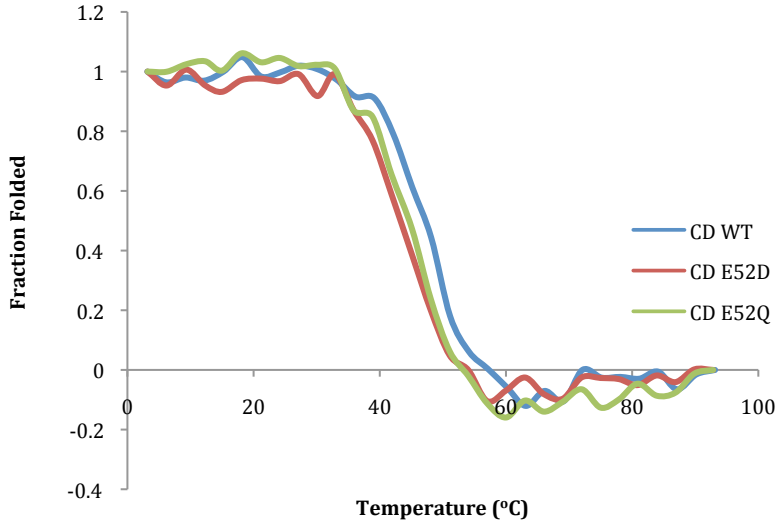

Figure 3.9. Thermal denaturation monitored by circular dichroism at 222 nm of HP1α chromodomain WT (blue), E52D (red), and E52Q (green) in 10 mM sodium phosphate pH 7.4 and 2 mM DTT.

Table 3.1. Approximate melting temperatures of chromodomain and the Glu52 mutants determined using the thermal denaturation data highlighted in Fig. 3.8 and Fig. 3.9.

	WT	**E52F**	**E52I**	**E52V**	**E52D**	**E52Q**
T_m (^{o}C)	47	53	39	42	43	43

iii. Isothermal Titration Calorimetry Studies

Isothermal titration calorimetry (ITC) was employed as an initial technique for measuring the dissociation constant and thermodynamic parameters of native HP1α chromodomain bound to H3 $K9Me_3$ (Fig. 3.10, Table 3.2). The *n* value was determined to be 1.1, which indicates a stoichiometric ration of 1:1 of chromodomain to histone tail. The binding event is enthalpically driven with a ΔH of -10.3 kcal/mol. The dissociation constant was determined to be 13±1 μM, which differs from the literature value previously published (Table 3.2). However any differences can be attributed to varying conditions as previous ITC measurements were taken at 15 ^{o}C instead of 25 ^{o}C, which has been shown to improve the dissociation constant when using monomethyllysine 9 histone tail peptide as the ligand.[19]

As will be discussed further in the following section, the dissociation constant between chromodomain and H3 $K9Me_3$ measured using fluorescence anisotropy was determined to be 17 μM (Table 3.3), similar to the constant measured by ITC. Therefore, the K_D was verified using two independent methods. Due to the large quantity of material required for the ITC experiment, anisotropy was chosen as the preferred method for all further measurements.

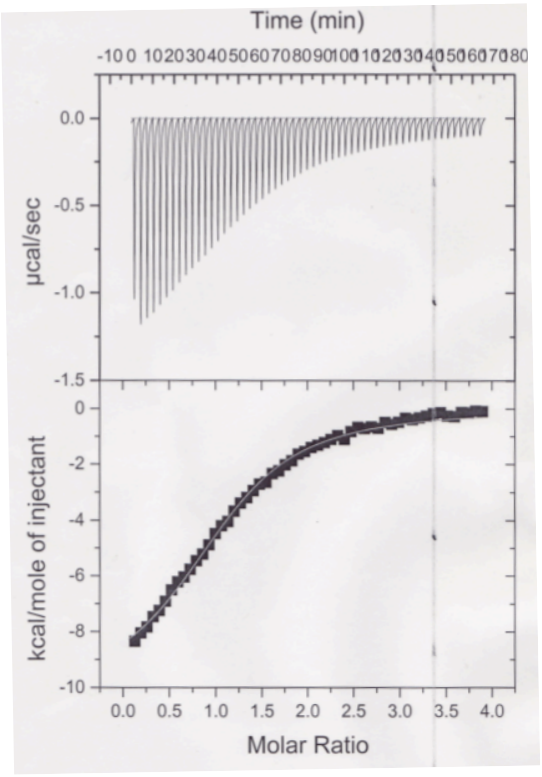

Figure 3.10. Binding HP1α chromodomain to H3 K9Me$_3$ histone tail by isothermal titration calorimetry. (Top) Raw data for peptide injections into the chromodomain (the first injection was omitted). (Bottom) Integrated heats of injection after subtracting the heat of dilution. Measurements were taken at 25 ^{o}C in 50 mM potassium phosphate pH 8.0, 25 mM NaCl, 2mM DTT.

Table 3.2. Summary of thermodynamic parameters from the ITC experiment in Fig. 3.10.

	N	K_D (μM)	ΔH (kcal/mol)	TΔS (kcal/mol)	ΔG (kcal/mol)
Literature[20]	0.99	2.5 ± 0.1	-9.83	-2.46	-7.36
Experimental[20]	1.1	13 ± 1	-10.3	-3.63	-6.7

iv. Binding Studies

Initially, fluorescence anisotropy experiments were performed using histone peptides labeled at the N-terminus with 5(6)-TAMRA. This fluorophore was chosen for its high quantum yield and its resistance to photobleaching as compared to 5(6)-FAM. Additionally, a single-cell Cary Eclipse Fluorescence Spectrophotometer from Varian was used. Several repetitions of anisotropy experiments with wild-type HP1α

chromodomain and H3 K9Me$_3$ yielded different dissociation constants with large error (Fig. 3.11).

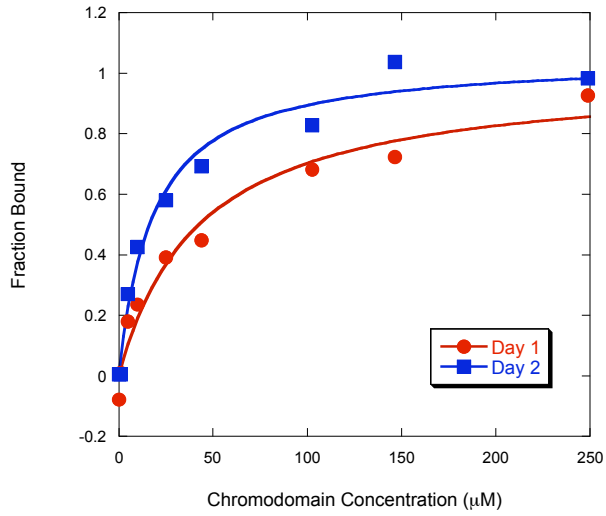

Figure 3.11. Fluorescence anisotropy binding experiments of 100 nM 5(6)-TAMRA H3 K9Me$_3$ histone tail with wild-type chromodomain from two different days. The experiments were performed in 50 mM potassium phosphate buffer pH 8.0, 25 mM NaCl, and 4 mM DTT at 25 °C. Each curve is an average of 2 runs. On day 1 the K_D was 42 ± 15 μM and the R^2 was 0.971. On day 2 the K_D was 17 ± 4 μM and the R^2 was 0.987.

A fluorescence emission experiment was used to determine if 5(6)-TAMRA was interacting with HP1α chromodomain. An increase in emission is indicative of a non-specific interaction between a fluorophore and the receptor. As shown in Fig. 3.12 fluorescence emission increased significantly with increased chromodomain concentration. A similar experiment was repeated using 5(6)-FAM at the fluorophore to determine whether this would be a viable substitute. Since no significant change in fluorescence emission was observed, 5(6)-FAM was chosen as the fluorophore for future studies. Additionally, a Polarstar plate reader was used for remaining studies. The concentration of peptide was also increased from 100 nM to 1 μM because the

dissociation constants were determined to be higher than 10 μM. The ideal concentration for a labeled ligand in a binding assay is at least ten-fold lower than the dissociation constant.

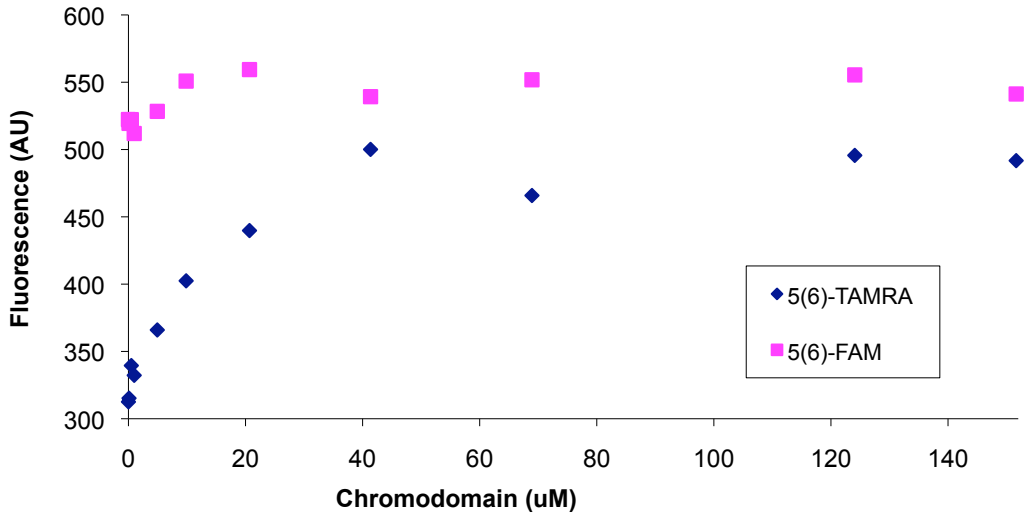

Figure 3.12. Fluorescence emission of 100 nM H3 K9Me$_3$ labeled with either 5(6)-TAMRA or 5(6)-FAM and increasing concentrations of HP1α Chromodomian in 50 mM potassium phosphate buffer pH 8.0, 25 mM NaCl, and 4 mM DTT at 25 °C. Each curve is an average of 2 runs.

The dissociation constants between the chromodomain and di- and tri-methyllysine 9 Histone H3 tail were measured using the new experimental anisotropy conditions (Fig. 3.13). The data show that the K_D values are nearly identical for both the di and tri-methylated peptides (K_D=20 μM and 17 μM respectively) thus demonstrating the lack of selectivity that chromodomain has for the higher methylation states.

Chromodomain E52 mutations involving the three hydrophobic residues, Phe (Fig. 3.14), Ile (Fig. 3.15), and Val (Fig. 3.16) had a two to three-fold decrease in binding affinity to both dimethyl and trimethyllysine histone tails (Table 3.3). It is possible that

substituting glutamate with residues that are dissimilar in polarity may have distorted the aromatic cage or disrupted any electrostatic interactions with lysine 9. Substitution of glutamate with bulkier residues such as phenylalanine may have also resulted in a steric clash with other neighboring amino acids that can distort the binding pocket. Additionally, E52 is a solvent-exposed acidic residue. Substituting such a residue with one that is hydrophobic results in an unfavorable solvation energy, which may also destabilize the aromatic cage. This distortion is consistent with the circular dichroism collected for E52I and E52V in which the exiton coupling peak at 232 nm, which is known to be influenced by the orientation of neighboring aromatic residues, was weakened for both mutants.[21]

Chromodomain E52D had a minimal effect on binding affinity to H3 K9Me$_2$ with a K_D of 19 μM (Fig. 3.17), which demonstrates that the aspartate may still be able to maintain the water-mediated H-bond to the dimethyllysine. However, binding to the trimethyllysine is improved by a factor of two with a K_D of 9 μM. Aspartate is a shorter amino acid than glutamate by one methylene. Therefore, the aromatic cage with aspartate may have a reduced steric clash with the third methyl group of trimethyllysine.

Interestingly, Chromodomain E52Q is a 2.5-fold weaker dissociation constant with H3 K9Me$_2$ (52 μM) compared to the native protein while the dissociation constant with H3 K9Me$_3$ (15 μM) is unaffected by the mutation (Fig. 3.18). The loss of the H-bond to the dimethyllysine can account for the difference in binding affinity. The similar conformation between glutamine and glutamate explains the comparable binding affinity to H3 K9Me$_3$. This observation supports the argument that the water-mediated H-bond does play a role in chromodomain binding to H3 K9Me$_2$.

Table 3.3. Dissociation constants (μM) of *Drosophila* chromodomain and H3 $K9Me_3$ and the mutants using the data from Fig. 3.10 through Fig. 3.13. The R^2 values were calculated using Kaleidagraph and are given in parenthesis. The ΔG (kcal/mol) is given in brackets and was calculated using the following equation: $\Delta G^o = -RT\ln(K_D)$. The data was measured in 50 mM potassium phosphate buffer (pH 8), 25 mM NaCl, with 4 mM DTT at 25 °C.

Chromodomain	H3 $K9Me_2$	H3 $K9Me_3$
Wild-Type	20 ± 4 (0.990) [-6.4 ± 0.1]	17 ± 3 (0.994) [-6.5 ± 0.1]
E52F	52 ± 5 (0.998) [-5.8 ± 0.1]	40 ± 9 (0.991) [-6.0 ± 0.1]
E52I	83 ± 20 (0.992) [-5.6 ± 0.1]	47 ± 8 (0.996) [-5.9 ± 0.1]
E52V	67 ± 11 (0.997) [-5.7 ± 0.1]	39 ± 9 (0.992) [-6.0 ± 0.1]
E52D	19 ± 2 (0.995) [-6.4 ± 0.1]	9 ± 1 (0.994) [-6.9 ± 1]
E52Q	52 ± 7 (0.995) [-5.8 ± 0.1]	15 ± 3 (0.990) [-6.6 ± 0.1]

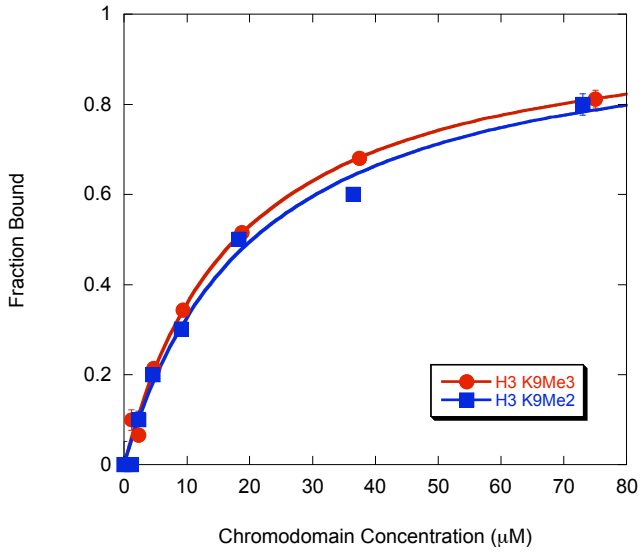

Figure 3.13. Fluorescence anisotropy binding experiments of 1 μM 5(6)-FAM H3 $K9Me_{2/3}$ histone tail with wild-type chromodomain. The experiments were performed in 50 mM potassium phosphate buffer pH 8.0, 25 mM NaCl, and 4 mM DTT at 25 °C. Each curve is an average of 3 runs.

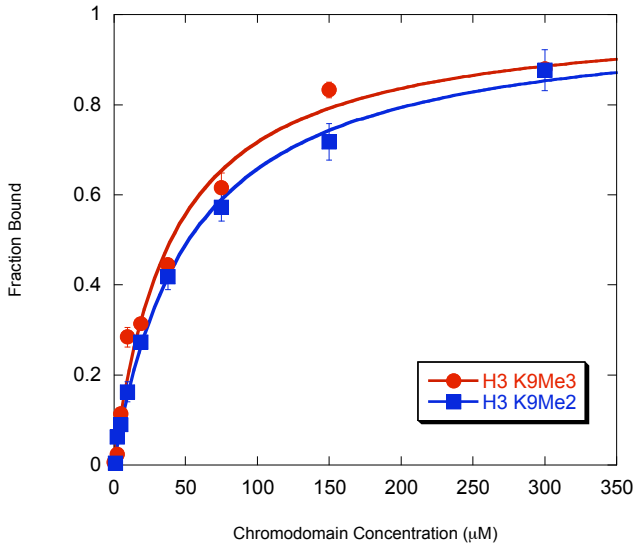

Figure 3.14. Fluorescence anisotropy binding experiments of 1 μM 5(6)-FAM H3 K9Me$_{2/3}$ histone tail with E52F chromodomain. The experiments were performed in 50 mM potassium phosphate buffer pH 8.0, 25 mM NaCl, and 4 mM DTT at 25 °C. Each curve is an average of 3 runs.

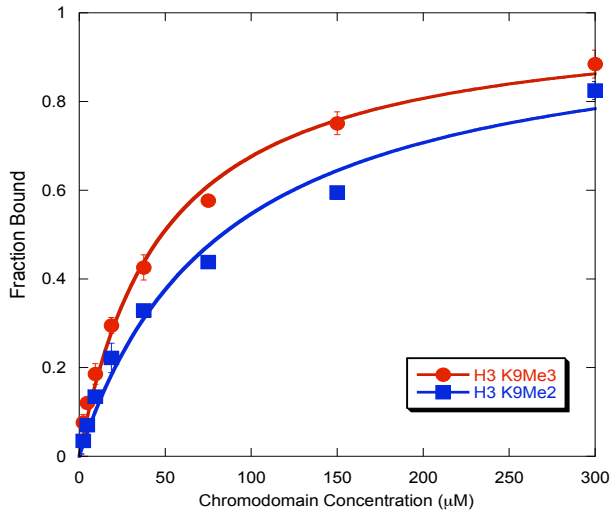

Figure 3.15. Fluorescence anisotropy binding experiments of 1 μM 5(6)-FAM H3 K9Me$_{2/3}$ histone tail with E52I chromodomain. The experiments were performed in 50 mM potassium phosphate buffer pH 8.0, 25 mM NaCl, and 4 mM DTT at 25 °C. Each curve is an average of 3 runs.

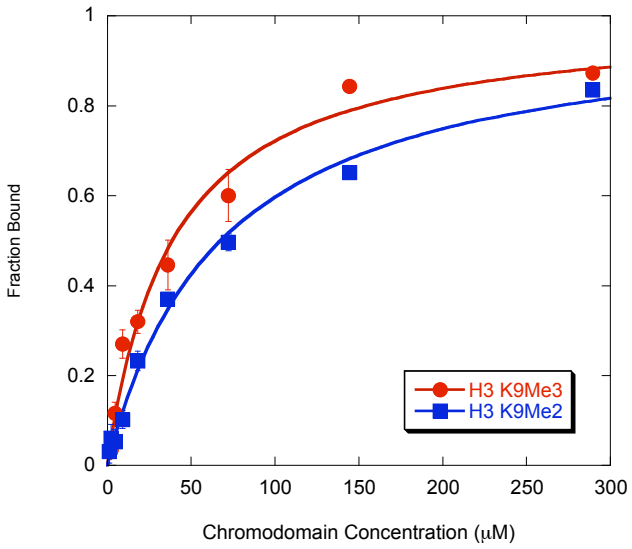

Figure 3.16. Fluorescence anisotropy binding experiments of 1 μM 5(6)-FAM H3 K9Me$_{2/3}$ histone tail with E52V chromodomain. The experiments were performed in 50 mM potassium phosphate buffer pH 8.0, 25 mM NaCl, and 4 mM DTT at 25 °C. Each curve is an average of 3 runs.

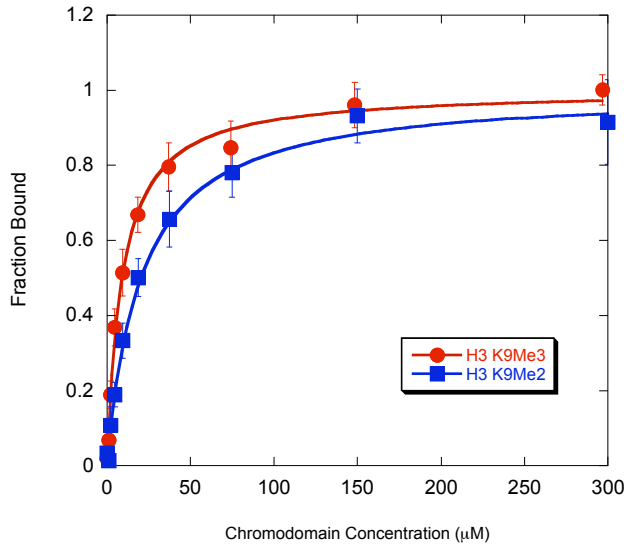

Figure 3.17. Fluorescence anisotropy binding experiments of 1 μM5(6)-FAM H3 K9Me$_{2/3}$ histone tail with E52D chromodomain. The experiments were performed in 50 mM potassium phosphate buffer pH 8.0, 25 mM NaCl, and 4 mM DTT at 25 °C. Each curve is an average of 3 runs.

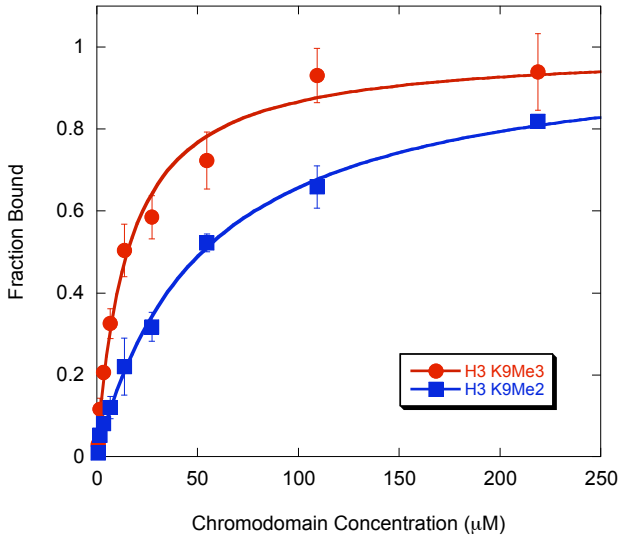

Figure 3.18. Fluorescence anisotropy binding experiments of 1 μM 5(6)-FAM H3 $K9Me_{2/3}$ histone tail with E52Q chromodomain. Experiments were performed in 50 mM potassium phosphate buffer pH 8.0, 25 mM NaCl, and 4 mM DTT at 25 °C. Each curve is an average of 3 runs.

D. Discussion

The aromatic cage within the HP1α chromodomain is critical for recognition of methyllysine 9 on the Histone H3 tail and has been shown to have only a small preference for trimethyllysine. The purpose of this project was to investigate how selectivity is maintained by the aromatic cage and to improve the selectivity of HP1α chromodomain for H3 $K9Me_3$ over H3 $K9Me_2$. This goal was to be accomplished by substituting E52, which forms a water-mediated H-bond to the lone electron pair on dimethyllysine, with residues that would form favorable contacts with trimethyllysine while removing the H-bond to dimethyllysine.

The E52F mutation was incorporated to explore the effects of adding a forth cation-π interaction while E52V and E52I were incorporated to explore hydrophobic

contacts with the methyl groups on lysine 9. The E52F and E52V mutations weakened binding by at least two-fold while showing no improvement in selectivity. The E52I mutation improved selectivity by two-fold, but the binding to both di- and tri-methylated peptides were also significantly weakened. The negative charge and conformation of glutamate may be key to stabilizing the recognition of the aromatic cage for both di- and trimethyllysine. Without this charge no H-bond network can be formed to dimethyllysine and no electrostatic interactions can occur with trimethyllysine.

Substituting glutamate for the two polar residues, glutamine and aspartate, both improved selectivity for H3 K9Me$_3$. Chromodomain E52D maintained the same binding affinity to H3 K9Me$_2$ while improving affinity to H3 K9Me$_3$ by two-fold (K_D=9 μM). It is likely that the stabilizing water-mediated H-bond is maintained between E52D and K9Me$_2$. However, the two-fold enhancement of binding to H3 K9Me$_3$ may be attributed to the shorter alkyl chain of aspartate, which provides additional space within the aromatic cage for the trimethyllysine to fit into.

Chromodomain E52Q had a 2.5 fold weaker binding affinity to H3 K9Me$_2$ (K_D=52 μM) and maintained the same binding affinity to H3 K9Me$_3$ (K_D=15 μM). The significant loss in binding affinity to the dimethylated histone peptide is likely to be due to the weakened H-bond between dimethyllysine and glutamine. Glutamine, though a polar amino acid, is not a strong H-bond acceptor compared to glutamate and, therefore, cannot form the water-mediated H-bond to dimethyllysine. This observation is consistent with the results from the hydrophobic mutations, which displayed a weakened binding affinity to both methylated peptides. However, the unaltered binding affinity to the trimethyllysine implies that the negative charge of glutamate is not the major driving

force for recognition. This observation was surprising because glutamate is able to form a favorable electrostatic interaction with the positively charged trimethyllysine, which was expected to be important for recognition. Rather, the similar structures of glutamine and glutamate can be important for maintaining the integrity of the aromatic cage structure and the polarity of glutamine may be important for favorable solvation energy.

The aromatic cage in a methyllysine recognition domain is important for maintaining selectivity for specific methylation states. Several factors that are suspected to contribute to selectivity include the depth of the binding pocket and the composition of the aromatic cage. While there appears to be some trends in binding pocket composition, for example more aromatic residues in the cage aids in the recognition of higher methylation states, the trends are not always consistent and not well understood. Understanding the factors that contribute to this selectivity is critical for understanding the readout of the Histone Code. From these studies it has been demonstrated that introducing glutamine, which is a neutral polar residue with a structure similar to glutamate, is a successful method for enhancing the specificity of chromodomain for trimethyllysine 9 of the Histone H3 tail.

E. Experimental

i. Protein Expression and Purification

The Khorasanizadeh Lab at the University of Virginia supplied the PET11a plasmid containing the coding region of *Drosophila* HP1α chromodomain (residues 17-76) with an N-terminal 6-Histidine tag.[10] Mutagenesis was carried out as described below. The total reaction volumes were 50 μL with 1 μL DNA plasmid (~30 ng/μL), 1 μL dimethyl sulfoxide (DMSO), 1 μL of forward and reverse primers (0.01 mmol), 2.5

μL dNTP mix (10 mM), 5 μL 5X PFU buffer, 36.5 μL dH_2O, and 2 μL PfuUltra hotstart DNA polymerase (Strategene) was added last. The thermocycler settings are described in Table 3.4 and primers are given in Table 3.5. The sequences were confirmed by next-generation sequencing at the UNC core facility. The DNA was expressed and isolated from DH5α *E. coli* cells using a Fermentas Genejet Plasmid miniprep kit. *E. coli* BL21 (DE3) gold cells were transformed with the plasmid and were grown on ampicillin-containing plates at 37°C over night. A colony was selected and grown in 100 mL LB with 50 mg/mL Amp overnight at 37°C. The next morning 15 mL of the starter culture were added 1.5 L LB media with 50 mg/L ampicillin at 37 °C. At A_{600}=0.5-0.7, 0.1 mM IPTG was added to the cultures and the temperature was reduced to 18 °C overnight. The cells were harvested by centrifugation for 20 mins at 4500 rpm. The cells were resuspended in approximately 30 mL NiA buffer (5 mM imidazole, 50 mM potassium phosphate, pH 7.4, 150 mM NaCl, 0.01% sodium azide) and stored at -80 °C.

The cells were lysed and purified as described in Chapter II. Representative figures of the wild-type chromodomain after purification are shown in Fig. 3.19A. The protein was then dialyzed in 50 mM potassium phosphate pH 8.0, 25 mM NaCl. If purity of the chromodomain proteins were less than 95% then the proteins were subsequently purified by size exclusion using an S75 superdex FPLC column at 4 °C. The first chromodomain purified showed two proteins after FPLC purification (Fig. 3.19B). There is a naturally occurring cysteine within HP1α chromodomain. A sample of the purified protein was treated with reducing and denaturing agents to confirm that the impurity was due to dimerization, which can disrupted using DTT as described in the anisotropy experiments (Fig. 3.19C).

(A)

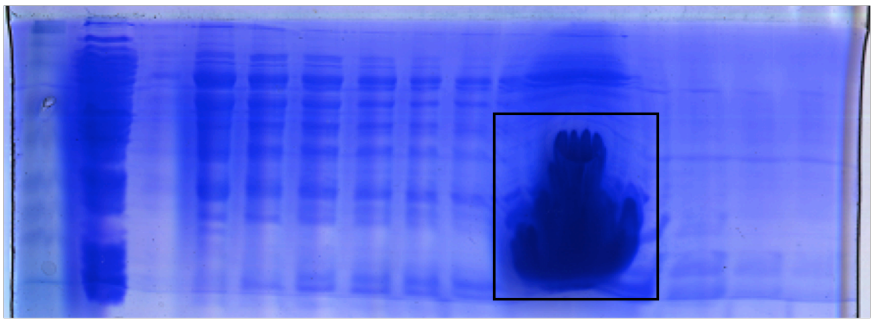

(B)

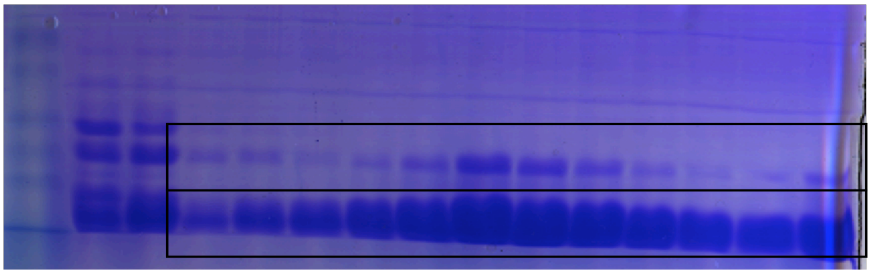

(C)

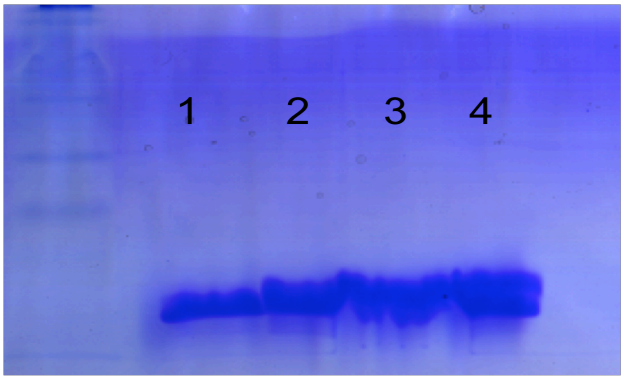

Figure 3.19. (A) Purity of HP1α chromodomain on a 15% SDS-PAGE after purification by Ni affinity chromatography. (B) Purity of HP1α chromodomain on a 15% SDS-PAGE after purification by size exclusion following Ni affinity. (C) The disulfide bonds were reduced by adding the following denaturants to a small sample of purified HP1α chromodomain for SDS-PAGE analysis: (1) 2 mM DTT, (2) 100 mM DTT, (3) 1% Triton X-100, and (4) 4 mM urea.

Table 3.4. Thermocycler conditions for Site-Directed Mutagenesis.

Temperature (°C)	Time	Cycles
Hot start: 95	30 sec	1
Melt: 95	1 min	
Anneal: 60	1 min	5
Extend: 68	13 min	
Melt: 95	1 min	
Anneal: 55	1 min	16
Extend: 68	10 min	
Find extend: 72	5 min	1
Pause: 4	hold	

Table 3.5. The forward primers used for mutagenesis. The site of mutation is in red.

Mutant	Primer Sequence
E52F	GGC TAT CCC GAA ACT TTT AAC ACG TGG GAG CCG
E52W	GGC TAT CCC GAA ACT TGG AAC ACG TGG GAG CCG
E52V	GGC TAT CCC GAA ACT GTG AAC ACG TGG GAG CCG
E52L	GGC TAT CCC GAA ACT CTG AAC ACG TGG GAG CCG
E52I	GGC TAT CCC GAA ACT ATC AAC ACG TGG GAG CCG
E52D	GC TAT CCC GAA ACT GAT AAC ACG TGG GAG C
E52Q	GC TAT CCC GAA ACT CAG AAC ACG TGG GAG C

ii. Peptide Synthesis

Histone tails (residues 1-15 of the H3 tail with a C-terminal tyrosine) were synthesized using automated solid phase peptide synthesis with a Thuramed tetras synthesizer on a 0.06 mmol scale. Fmoc protected amino acids were used with a Wang resin from Peptides International, Inc. Amino acid residues were activated with HBTU (O-benzotriazole-N,N,N',N',-tetramethyluronium hexafluorophosphate) and HOBT (N-hydroxybenzotriazole) with DIPEA (diisopropylethylamine) in DMF (N,N-dimethylformamide). Amino acids were deprotected twice with 2% DBU (1,8-diazabicyclo[5.4.0]undec-7-ene) and 2% piperidine in DMF for 15 mins each step. Each amino acid was coupled on double cycles of 30 mins each to improve coupling. Fmoc protected dimethyllysine was coupled at position 9, which was methylated before the final Fmoc-deprotection of the N-terminal alanine with 10.8 mL MTBD and 37.4 mL iodomethane in 5mL DMF and bubbled with N_2 for 4-5 hrs. The final Fmoc was cleaved with 2 washes with 20% piperidine for 15 mins each and 5(6)-carboxyfluorescein (Anaspec) was coupled using 2 equivalents of the fluorophore, HOBt, HBTU, and DIPEA and allowed to react overnight under nitrogen gas. Cleavage of the peptides from the resin was performed in 95% trifluoroacetic acid (TFA), 2.5% H_2O, 2.5% triisopropylsilane (TIPS) for three hrs. The TFA was evaporated off by blowing the reaction with nitrogen. Cold diethyl ether was used to precipitate the product. The product was extracted with deionized water and subsequently lyophilized to a powder for HPLC.

Peptides were purified by reversed-phase HPLC. A waters semi-preparative HPLC system with an Atlantis Prep OBD dC-18 semi-preparative column was used for

separation with a gradient of 0% to 100% solvent B over 60 mins with solvent A (95:5 water:acetonitrile, 0.1% TFA) and solvent B (95:5 acetonitrile:water, 0.1% TFA). Peptides were then lyophilized and the molecular weight of the peptide was confirmed by ESI-TOF mass spectrometry (Table 3.6).

iii. Circular Dichroism

CD measurements were performed on an Aviv 62DS Circular Dichroism Spectrometer. CD data was obtained for the chromodomain at 33.3 μM concentration in 10 mM Na_2HPO_4, pH 7.4, 2 mM DTT. Wavelength scans were performed in triplicate and averaged. Scans were performed at 25 ^{o}C from 260-185 nm. All scans were corrected by subtracting the spectrum of the buffer used in the experiment and the signal was converted to Mean Residue Ellipticity (MRE) using Eq. 3.1. Where signal refers to circular dichroism signal, ℓ is path length in cm, c is concentration in M, and r is the number of amino acid residues.

$$\Theta = \frac{signal}{10 \cdot \ell \cdot c} \cdot \frac{1}{r} \qquad \text{Eq. 3.1}$$

3Thermal denaturation experiments were preformed using the same buffer and concentrations as described above and measurements were taken between 275 and 366 K. The melting curves were normalized to show the fraction folded using Eq. 3.2 where Θ_O is MRE, Θ_D is the MRE for the fully denatured protein, and Θ_F is MRE for the fully folded protein

$$Fraction\ Folded = \frac{\Theta_O - \Theta_D}{\Theta_F - \Theta_D} \qquad \text{Eq. 3.2}$$

iv. Anisotropy

Binding assays were performed using a POLARstar Omega microplate reader using untreated 96 half area flat bottom plates. Chromodomain was prepared by making serial 1:2 dilutions in the 0 to 600 μM range and mixed by pipetting 15 times while avoiding adding any air bubbles. The samples were centrifuged for 1 minute at 4000 rpm to draw any particulates to the bottom and removed air bubbles. A 2 μM stock of H3 $K9Me_{2/3}$ was prepared (ε_{492}=78,000 $cm^{=1}M^{-1}$) in 50 mM potassium phosphate buffer, pH 8, 25 mM NaCl, 8mM DTT. The chromodomain and peptide were mixed in the microplate with 50 μL of chromodomain and 50 μL of peptide. This reduced the concentration of peptide, DTT, and chromodomain by half (1 μM peptide, 4 mM DTT, 0 μM to 300 μM chromodomain). The samples were mixed by pipetting them ten times while introducing as few air bubbles as possible. The samples were centrifuged for 1 minute at 4000 rpm to remove any air bubbles and allowed to reach equilibrium for 30 mins prior to analysis at 25 ^{o}C. Measurements were taken with an excitation wavelength of 485 nm and an emission wavelength at 520 nm. The data was fitted using Eq. 2.3. The fraction of chromodomain bound was calculated using Equation 2.4. The data was re-plotted as fraction bound as a function of chromodomain concentration to give the final data as shown in Fig. 3.6. The binding energy (ΔG^{o}) was calculated using equation 3.3:

$$\Delta G^{o} = -RT\ln(K_D) \qquad \text{Eq. 3.3}$$

Table 3.6. Mass spectrometry data for the peptides synthesized for this study.

Peptide	Expected Mass (Da)	Experimental Mass (Da)
H3 K9Me$_2$	2109.0	2110.0
H3 K9Me$_3$	2124.1	2124.7

v. Isothermal Titration Calorimetry

ITC was performed using a Micro Cal VP-ITC. The dialysis buffer (50 mM potassium phosphate pH 8, 25 mM NaCl) that had been used to dialyze chromodomain was also used for ITC with 2 mM DTT subsequently added. Desalted and lyophilized H3 K9Me$_3$ peptide was dissolved in the same buffer, also with 2 mM DTT to obtain a concentration of 947 μM histone tail peptide and degassed for 10 mins. Measurements were made using 55 automatic injections of 5 μL peptide into 50 mM chromodomain at 25 ^{o}C with 3 mins between injections. The heat of dilution was measured by titrating peptide into buffer and subtracted from the raw data. The curves were analyzed with the Micro Cal software using a non-linear least squares fitting.

References

1. Martens, J. H. A.; O'Sullivan, R. J.; Braunschweig, U.; Opravil, S.; Radolf, M.; Stainlein, P.; Jenuwein, T., The Profile of Repeat-Associated Histone Lysine Methylation States in the Mouse Epigenome. *EMBO J* **2005,** *24*, 800-812.

2. Zhang, K.; Tang, H.; Huang, L.; Blankenship, J. W.; Jones, P. R.; Xiang, F.; Yau, P. M.; Burlingame, A. L., fication of Acetylation and Methylation Sites of Histone H3 from Chicken Erythrocytes by High-Accuracy Matrix-Assisted Laser Desorption Ionization–Time-of-Flight, Matrix-Assisted Laser Desorption Ionization–Postsource Decay, and Nanoelectrospray Ionization Tandem Mass Spectrometry. *Anal Biochem* **2002,** *306*, 259-269.

3. Peters, A. H.; Kubicek, S.; Mechtler, K.; O'Sullivan, R. J.; Derijck, A. A. H. A.; Perez-Burgos, L.; Kohimaler, A.; Opravil, S.; Tachibana, M.; Shinkal, Y.; Martens, J. H. A.; Jenuwein, T., Partitioning and Plasticity of Repressive Histone Methylation States in Mammalian Chromatin. *Mol Cell* **2003,** *12*, 1577-1589.

4. Nakayama, J.-I.; Rice, J. C.; Strahl, B. D.; Allis, C. D.; Grewal, S. I. S., Role of Histone H3 Lysine 9 Methylation in Epigenetic Control of Heterochromatin Assembly. *Science* **2001,** *292*, 110-113.

5. Peters, A. H.; Mermoud, J. E.; O'Carroll, D.; Pagani, M.; Schweizer, D.; Brockdorff, N.; Jenuwein, T., Histone H3 Lysine 9 Methylation is an Epigenetic Imprint of Facultative Heterochromatin. *Nat Genet* **2001,** *30*, 77-80.

6. Noma, K.-i.; Allis, C. D.; Grewal, S. I. S., Transitions in Distinct Histone H3 Methylation Patterns at the Heterochromatin Domain Boundaries. *Science* **2001,** *293*, 1150-1155.

7. Hughes, R. M.; Wiggins, K. R.; Khorasanizadeh, S.; Waters, M. L., Recognition of Trimethyllysine by a Chromodomain is not Driven by the Hydrophobic Effect. *Proc Natl Acad Sci* **2007,** *104*, 11184-11188.

8. Ma, J. C.; Dougherty, D. A., The Cation-π Interaction. *Chem Rev* **1997,** *97*, 1303.

9. Lan, F.; Collins, R. E.; Cegli, R. D.; Alpatov, R.; Horton, J. R.; Shi, X.; Gozani, O.; Cheng, X.; Shi, Y., Recognition of Unmethylated Histone H3 Lysine 4 Links BHC80 to LSD1-Mediated Gene Repression. *Nature* **2007,** *448*, 718-722.

10. Jacobs, S. A.; Khorasanizadeh, S., Structure of HP1 Chromodomain Bound to a Lysine 9-Methylated Histone H3 Tail. *Science* **2002,** *295*, 2080-2083.

11. Guo, Y.; Nady, N.; Qi, C.; Allali-Hassani, A.; Zhu, H.; Pan, P.; Adams-Cioaba, M. A.; Amaya, M. F.; Dong, A.; Vedadi, M.; Schapira, M.; Read, R. J.; Arrowsmith, C.

H.; Min, J., Methylation-State-Specific Recognition of Histones by the MBT Repeat Protein L3MBTL2. *Nucl Acids Res* **2009,** *37*, 2204-2210.

12. Botuyan, M. V.; Lee, J.; Ward, I. M.; Kim, J. E.; Thompson, J. R.; Chem, J.; Mer, G., Structural Basis for the Methylation Sate-Specific Recognition of Histone H4-K20 by 53BP1 and Crb2 in DNA Repair. *Cell* **2006,** *127* (1361-1373).

13. Flanagan, J. F.; Mi, L. Z.; Chruszcz, M.; Cymborowski, M.; Clines, K. L.; Kim, Y.; Minor, W.; Rastinejad, F.; Khorasanizadeh, S., Double Chromodomains Cooperate to Recognize the Methylated Histone H3 Tail. *Nature* **2005,** *438*, 1181-1185.

14. Taverna, S. D.; Li, H.; Ruthenburg, A. J.; Allis, C. D.; Patel, D. J., How Chromatin-Binding Modules Interpret Histone Modifications: Lessons from Professional Pocket Pickers. *Nat Struct Mol Biol* **2007,** *14*, 1025-1040.

15. Li, H.; Llin, S.; Wang, W.; Duncan, E. M.; Wysocka, J.; Allis, C. D.; Patel, D. J., Molecular Basis for Site-Specific Read-Out of Histone H3K4me3 by the BPTF PHD Finger of NURF. *Nature* **2006,** *442*, 91-95.

16. Li, H.; Fischle, W.; Wang, W.; Duncan, E. M.; Liang, L.; Murakami-Ishibe, S.; Allis, C. D.; Patel, D. J., Structural Basis for Lower Lysine Methylation Sate-Specific Readout by MBT Repeats of L3MBTL1 and an Engineered PHD Finger. *Mol Cell* **2007,** *28*, 677-691.

17. Gallivan, J. P.; Dougherty, D. A., Cation-π Interactions in Structural Biology. *Proc Natl Acad Sci* **1999,** *96*, 9459-9464.

18. Greenfield, N. J., Methods to Estimate the Conformation of Proteins and Polypeptides from Circular Dichroism Data. *Anal Biochem* **1996,** *235*, 1-10.

19. Jacobs, S. A.; Taverna, S. D.; Zhang, Y.; Briggs, S. D.; Li, J.; Eissenberg, J. C.; Allis, C. D.; Khorasanizadeh, S., Specificity of the HP1 Chromo Domain for the Methylated N-Terminus of Histone H3 *EMBO J* **2001,** *20*, 5232-5241.

20. Nielson, R. R.; Nietlispach, D.; Mott, H. R.; Callaghan, J.; Bannister, A.; Kousarides, T.; Murzin, A. G.; Murzina, N. V.; Laue, E. D., Stucture of the HP1 Chromodomain Bound to Histone H3 Methylated at Lysine9. *Nature* **2002,** *416*, 103-107.

21. Kelly, S. M.; Price, N. C., The Use of Circular Dichroism in the Investigation of Protein Structure and Function. *Curr Protein Pept Sci* **2000,** *1*, 349-38

Chapter IV

β-SHEET INTERACTIONS BETWEEN HP1α CHROMODOMAIN AND TRIMETHYLLYSINE 9 OF HISTONE H3

A. Background

i. Read-out of Trimethyllysine 9 of Histone H3 by HP1α chromodomain

Methylation of the Histone H3 protein at various lysine residues is among the most important and complex modifications.[1] For example, trimethyllysine 9 of histone H3 (H3 K9Me_3) is a modification that recruits the effector protein, heterochromatin protein 1 (HP1) via the highly conserved chromodomain.[2-5] Once recruited to the nucleosome, HP1 is believed to prevent gene expression by condensing DNA into tightly packed and genetically silent heterochromatin.[6]

However, there are a wide variety of other effector proteins containing chromodomains that recognize methyllysine marks and they can have opposing effects on gene expression. The mode of sequence selectivity of effector proteins for different methylated lysine residues has been difficult to elucidate due to the high sequence homology between different chromodomains and the sequences surrounding methyllysines on histone tails (Fig. 4.1).[7]

(A)

(B)

N-terminus-ARTKQTARK(Me_3)STGGKAPRKQLATKAARK(Me_3)SAPATGGVK…

Figure 4.1. (A) Sequence alignment of chromodomains from *Drosophila* (Dm) HP1α and polycomb proteins and the corresponding human (Hs) isoforms. The conserved residues are highlighted in black and the similar residues are highlighted in grey. The aromatic residues that make up the cage are highlighted in yellow. Ala25 and Asp62 of HP1α chromodomain, which make up the binding region, and the corresponding residues in the isoforms are highlighted in red (NCBI Accession numbers in the order that each sequence is listed are: AAF52618, CAG33047, NP_009207, CAG33699, NP_524199, CAA54839, AAH14967, NP_055107, CAQ07275, NP_065700). (B) Residues 1-36 of the Histone H3 tail. The residues surrounding Lys9 and Lys27 are highlighted in yellow and green respectively.

Crystallography and NMR studies of the HP1α chromodomain bound to the H3 K9Me_3 tail have been used to understand the nature of the interactions between the chromodomain and trimethylated histone tail.[2] The binding of H3 K9Me_3 by the chromodomain is mediated by two modes of recognition. The first is the cation-π interaction between the trimethyllysine 9 of the Histone H3 tail and a three-member aromatic cage of the chromodomain.[8] The second is the formation of an anti-parallel three-stranded β-sheet motif with four amino acids surrounding Lysine 9 of the Histone H3 tail (TARK^{9}S) as the central strand and two β-strands of the chromodomain as the edge strands (Figure 4.2). Van der Waals contacts between side chains and H-bonds between the amide backbones of the chromodomain and histone tail are key for selectivity and for stabilizing the complex.[7, 9]

(A)

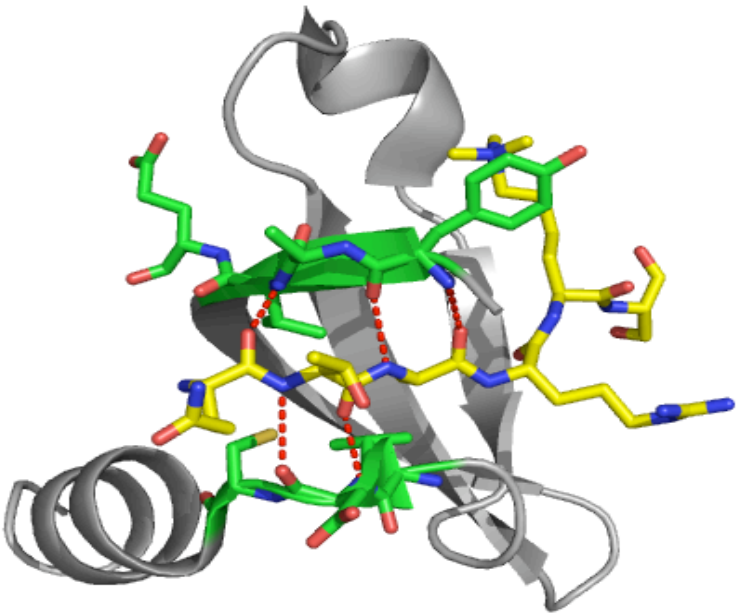

(B)

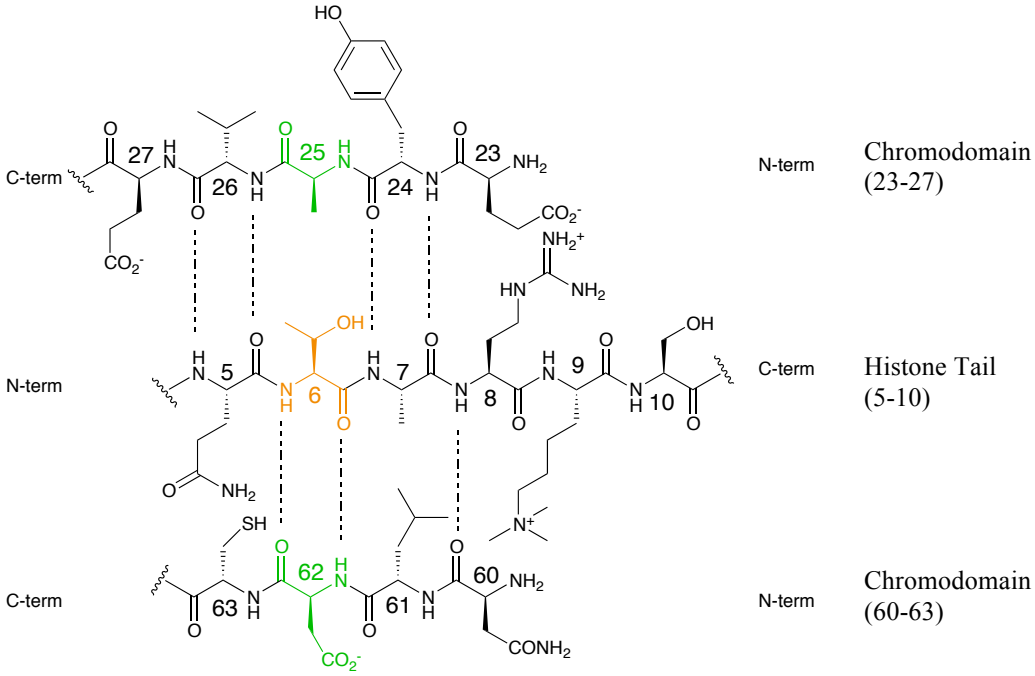

Figure 4.2. (A) Pymol representation of the crystal structure of HP1α chromodomain (green) in complex with H3 K9Me$_3$ histone tail (yellow) with the backbone H-bonds in red. (B) β-strands of the chromodomain and histone tail with the H-bonds between the backbones shown by dashes. The Ala25 and Asp62 of chromodomain are highlighted in green and Thr6 of the histone tail is highlighted in yellow.[2]

ii. β-Sheet Structure

Applying the factors that contributed to β-sheet stability to understanding the selectivity of the HP1α chromodomain for H3 K9Me$_3$ is a method that has not yet been considered for understanding the chromodomain-histone tail complex. A β-sheet can either be parallel with the N-termini of two strands aligned or the antiparallel motif with the C-terminus of one strand aligned with the N-terminus of the other, which is observed in the histone tail-chromodomain complex (Fig. 4.2).

In the anti-parallel β-sheet there are two type of positions referred to as the non-hydrogen bonded (NHB) site and the hydrogen bonded (HB) site (Fig. 4.3). In the NHB site the amide backbone of two cross-strand amino acids are not involved in H-bonds. The NHB and HB sites have significant differences that influence which amino acids are favored in those sites. First, the α-carbons in HB sites are separated by 5.5 Å while α-carbons in NHB are only separated by 4.5 Å. Second, rotamer conformations differ significantly in the two sites, which influences which residues have a higher preference in the NHB versus HB sites.[10, 11]

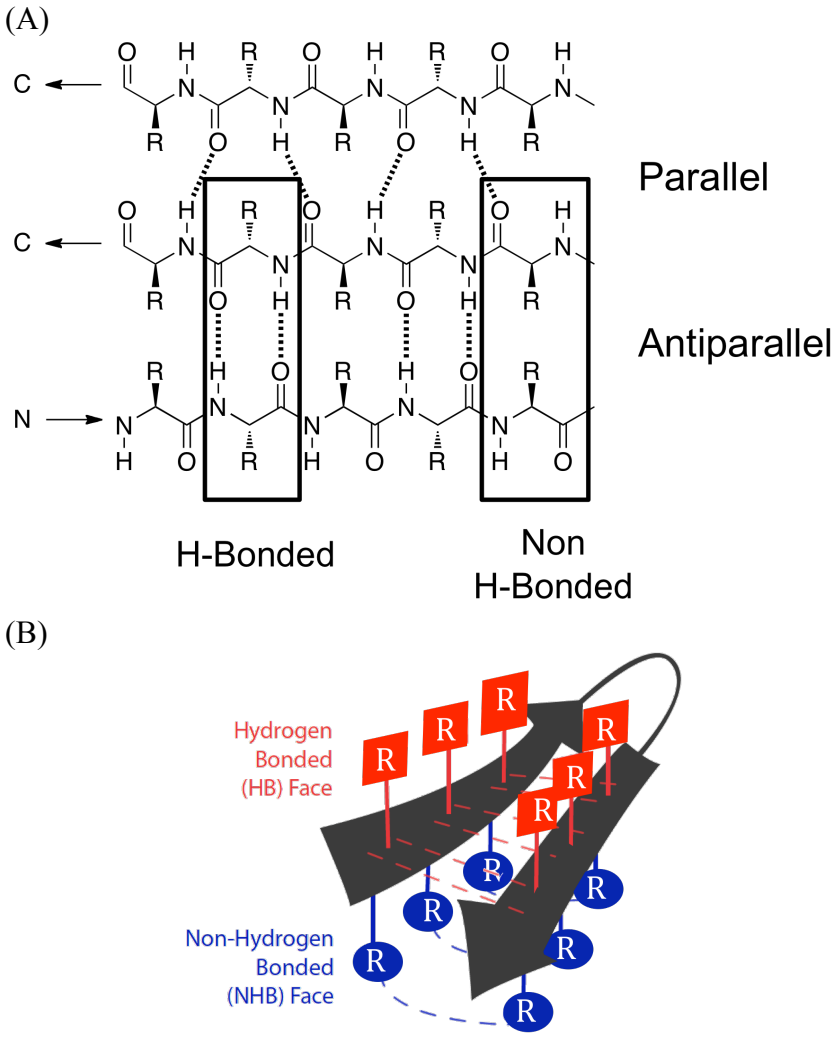

Figure 4.3. (A) An example of both a parallel and antiparallel β-sheet structure with the NHB and HB sites of the antiparallel strands. (B) Side view of an antiparallel β-hairpin with the amino acid side chains depicted as "R".

Extensive research has been performed to establish what amino acids have the highest propensity in β-sheets and which are the most stabilizing. Early statistical analyses were performed using structures from the Protein Data Bank to measure the distribution of amino acids in β-sheets. Amino acids with β-branched or aromatic side chains were shown to have the highest β-sheet propensity. Amino acids that are small, conformationally restrictive (proline), or charged had the lowest propensity.[12, 13] Wouters

and Curmi also performed statistical correlation analysis to determine which cross-strand amino acids are preferred in the HB or NHB sites. One important finding demonstrated that β- and γ-branched amino acids are most commonly found in NHB sites.[11]

Smith and Regan measured interaction energies between cross-strand amino acid pairs by making pair-wise mutations to the B1 domain of Streptococcal protein G in an solvent-exposed HB site.[14] Their findings corroborated the initial statistical analysis showing that pairs composed of β-branched and aromatic residues had the most favorable interaction energy and favorable charge-charge interactions between side chain pairs were the least stabilizing.[14]

Previous studies involving β-hairpins have shown that π-π interactions between two cross-strand aromatic residues, such as two Trp [15] and two Phe residues,[16] are highly stabilizing. The cation-π interaction of Trp and Phe with Lys and Arg is another favorable cross-strand interaction.[17]

B. Goal

Herein we have substituted naturally occurring amino acids at the A25 position of HP1α chromodomain, the T6 position of H3 K9Me3, and the D62 position of HP1α chromodomain for those with higher β-sheet propensity. We also incorporated known favorable cross-strand pairs into the D62 and A25 sites. The purpose of this research is three-fold. First is to evaluate the selectivity of the recognition domain for H3 K9Me_3, the second is to determine whether binding can be optimized by mutating residues within the chromodomain and histone tail peptide. The third goal is to measure how previous studies from β-sheet models and statistical studies compare in the context of protein-protein recognition and the HP1α chromodomain-H3 K9Me3 complex provides a simple

model to meet this end. The results from these studies demonstrate how information about β-sheet propensity and stability from statistics and model systems can be applied to a biologically relevant system to manipulate protein-protein recognition.

C. Results

i. Experimental Design

The β-sheet interactions between H3 K9Me$_3$ and the HP1α chromodomain were explored using a number of trimethyllysine 9 Histone H3 tail peptides with mutations to the Thr6 position and HP1α chromodomain proteins with mutations to either the Ala25 or Asp62 positions. The Thr6 residue of the histone tail was chosen because alanine scans have demonstrated its significance in binding and sequence selectivity. The threonine is also solvent exposed and does not make significant contacts with the interior of the protein. The Ala25 and Asp62 positions were chosen, in part, due to their cross-strand location from Thr6 in the binding pocket. These two residues in the chromodomain were also ideal because they are not known to have high β-sheet propensity or to form particularly favorable cross-strand interactions with threonine. Sidechain-sidechain (SC-SC) interactions vary depending on whether residues are in the NHB or HB positions.[11, 13] Since the Ala25-Thr6 and Thr6-Asp62 pairs occur in NHB and HB positions respectively, the histone tail-chromodomain complex is an ideal system to further explore which interactions are preferred in each position. Additionally, they are solvent exposed residues that appear to form minimal contacts with other amino acids within the chromodomain or histone tail. Therefore these residues were mutated to those with higher β-sheet propensity such as β-branched residues including isoleucine and threonine and the aromatic residue, phenylalanine. Mutations were also incorporated to

include amino acid residues known to form favorable SC-SC interactions including hydrophobic packing, H-bonding, cation-π, and π–π interactions. By incorporating amino acids known to stabilize β-sheet structure into the HP1α chromodomain and histone, the β-sheet-mediated interaction between the two molecules should be stabilized.

ii. Structural Characterization

Circular dichroism experiments were used to investigate the effect that various mutations had on global structure of the chromodomain. Since the signal from the α-helix at 208 nm and 222 nm was expected to mask any signal from β-sheet structure at 210 nm, only two minima at 208 nm and 222 nm were expected to be observed.[18] These minima are present and similar in the spectra of the Ala25 chromodomain mutants (Fig. 4.4). The global structures of the Asp62 mutants deviate more from the wild-type chromodomain, but still have the strong minima at 208 nm and 222 nm and the exciton coupling peak at 232 nm, which arises from interactions between aromatic residues in the aromatic cage (Fig. 4.5). Thus, there appears to be no significant alteration in the global structure due to the various mutations.

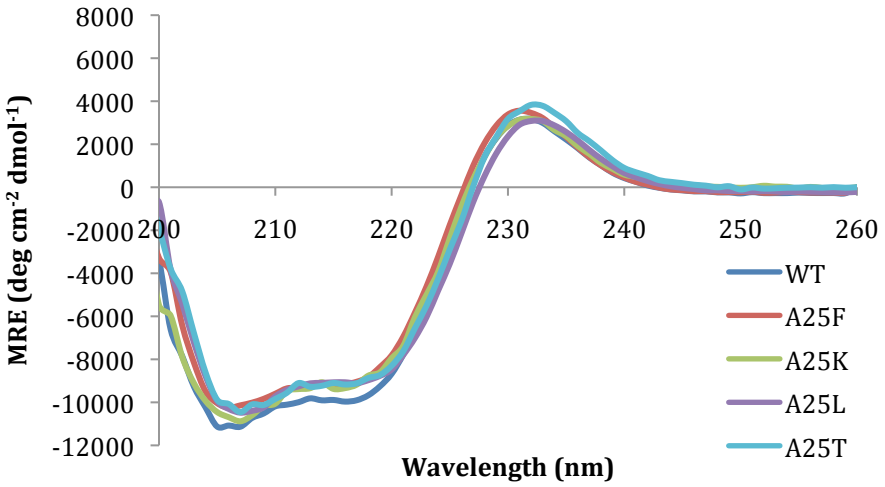

Figure 4.4. Circular dichroism spectra comparison of HP1α chromodomain to the Ala25 mutants at 25 °C in 10 mM sodium phosphate pH 7.4 with 2 mM DTT. These are the averages of three runs.

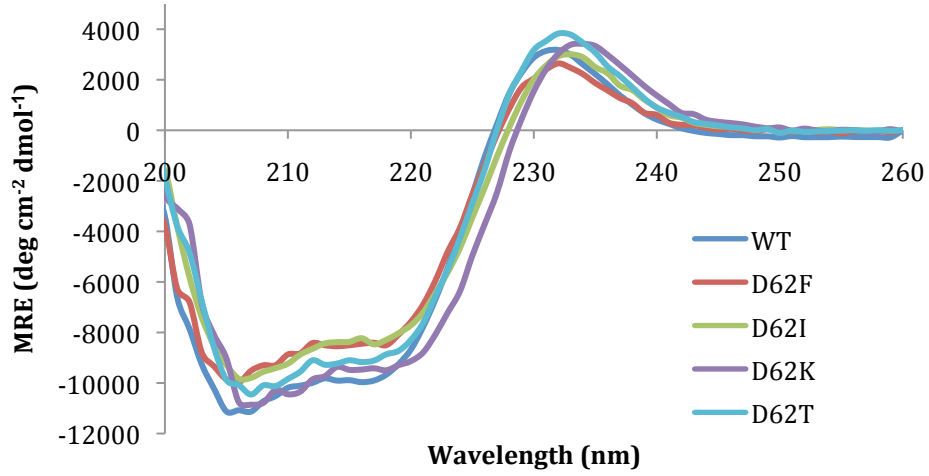

Figure 4.5. Circular dichroism spectra comparison of HP1α chromodomain to the Asp25 mutants at 25 °C in 10 mM sodium phosphate pH 7.4 with 2 mM DTT. These are the averages of three runs.

Thermal denaturation profile of the HP1α chromodomain and the mutants were monitored by circular dichroism at 222 nm to determine how the different point mutations affected the overall stability of the chromodomain. Exploring the stability of the chromodomain and the five mutants is very relevant to the research because it is

necessary to confirm that any decreases in binding affinity are not due to the instability of the protein. It is also important to confirm whether any improvement in binding affinity is due to an increased stability of the mutant chromodomains is a result of favorable interactions between the histone tail and the non-native amino acid residues in the Asp62 or Ala25 positions. The melting temperature of the wild-type protein was measured to be approximately 47 ^{o}C (Fig. 4.6, Fig. 4.7, Table 4.1). Each of the mutants had a melting temperature between 45 ^{o}C and 49 ^{o}C, clearly showing that the various point mutations resulted in an insignificant effect on global stability. This experiment also indicates that wild-type and mutant chromodomains are thermally stable at 25 ^{o}C, the temperature at which all subsequent binding experiments were carried out.

Thermal denaturation and renaturation experiments were also carried out to demonstrate that once denatured, mutant chromodomain are able to refold equally as well as the wild-type protein (Fig. 4.8). Only D62I and A25K mutants were used in these experiments as representatives of the other Asp62 and Ala 25 mutants. As expected, once denatured, the chromodomain is not able to fully refold into its native structure. However about 80% of the protein refolds as do the mutant chromodomains. Once again, these experiments confirm that the mutant proteins are as stable as the wild-type protein.

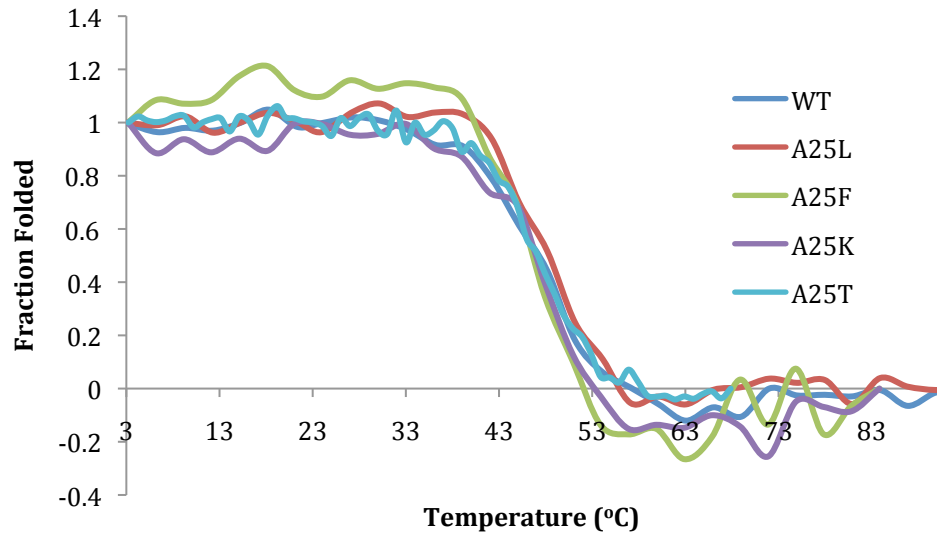

Figure 4.6. Thermal denaturation curves monitored by circular dichroism at 222 nm of HP1α chromodomain Ala25 mutants in 10 mM sodium phosphate pH 7.4 with 2 mM DTT.

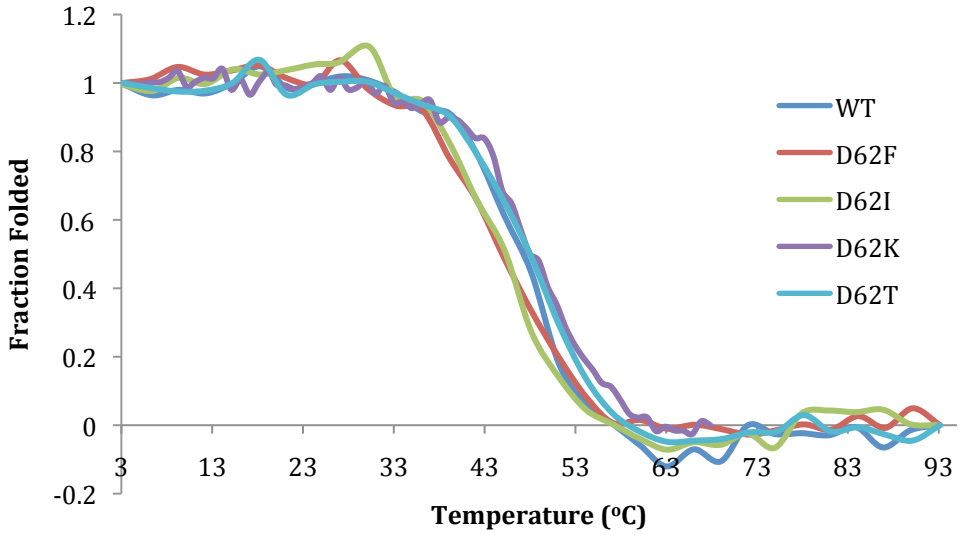

Figure 4.7. Thermal denaturation curves monitored by circular dichroism at 222 nm of HP1α chromodomain Asp62 mutants in 10 mM sodium phosphate pH 7.4 with 2 mM DTT.

Table 4.1. Approximate melting temperatures of HP1α chromodomain Ala25 and Asp62 mutants determined using the thermal denaturation data highlighted in Fig. 4.5 and Fig. 4.6.

HP1α chromodomain mutants	T_m (^oC)
Wild-type	47
A25F	47
A25K	47
A25L	48
A25T	47
D62F	45
D62I	45
D62K	48
D62T	48

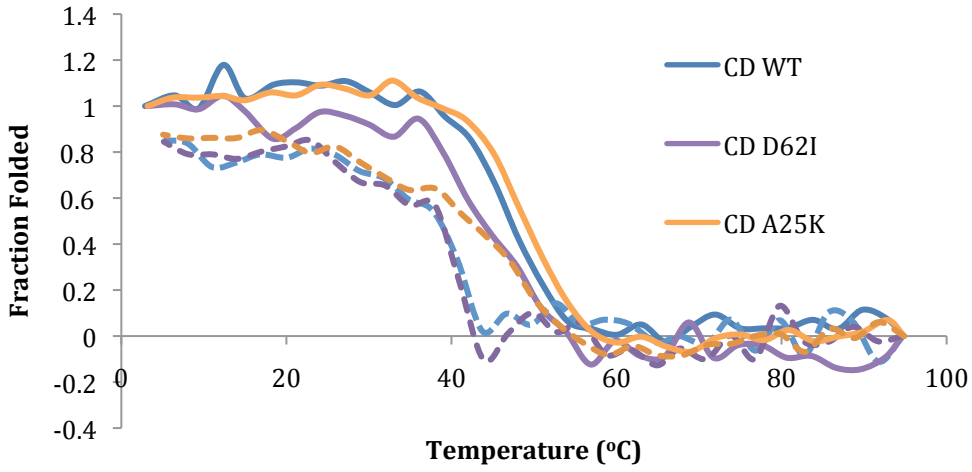

Figure 4.8. Thermal denaturation and renaturation curves monitored by circular dichroism at 222 nm of wild-type HP1α chromodomain and the D62I and A25K mutants in 10 mM sodium phosphate pH 7.4 with 2 mM DTT. The solid line indicates denaturation while the dotted line indicates renaturation

iii. Native Chromodomain-Histone Tail Binding

The dissociation constants between chromodomain and histone tail were measured using fluorescence anisotropy. In previous binding studies, which were performed at 15 ^oC, a K_D value of 10 μM was measured for the HP1α chromodomain and H3 K9Me$_3$.[8] However, the PolarStar platereader used in the Waters lab is unable to take

measurements below a temperature of 25 ^{o}C. Therefore, a new dissociation constant between the native histone tail and HP1α chromodomain was measured at 25 ^{o}C and was determined to be 17 μM. This decrease in binding affinity was expected based on previous binding studies between HP1α chromodomain and monomethyllysine 9 Histone H3 tail, which demonstrated a decrease in binding affinity when the temperature was raised from 15^{o} C to 25^{o} C.[19]

iv. Mutations to H3 K9Me3 at T6 with Wild-Type Chromodomain

Jacobs *et al.* previously reported alanine scans of H3 K9Me$_3$ and found that T6A hindered binding by 7-fold, which was proposed to be due to loss of complementary interactions between the larger threonine residue and the chromodomain.[2] However, no other mutations were explored to examine the scope of the selectivity between the chromodomain and H3 K9Me$_3$. Hence, Thr6 was replaced with four other amino acids know to have high β-sheet propensity including lysine, isoleucine, phenylalanine and leucine which were expected to make favorable SC-SC interactions with A25 and D62 as well as the other chromodomain mutants (Fig. 4.9).

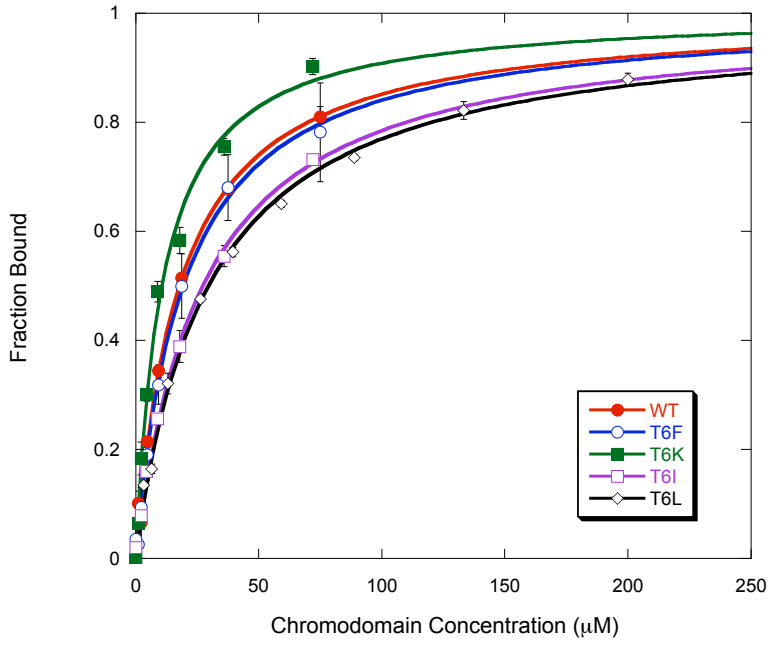

Figure 4.9. Fluorescence anisotropy binding experiments of 1 μM 5(6)-FAM H3 K9Me$_3$ histone tail T6 mutants with wild-type chromodomain. The experiments were performed in 50 mM potassium phosphate buffer pH 8.0, 25 mM NaCl, and 4 mM DTT at 25 °C. Each curve is an average of 3 runs.

Interestingly, none of the four point mutations had a significantly negative effect on binding to the wild-type chromodomain. The T6K histone tail had a slightly improved binding constant to the native chromodomain (10 μM versus 17 μM, respectively). Complementary charged residues in a β-sheet are known to have a favorable side-chain interaction in the H-bonded (HB) site of a β-sheet.[14,11] In this case, having a basic lysine cross-strand from aspartic acid, which is an HB site, may result in a favorable electrostatic interaction. Additionally, the long hydrophobic chain of lysine can form van der Waals contacts with Ala25. The other amino acids substituted into the T6 position of the histone tail also have hydrophobic character, potentially allowing them to maintain similar packing interactions within the binding pocket that T6A could not. A

recent study demonstrated the mammalian HP1α chromodomain, which has 70% homology to *Drosophila* HP1α chromodomain, is more promiscuous than previously believed and recognizes dimethyllysine27 of histone H1.4.[20] The sequence surrounding K27 of H1.4 is KARK(me)$_3$S as opposed to TARK(me)$_3$S. From these studies it is evident that *drosophila* HP1α can interact with other methyllysine marks *in vitro* and may be able to do so *in vivo* as well.

v. Chromodomain Mutations at A25 with Wild-Type H3 K9Me$_3$

Four point mutations to the Ala25 position were studied, which include A25F, A25K, A25L, and A25T (Fig. 4.10, Table 4.2). As expected, A25F, A25L, and A25T had either similar or more favorable binding affinities than the native chromodomain. The residues, Phe, Leu, and Thr have all been shown statistically to have higher β-sheet propensities and are thermodynamically favored in β-sheets over alanine (Table 4.3).[12,21] Incorporating residues known to have a stabilizing effect on β-sheet structures may also stabilize the three-stranded β-sheet formed when chromodomain binds to the histone tail. However, the A25K mutant chromodomain was shown to hinder binding to the histone tail peptide, which will be discussed in further detail below.

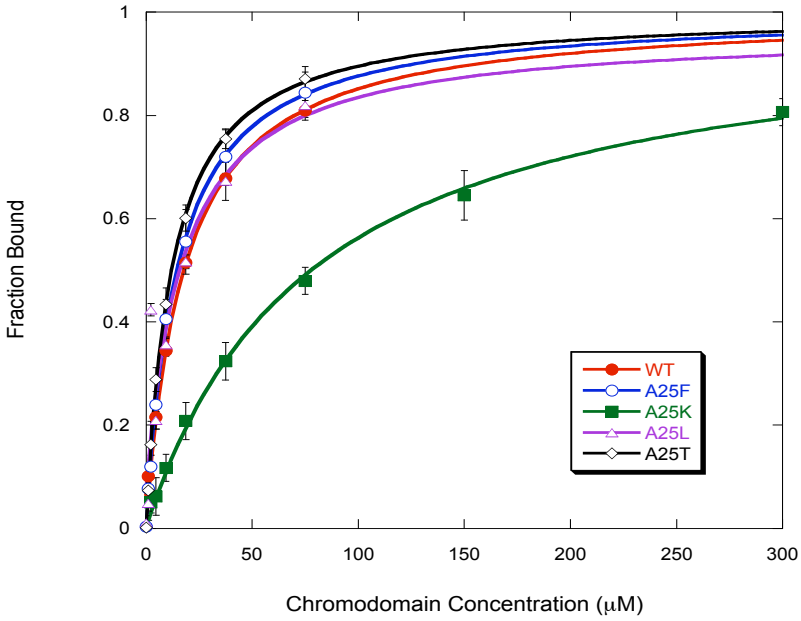

Figure 4.10. Fluorescence anisotropy binding experiments of 1 μM 5(6)-FAM H3 K9Me$_3$ histone tail with Ala25 mutants. The experiments were performed in 50 mM potassium phosphate buffer pH 8.0, 25 mM NaCl, and 4 mM DTT at 25 °C. Each curve is an average of 3 runs.

Table 4.2. Dissociation constants (μM) of *Drosophila* HP1α chromodomain and H3 K9Me$_3$ and the mutants with R^2 value given in parenthesis. The ΔG^o values are given in brackets (kcal/mol) and were calculated using the following equation: $\Delta G^o = -RT\ln(K_D)$. The data was measured in 50 mM potassium phosphate buffer (pH 8.0), 25 mM NaCl, with 4 mM DTT at 25 °C.

Chromodomain	Histone Tail				
	WT	**T6K**	**T6I**	**T6F**	**T6L**
WT	17±3 (0.994) [-6.5±0.1]	10±1 (0.998) [-6.8]	27± 5(0.993) [-6.2]	20±2 (0.996) [-6.4]	24±4 (0.996) [-6.3]
A25F	14±1 (0.999) [-6.6]	16±1 (0.999) [-6.5]	46±5 (0.997) [-5.9]	66±6 (0.998) [-5.7]	33±4 (0.998) [-6.1]
A25K	77±8 (0.997) [-5.6]	253±33 (0.998) [-4.9]	180±26 (0.997) [-5.1]	203±18 (0.999) [-5.0]	376±72 (0.996) [-4.7]
A25L	17±1 (0.999) [-6.5]	13±3 (0.991) [-6.7]	19±2 (0.997) [-6.4]	26±4 (0.995) [-6.2]	26±6 (0.990) [-6.2]
A25T	9±1 (0.998) [-6.9]	10±1 (0.998) [-6.8]	47±5 (0.996) [-5.9]	64±5 (0.998) [-5.7]	44±3 (0.999) [-5.9]
D62F	6±1 (0.995) [-7.1]	12±2 (0.997) [-6.7]	24±4 (0.996) [-6.3]	13±2 (0.995) [-6.7]	28±3 (0.995) [-6.2]
D62I	37±3 (0.999) [-6.0]	46±5 (0.998) [-5.9]	48±4 (0.990) [-5.9]	108±20 (0.992) [-5.7]	45±13 (0.989) [-5.9]
D62K	9±2 (0.990) [-6.9]	30±3 (0.998) [-6.2]	17±3 (0.994) [-6.5]	16±2 (0.996) [-6.5]	10±1 (0.996) [-6.8]
D62T	39±4 (0.997) [-6.0]	58±8 (0.996) [-5.8]	76±11 (0.996) [-5.6]	138±20 (0.996) [-5.3]	26±5 (0.993) [-6.2]

Table 4.3. β-Sheet forming propensities of amino acids relevant to this study.

Amino Acid	Statistical[a]	B1[b]
Ile	1.67	-1.25
Phe	1.33	-1.08
Leu	1.22	-0.45
Thr	1.17	-1.36
Ala	0.72	0
Lys	0.69	-0.35
Asp	0.39	0.85

[a] The normalized frequencies of each amino acid in a β-sheet.[12]

[b] $\Delta\Delta G_{333K}$ (kcal/mol) of amino acid residues relative to alanine when substituted into position 53 of the B1 domain of *Staphylococcal* IgG binding protein G.[21]

vi. Chromodomain A25K Analyzed by the Double-Mutant Cycle

One interesting chromodomain mutant was A25K, a mutation that inhibited binding to every histone tail peptide. Lysine is known to have a high β-sheet propensity. Additionally, lysine residues can participate in favorable cation-π interactions, which can stabilize β-hairpins and β-sheets. Therefore, the A25K mutation to the chromodomain was expected to enhance binding to the T6F histone tail. However, the dissociation constants of A25K to the native and T6F histone tail were 77 μM and 203 μM, respectively. Additionally, the dissociation constants to the other histone tail T6 mutants were at least an order of magnitude greater than the native chromodomain (Fig. 4.11, Table 4.1).

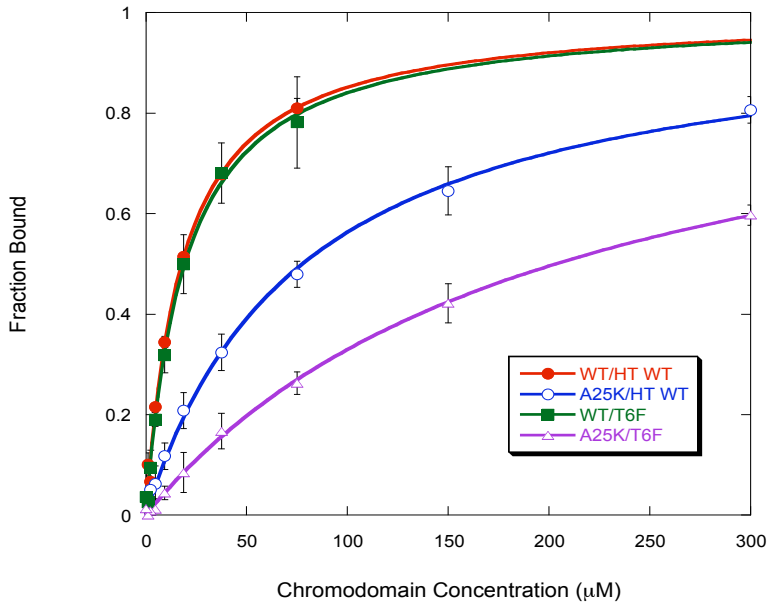

Figure 4.11. Fluorescence anisotropy binding experiments of 1 μM 5(6)-FAM H3 K9Me$_3$ histone tail (wild-type and T6F) with chromodomain (wild-type and A25K). The experiments were performed in 50 mM potassium phosphate buffer pH 8.0, 25 mM NaCl, and 4 mM DTT at 25 °C. Each curve is an average of 3 runs.

Two possible explanations can account for the drastic decrease in binding affinity. First, the incorporation of a basic residue into the chromodomain may have resulted in an electrostatic repulsion with the histone tail, which is a highly basic peptide. For example, R8 of H3 may be involved in a charge-charge repulsion with A25K. Second, there is a highly conserved lysine at position 46, which is in a loop region of the chromodomain. The K46 is also cross-strand from A25K and neighbors the aromatic residues that form the cage around K9 of the histone tail (Fig. 4.12). A charge-charge repulsion may disrupt this region of the chromodomain and may be responsible for the weakened binding affinity to the histone tail peptides. To address this question a double-mutant cycle was used to determine unfavorable or favorable interaction energy between A25K and K46 on binding to the H3 K9Me_3 peptide (Fig. 4.13).[22] This study cannot be used to investigate interaction energies between R8 and A25K because R8 is required for binding, which will be addressed later in this chapter.

A double-mutant cycle is a common technique used to measure the interaction energy between two amino acids of interest, which can either be in the same protein or be involved protein-protein recognition.[22] In a double-mutant cycle each amino acid is individually mutated to an amino acid that is not expected to be involved in stabilizing or destabilizing interactions with the other amino acid. This change may still have an effect on the stability of the protein and, therefore, both amino acids are mutated to create the double-mutant. Performing a double mutation should correct for any effects the single change may have had. If the two residues are not coupled, then the free energy of the native protein equals the energy of the double-mutant minus the energies of the single

mutants. If the residues are coupled then a change in the free energy will be observed.[22, 23]

To measure the interaction energy between K46 and A25K, the residues were individually changed to alanine and then the double-mutant was constructed to complete the cycle. The sum of the energies from chromodomain A25K/K46 and A25/K46A minus the sum of A25/K46 and A25K/K46A gives the interaction energy between A25K and K46. The data from the double-mutant cycle was highly unanticipated. For a double-mutant cycle to be effective, replacing two interacting residues with two non-interacting residues should account for any perturbation a single mutation has on the system. This way the ΔΔG between two residues of interest can be calculated. In this study if K46 and A25K have a repulsive interaction then changing K46 to alanine should improve binding. Since two cross-strand alanine side chains are not involved in non-covalent interactions, the chromodomain A25/K46A mutant should slightly recover binding, but not enhance binding compared to the native chromodomain. Here, the K46A mutation significantly improved binding by nearly an order of magnitude (K_D=2 μM) and was in fact the best binder of all chromodomain mutants. The double mutation A25K/K46A mutation recovered the binding affinity of the chromodomain A25K mutant and corrected for the effects of the single mutants (Fig. 4.14, Table 4.4). The calculated ΔΔG between A25K and K46 was calculated to be -0.1 kcal/mol, which is within error of 0 kcal/mol indicating a minimal interaction between A25K and K46. Therefore, the A25K mutant may weaken binding due to a charge-charge repulsion with the basic histone tail.

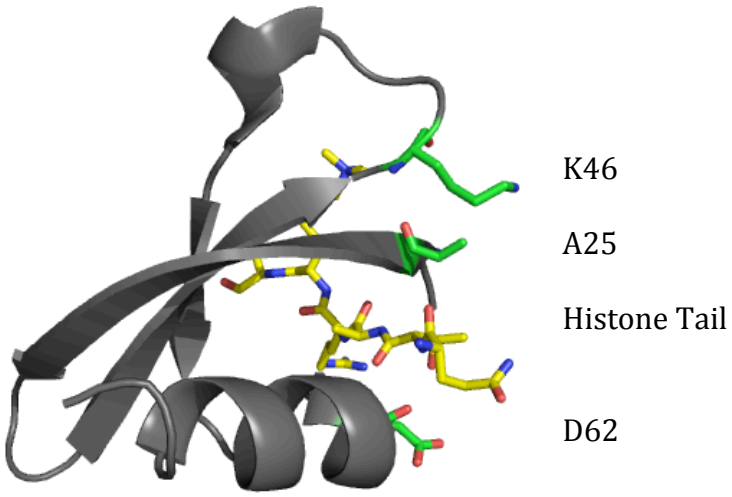

Figure 4.12. Structure depicting the chromodomain (silver) bound to histone tail (yellow). Residues K46, A25, and D62 are shown in green (PDB: 1KNE). [2] This structure was generated using PyMol.

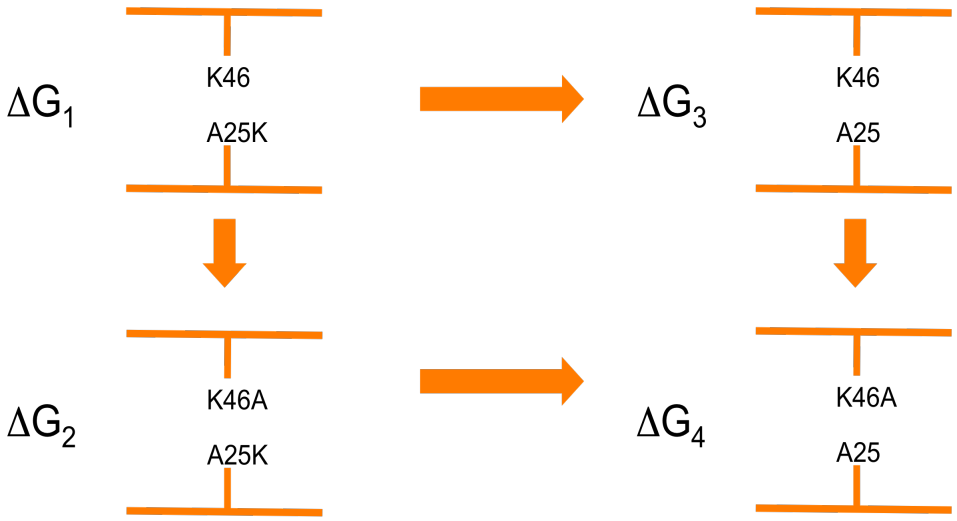

Figure 4.13. Depiction of the double-mutant cycle used to measure the interaction energy between A25K and K46 of the HP1α chromodomain and the histone tail.

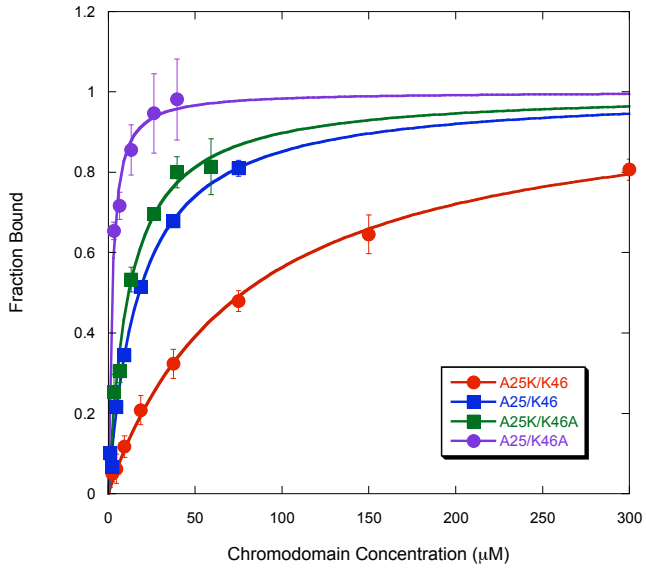

Figure 4.14. Fluorescence anisotropy binding experiments of 1 μM 5(6)-FAM H3 K9Me$_3$ wild-type histone tail with chromodomain for the A25K/K46 double-mutant cycle. The experiments were performed in 50 mM potassium buffer pH 8.0, 25 mM NaCl, and 4 mM DTT at 25 °C. Each curve is an average of 3 runs.

Table 4.4. Fluorescence anisotropy binding data from Fig. 4.21 for the HP1α chromodomain A25K/K46 double-mutant cycle. The K_D values are in μM with R^2 in parenthesis. The ΔG values are given in brackets (kcal/mol) and were calculated using the following equation: $\Delta G^o = -RT\ln(K_D)$The experiments were performed in 50 mM potassium phosphate buffer pH 8.0, 25 mM NaCl, and 4 mM DTT at 25 °C. Each curve is an average of 3 runs.

chromodomain mutants	H3 K9Me$_3$ WT
A25K/K46	77±8 (0.997) [-5.6]
A25/K46 (wild-type)	17±3 (0.994) [-6.5]
A25K/K46A	11±2 (0.991) [-6.8]
A25/K46A	2±0.5 (0.991) [-7.8]

NMR studies by Jacobs and coworkers demonstrated the region in which K46 to have a minimal change in $\{^1H\}-^{15}N$ NOE values between the bound and unbound state, which demonstrates the importance of pre-organization of chromodomain when binding

to H3 K9Me$_3$. Alanine is also known to be residue with the highest α-helix propensity compared to other amino acids including lysine.[24] Since K46 occurs between a β-strand and short α-helix (Fig. 4.12), it may be that replacing lysine with alanine altered the structure of the random-coiled region, which may improve binding affinity.

To address this question, circular dichroism studies were performed to ascertain how the K46A mutation affected both the global structure and thermal stability of HP1α chromodomain (Fig. 4.15, Fig. 4.16). The global structures of the proteins that were used in the double-mutant cycle are all consistent with distinct minima at 208 nm and 222 nm and a maximum at 232 nm. The A25K/K46A mutant gives a slightly enhanced signal compared to the other three. The thermal denaturation experiments showed that the A25K mutant and the A25K/K46A mutant have melting temperatures similar to the wild-type protein. However, the K46A mutant has a melting temperature about 9 ^{o}C lower than the wild-type chromodomain (Fig. 4.16, Table 4.5). These results suggest that there is one of two possibilities. First, any change in conformation near the binding pocket of chromodomain due to the K46A mutation is too subtle to be detected by circular dichroism. Second, the K46A mutation may not enhance the stability of the chromodomain, but instead affect conformation or molecular interactions with the histone tail peptide by replacing a basic amino acid with a neutral one.

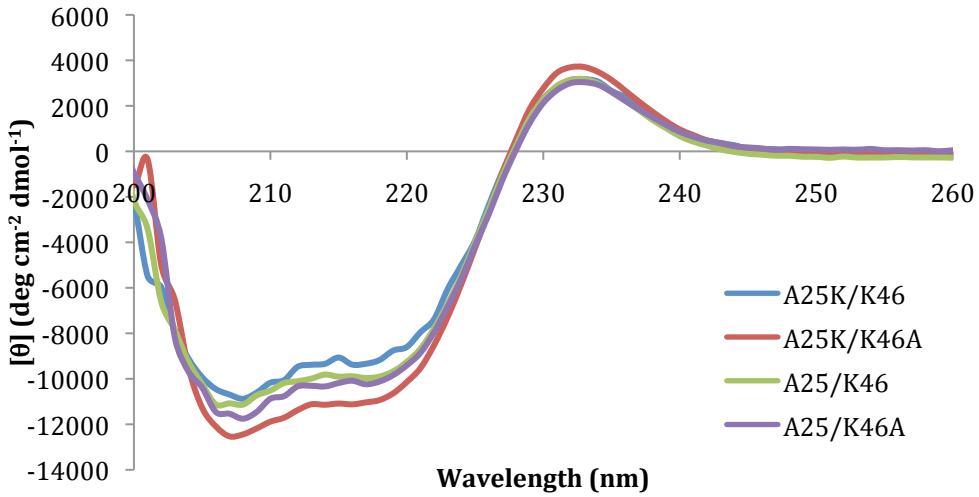

Figure 4.15. Circular dichroism spectra of HP1α chromodomain (wild-type and A25/K46 mutants) to for A25K/K46 double-mutant cycle at 25 °C in 10 mM sodium phosphate pH 7.4 with 2 mM DTT. These are the averages of three runs.

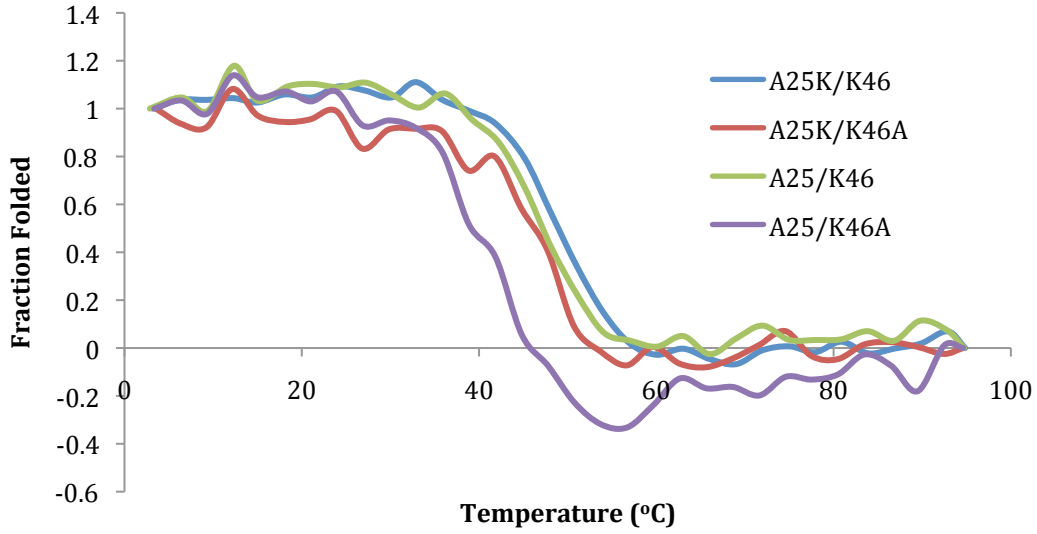

Figure 4.16. Thermal denaturation monitored by circular dichroism (222 nm) of HP1α chromodomain (wild-type and A25/K46 mutants) to for A25K/K46 double-mutant cycle at 25 °C in 10 mM sodium phosphate pH 7.4 with 2 mM DTT. These are the averages of three runs.

Table 4.5. Approximate melting temperatures of HP1α chromodomain wild-type and A25/K46 mutants determined using the thermal denaturation data highlighted in Fig. 4.16.

chromodomain mutants	T_m (^oC)
Wild-type	47
A25K/K46	48
A25K/K46A	45
A25/K46A	38

vii. Chromodomain Mutations at D62 with Wild-Type H3 K9Me$_3$

The mutations to the D62 position of the chromodomain that were studied include D62F, D62I, D62K, and D62T (Fig. 4.17, Table 4.2). The only mutant that had a weaker binding to the native histone tail was D62I (37 μM versus 17 μM for the wild-type). Despite isoleucine having a higher β-sheet propensity compared to aspartate, incorporating a hydrophobic residue to the most solvent exposed strand of the chromodomain-histone tail complex results in weaker binding. This may be a result of unfavorable solvation energy or a steric clash with T6.

Unlike A25K, the D62K mutation improved binding to the native histone tail by 2-fold compared to the wild-type chromodomain. The difference between affinities of A25K and D62K may be explained because the exposed basic amine of lysine is readily solvated rather than forming unfavorable charge-charge repulsion with basic residues on the histone tail such as R8.

The improved binding affinity of D62K compared to the wild-type chromodomain for H3 K9Me$_3$ is consistent with previous thermodynamic studies by Smith and Regan. [21] Lysine was shown to have a significantly higher β-sheet propensity compared to aspartate with a ΔΔG of -1.1 kcal/mol when measured in an HB site. Additionally, the alkyl chain of lysine may be able to form a hydrophobic packing interaction with threonine.

Interestingly, a phenylalanine mutation at the D62 position favors binding to the histone tail by approximately 3-fold, with a K_D of 6 μM (Fig. 4.17). There are a number of factors that may contribute to this observed improvement. Aromatic residues such as phenylalanine have been shown in both statistical, mutational, and hairpin studies to have a significantly higher β-sheet propensity than aspartate.[13,14,25] Additionally, previous research has demonstrated the stabilizing effects of a diagonal cation-π interaction in β-hairpins.[17,26] In the chromodomain-histone tail complex, D62 is in a diagonal cross-strand position from R8 of the histone tail and may form a cation-π interaction, which can stabilize the complex. A double-mutant cycle to determine the interaction energy with D62F and R8 of the histone tail was not possible due to the importance of R8 for binding.

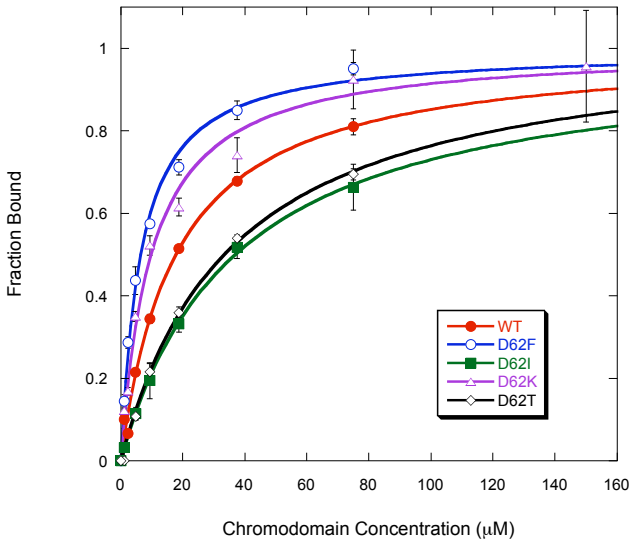

Figure 4.17. Fluorescence anisotropy binding experiments of 1 μM 5(6)-FAM H3 K9Me_3 histone tail with Asp62 mutants. The experiments were performed in 50 mM potassium phosphate buffer pH 8.0, 25 mM NaCl, and 4 mM DTT at 25 °C. Each curve is an average of 3 runs.

viii. Trends Between Mutant Chromodomain and Histone Tails

There are some general trends between mutant chromodomain and mutant histone tails. For example, A25F and A25T both had similar binding affinities for the wild-type histone tail and the T6K histone tail. However, binding affinity is less favorable when a bulky or β-branched residue is substituted in the T6 position of the histone tail. Steric clash is a likely explanation for the decrease in affinity. The D62T and D62F mutations have very different trends, which will be discussed in detail below.

ix. Orientation of Cross-Strand Pairs

Extensive consideration has previously been given to the orientation of cross-strand amino acids residues. It is evident from mutational studies to the B1 domain of *Streptococcal* protein G and in β-hairpin model systems that reversing the cross-strand positions of two amino acids significantly decreases the stability of the protein.[14,27] This is an observation that was further explored by investigating the effects of amino acid orientation in the HP1α chromodomain and histone tail complex.

The results indicate that reversing the orientation of two residues has a drastic effect on the binding of the histone tail by the chromodomain. The previous study using the B1 domain explored Thr-Phe cross-strand pairs and the interaction energies improved when threonine was located on the N-terminal β-strand and phenylalanine on the C-terminal β-strand. However, when positions were reversed the ΔG was disfavored by 0.55 kcal/mol. This discrepancy in interaction energy was credited to differences in local geometry around each amino acid.[14]

In the case of the chromodomain-H3 K9Me_3 complex, the chromodomain D62F mutant improved binding by 3-fold as previously discussed (Fig. 4.18). However when

the orientation of the Thr and Phe residues was reversed (D62T/T6F), the dissociation constant increased to 138 μM (ΔΔG=1.8 kcal/mol). This measurement is consistent with the loss of a diagonal cation-π interaction between D62F and R8 of the histone tail that occurs by reversing the positions of the Thr and Phe residues (Fig. 4.19). Additionally, there is probably a steric clash due to rotamer preferences of the D62T and T6F. An interaction of this type may not be visible between the T6F mutant and the native chromodomain if there is a favorable electrostatic interaction between R8 and D62, which is lost when D62 is mutated to a threonine. Additionally, incorporating a bulky amino acid such as phenylalanine in a central β-strand has been suggested to result in steric crowding.[11]

Consistent with the D62F/T6 pair, the A25F/T6 pair was favored relative to the A25T/T6F pair by a factor of four (ΔΔG=0.9 kcal/mol) (Fig. 4.18). Thus, based on the studies involving the D62F/T and A25F/T mutants, the intrinsic β-sheet forming propensities of the amino acid residues are not the only contributing factors to the formation of the chromodomain-histone tail complex. The interactions of the amino acids with neighboring residues and water molecules must play an important role as well, as has been shown in other systems.[28]

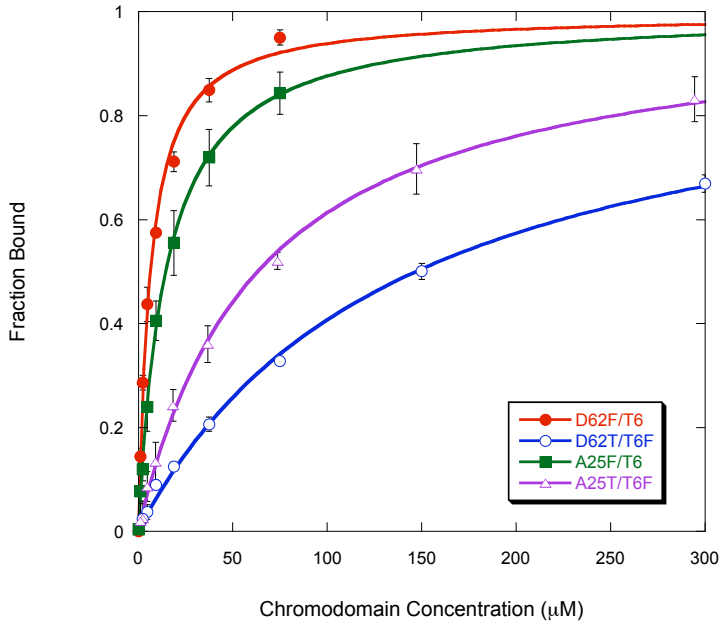

Figure 4.18. Comparison of the various fluorescence anisotropy binding experiments of 5(6)-Fam-labeled H3 K9Me$_3$ with chromodomain, focusing on Thr/Phe pairs. Experiments were done in 50 mM potassium phosphate buffer pH 8.0, 25 mM NaCl, and 4 mM DTT at 25 °C. Each curve is an average of 3 runs.

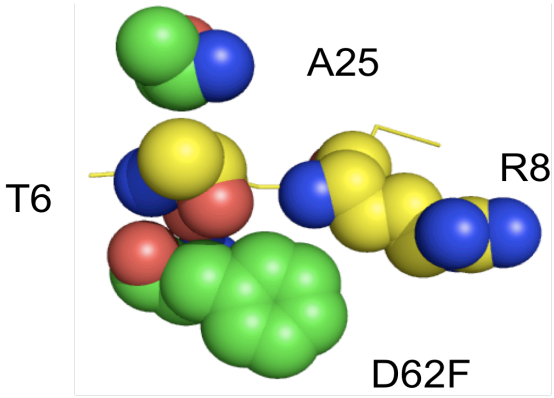

Figure 4.19. PyMol image of H3 K9Me$_3$ (yellow) bound to HP1α chromodomain D62F (green). The conformation of D62F represents the context dependent preferred rotamer and does not reflect an energy-minimized structure (PDB 1KNE).

A double-mutant cycle was used to measure the interaction energy between D62F and R8 to determine whether they are involved in a cation-π interaction. In a double-mutant cycle, the two residues of interest are systematically mutated for an amino acid that should have little to no effect on interaction energy. To complete the cycle both residues are mutated (Fig. 4.20).

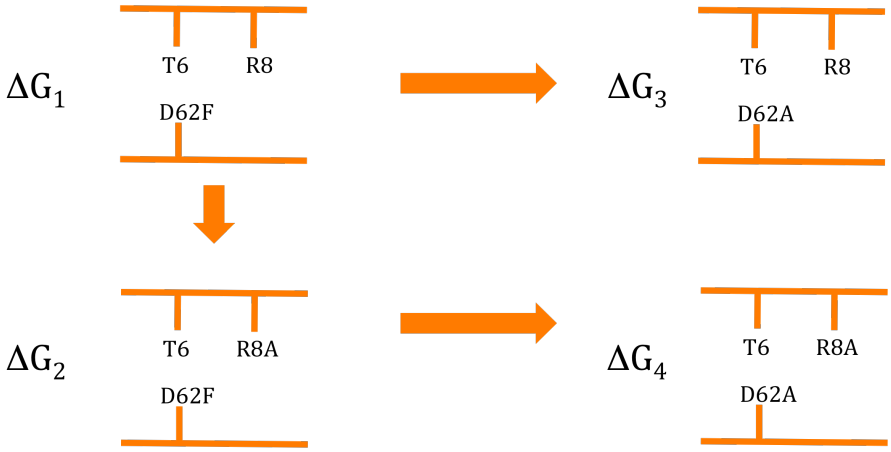

Figure 4.20. Depiction of the double-mutant cycle used to measure the interaction energy between R8 of the histone tail and D62 of the chromodomain.

The results from the double-mutant cycle proved to be inconclusive. Due to the significance of R8 in the histone tail in chromodomain recognition, binding to the R8A mutant was severely inhibited (Fig. 4.21, Table 4.6). As shown in Table 4.3, both the D62A and D62F chromodomain mutants had a K_D of over 200 μM to the R8A histone tail. It was interesting to see that chromodomain D62A had a K_D of 8 μM to the native histone tail. Alanine has a statistically higher β-sheet propensity than asparate and has been reported to be more energetically favorable by -0.85 kcal/mol in an HB site.[21] Therefore substitution of D62 with alanine may have a stabilizing effect on β-sheet interactions with the histone tail peptide.

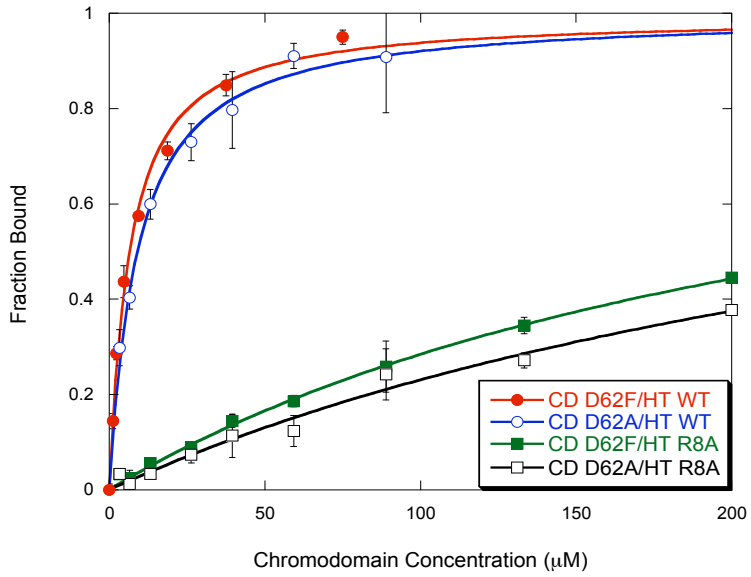

Figure 4.21. Fluorescence anisotropy binding experiments of 1 μM 5(6)-FAM H3 K9Me$_3$ histone tail with chromodomain for the D62/R8 double-mutant cycle. The experiments were performed in 50 mM potassium phosphate buffer pH 8.0, 25 mM NaCl, and 4 mM DTT at 25 °C. Each curve is an average of 3 runs.

Table 4.6. Fluorescence anisotropy binding data from Fig. 4.14. The dissociation constants are in μM with the R^2 in parenthesis. The ΔG values are given in brackets (kcal/mol) and were calculated using the following equation: $\Delta G^o = -RT\ln(K_D)$.

	H3 K9Me$_3$ WT	**H3 K9Me$_3$ R8A**
D62F	6±1 (0.995) [-7.1]	251±53 (0.995) [-4.9]
D62A	8±1 (0.995) [-6.9]	332±165 (0.981) [-4.7]

x. Comparison of Hydrogen-Bonded and Non-Hydrogen-Bonded Sites

The differences between cross-strand pairs in HB and NHB sites have been extensively explored using statistical correlation studies.[11] Therefore, significant comparisons were made between the NHB and HB sites of the chromodomain-histone tail complex (A25/T6 and T6/D62 respectively).

The D62F/T6 pair in the HB site favored binding affinity over the A25F/T6 pair in the NHB site (Fig. 4.14). Statistical correlation studies have demonstrated that there is a 2-fold higher correlation of Phe/Thr pairs in the HB site than in the NHB site of a β-sheet.[11] Based on simple modeling with PyMol, which places the side chain in its statistically preferred conformation, it is possible that the phenylalanine is splayed away from the histone tail. Additionally, the right-handed twist of the β-sheet formed between the chromodomain and histone tail would likely direct side-chains at position 25 away from R8. Therefore, the cation-π interaction with R8 of the histone tail compared to D62F would be weakened (Fig. 4.22).

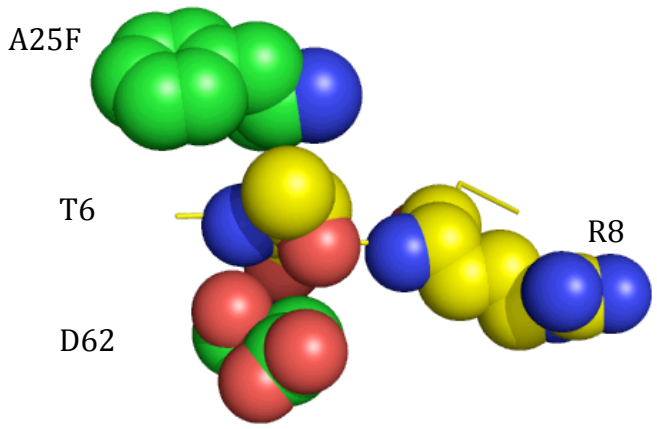

Figure 4.22. PyMol image of H3 K9Me$_3$ (yellow) bound to HP1α chromodomain A25F (green). The conformation of A25F represents the context dependent preferred rotamer and does not reflect an energy-minimized structure (generated from PDB 1KNE).

The interaction between two aromatic rings, which are known to be an important element in protein stability and recognition[16,29,30], also showed different binding preferences depending on whether they were placed in the HB or NHB site. chromodomain D62F in complex with H3 K9Me$_3$ T6F has a slightly improved affinity of 13 μM (Fig. 4.23). Using PyMol as a simplistic model, the two aromatic phenylalanine

residues are shown to align ideally to form the favorable aromatic offset-stacked motif in their preferred rotomeric states to allow for a favorable quadrupole-quadrupole interaction (Fig. 4.24A).[29] Although this is an unminimized structure, it suggests that the preferred conformation will predispose these side-chains to interact favorably. This structure is also consistent with the statistical analysis by Wouters and Curmi who showed that Phe-Phe pairs often take a gauche-/gauche+ conformation, which results in an offset stacked π-π interaction.[11]

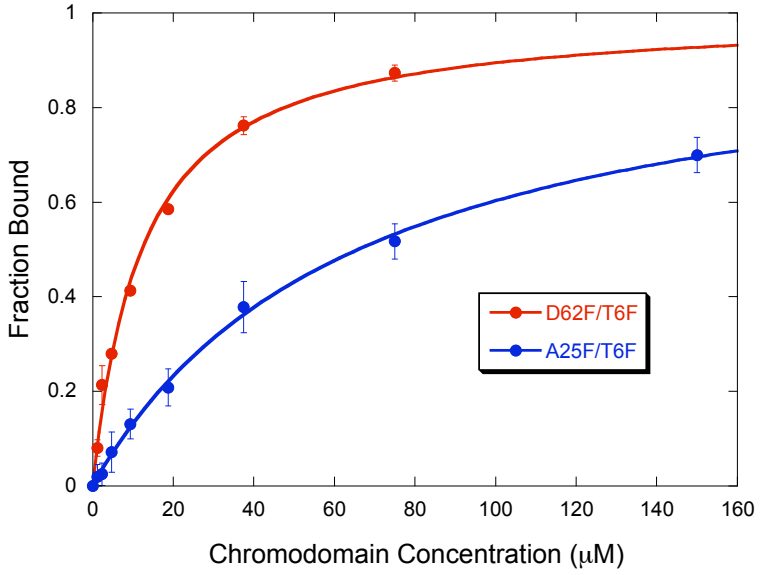

Figure 4.23. Comparison of the fluorescence anisotropy binding experiments of 5(6)-Fam-labeled H3 K9Me$_3$ with chromodomain focusing on Phe/Phe interactions. Experiments were done in 50 mM potassium phosphate buffer pH 8.0, 25 mM NaCl, and 4 mM DTT at 25 °C. Each curve is an average of 3 runs.

(A) (B)

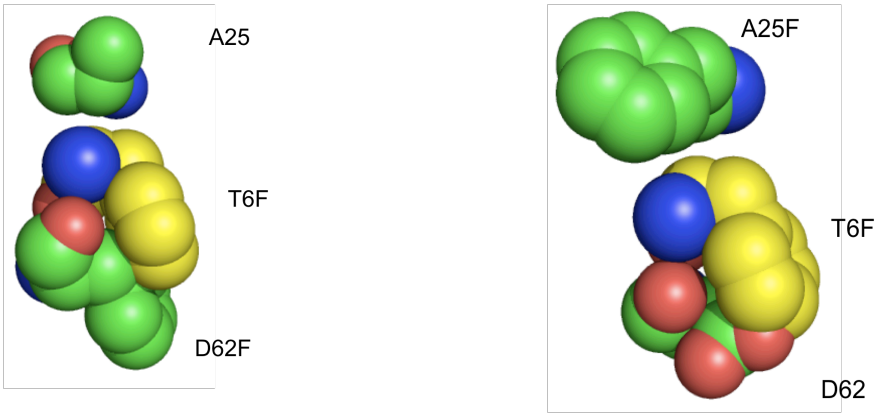

Figure 4.24. PyMol image of (A) H3 K9Me$_3$ T6F (yellow) bound to HP1α chromodomain D62F (green) and (B) H3 K9Me$_3$ T6F (yellow) bound to HP1α chromodomain A25F (green). The conformation of the mutants represents the context dependent preferred rotamer and does not reflect an energy-minimized structure (generated from PDB 1KNE).

In contrast, chromodomain A25F binds H3 K9Me$_3$ T6F with a K_D of 66 μM, which is 4-fold weaker than with the native histone tail and between chromodomain D62F and the T6F peptide (Fig. 4.23). It is possible that introducing two bulky aromatic residues to the interior and conformationally restricting two β-strands of the 3-stranded β-sheet results in steric hindrance. Furthermore, R8 of the histone tail, which is in close proximity to D62F, is further from A25F due to the right-handed twist of the β-sheet. Thus a favorable cation-π interaction between R8 and D62F is likely not able to form. Lastly, statistical analysis has shown that Phe-Phe pairs have a significantly higher correlation in a HB site over a NHB site. This difference is attributed to the favorable offset-stacked orientation observed in the HB site that doesn't necessarily occur in the NHB site (Fig. 4.24).[11] Interestingly, the favored D62F/T6F pair occurs in the HB site while the A25F/T6F pair is in the NHB site, which is consistent with the previous statistical analysis.

Binding affinity between chromodomain and histone tails with cross-strand threonine pairs is also site-specific. Incorporating a threonine mutation at position 62 reduces binding affinity to H3 K9Me$_3$ by two-fold (K_D=39 μM) compared to the native chromodomain (K_D=17 μM) while incorporating a threonine at position 25 enhances binding affinity by two-fold compared to the native chromodomain (K_D=9 μM) (Fig. 4.25).

In general, β-branched residues have a higher statistical pair correlation in HB sites compared to NHB sites, including Thr-Thr pairs.[10, 11] Statistical analyses have demonstrated that cross-strand Thr-Thr pairs have a preference for the gauche+ rotamer conformation, which favors inter-residue H-bond between the hydroxyl groups of the threonine side chains (Fig. 4.26). In an HB site, both Thr residues must be in the unfavorable gauche- rotamer conformation to accommodate the H-bond between the hydroxyl groups.[10] Experimental results reported Smith and Regan supported the analysis that Thr-Thr pairs are disfavored in the HB position when various cross-strand pairs were incorporated into a HB position of the B1 domain of Streptococcal protein G. They showed that Thr-Thr pairs had an unfavorable interaction energy,[14] which is consistent with the findings here showing the Thr-Thr pairs in the HB site of the chromodomain-histone tail complex (positions 6 and 62 respectively) weakened binding affinity.

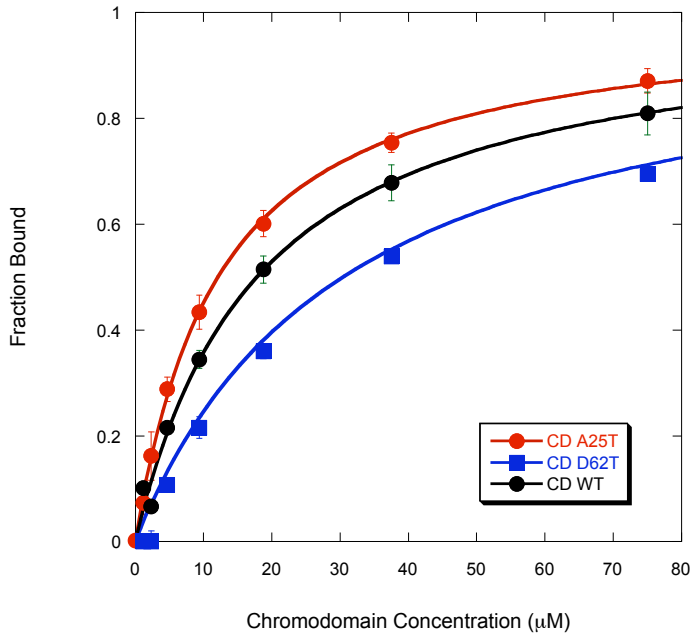

Figure 4.25. Comparison of the fluorescence anisotropy binding experiments of 5(6)-Fam-labeled H3 K9Me$_3$ with chromodomain focusing on Thr/Thr interactions. Experiments were done in 50 mM potassium phosphate buffer pH 8.0, 25 mM NaCl, and 4 mM DTT at 25 °C. Each curve is an average of 3 runs.

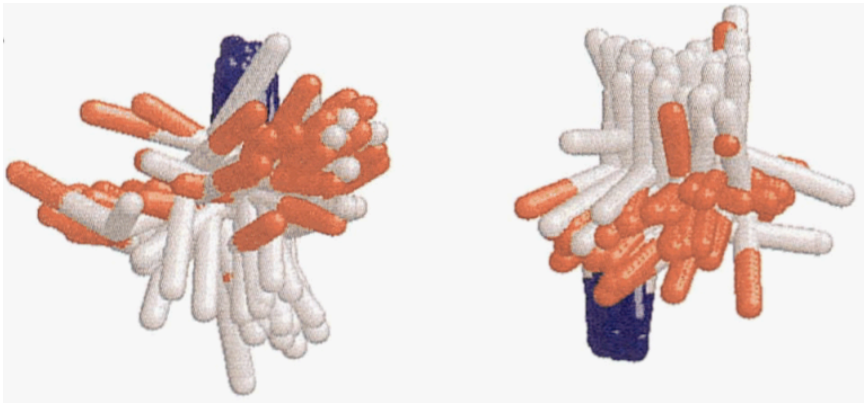

Figure 4.26. Superposition of 37 Thr-Thr pairs that shows the preference for the gauche+ gauche+ conformation. Most of the hydroxyl groups in the side chains are aligned to accommodate a inter-residue H-bond. Hydroxyl group are red while amides are blue and carbons are white.[10]

D. Conclusions

We have used the HP1α chromodomain and H3 K9Me$_3$ peptide to investigate how information gleaned from β-hairpin models and statistical analysis of β-sheet propensity and stability apply to protein-protein recognition. Additionally, these studies

permitted us to examine the scope of the selectivity of the HP1α chromodomain for its intended target. Our data has shown that changing residues not known to be favored in β-sheet structures such as alanine or aspartic acid to those such as lysine, threonine, and phenylalanine[21] can have a drastic positive or negative effect on binding depending on the site of the mutation. The system is complicated by the surrounding amino acids, which can form unfavorable charge-charge interactions, such as between A25K and R8 of the histone tail of the chromodomain repulsion or favorable cation-π interactions such as D62F of the chromodomain and R8. Solvation and steric hindrance are two additional factors that may also influence how the orientation of two cross-strand residues affects binding. The findings have also demonstrated the possible variations at the T6 position of the Histone H3 tail. While alanine scans have shown that shortening the residue reduces binding by 7-fold, incorporating bulky amino acids capable of packing against A25 and D62 is equally as favorable as the native threonine.

The information gathered from these studies can be utilized in a number of applications. Regan *et al* recently redesigned tetratricopeptide repeat and its ligand with a K_D in the low micromolar range to enhance selectivity and applied their findings for use in Western blots.[31] Detection of PTMs in histone proteins is a difficult, but important endeavor necessary for unveiling the "Histone Code". Mass spectrometry has its limitations[32] and antibodies are expensive and difficult to manufacture. Using the chromodomain mutants with higher affinity H3 K9Me_3 and incorporating the E52Q mutation discussed in Chapter III, which will give higher selectivity for trimethyllysine, can be used as a detection method for PTMs in the future.

E. Experimental

i. Protein Expression and purification

The DNA plasmid containing the cloning region of *Drosophila* HP1α chromodomain was supplied by the Khorasanizadeh lab.[19] Mutagenesis, expression, and purification were performed as previously described in Chapter III and purity was confirmed by SDS-PAGE. The primers used for mutagenesis are given in Table 4.7.

Table 4.7. Forward primers used for mutagenesis of HP1α chromodomain at Ala25 and Asp62. The site of mutation is in red.

Mutant	Primer Sequence
A25F	GAG GAG GAG GAG TAC TTC GTG GAA AAG ATC ATC
A25K	GAG GAG GAG GAG TAC AAA GTG GAA AAG ATC ATC
A25L	GAG GAG GAG GAG TAC CTC GTG GAA AAG ATC ATC
A25T	GAG GAG GAG GAG TAC ACC GTG GAA AAG ATC ATC
A25W	G GAG GAG GAG TAC TGG GTG GAA AAG ATC
D62F	CCG GAG AAC AAT CTC TTC TGC CAG GAT CTT ATC CAG
D62I	CCG GAG AAC AAT CTC ATC TGC CAG GAT CTT ATC CAG
D62K	CCG GAG AAC AAT CTC AAA TGC CAG GAT CTT ATC
D62T	CCG GAG AAC AAT CTC ACC TGC CAG GAT CTT ATC CAG
D62A	CCG GAG AAC AAT CTC GCC TGC CAG GAT CTT ATC
K46A	G TAC TAT CTG AAA TGG GCG GGC TAT CCC GAA AC

ii. Peptide synthesis and purification

Histone peptides were synthesized as previously described in Chapter III. See Table 4.8 for mass spec analysis.

Table 4.8. Mass spectrometry data for the peptides synthesized for this study.

Peptide	Expected Mass (Da)	Experimental Mass (Da)
H3 K9Me$_3$	2124.1	2124.7
H3 K9Me$_3$ T6F	2170.1	2169.8
H3 K9Me$_3$ T6I	2136.1	2136.1
H3 K9Me$_3$ T6K	2151.1	2151.0
H3 K9Me$_3$ T6L	2136.1	2136.1
H3 K9Me$_3$ T6A	2094.0	2094.0
H3 K9Me$_3$ R8A	2039.0	2038.8

iii. Circular Dichroism

CD measurements were performed on an Aviv 62DS Circular Dichroism Spectrometer. All CD experiments were performed as described in Chapter III.

iv. Anisotropy

As explained in Chapter III, all experiments were carried using a Polarstar plate reader with 1 μM histone tail peptide labeled with 5(6)-carboxyfluorescein. However, during the initial studies using the β-sheet mutants, a number of inconsistencies were observed. Much like with the CHD1 chromodomain studies nonspecific binding was observed at higher chromodomain concentrations and, therefore, had to omit data points.[33]

Several controls were performed to determine the optimal experimental conditions. To control for aggregation, a sample of chromodomain was centrifuged in a microcentrifuge at 13,000 rpm for 10 mins using a Sorvall Biofuge pico centrifuge with rotor number 3325B to remove precipitates and binding to H3 K9Me$_3$ T6K was compared to chromodomain that had not been centrifuged (Fig.4.27, Table 4.9). The dissociation constants measured using the centrifuged samples and non-centrifuged samples are very similar and the concentrations before and after centrifugation were the same. Therefore, protein aggregation was not a concern.

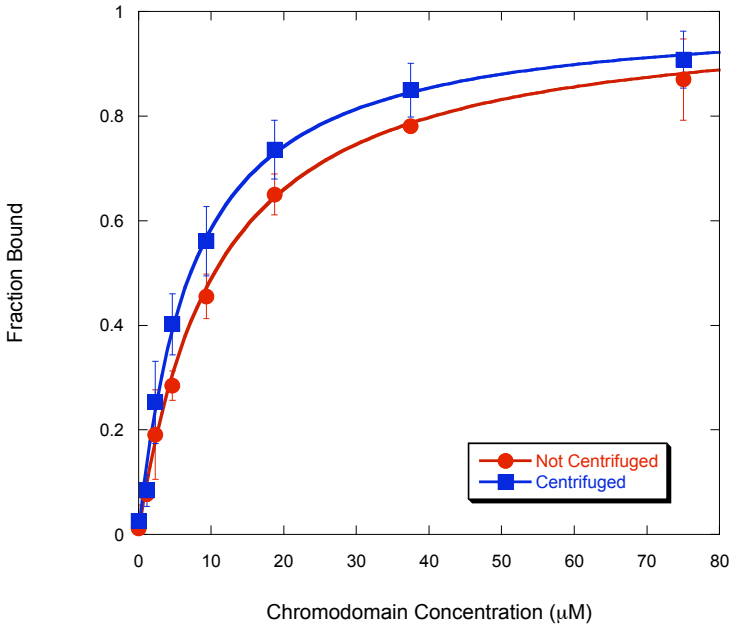

Figure 4.27. Fluorescence anisotropy binding experiments of 1 μM 5(6)-FAM H3 K9Me$_3$ T6K histone tail with wild-type chromodomain. The centrifuged sample of chromodomain was centrifuged at 13000 rpm for ten minutes at 4 °C. The experiments were performed in 50 mM potassium phosphate buffer pH 8.0, 25 mM NaCl, and 4 mM DTT at 25 °C. Each curve is an average of 3 runs.

Table 4.9. A summary of the dissociation constants (μM) with R^2 in parenthesis. The data corresponds to the curves in Figure 4.27.

Not Centrifuged	Centrifuged
10±1 (0.998)	7±1 (0.995)

Another variable that had to be controlled for was the type of microplate used for the measurements. Costar produces plates with a treated surface to prevent protein and small molecules from binding to the plate as well as a plate with an untreated surface. Binding of the wild-type chromodomain to the H3 K9Me$_3$ T6K peptide was measured using both microplates (Fig. 4.28, Table 4.10). The data from the untreated plates provided more favorable dissociation constants and the error was considerably lower. The chromodomain does not interact with the untreated hydrophobic polystyrene plates,

but may interact with the hydrophilic surface of the treated plate. Therefore, the untreated plates were used for all anisotropy experiments.

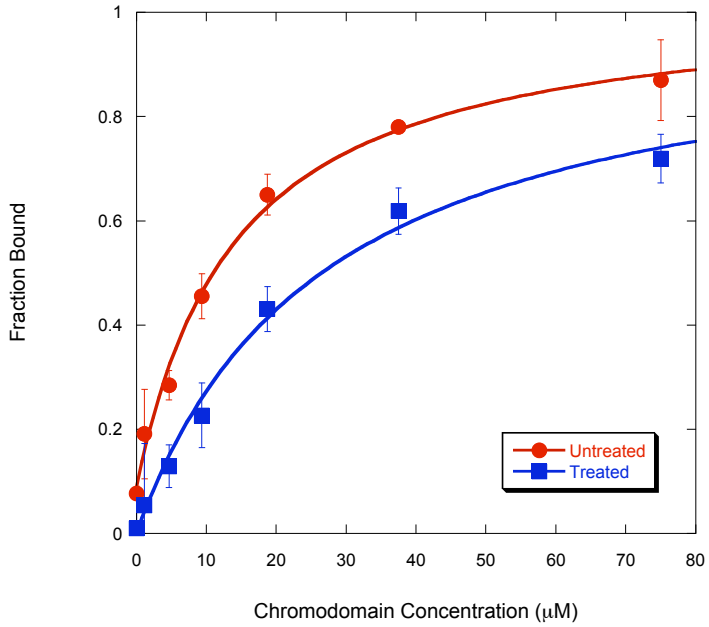

Figure 4.28. Fluorescence anisotropy binding experiments of 1 μM 5(6)-FAM H3 K9Me$_3$ T6K histone tail with wild-type chromodomain using untreated and treated microplates. The experiments were performed in 50 mM potassium phosphate buffer pH 8.0, 25 mM NaCl, and 4 mM DTT at 25 °C. Each curve is an average of 3 runs.

Table 4.10. A summary of the K_D (μM) with R^2 in parenthesis. The data corresponds to the curves in Figure 4.28.

Untreated Plate	Treated Plate
10±1 (0.998)	26±6 (0.993)

A final control that was performed tested whether 5(6)-carboxyfluorescein was interacting with the chromodomain directly. Therefore the fluorescence signal from all chromodomain and histone tail data was calculated from the raw polarization measurements using the Polarstar software. A 25% decrease in fluorescence signal was

observed in all of the data that had been collected from 0 to 300 μM chromdomain (Fig. 4.27). Fluorescence intensity of fluorescein depends strongly on the environment such as varying protein concentrations. Since the decrease in signal was consistent irrespective of the binding affinity and because 5(6)-carboxyfluorescein is the standard fluorophore used for investigating chromodomain-histone tail interactions, the fluorophore was used for all binding studies.

After all controls were performed the final experimental conditions were established. A POLARstar Omega microplate reader with untreated 96 half-area flat bottom plates (Costar 3694) was used for anisotropy measurements. Concentrated stocks of histone peptide with 5(6)-FAM on the N-terminus were prepared in 50 mM potassium phosphate, pH 8.0, 25 mM NaCl. The concentrations were measured using e_{492}=78,000 $M^{-1}cm^{-1}$ with a Perkin Elmer Lambda35 UV/VIS Spectrometer. A histone tail solution was then prepared with 2 μM peptide, 8 mM DTT and the same buffer as described above. Using a multichannel pipette, 50 μL peptide was added to each well of the Costar 3694 plate.

The chromodomain was thawed on ice and a 400 μL solution was prepared at 600 μM and 8 subsequent serial dilutions were made (1:2). Solutions were mixed by pipetting approximately twenty times and rather than by vortexing to avoid introducing air bubbles into the sample. The solutions were added to clear microplates (Costar 3795) with buffer as a blank, centrifuged for 1 min at 4,000 rpm to remove air bubbles and to draw any particulates to the bottom of the wells. Then 50 μL of chromodomain sample was added to the Costar 3694 plates using a multichannel pipette and mixed with the H3 peptide by pipetting the solution approximately ten times. This method of preparation

reduced the final concentrations of chromodomain, peptide, and DTT by half. The plates were centrifuged at 4000 rpm for 1 min to remove air bubbles.

All samples were allowed to reach equilibrium for 30-60 mins before measurements were taken. A timed experiment confirmed that there was no change in anisotropy signal between 30 and 60 mins. Measurements were taken with an excitation wavelength of 485 nm and an emission at 520 nm. The data was analyzed using Eq. 2.3 and the fraction of histone tail bound was calculated using Eq 2.4. The ΔG^o was calculated using Eq. 3.3. All binding curves except those previous highlighted are shown below in Fig. 4.29-4.36. Not all of the binding curves show a plateau because at the higher concentrations required for saturation, the chromodomain would aggregate.

v. Double-Mutant Cycle

Single and double mutations for studying A25K/K46 interactions were made to the HP1α chromodomain by expressing the following mutants: A25K/K46A, A25K/K46A, A25/K46A. The circular dichroism spectra and melting temperatures were measured as described above as where the dissociation constants. The ΔΔG was calculated as shown in Eq. 4.4:

$$\Delta\Delta G_{A25K-K46} = \Delta G^{o}{}_{A25K/K46} - \Delta G^{o}{}_{A25/K46} - \Delta G^{o}{}_{A25K/K46A} - \Delta G^{o}{}_{A25/K46A} \quad \text{Eq. 4.4}$$

Single mutations for studying D62F/ H3 R8 interactions were made to the HP1α chromodomain by expressing D62F and D62A chromodomain mutants. The histone tail, H3 K9Me_3 R8A was synthesized as previously described in Chapter III (see Table 4.4 for masses). The circular dichroism spectra and melting temperatures were measured as

described above as where the dissociation constants. The ΔΔG was calculated as shown in equation 4.5:

$$\Delta\Delta G_{D62F-R8} = \Delta G^{o}{}_{D62F/R8} - \Delta G^{o}{}_{D62F/R8A} - \Delta G^{o}{}_{D62A/R8} - \Delta G^{o}{}_{D62A/R8A} \quad \text{Eq. 4.5}$$

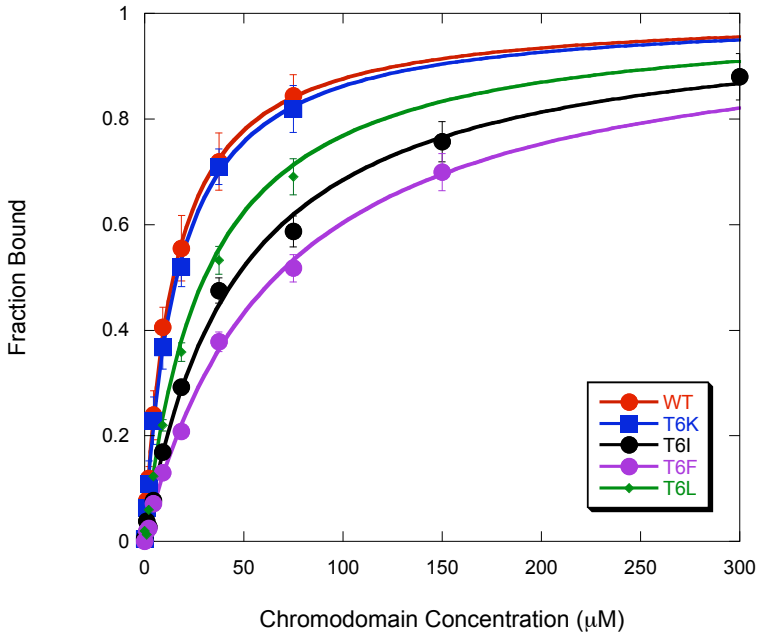

Figure 4.29. Fluorescence anisotropy binding experiments of 1 μM 5(6)-FAM H3 K9Me$_3$ histone tail mutants with chromodomain A25F. The experiments were performed in 50 mM potassium phosphate buffer pH 8.0, 25 mM NaCl, and 4 mM DTT at 25 °C. Each curve is an average of 3 runs.

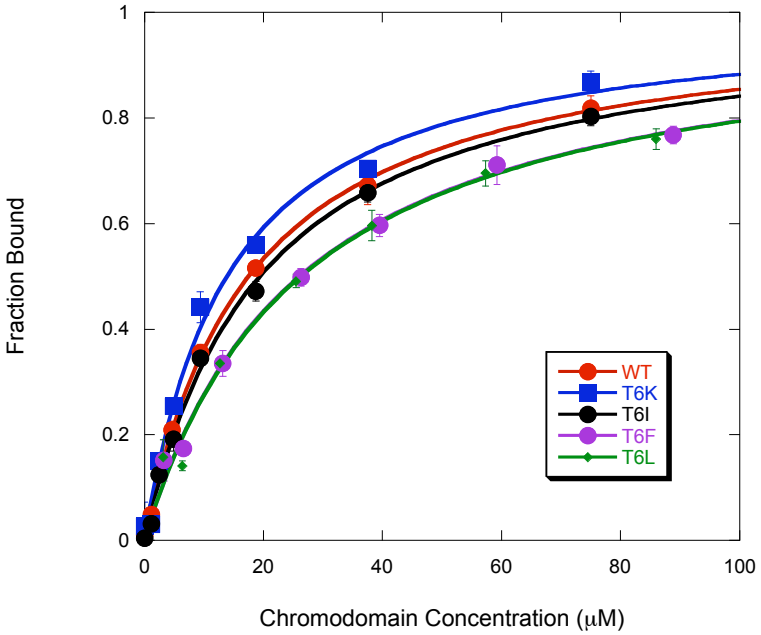

Figure 4.30. Fluorescence anisotropy binding experiments of 1 μM 5(6)-FAM H3 K9Me$_3$ histone tail mutants with chromodomain A25L. The experiments were performed in 50 mM potassium phosphate buffer pH 8.0, 25 mM NaCl, and 4 mM DTT at 25 °C. Each curve is an average of 3 runs.

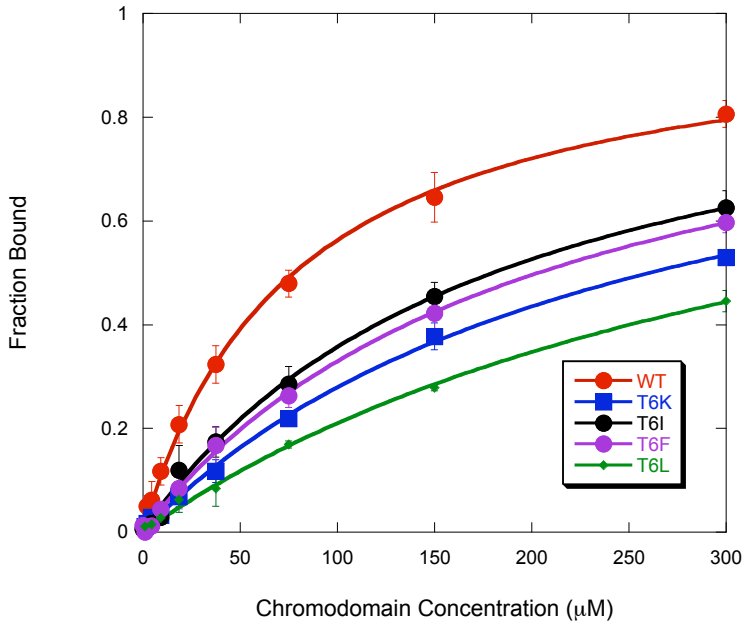

Figure 4.31. Fluorescence anisotropy binding experiments of 1 μM 5(6)-FAM H3 K9Me$_3$ histone tail mutants with chromodomain A25K. The experiments were performed in 50 mM potassium phosphate buffer pH 8.0, 25 mM NaCl, and 4 mM DTT at 25 °C. Each curve is an average of 3 runs.

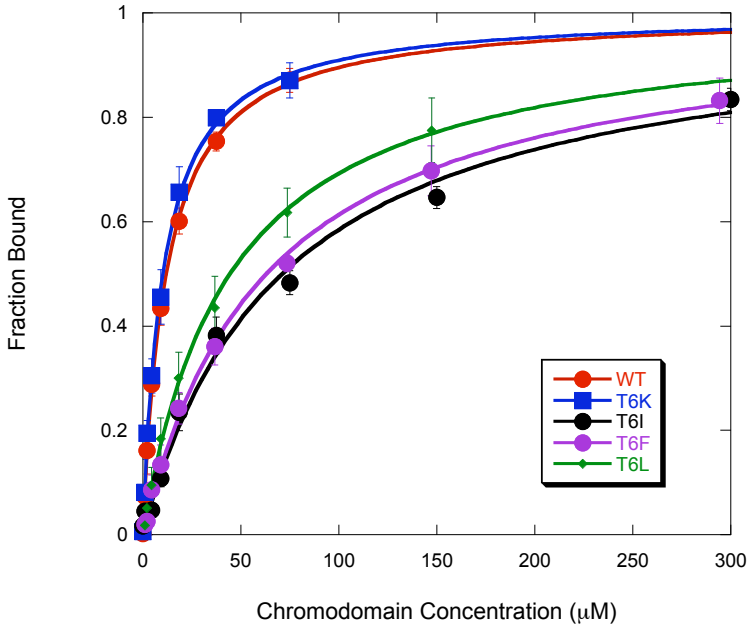

Figure 4.32. Fluorescence anisotropy binding experiments of 1 μM 5(6)-FAM H3 K9Me$_3$ histone tail mutants with chromodomain A25T. The experiments were performed in 50 mM potassium phosphate buffer pH 8.0, 25 mM NaCl, and 4 mM DTT at 25 °C. Each curve is an average of 3 runs.

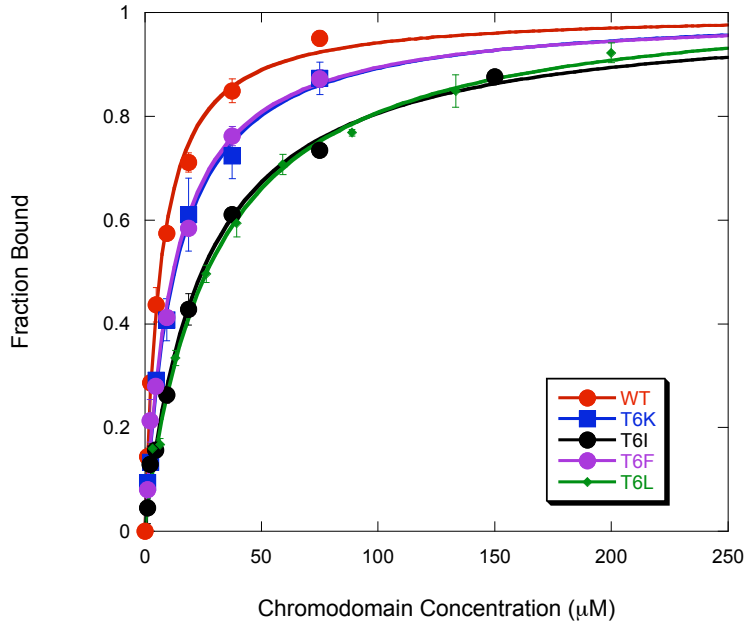

Figure 4.33. Fluorescence anisotropy binding experiments of 1 μM 5(6)-FAM H3 K9Me$_3$ histone tail mutants with chromodomain D62F. The experiments were performed in 50 mM potassium phosphate buffer pH 8.0, 25 mM NaCl, and 4 mM DTT at 25 °C. Each curve is an average of 3 runs.

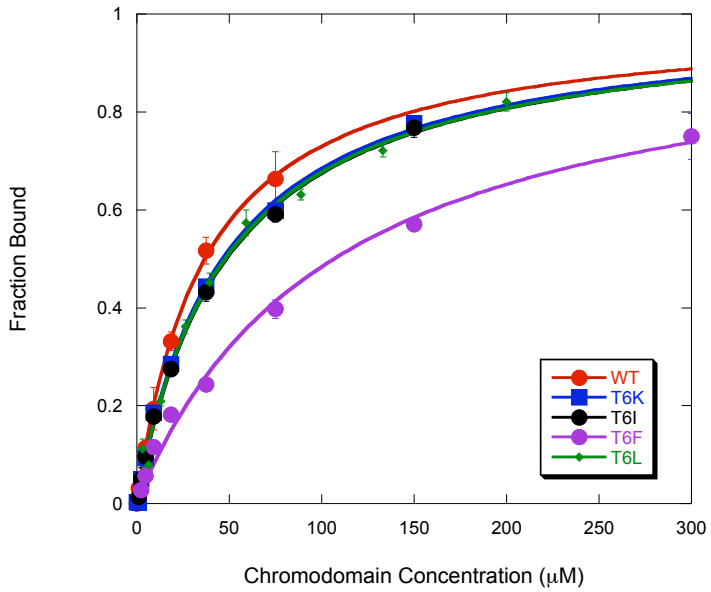

Figure 4.34. Fluorescence anisotropy binding experiments of 1 μM 5(6)-FAM H3 K9Me$_3$ histone tail mutants with chromodomain D62I. The experiments were performed in 50 mM potassium phosphate buffer pH 8.0, 25 mM NaCl, and 4 mM DTT at 25 °C. Each curve is an average of 3 runs.

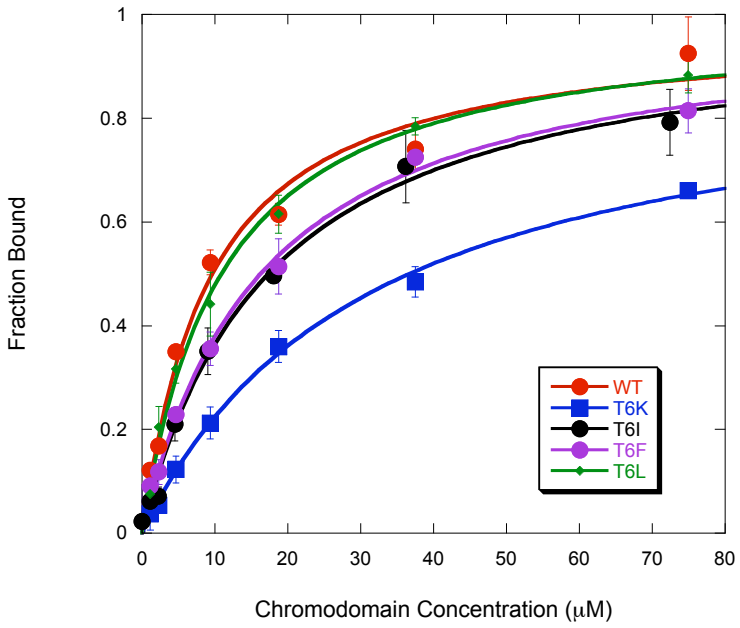

Figure 4.35. Fluorescence anisotropy binding experiments of 1 μM 5(6)-FAM H3 K9Me$_3$ histone tail mutants with chromodomain D62K. The experiments were performed in 50 mM potassium phosphate buffer pH 8.0, 25 mM NaCl, and 4 mM DTT at 25 °C. Each curve is an average of 3 runs.

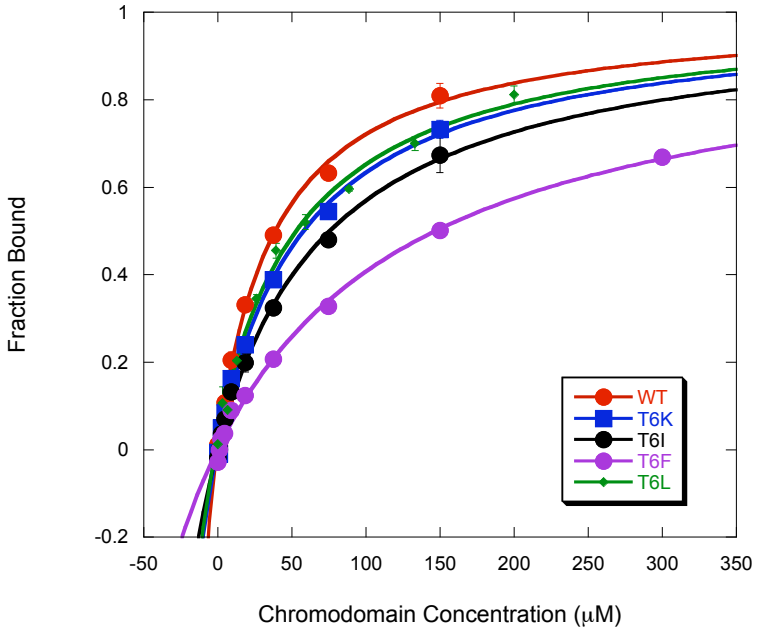

Figure 4.36. Fluorescence anisotropy binding experiments of 1 μM 5(6)-FAM H3 K9Me$_3$ histone tail mutants with chromodomain D62T. The experiments were performed in 50 mM potassium phosphate buffer pH 8.0, 25 mM NaCl, and 4 mM DTT at 25 °C. Each curve is an average of 3 runs.

References

1. Lee, D. Y.; Teyssier, C.; Strahl, B. D.; Stallcup, M. R., Role of Protein Methylation in Regulatio of Transcription. *Endocr Rev* **2005,** *26*, 147-170.

2. Jacobs, S. A.; Khorasanizadeh, S., Structure of HP1 chromodomain Bound to a Lysine 9-Methylated Histone H3 Tail. *Science* **2002,** *295*, 2080-2083.

3. Bannister, A. J.; Zegerman, P.; Partidge, J. F.; Miska, E. A.; Thomas, J. O.; Allshire, R. C.; Kouzarides, T., Selective Recognition of Methylated Lysine 9 on Histone H3 by the HP1 Chromo Domain. *Nature* **2001,** *410*, 120-124.

4. Lachner, M.; O'Carroll, D.; Rea, S.; Mechtler, K.; Jenuwein, T., Methylation of Histone H3 Lysine 9 Creates a Binding Site for HP1 Proteins. *Nature* **2001,** *410*, 116-120.

5. Nakayama, J.-I.; Rice, J. C.; Strahl, B. D.; Allis, C. D.; Grewal, S. I. S., Role of Histone H3 Lysine 9 Methylation in Epigenetic Control of Heterochromatin Assembly. *Science* **2001,** *292*, 110-113.

6. Maison, C.; Bailly, D.; Peters, H. E. M.; Quivy, J. P.; Roche, D.; Taddei, A.; Jenuwein, T.; Almousni, G., Higher-Order Structure in Pericentric Heterochromatin Involves a Distinct Pattern of HIstone Modification and an RNA Component. *Nat Genet* **2002,** *30*, 329-334.

7. Nielson, R. R.; Nietlispach, D.; Mott, H. R.; Callaghan, J.; Bannister, A.; Kousarides, T.; Murzin, A. G.; Murzina, N. V.; Laue, E. D., Stucture of the HP1 chromodomain Bound to Histone H3 Methylated at Lysine9. *Nature* **2002,** *416*, 103-107.

8. Hughes, R. M.; Wiggins, K. R.; Khorasanizadeh, S.; Waters, M. L., Recognition of Trimethyllysine by a chromodomain is not Driven by the Hydrophobic Effect. *Proc Natl Acad Sci* **2007,** *104*, 11184-11188.

9. Fischle, W.; Wang, Y.; Jacobs, S. A.; Kim, Y.; Allis, C. D.; Khorasanizadeh, S., Molecular Basis for the Discrimination of Repressive Methyl-Lysine Marks in Histone H3 by Polycomb and HP1 chromodomains. *Genes Dev* **2003,** *17*, 1870-1881.

10. Hutchinson, E. G.; Sessions, R. B.; Thornton, J. M.; Woolfson, D. N., Determinants of Strand Register in Antiparallel β-sheets of Proteins. *Protein Sci* **1998,** *7*, 2287-2300.

11. Wouters, M. A.; Curmi, P. M. G., An Analysis of Side Chain Interactions and Pair Correlations Within Antiparallel β-Sheets: The Differences Between Backbone H-bonded and Non-H-bonded Residue Pairs. *Proteins* **1995,** *22*, 119-131.

12. Williams, R. W.; Chang, A.; Juretić, D.; Loughran, S., Secondary Structure Predictions and Medium Range Interactions. *Biochim Biophys Acta* **1987,** *916*, 200-204.

13. Smith, C. K.; Regan, L., Construction and Design of β-Sheets. *Acc Chem Res* **1997,** *30*, 153-161.

14. Smith, C. K.; Regan, L., Guidelines for Protein Design: The Energetics of β--Sheet Side Chain Interactions. *Science* **1995,** *270*, 980-982.

15. Russell, S. J.; Cochran, A. G., Designing Stable β-Hairpins: Energetic Contributions from Cross-Strand Residues. *J Am Chem Soc* **2000,** *122*, 12600-12601.

16. Tatko, C. D.; Waters, M. L., Selective Aromatic Interactions in β-Hairpin Peptides. *J Am Chem Soc* **2002,** *124*, 9372-9373.

17. Tatko, C. D.; Waters, M. L., The Geometry and Efficacy of Cation-π Interactions in a Diagonal Position of a Desgined β-Hairpin. *Protein Sci* **2003,** *12*, 2443-2452.

18. Greenfield, N. J., Methods to Estimate the Conformation of Proteins and Polypeptides from Circular Dichroism Data. *Anal Biochem* **1996,** *235*, 1-10.

19. Jacobs, S. A.; Taverna, S. D.; Zhang, Y.; Briggs, S. D.; Li, J.; Eissenberg, J. C.; Allis, C. D.; Khorasanizadeh, S., Specificity of the HP1 Chromo Domain for the Methylated N-Terminus of Histone H3 *EMBO J* **2001,** *20*, 5232-5241.

20. Daujat, S.; Zeissler, U.; Waldmann, T.; Happel, N.; Schneider, R., HP1 Bind Specifically to Lys^{26} Methylated Histone 1.4, Whereas Simultaneous Ser^{27} Phosphorylation Blocks HP1 Binding. *J Biol Chem* **2005,** *280*, 28090-28095.

21. Smith, C. K.; Withka, J. M.; Regan, L., A Thermodynamic Sale for the β-Sheet Forming Tendencies of the Amino Acids. *Biochemistry* **1994,** *33*, 5510-5517.

22. Schreiber, G.; Fersht, A. R., Energetics of Protein-Protein Interactions: Analysis of the Barnase-Barstar Interface by Single Mutations and Double Mutant Cycles. *J Mol Biol* **1995,** *248*, 478-486.

23. Riemen, A. J.; Waters, M. L., Controlling Peptide Folding with Repulsive Interactions Between Phosphorylated Amino Acids and Tryptophan. *J Am Chem Soc* **2009,** *131*, 14081-14087.

24. Pace, C. N.; Scholtz, J. M., A Helix Propensity Scale Based on Experimental Studies of Peptides and Proteins. *Biophys J* **1998,** *75*, 422-427.

25. Chochran, A. G.; Tong, R. T.; Starovasnik, M. A.; Park, E. J.; McDowell, R. S.; Theaker, J. E.; Skelton, N. J., A Minimal Peptide Scaffold for β-Turn Display:

Optimizing a Strand Position in Disulfide-Cyclized β-Hairpins. *J Am Chem Soc* **2001,** *123*, 625-632.

26. Syud, F. A.; Stanger, H. E.; Gellman, S. H., Interstrand Side Chain-Side Chain Interactions in a Designed β-Hairpin: Significance of Both Lateral and Diagonal Pairings. *J Am Chem Soc* **2001,** *123*, 8667-8677.

27. Russell, S. J.; Blandl, T.; Skelton, N. J.; Cochran, A. G., Stability of Cyclic β-Hairpins: Asymmetric Contributions from Side Chains of a H-bonded Cross-Strand Residue Pair. *J Am Chem Soc* **2002,** *124*, 388-395.

28. Minor, D. L.; Kim, P. S., Context is a Major Determinant of β-Sheet Propensity. *Nature* **1994,** *371*, 264-267.

29. Meyer, E. A.; Catellano, R. K.; Diederich, F., Interactions with Aromatic Rings in Chemical and Biological Recognition. *Angew Chem Int Ed* **2003,** *42*, 1210-1250.

30. Hunter, C. A.; Lawson, K. R.; Perkins, J.; Urch, C. J., Aromatic Interactions. *J Chem Soc-Prkin Trans* **2001,** *2*, 651-669.

31. Jackrel, M. E.; Valverde, R.; Regan, L., Redesign of a Protein-Peptide Interaction Characterization and Applications. *Protein Sci* **2009,** *18*, 762-774.

32. Chait, B. T., Mass Spectrometry: Bottom-Up or Top-Down? *Science* **2006,** *2006* (314), 65-66.

33. Schalch, T.; Job, G.; Noffsinger, V. J.; Shanker, S.; Kuscu, C.; Joshua-Tor, L.; Partridge, J. F., High-Affinity Binding of Chp1 chromodomaini to K9 Methylated Histone H3 Is Required to Establish Centromeric Heterochromatin. *Mol Cell* **2009,** *34*, 36-46.

34. Invitrogen, Chapter 8: Analysis of FP Binding Data. *Invitrogen Corporation*.

Chapter V

TOWARDS DEVELOPING RECEPTORS FOR DETECTING DUAL POST-TRANSLATIONAL HISTONE MODIFICATIONS

A. Background

i. Cross-Regulation Between Post-Translational Modifications

Histone modifications most commonly occur in combination to create a "code", which can drastically alter how they are "read" by effector proteins. For example when Ser10 on H3 becomes phosphorylated it acts as a switch, ejecting HP1 from this histone to reactivate gene expression.[1] Dual modifications are also capable of recruiting multivalent effector proteins such as TAF1 (TATA-binding protein-associated factor-1), which can bind to multi-acetylated sites.[2] Some modifications are also known to promote or inhibit further modifications. For example, specific lysine methyl marks can recruit histone deacetylases (HDAC) or histone acetyltransferases (HATs) to perpetuate gene silencing or expression.[3] Significant research has been performed to determine which modifications occur in conjunction with one another and to understand how multiple modifications elicit specific biological functions. However, there are still many modifications and potential combinations of modifications that must be identified.

ii. Identifying Post-Translational Modifications

Two techniques are presently used to identify PTMs in histones: mass spectrometry and antibodies for ChIP and Western blot analysis.[4] Both of these methods are excellent for identifying a single PTM in proteins, but they are not necessarily practical for identifying combinations of PTMs within a single protein.[5]

Two protocols can be applied to mass spectrometry to analyze PTMs including the "bottom-up" approach and the "top-down" approach (Fig. 5.1). In the "bottom-up" approach, proteins are digested with proteases into peptide fragments, which are then analyzed by ESI. This technique gives information on the peptide sequences as well as the exact location of the modifications. However, since multiple proteins, which may have varying modifications, are present within the digest it is difficult to determine if two modifications came from the same protein. Additionally, some fragments may be too small or not in a high enough level to detect.[5, 6]

In the "top-down" method the proteins are fragmented in the gas phase within the mass spectrometer to produce a "ladder" of peptide fragments. The primary structure of the modified protein can be compared to an unmodified protein to isolate the site of modification. Often, the protein is not fully fragmented to generate the entire ladder and some of the more labile modifications such as phosphorylation can be dislodged from the protein and will remain undetected.[5, 6] It is also difficult to differentiate modifications that have similar molecular weights, such as KMe_3 and KAc, which differ by only one mass unit. While it is possible to fully characterize a modified protein by mass spectrometry, the combination of approaches required does not make this a practical method.

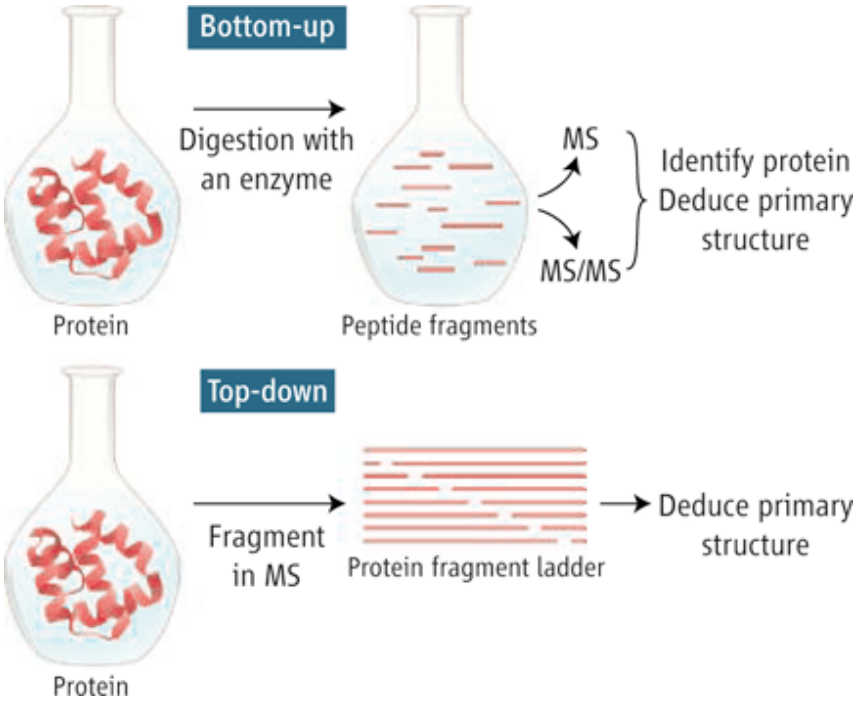

Figure 5.1. In the bottom-up approach (top), proteins of interest are digested with a protease, and the resulting peptides are analyzed in the gas phase by mass spectrometry. MS is used to determine the mass of the peptides and MS/MS is used to determine the peptide sequences and the modifications. In the top-down approach (bottom), protein ions are fragmented while in the gas phase and analyzed in the mass spectrometer, yielding the molecular mass of the protein as well as protein ion fragment ladders, which is used to determine the primary structure of the protein.[6]

The use of antibodies is also a very common strategy for identifying PTMs and for isolating them. This powerful technique can be used to identify specific PTM sites within a mixture of proteins. However, there are several drawbacks to using antibodies in addition to their cost and their inconsistency. Antibodies are not always sequence selective, they do not always select for specific methylation states, and they are influenced by the presence of neighboring PTMs, which makes determining which modifications are present within a sample difficult and uncertain.[7] Mixed protein samples with various PTMs are often difficult to visualize using both one- and two-dimensional gel electrophoresis especially if some proteins are in lower populations or if they co-

migrate. Additionally, it is nearly impossible to determine whether multiple PTMs that are visualized with antibodies are present in the same protein or in two different proteins.[5]

B. Goal

A new approach that overcomes the limitations of the methods available to analyze PTMs would be highly beneficial. In this research two PTM-recognition domains, or receptors, derived from naturally occurring effector proteins were coupled together to create a coupled-receptor construct to visualize dual modifications on a single histone tail. I first coupled two HP1α chromodomains to determine if they were functional for detecting a synthetic peptide with two H3 K9Me_2 sequences as proof that coupled receptors can have cooperative binding for a peptide with two methyllysine marks.

C. Results and Discussion

i. Initial System Design

The initial design of the coupled receptors involved linking them non-covalently so the recognition domains could be easily interchangeable to detect different sets of PTMs. To do this, the receptors were to be linked to one of two different peptides, which are capable of forming a parallel, heterodimeric coiled-coil motif. The peptides were to have either a FRET donor or acceptor on the N-terminus and a thiol-reactive maleimide linker on the C-terminus so the peptides could be conjugated to the chromodomain via a cysteine (Fig. 5.2). If the coiled-coils have favorable binding then the receptors should be dimerized in solution to promote cooperative binding to the modified histone peptide.

As long as cooperative binding results in 100-fold enhanced binding then background noise from a receptor binding to a single PTM should be relatively low. Such phenomenon is not unprecedented as demonstrated by Melkko and coworkers who used duplex DNA as a scaffold to generate a bidentate biotin ligand for streptavidin.[8] The bidentate ligand had a 2000-fold improvement in binding affinity to streptavidin compared to the free biotin due to the chelate effect. Williams and coworkers used duplex DNA as a scaffold for two peptides to form a bivalent affinity reagent, which is able to bind to two different sites of a protein.[9] The bivalent reagent with two peptides had an affinity to the target protein 4000-fold more favorable than the individual peptides.

(A)

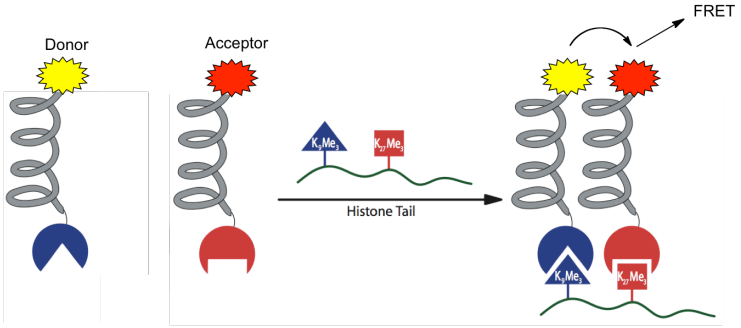

(B)

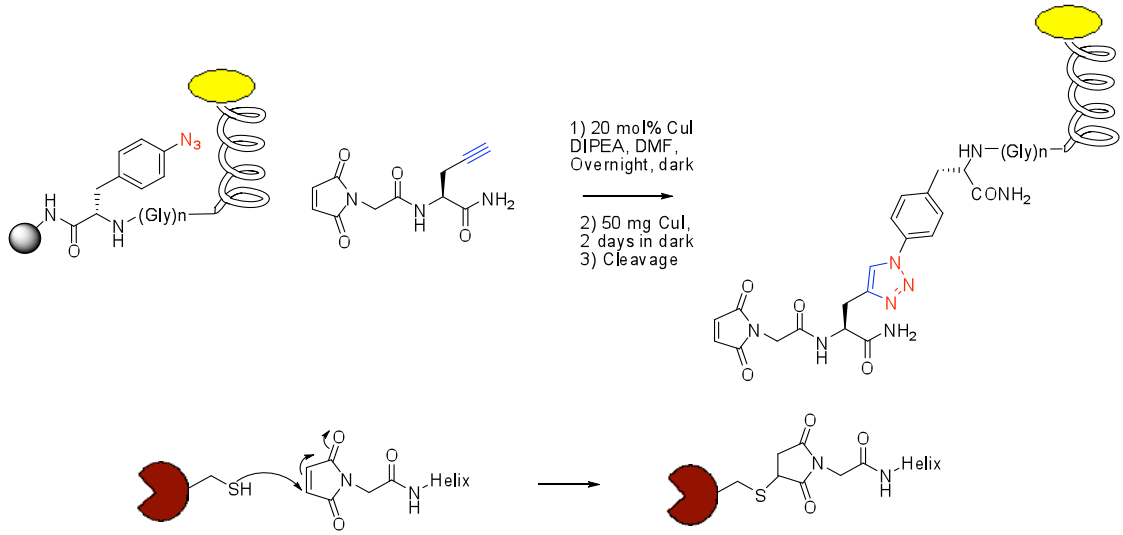

Figure 5.2. (A) Initial design of the coupled receptors. The coiled-coil peptides are labeled with a FRET pair and will dimerize when the recognition domains bind the dual-modified histone tail. FRET will be used to visualize the presence of two modifications of interest, which in this case are H3 K9Me$_3$ and H3 K27Me$_3$. (B) Synthetic scheme for the initial design.

ii. Chromodomain Cysteine Mutants

The receptors were to be conjugated using a cysteine within the receptor and a thiol-reactive functional group such as a maleimide or bromoacetamide within the coiled-coil peptides. A naturally occurring cysteine is already located near the binding pocket of HP1α chromodomain at position 63. The cysteine, which is shown to face the interior of the protein in the crystal structure, appeared to be unreactive and biotin-maleimide could not be conjugated to the chromodomain. Therefore, four cysteine point mutations were

made to the chromodomain at locations shown to be more solvent exposed and appeared to be involved in minimal interactions with other neighboring residues (Fig. 5.3).

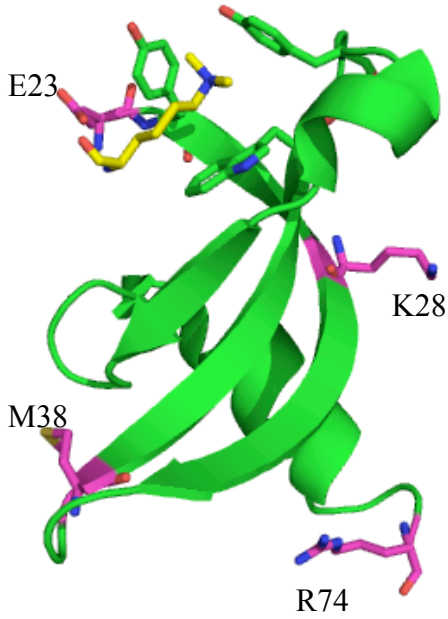

Figure 5.3. The location of the four different cysteine point mutations made to the HP1α chromodomain. The chromodomain is shown in green. The mutated amino acids are shown in purple. The trimethyllysine is shown in yellow. The aromatic cage is shown in green sticks (PDB 1KNE).

(1) Structural Characterization

Circular dichroism spectrum of each mutant was collected to determine how the cysteine mutations affected the global structure of the chromodomain (Fig. 5.4). The minima at 208 nm and 222 nm and the exciton coupling peak at 232 nm for each mutant are consistent with the native chromodomain. Therefore the global structure was not perturbed by the point mutations. The thermal stability was also ascertained by thermal denaturation monitored at 222 nm by circular dichroism (Fig. 5.5). All mutants have a melting temperature within 2 ^{o}C of the wild-type proteins, confirming the stability of each chromodomain.

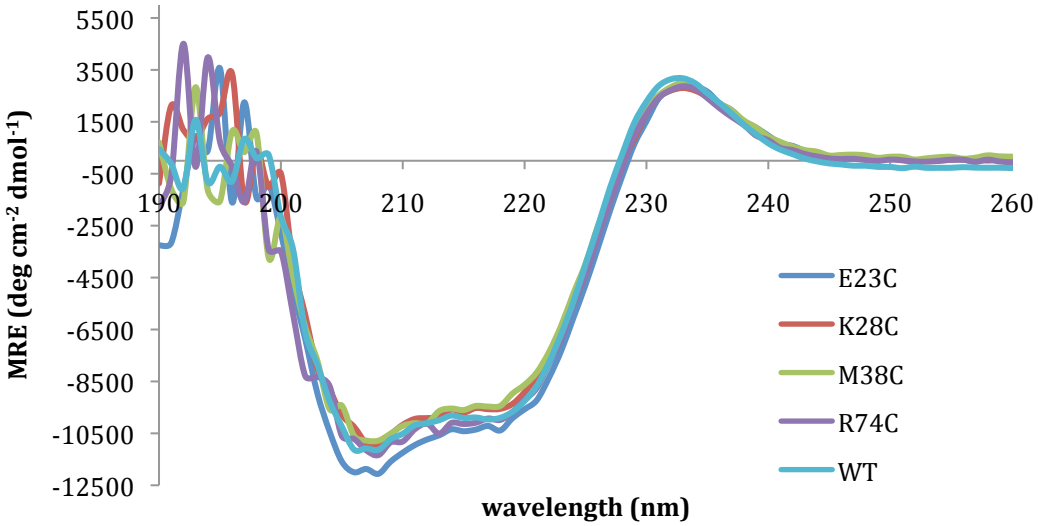

Figure 5.4. Circular dichroism spectra comparison of HP1α Chromodomain to the cysteine mutants at 25°C in 10 mM sodium phosphate pH 7.4 with 2 mM DTT. These are the averages of three runs.

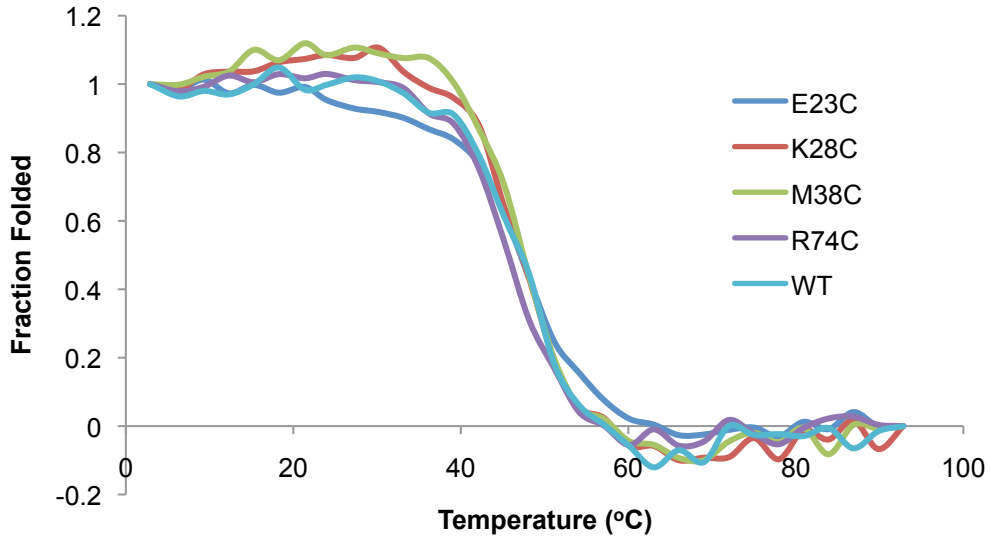

Figure 5.5. Thermal denaturation monitored by circular dichroism at 222 nm of HP1α Chromodomain WT and the cysteine mutants in 10 mM sodium phosphate pH 7.4 and 2 mM DTT.

Table 5.1. Melting temperatures of HP1α chromodomain and the cysteine mutants determined using the thermal denaturation curves in Fig. 5.5. The T_m values were estimated from the inflection points of the curve.

	WT	**E25C**	**K28C**	**M38C**	**R74C**
T_m (^oC)	47	47	47	46	45

(2) Binding Studies

The HP1α chromodomain cysteine mutants must maintain binding affinity to the H3 K9Me_3 for them to be viable receptors. The affinity of the chromodomain cysteine mutants for the H3 K9Me_3 histone tail was confirmed using fluorescence anisotropy. The binding curves are shown in Fig. 5.6 through Fig. 5.9 and the dissociation constants are summarized in Table 5.2. In each case the cysteine mutants have similar or even slightly higher binding affinity for the trimethyllysine 9 Histone H3 peptide. Therefore the residues that were mutated are not important for binding affinity and can be manipulated without having and effect on binding affinity.

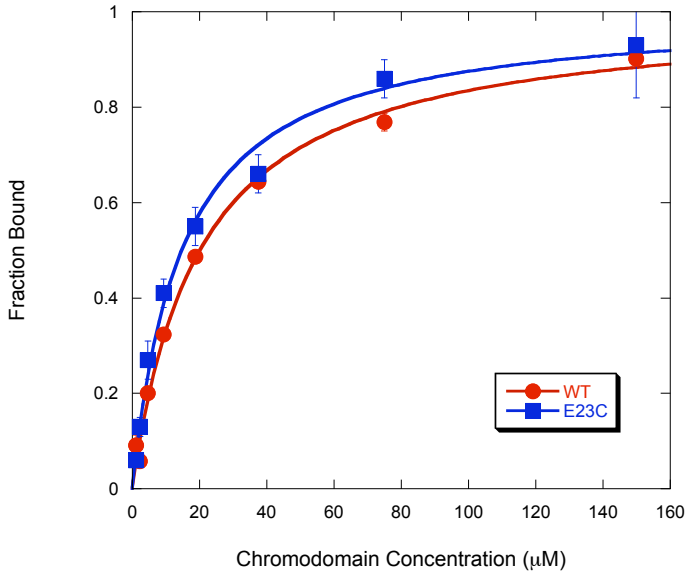

Figure 5.6. Fluorescence anisotropy binding experiments of 1 μM 5(6)-FAM H3 K9Me$_3$ histone tail with chromodomain wild-type and E23C. The experiments were performed in 50 mM potassium buffer pH 8.0, 25 mM NaCl, and 4 mM DTT at 25 °C. Each curve is an average of 3 runs.

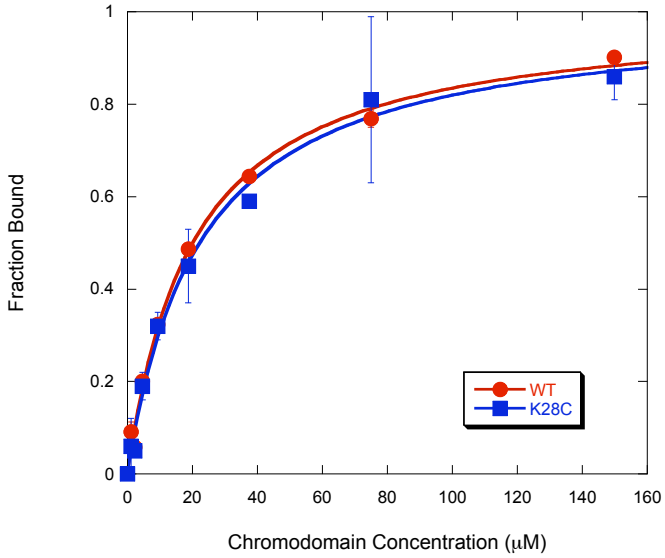

Figure 5.7. Fluorescence anisotropy binding experiments of 1 μM 5(6)-FAM H3 K9Me$_3$ histone tail with chromodomain wild-type and K28C. The experiments were performed in 50 mM potassium buffer pH 8.0, 25 mM NaCl, and 4 mM DTT at 25 °C. Each curve is an average of 3 runs.

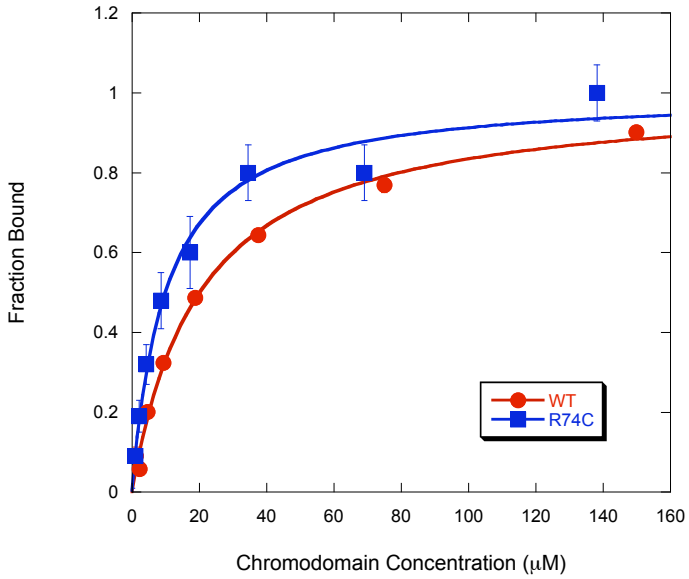

Figure 5.8. Fluorescence anisotropy binding experiments of 1 μM 5(6)-FAM H3 K9Me$_3$ histone tail with chromodomain wild-type and M38C. The experiments were performed in 50 mM potassium buffer pH 8.0, 25 mM NaCl, and 4 mM DTT at 25 °C. Each curve is an average of 3 runs.

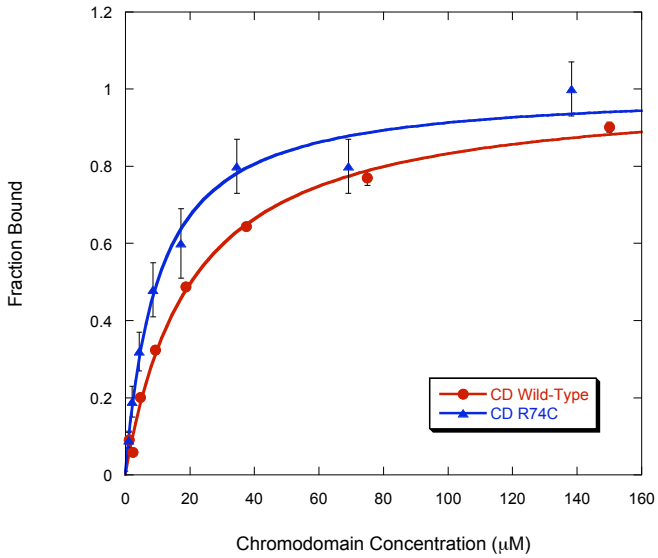

Figure 5.9. Fluorescence anisotropy binding experiments of 1 μM 5(6)-FAM H3 K9Me$_3$ histone tail with chromodomain wild-type and R74C. The experiments were performed in 50 mM potassium buffer pH 8.0, 25 mM NaCl, and 4 mM DTT at 25 °C. Each curve is an average of 3 runs.

Table 5.2. Fluorescence anisotropy binding data from Fig. 5.6 through Fig. 5.9 of HP1α chromodomain with H3 K9Me$_3$. The dissociation constants are in μM with the R^2 in parenthesis. The experiments were performed in 50 mM potassium buffer pH 8.0, 25 mM NaCl, and 4 mM DTT at 25 °C. Each curve is an average of 3 runs.

Chromodomain	K_D (μM)
WT	17 ± 1 (0.999)
E23C	14 ± 2 (0.993)
K28C	22 ± 3 (0.993)
M38C	11 ± 1 (0.998)
R74C	10 ± 2 (0.987)

iii. Coiled-coil Design

Alpha-helical coiled-coils are protein motifs that are ubiquitous in biological systems. They are important for cytoskeleton formation, mediation of protein-protein interactions involved in DNA expression, viral pathogenesis, and a number of other biological functions. Therefore the structure and design of coiled-coils have been extensively characterized.[10]

A coiled-coil is a structure that consists of two to four strands of amphipathic peptides engaged in a left-handed twist. The peptide sequences consist of seven-residue or heptad repeats commonly denoted as **a-b-c-d-e-f-g** (Fig. 5.10). To promote coiled-coil packing, hydrophobic residues are placed in three and four residues apart (positions **a** and **d**). Isoleucine residues placed in position **a** and leucine residues are placed in position **d** to promote dimmer formation and disfavor trimers.[11] Residues **e** and **g** neighbor the hydrophobic core and consist of charged side chains that can promote either a heterodimer or homodimer depending on the charge of the residues.[12]

(A)

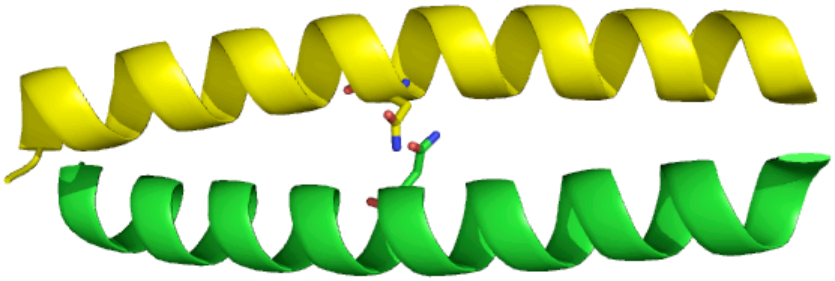

(B)

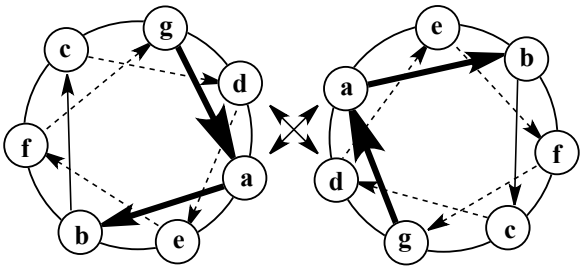

Figure 5.10. **(A)** X-ray structure of the GCN4 leucine zipper (pdb 2azt). (B) Generic helical wheel diagram.

The coiled-coil used in this study was based on the *de novo* three-heptad repeat, ISAL E3/K3 sequence, which was designed by Hodges and coworkers. The coiled-coil was designed with a hydrophobic core consisting of isoleucines and leucines, which interlock in a knobs-in-holes fashion and has a reported K_D of 9 μM.[13, 14] Like the original sequences, glutamates were incorporated in the **g** and **e** positions of the E3 peptide and lysine residues were incorporated in the **g** and **e** positions of the K3 peptide. Having complementary charged residues in these positions promotes the formation of heterodimers so two different PTM receptors are coupled together (Fig. 5.11A).[13, 15] The two receptors must also be aligned in the same direction so they can bind to a single histone tail. Proper alignment was accomplished designing parallel coiled-coils. In nature, parallel GCN4 leucine zippers contain an asparagine in a single **a** position of each

peptide (Fig. 5.10A). Though the incorporation of polar residues within the core is destabilizing, they form an intermolecular H-bond in a parallel coiled-coil, but are misaligned in an anti-parallel coiled-coil. Thus, they are significantly disfavored in antiparallel coiled-coils and in trimers and promote parallel dimers.[16] In the *de novo* design one asparagine was incorporated into the hydrophobic core (**a**2 position) of each peptide to promote a parallel orientation orientation.[17]

(A)

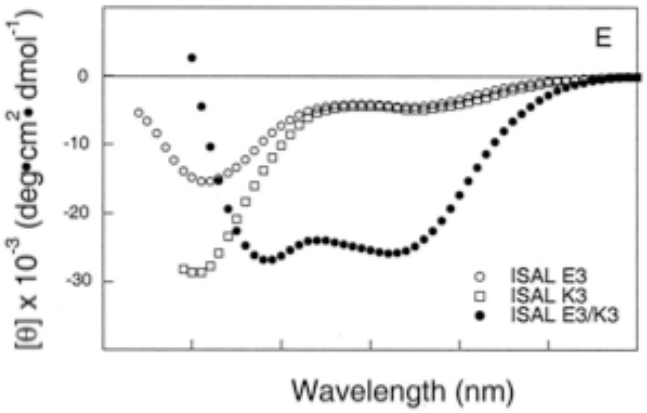

(B)

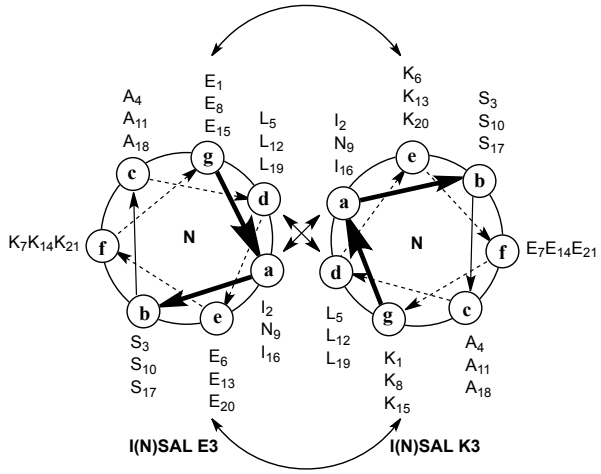

Figure 5.11. (A) Circular dichroism spectra of the ISAL E3/K3.[13] (B) Helical wheel diagram of the I(N)SAL E4/K4 sequences. Arrows indicate point of interaction between the two peptides.

The peptides were initially synthesized without the linker or fluorophore for preliminary characterization by circular dichroism (Fig. 5.12). The minimum at approximately 200 nm indicates that the two peptides do not form a coiled-coil, even in an equi-molar heterogeneous mixture. Though the ISAL E3/K3 peptides are capable of forming heterodimers, the asparagines are likely too destabilizing to the hydrophobic core.

To further stabilize the structure, the coiled-coil was extended to a four-heptad repeat with a tyrosine at position 21 for measuring concentration by UV/VIS (I(N)SAL E4/K4). The CD spectra of the individual peptides show a minimum at 200 nm, which indicates a random coil structure. An equi-molar mixture of the two peptides yields two minima at 208 nm and 222 nm, which confirm α-helix structure (Fig. 5.13).

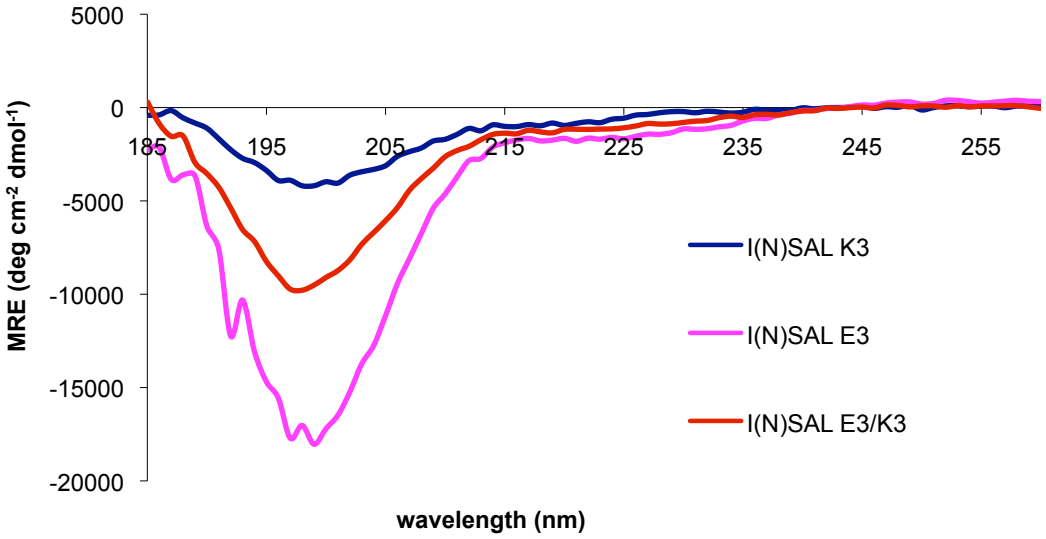

Figure 5.12. Circular dichroism spectra of I(N)SAL E3/K3 peptides. Measurements were taken in 10 mM $NaPO_4$ pH 7.0 with a total peptide concentration of 100 μM (50 μM of each peptide for the equi-molar E3/K3 mixture).

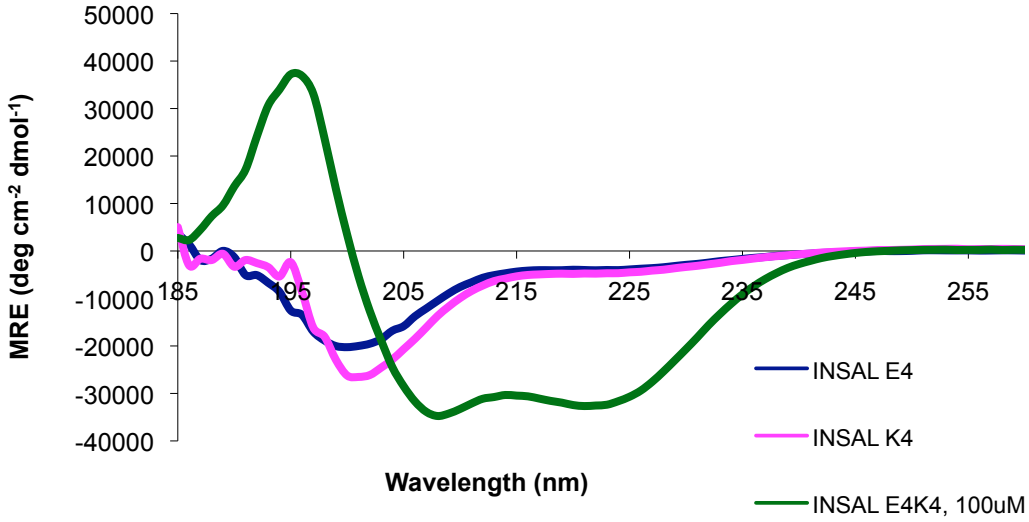

Figure 5.13. Circular dichroism spectra of I(N)SAL E4/K4 peptides. Measurements were taken in 10 mM $NaPO_4$ pH 7.0 with a total peptide concentration of 100 μM (50 μM of each peptide for the mixture).

A low dissociation constant in the nanomolar range between the coiled-coil peptides was necessary to promote cooperative binding of the coupled receptor to the dual-modified histone tail The low nanomolar range is ideal because the coiled-coils will be dimerized in solution. Guanidine denaturation was used to measure the dissociation constant between the two peptides. Samples of 100 μM mixtures of I(N)SAL E4/K4 peptides were prepared with increasing concentrations of guanidine hydrochloride. Denaturation was monitored by circular dichroism at 222 nm, which is a characteristic minimum for α-helices. The concentration of guanidine was increased until the denaturation curve reached a plateau (Fig. 5.14). From this data, the ΔG of folding in the presence of various concentrations of guanidine was calculated using the data in the most linear region of the denaturation curve (Fig. 5.15). The ΔG of folding in the absence of denaturant was determined by extrapolation to yield a final K_D of 3 μM. Though this is a strong K_D compared to the previously reported value for ISAL E3/K3 (9 μM), a value in

the low nanomolar range was desired. A dissociation constant in the nanomolar range is preferred so the receptors will be dimerized in solution prior to binding to the histone peptides.[13] Therefore, the coupled receptors were redesigned to incorporate a covalent link between the coiled-coil peptides at the C-terminus as opposed to relying on self-assembly.

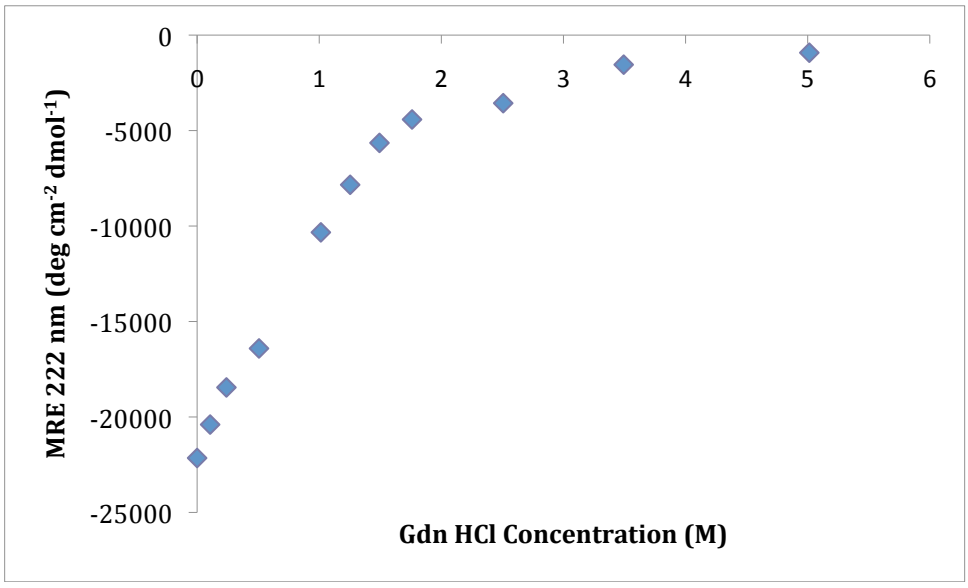

Figure 5.14. Guanidine denaturation of I(N)SAL E4/K4 monitored by CD at 222 nm in 50 mM potassium phosphate pH7.0, 100 mM NaCl buffer at 25°C.

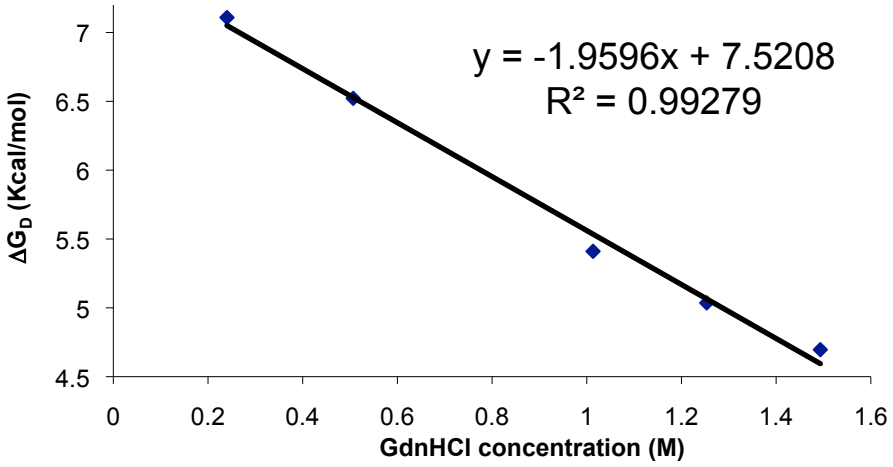

Figure 5.15. The ΔG of folding in the presence of various concentrations of guanidine was calculated using the data from the linear region of the denaturation curve in Fig. 5.15.

iv. New System Design

(1) Covalently Linked Coiled-coils

In the new design, we introduced a covalent link at the C-terminus of the coiled-coils. Since the coiled-coils were covalently linked at the C-terminus, there was no longer a need for asparagines within the hydrophobic core of the peptide to promote a parallel coiled-coil. The ISAL E4/K4 peptides were also reduced to a three-heptad repeat due to the added stability of linking the two peptides and the removal of the polar residue from the core. Shortening the peptides by seven amino acids improved the yield of the peptides and the length of time required for solid phase peptide synthesis.

First, the coiled-coils were covalently linked using a disulfide bond between two cysteine residues at the C-terminus with two glycine residues as spacers at both the N- and C-termini. Disulfide exchange of the peptide was monitored over the course of four days to confirm that the parallel heterodimer is favored over parallel homodimer (Fig.

5.16). As shown on Day 1, the peptides first appeared as monomers with a small amount of homodimer or heterodimer. By the fourth day, equilibration was complete and the primary peak observed in the heterogeneous mixture was the heterodimer with only a small peak for the ISAL K3-GGC monomer, due to a presence of a slight excess of the peptide. The K_{eq} was calculated to be 79 with a favorable ΔG of -1.8 Kcal/mol while a statistical mixture of homodimers to heterodimer would yield a K_{eq} of only 4. Thus, the equilibrium strongly favors the heterodimer over the two homodimers.

The structure of the peptide was also characterized using circular dichroism to confirm the presence of α-helical structure (Fig. 5.17). It is clear that the mixture of the two different peptides results in the formation of α-helix while the homogenous mixtures remain as random coil, which demonstrates the stability of the heterodimer compared to the homodimers.

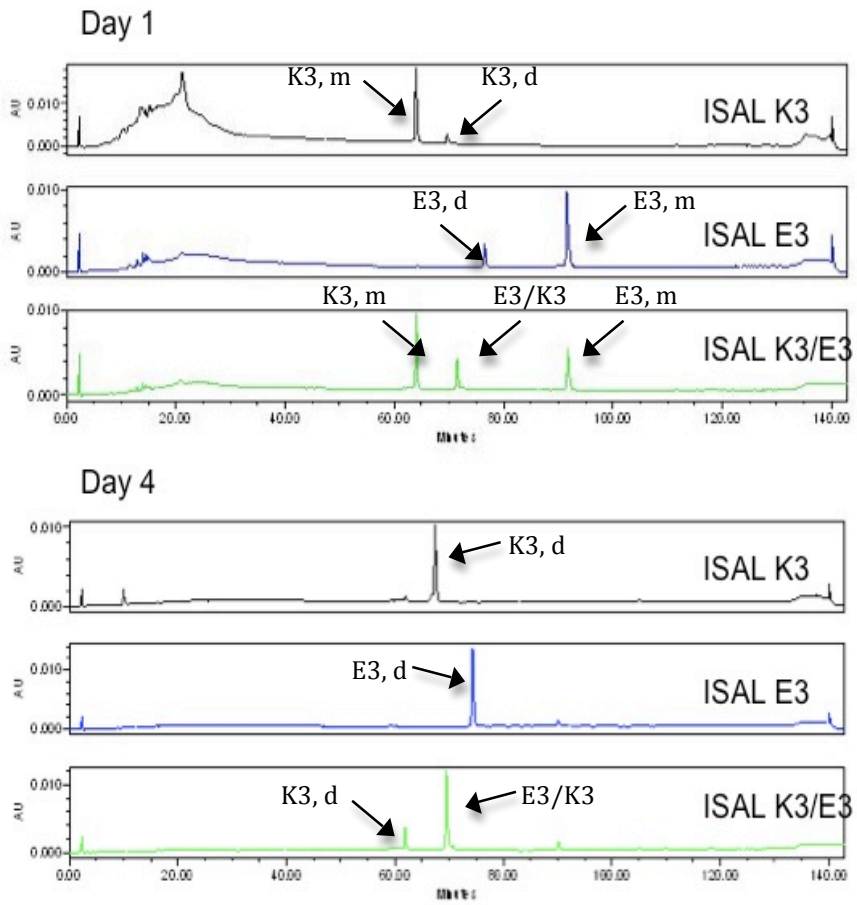

Figure 5.16. Disulfide exchange of ISAL E3/K3 peptides monitored by analytical HPLC. K3,m and K3,d refer to K3 monomer and homodimer respectively. E3,m and E3,d refer to E3 monomer and homodimer respectively. E3/K3 refers to heterodimer. The peaks were confirmed by mass spectrometry.

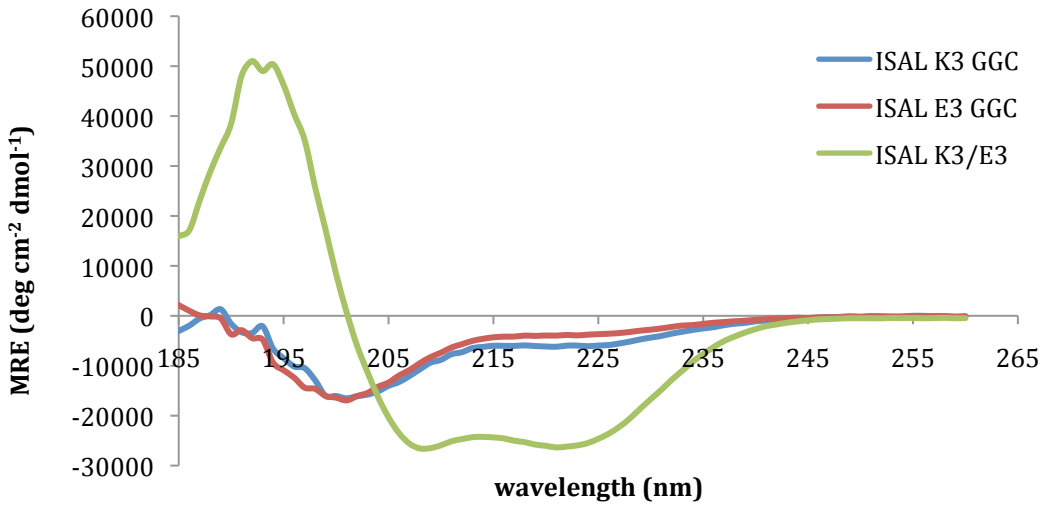

Figure 5.17. Circular dichroism spectra of ISAL E3/K3 peptides after 4 days of disulfide exchange. Measurements were taken in 10 mM $NaPO_4$ pH 7.0 with a total monomer concentration of 100 μM.

Though disulfide linkages are commonly used for covalent bonds, this method is not practical for the design of the coupled receptors because the peptides will be linked to the chromodomain using a thiol-reactive linker on the peptides and a cysteine within the chromodomain. Therefore, the bioorthogonal copper-catalyzed Huisgen cycloaddition was used to covalently link the ISAL E3/K3 peptides (Fig. 5.18). An azido-lysine was incorportated at the C-terminus of the ISAL K3 peptide with a 2-glycine spacer (BrAc-ISAL K3-azidoK). A propargyl glycine was incorportated at the C-terminus of the ISAL E3 peptide with a 2-glycine spacer (BrAc-ISAL E3-propargylG). The peptides were both capped with a 2-glycine spacer with a bromoacetate on the N-terminus.

The α-helical structure of the linked coiled-coiled coils was verified by circular dichroism and compared to the coiled-coils before cycloaddition (Fig. 5.19). While both have α-helical structure, it is clear that linking the two peptides promotes assembly, which will be necessary for proper alignment of the two receptors.

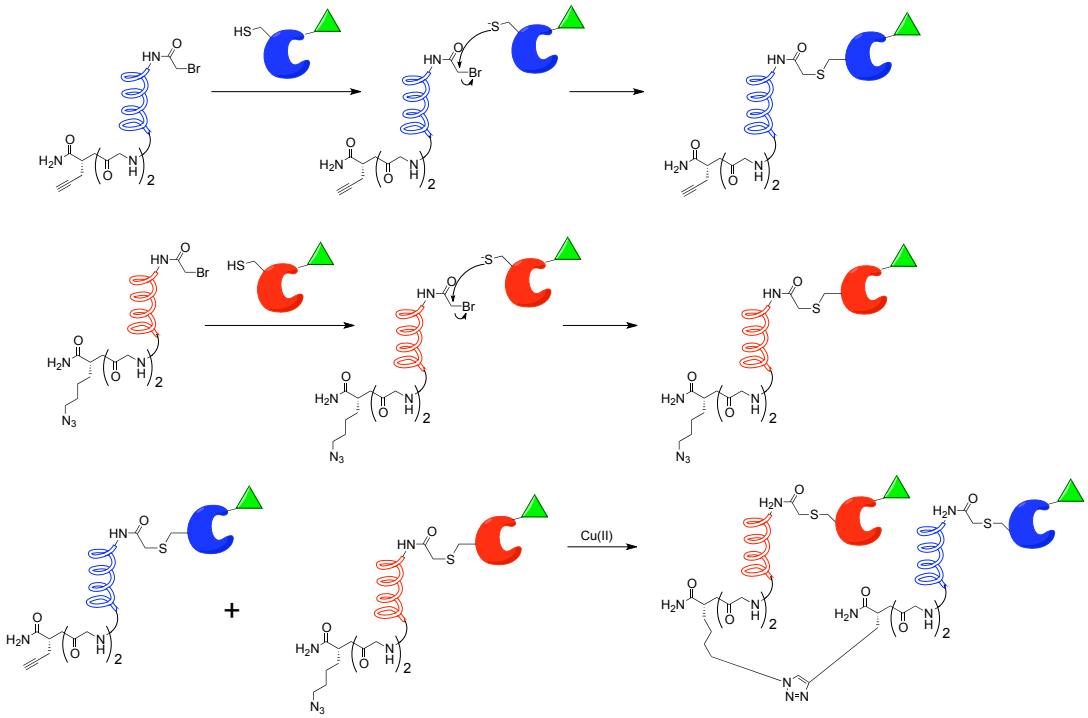

Figure 5.18. Final construction of the coupled receptors using the Huisgen cycloaddition, with a myc tag (green) fused to the chromodomain (red and blue).

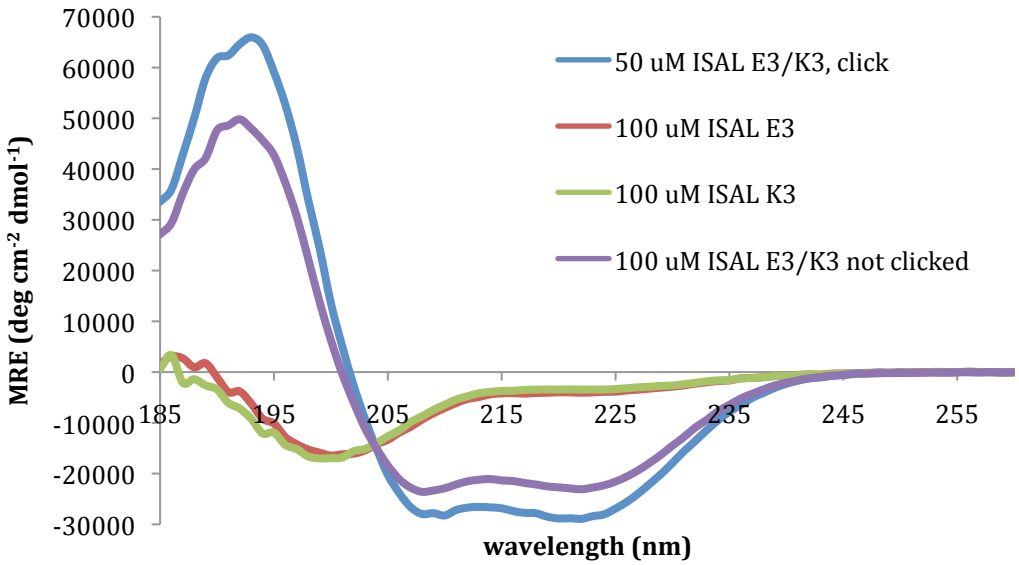

Figure 5.19. Circular dichroism spectra of the BrAc-ISAL E3-propargylG and BrAc-ISAL K3-azidoK peptides before and after cycloaddition. Measurements were taken in 10 mM $NaPO_4$ pH 7.0.

(2) Tagging the Receptors

Since the two receptors will be covalently linked, FRET is not longer necessary for detection. Use of a tag for an antibody rather than a FRET pair is more sensitive and requires less optimization. Therefore a myc-tag was inserted into the HP1α chromodomain on the N-termins preceding the N-terminal histidine tag.

The HP1α chromodomain-myc fusion protein was visualized on a microarray and is selective for the H3 K9Me_3 peptide over lower methylation states and phosphorylated peptides (Fig. 5.20). The peptides and layout used in the microarry can be found in Table 5.3 and Table 5.4. As expected, the signal is strongest for H3 K9Me_3 peptide then the H3 K9Me_2 (Table 5.5). Only a small signal is visualized for the monomethylated peptide and no signal for the phosphorylated peptides or peptides with no methyl marks. The results are positive in that the chromodomains can be used to supplement antibodies. However this data emphasizes the importance of optimizing the conditions such that only dual modifications are visualized on the blot and minimal background signal from single modifications is observed. Lowering receptor concentrations used in the microarray and increasing the number of washes can minimize the background signal.

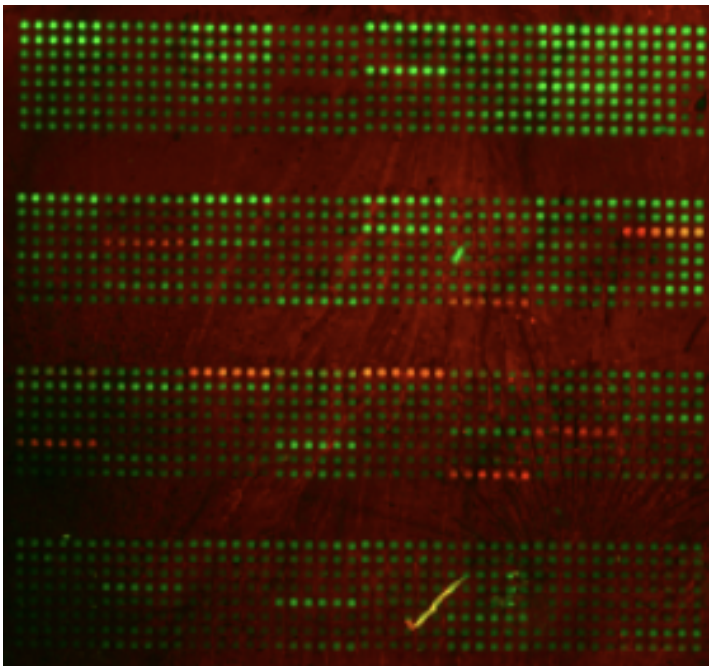

Figure 5.20. Peptide array where positive binding by myc-HP1α chromodomain was visualized using an anti-mic antibody and Alexafluor 647 labeled anti-mouse secondary antibody. Positive binding is shown as red spots and negative interactions are shown as green spots.

Table 5.3. List of all peptides and their identifying number used in the microarray in Fig. 5.20.

Peptide #	Sequence
	H3 [1-20]
1	ARTKQTARKSTGGKAPRKQL-K(Biot)-NH_2
2	ARTKQTARKSTGGK(Ac)APRKQL-K(Biot)-NH_2
3	ARTKQTARK(Ac)STGGKAPRKQL-K(Biot)-NH_2
4	ARTK(Ac)QTARKSTGGKAPRKQL-K(Biot)-NH_2
5	ARTK(Ac)QTARKSTGGK(Ac)APRKQL-K(Biot)-NH_2
6	ARTKQTARK(Ac)STGGK(Ac)APRKQL-K(Biot)-NH_2
7	ARTK(Ac)QTARK(Ac)STGGKAPRKQL-K(Biot)-NH_2
8	ARTK(Ac)QTARK(Ac)STGGK(Ac)APRKQL-K(Biot)-NH_2
10	ARTKQTARKSTGGKAPRK(Ac)QL-K(Biot)-NH_2
11	ARTKQTARKSTGGK(Ac)APRK(Ac)QL-K(Biot)-NH_2
12	ARTKQTARK(Ac)STGGKAPRK(Ac)QL-K(Biot)-NH_2
13	ARTK(Ac)QTARKSTGGKAPRK(Ac)QL-K(Biot)-NH_2
14	ARTKQTARK(Ac)STGGK(Ac)APRK(Ac)QL-K(Biot)-NH_2
15	ARTK(Ac)QTARKSTGGK(Ac)APRK(Ac)QL-K(Biot)-NH_2
16	ARTK(Ac)QTARK(Ac)STGGKAPRK(Ac)QL-K(Biot)-NH_2
17	ARTK(Ac)QTARK(Ac)STGGK(Ac)APRK(Ac)QL-K(Biot)-NH_2
18	ARTK(Me_3)QTARKSTGGKAPRKQL-K(Biot)-NH_2

19	ARTK(Me$_3$)QTARK(Ac)STGGKAPRKQL-K(Biot)-NH$_2$
20	ARTK(Me$_3$)QTARKSTGGK(Ac)APRKQL-K(Biot)-NH$_2$
21	ARTK(Me$_3$)QTARKSTGGKAPRK(Ac)QL-K(Biot)-NH$_2$
22	ARTK(Me$_3$)QTARK(Ac)STGGK(Ac)APRKQL-K(Biot)-NH$_2$
23	ARTK(Me$_3$)QTARK(Ac)STGGKAPRK(Ac)QL-K(Biot)-NH$_2$
24	ARTK(Me$_3$)QTARKSTGGK(Ac)APRK(Ac)QL-K(Biot)-NH$_2$
25	ARTK(Me$_3$)QTARK(Ac)STGGK(Ac)APRK(Ac)QL-K(Biot)-NH$_2$
26	ARpTK(Me$_3$)QTARK(Ac)STGGK(Ac)APRK(Ac)QL-K(Biot)-NH$_2$
27	ArpTK(Me$_3$)QTARKSTGGKAPRKQL-K(Biot)-NH$_2$
28	AR(Me$_2$a)pTK(Me$_3$)QTARK(Ac)STGGK(Ac)APRK(Ac)QL-K(Biot)-NH$_2$
29	AR(Me$_2$a)pTK(Me$_3$)QTARKSTGGKAPRKQL-K(Biot)-NH$_2$
30	AR(Me$_2$a)TK(Me$_3$)QTARKSTGGKAPRKQL-K(Biot)-NH$_2$
31	5-Fam-ARTKQTARKSTGGKAPRKQL-K(Biot)-NH$_2$
32	ARTK(Me$_2$)QTARKSTGGKAPRKQL-K(Biot)-NH$_2$
33	ARTK(Me$_2$)QTARK(Ac)STGGK(Ac)APRK(Ac)QL-K(Biot)-NH$_2$
34	ARTK(Me)Q TARKSTGGKAPRKQL-K(Biot)-NH$_2$
35	ARTK(Me)QTARK(Ac)STGGK(Ac)APRK(Ac)QL-K(Biot)-NH$_2$
36	ARTKQTARKpSTGGKAPRKQL-K(Biot)-NH$_2$
37	ARTK(Ac)QTARK(Ac)pSTGGK(Ac)APRK(Ac)QL-K(Biot)-NH$_2$
38	ARTK(Me$_3$)QTARKpSTGGKAPRKQL-K(Biot)-NH$_2$
39	ARTK(Me$_3$)QTARK(Ac)pSTGGK(Ac)APRK(Ac)QL-K(Biot)-NH$_2$
40	AR(Me$_2$a)TK(Me$_3$)QTARKpSTGGKAPRKQL-K(Biot)-NH$_2$
41	AR(Me$_2$a)TK(Me$_3$)QTARK(Ac)pSTGGK(Ac)APRK(Ac)QL-K(Biot)-NH$_2$
42	ARTKQTARK(Me$_3$)STGGKAPRKQL-K(Biot)-NH$_2$
43	ARTK(Ac)QTARK(Me$_3$)STGGK(Ac)APRK(Ac)QL-K(Biot)-NH$_2$
44	ARTK(Me$_2$)QTARK(Ac)STGGKAPRK(Ac)QL-K(Biot)-NH$_2$
45	ARTK(Me)QTARK(Ac)STGGKAPRK(Ac)QL-K(Biot)-NH$_2$
47	AR(Me$_2$a)TKQTARKSTGGKAPRKQL-K(Biot)-NH$_2$
48	AR(Me$_2$a)TK(Ac)QTARK(Ac)STGGK(Ac)APRK(Ac)QL-K(Biot)-NH$_2$
50	AR(Me$_2$a)TK(Me$_3$)QTARK(Ac)STGGK(Ac)APRK(Ac)QL-K(Biot)-NH$_2$
51	AR(Me)TK(Me$_3$)QTARKSTGGKAPRKQL-K(Biot)-NH$_2$
52	AR(Me)TK(Me$_3$)QTARK(Ac)STGGK(Ac)APRK(Ac)QL-K(Biot)-NH$_2$
53	ACitTKQTARKSTGGKAPRKQL-K(Biot)-NH$_2$
54	AcitTK(Me$_3$)QTARKSTGGKAPRKQL-K(Biot)-NH$_2$
55	AcitTK(Me$_3$)QTARK(Ac)STGGK(Ac)APRK(Ac)QL-K(Biot)-NH$_2$
56	AcitTK(Ac)QTARK(Ac)STGGK(Ac)APRK(Ac)QL-K(Biot)-NH$_2$
	H4 [1-23]
58	Ac-SGRGKGGKGLGKGGAKRHRKVLR-Peg-Biot
59	Ac-SGRGK(Ac)GGK(Ac)GLGK(Ac)GGAK(Ac)RHRKVLR-Peg-Biot
66	Ac-SGRGK(Ac)GGKGLGKGGAKRHRKVLR-Peg-Biot
67	Ac-SGRGKGGK(Ac)GLGKGGAKRHRKVLR-Peg-Biot
68	Ac-SGRGKGGKGLGK(Ac)GGAKRHRKVLR-Peg-Biot
69	Ac-SGRGKGGKGLGKGGAK(Ac)RHRKVLR-Peg-Biot
70	Ac-SGRGK(Ac)GGKGLGK(Ac)GGAKRHRKVLR-Peg-Biot
71	Ac-SGRGKGGK(Ac)GLGKGGAK(Ac)RHRKVLR-Peg-Biot
72	Ac-SGRGK(Ac)GGK(Ac)GLGK(Ac)GGAKRHRKVLR-Peg-Biot

	H3 [15-41]
90	Ac-APRK^{18}QLATK^{23}AARK^{27}SAPSTGGVK^{36}K^{37}PHRY-GG-K(Biot)-NH_2
91	Ac-APRK(Me$_3$)QLATKAARKSAPSTGGVKKPHRY-GG-K(Biot)-NH_2
93	Ac-APRKQLATKAARKSAPSTGGVK(Me$_3$)KPHRY-GG-K(Biot)-NH_2
95	Ac-APRK(Me$_3$)QLATKAARKSAPSTGGVK(Me$_3$)KPHRY-GG-K(Biot)-NH_2
	H3 [74-84]
100	Ac-IAQDFK^{79}TDLRF-Peg-K(Biot)-NH_2
101	Ac-IAQDFK(Me$_3$)TDLRF-Peg-K(Biot)-NH_2
102	Ac-IAQDFK(Me$_2$)TDLRF-Peg-K(Biot)-NH_2
103	Ac-IAQDFK(Me)TDLRF-Peg-K(Biot)-NH_2
104	IAQDFKTDLRF-Peg-K(Biot)-NH_2
	H3 [27-45]
120	KSAPSTGGVK(Me$_3$)KPHRYKPGT-G-K(Biot)-NH_2
121	KSAPSTGGVK(Me$_2$)KPHRYKPGT-G-K(Biot)-NH_2
122	KSAPSTGGVK(Me)KPHRYKPGT-G-K(Biot)-NH_2
123	KSAPSTGGVK(Ac)KPHRYKPGT-GG-K(Biot)-NH_2
124	KSAPSTGGVK^{36}K^{37}PHRYKPGT-GG-K(Biot)-NH_2
	H3 [1-20]
132	ARTK(Me$_3$)QTARK(Me$_3$)STGGKAPRKQL-K(Biot)-NH_2
133	ARTKQTARK(Me$_2$)STGGKAPRKQL-K(Biot)-NH_2
134	ARTKQTARK(Me)STGGKAPRKQL-K(Biot)-NH_2
137	ARTKQTARKSTGGKAPRK(Me$_3$)QL-K(Biot)-NH_2
138	ARTKQTARKSTGGKAPRK(Me$_2$)QL-K(Biot)-NH_2
139	ARTKQTARKSTGGKAPRK(Me)QL-K(Biot)-NH_2
144	ARTKQTARK(Ac)phSTGGKAPRKQL-K(Biot)-NH_2
145	ARTKQTARK(Me$_3$)phSTGGKAPRKQL-K(Biot)-NH_2
146	ARTKQTARK(Me$_2$)phSTGGKAPRKQL-K(Biot)-NH_2
147	ARTKQTARK(Me)phSTGGKAPRKQL-K(Biot)-NH_2
148	ARTK(Me$_3$)QTARK(Ac)phSTGGKAPRKQL-K(Biot)-NH_2
157	AR(Me$_2$s)TK(Me$_3$)QTARKSTGGKAPRKQL-K(Biot)-NH_2
162	ARTKQpTARKSTGGKAPRKQL-K(Biot)-NH_2
163	ARTK(Me$_3$)QpTARKSTGGKAPRKQL-K(Biot)-NH_2
164	ARTK(Me$_2$)QpTARKSTGGKAPRKQL-K(Biot)-NH_2
165	ARTKQpTARK(Ac)STGGK(Ac)APRK(Ac)QL-K(Biot)-NH_2
166	ARTK(Me$_3$)QpTARK(Ac)STGGK(Ac)APRK(Ac)QL-K(Biot)-NH_2
167	ARTK(Me$_2$)QpTARK(Ac)STGGK(Ac)APRK(Ac)QL-K(Biot)-NH_2
	H2A[1-17]
300	Ac-SGRGK^{5}QGGK^{9}ARAK^{13}AK^{15}TR-Peg-Biot
301	Ac-SGRGK(Ac)QGGK(Ac)ARAK(Ac)AK(Ac)TR-Peg-Biot
302	Ac-SGRGK(Ac)QGGKARAKAKTR-Peg-Biot
303	Ac-pSGRGK(Ac)QGGKARAKAKTR-Peg-Biot
304	Ac-SGR(Me$_2$a)GK(Ac)QGGKARAKAKTR-Peg-Biot
305	Ac-pSGR(Me$_2$a)GK(Ac)QGGKARAKAKTR-Peg-Biot
306	Ac-SGCitGK(Ac)QGGKARAKAKTR-Peg-Biot
307	Ac-pSGCitGK(Ac)QGGKARAKAKTR-Peg-Biot
308	Ac-pSGRGK(Ac)QGGK(Ac)ARAK(Ac)AK(Ac)TR-Peg-Biot

309	SGRGK(Ac)QGGK(Ac)ARAK(Ac)AK(Ac)TR-Peg-Biot
310	pSGRGK(Ac)QGGK(Ac)ARAK(Ac)AK(Ac)TR-Peg-Biot
	H2B[1-24]
400	PEPAKSAPAPKKGSKKAVTKAQKK-Peg-Biot
401	PEPAK(Me_3)SAPAPKKGSKKAVTKAQKK-Peg-Biot
402	PEPAK(Me_2)SAPAPKKGSKKAVTKAQKK-Peg-Biot
403	PEPAK(Me)SAPAPKKGSKKAVTKAQKK-Peg-Biot

Table 5.4. A map of the microarry in Fig. 5.20 with the peptides listed by their identifying number.[1]

subarray 1 and 3

IgG (A1-A6)	1 (A7-A12)	IgG (A13-A18)	2 (A19-A24)	IgG (A25-A30)	3 (A31-A36)	IgG (A37-A42)	4 (A43-A48)
F (B1-B6)	5 (B7-B12)	100 (B13-B18)	6 (B19-B24)	120 (B25-B30)	7 (B31-A36)	58 (B37-B42)	8 (B43-B48)
90 (C1-C6)	10 (C7-C12)	F (C13-C18)	11 (C19-C24)	121 (C25-C30)	12 (C31-C36)	59 (C37-C42)	13 (C43-C48)
91 (D1-D6)	14 (D7-D12)	101 (D13-D18)	15 (D19-D24)	F (D25-D30)	16 (D31-D36)	66 (D37-D42)	17 (D43-D48)
93 (E1-E6)	18 (E7-E12)	102 (E13-E18)	19 (E19-E24)	122 (E25-E30)	20 (E31-E36)	F (E37-E42)	21 (E43-E48)
95 (F1-F6)	22 (F7-F12)	103 (F13-F18)	23 (F19-F24)	123 (F25-F30)	24 (F31-F36)	67 (F37-F42)	25 (F43-F48)
69 (G1-G6)	26 (G7-G12)	104 (G13-G18)	27 (G19-G24)	123 (G25-G30)	28 (G31-G36)	68 (G37-G42)	29 (G43-G48)
162 (H1-H6)	145 (H7-H12)	144 (H13-H18)	137 (H19-H24)	147 (H25-H30)	138 (H31-H36)	148 (H37-H42)	139 (H43-H48)
blank (I1-I6)	blank (I7-I12)	blank (I13-I18)	blank (I19-I24)	blank (I25-I30)	blank (I31-I36)	blank (I37-I42)	blank (I43-I48)
blank (J1-J6)	blank (J7-J12)	blank (J13-J18)	blank (J19-J24)	blank (J25-J30)	blank (J31-J36)	blank (J37-J42)	blank (J43-J48)
blank (K1-K6)	blank (K7-K12)	blank (K13-K18)	blank (K19-K24)	blank (K25-K30)	blank (K31-K36)	blank (K37-K42)	blank (K43-K48)
blank (L1-L6)	blank (L7-L12)	blank (L13-L18)	blank (L19-L24)	blank (L25-L30)	blank (L31-L36)	blank (L37-L42)	blank (L43-L48)
IgG (M1-M6)	30 (M7-M12)	IgG (M13-M18)	32 (M19-M24)	IgG (M25-M30)	33 (M31-M36)	IgG (M37-M42)	34 (M43-M48)
70 (N1-N6)	35 (N7-N12)	301 (N13-N18)	36 (N19-N24)	305 (N25-N30)	37 (N31-N36)	F (N37-N42)	38 (N43-N48)
71 (O1-O6)	39 (O7-O12)	302 (O13-O18)	40 (O19-O24)	F (O25-O30)	41 (O31-O36)	309 (O37-O42)	42 (O43-O48)
72 (P1-P6)	43 (P7-P12)	F (P13-P18)	44 (P19-P24)	306 (P25-P30)	45 (P31-P36)	310 (P37-P42)	157 (P43-P48)

F (Q1-Q6)	47 (Q7-Q12)	303 (Q13-Q18)	48 (Q19-Q24)	307 (Q25-Q30)	50 (Q31-Q36)	400 (Q37-Q42)	51 (Q43-Q48)
300 (R1-R6)	52 (R7-R12)	304 (R13-R18)	53 (R19-R24)	308 (R25-R30)	54 (R31-R36)	401 (R37-R42)	55 (R43-R48)
402 (S1-S6)	IgG (S7-S12)	403 (S13-S18)	167 (S19-S24)	56 (S25-S30)	IgG (S31-S36)	F (S37-S42)	IgG (S43-S48)
163 (T1-T6)	146 (T7-T12)	164 (T13-T18)	132 (T19-T24)	165 (T25-T30)	133 (T31-T36)	166 (T37-T42)	134 (T43-T48)
blank (U1-U6)	blank (U7-U12)	blank (U13-U18)	blank (U19-U24)	blank (U25-U30)	blank (U31-U36)	blank (U37-U42)	blank (U43-U48)
blank (V1-V6)	blank (V7-V12)	blank (V13-V18)	blank (V19-V24)	blank (V25-V30)	blank (V31-V36)	blank (V37-V42)	blank (V43-V48)
blank (W1-W6)	blank (W7-W12)	blank (W13-W18)	blank (W19-W24)	blank (W25-W30)	blank (W31-W36)	blank (W37-W42)	blank (W43-W48)
blank (X1-X6) subarray 2 and 4	blank (X7-X12)	blank (X13-X18)	blank (X19-X24)	blank (X25-X30)	blank (X31-X36)	blank (X37-X42)	blank (X43-X48)
134 (A1-A6)	166 (A7-A12)	133 (A13-A18)	165 (A19-A24)	132 (A25-A30)	164 (A31-A36)	146 (A37-A42)	163 (A43-A48)
IgG (B1-B6)	F (B7-B12)	IgG (B13-B18)	56 (B19-B24)	167 (B25-B30)	403 (B31-A36)	IgG (B37-B42)	402 (B43-B48)
55 (C1-C6)	401 (C7-C12)	54 (C13-C18)	308 (C19-C24)	53 (C25-C30)	304 (C31-C36)	52 (C37-C42)	300 (C43-C48)
51 (D1-D6)	400 (D7-D12)	50 (D13-D18)	307 (D19-D24)	48 (D25-D30)	303 (D31-D36)	47 (D37-D42)	F (D43-D48)
157 (E1-E6)	310 (E7-E12)	45 (E13-E18)	306 (E19-E24)	44 (E25-E30)	F (E31-E36)	43 (E37-E42)	72 (E43-E48)
42 (F1-F6)	309 (F7-F12)	41 (F13-F18)	F (F19-F24)	40 (F25-F30)	302 (F31-F36)	39 (F37-F42)	71 (F43-F48)
38 (G1-G6)	F (G7-G12)	37 (G13-G18)	305 (G19-G24)	36 (G25-G30)	301 (G31-G36)	35 (G37-G42)	70 (G43-G48)
34 (H1-H6)	IgG (H7-H12)	33 (H13-H18)	IgG (H19-H24)	32 (H25-H30)	IgG (H31-H36)	30 (H37-H42)	IgG (H43-H48)
blank (I1-I6)	blank (I7-I12)	blank (I13-I18)	blank (I19-I24)	blank (I25-I30)	blank (I31-I36)	blank (I37-I42)	blank (I43-I48)
blank (J1-J6)	blank (J7-J12)	blank (J13-J18)	blank (J19-J24)	blank (J25-J30)	blank (J31-J36)	blank (J37-J42)	blank (J43-J48)
blank (K1-K6)	blank (K7-K12)	blank (K13-K18)	blank (K19-K24)	blank (K25-K30)	blank (K31-K36)	blank (K37-K42)	blank (K43-K48)
blank (L1-L6)	blank (L7-L12)	blank (L13-L18)	blank (L19-L24)	blank (L25-L30)	blank (L31-L36)	blank (L37-L42)	blank (L43-L48)

139 (M1-M6)	148 (M7-M12)	138 (M13-M18)	147 (M19-M24)	137 (M25-M30)	144 (M31-M36)	145 (M37-M42)	162 (M43-M48)
29 (N1-N6)	68 (N7-N12)	28 (N13-N18)	124 (N19-N24)	27 (N25-N30)	104 (N31-N36)	26 (N37-N42)	69 (N43-N48)
25 (O1-O6)	67 (O7-O12)	24 (O13-O18)	123 (O19-O24)	23 (O25-O30)	103 (O31-O36)	22 (O37-O42)	95 (O43-O48)
21 (P1-P6)	F (P7-P12)	20 (P13-P18)	122 (P19-P24)	19 (P25-P30)	102 (P31-P36)	18 (P37-P42)	93 (P43-P48)
17 (Q1-Q6)	66 (Q7-Q12)	16 (Q13-Q18)	F (Q19-Q24)	15 (Q25-Q30)	101 (Q31-Q36)	14 (Q37-Q42)	91 (Q43-Q48)
13 (R1-R6)	59 (R7-R12)	12 (R13-R18)	121 (R19-R24)	11 (R25-R30)	F (R31-R36)	10 (R37-R42)	90 (R43-R48)
8 (S1-S6)	58 (S7-S12)	7 (S13-S18)	120 (S19-S24)	6 (S25-S30)	100 (S31-S36)	5 (S37-S42)	F (S43-S48)
4 (T1-T6)	IgG (T7-T12)	3 (T13-T18)	IgG (T19-T24)	2 (T25-T30)	IgG (T31-T36)	1 (T37-T42)	IgG (T43-T48)
blank (U1-U6)	blank (U7-U12)	blank (U13-U18)	blank (U19-U24)	blank (U25-U30)	blank (U31-U36)	blank (U37-U42)	blank (U43-U48)
blank (V1-V6)	blank (V7-V12)	blank (V13-V18)	blank (V19-V24)	blank (V25-V30)	blank (V31-V36)	blank (V37-V42)	blank (V43-V48)
blank (W1-W6)	blank (W7-W12)	blank (W13-W18)	blank (W19-W24)	blank (W25-W30)	blank (W31-W36)	blank (W37-W42)	blank (W43-W48)
blank (X1-X6)	blank (X7-X12)	blank (X13-X18)	blank (X19-X24)	blank (X25-X30)	blank (X31-X36)	blank (X37-X42)	Blank (X43-X48)

[1] Each peptide was printed as 6 sequential spots on the four subarrays. The layout of subarrays 1 through 4 are identical. Locations of a given peptide was printed are given in parenthesis.

Table 5.5. Quantification of fluorescence of HP1α chromodomain bound to histone peptides on the array shown in Fig. 5.20.

Histone H3 modification	Average intensity
k9me3	0.0666
k9me2	0.0433
k4me3 k9me3	0.0383
k9me3 + 3 ac	0.0239
k9me1	0.0047
k9me3 s10ph	0.0000
k9me2 s10ph	0.0000
k9me1 s10ph	0.0000

v. Putting the Components Together

Once the separate components were characterized for structure and binding affinity, the next step is to piece the components together. Though the ultimate goal is to combine receptors that are selective for two different Histone H3 modifications, two HP1α chromodomains were be combined because the protein is already expressed and well characterized. First, a single chromodomain R74C mutant with a myc-tag was conjugated to the BrAc-ISAL K3-azidoK peptide using approximately three equivalents of peptide with TCEP. After 24 hours the reaction was analyzed by LC/MS. The LC trace of the reaction is shown in Fig. 5.21A. There is one sharp peak (peak 1) and a smaller, uneven peak (peak 2). The peak 1 shows a mass corresponding to 3386.8 Da, which is consistent with BrAc-ISAL K3-azidoK (3215.7 Da) that has been substituted with TCEP on the N-terminus, which indicates that TCEP acts a nucelophile and should be omitted from reactions of this type (Fig. 5.21B). Peak 2 contains masses that closely correspond to both unconjugated and conjugated chromodomain (8516.3 Da and 11729.98 Da respectively) (Fig. 5.21C). The low resolution of the instrument made it difficult to measure the exact mass. Though the BrAc-ISAL K3-azidoK was in excess, much of it reacted with the TCEP (Fig. 5.22). Therefore, not all of the chromodomain was able to form conjugate with the peptide.

(A)

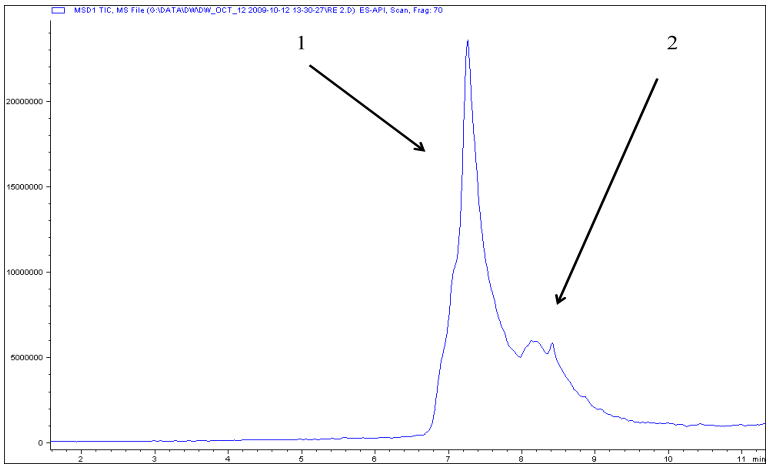

(B)

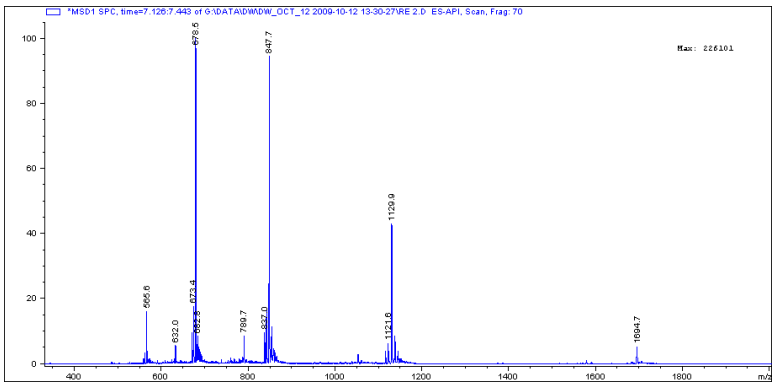

(C)

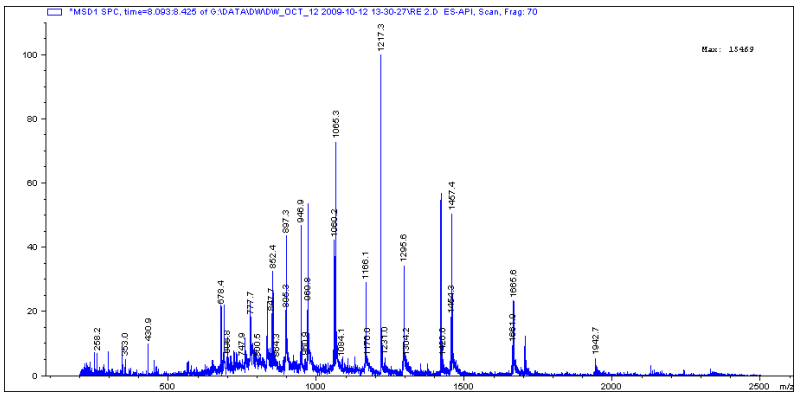

Figure 5.21. LC/MS of conjugation reaction between ISAL K3-azidoK and HP1α chromodomain R74C. (A) LC/MS trace of the conjugation reaction. (B) Mass spectrum of peak 1. (C) Mass spectrum of peak 2.

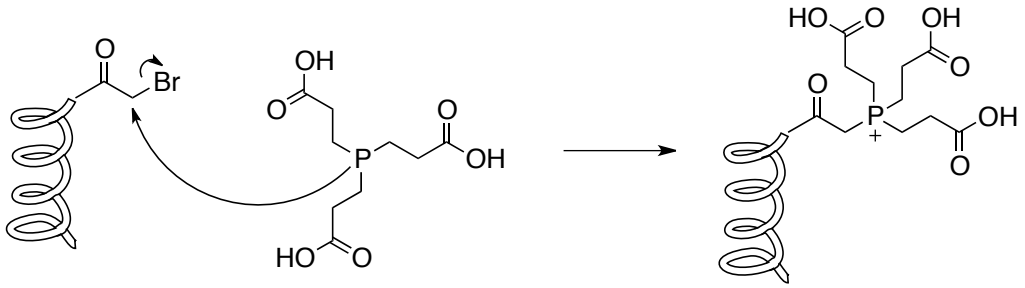

Figure 5.22. Reaction of TCEP with bromoacetate in BrAc-ISAL K3-azidoK

The AcBr-ISAL E3-propargylG and AcBr-ISAL K3-azidoK peptides were already linked using the copper-catalyzed cycloaddition. Therefore two HP1α chromodomain cysteine mutants were conjugated to the coiled-coil (Fig. 5.23). The first reaction had a 1:3 ratio of coiled-coil to chromodomain in 50 mM potassium phosphate, pH 8, 25 mM NaCl and the second had a 1:4 ratio of coiled-coil to chromodomain in the same buffer. The third was similar to the first reaction with 10 equivalents of TCEP, which was included before the TCEP was shown to react extensively with the bromoacetate cap. Each reaction was performed on a 9 nmol scale of coiled-coil in a total volume of 100 μL. The reactions were visualized by SDS-PAGE after 1 day then after 4 days at 4^{o} C (Fig. 5.24 and Fig. 5.25 respectively). Reactions one and two proceeded at approximately similar rates after four days regardless of the different chromodomain concentrations. The reaction with TCEP did not proceed after four days, most likely because the TCEP had reacted with the coiled-coil. There are some lighter bands indicating a large protein, which may indicate an impurity, aggregate, or a small side product due to the presence of the less reactive cysteine in the HP1α chromodomain.

The conditions for the first reaction were chosen for a larger scale reaction (0.336 μmol coiled-coil, 1.009 μmol chromodomain R74C) to minimize the use of material and once complete the fully reacted conjugate were isolated using size exclusion

chromatography. As shown in Fig. 5.26, a single band appears at approximately 20 kDa, which is consistent with the mass of the conjugated coiled-coil with two chromodomains.

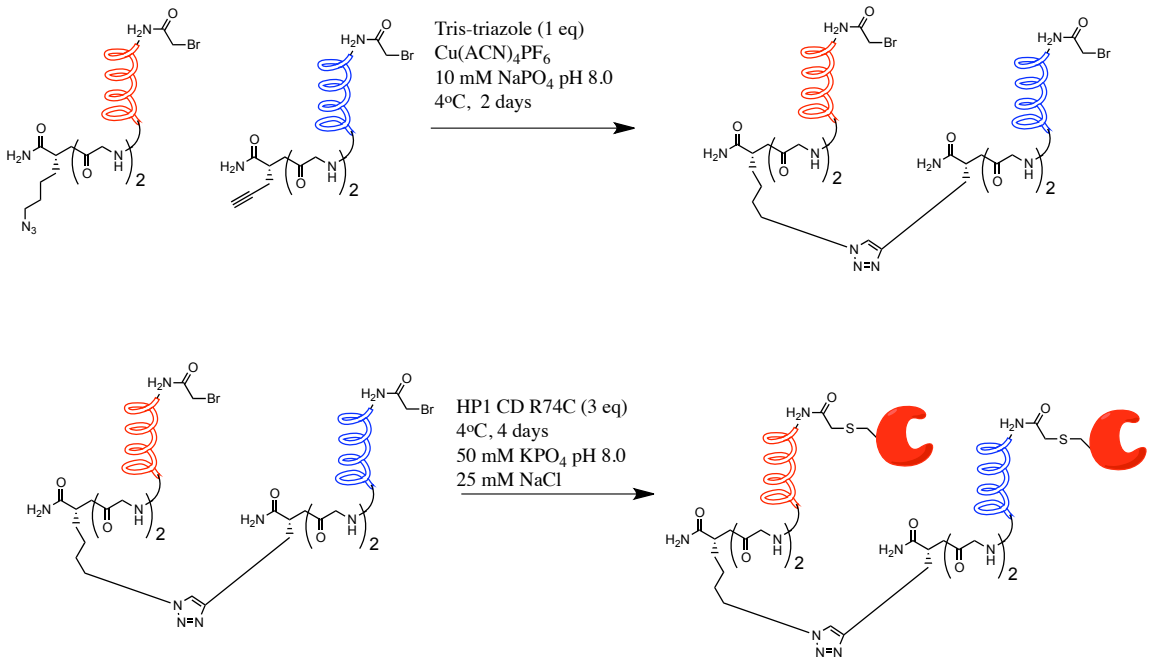

Figure 5.23. Conjugation of two HP1α chromodomain R74C mutants to linked coiled-coil peptides with the N-terminal bromoacetate.

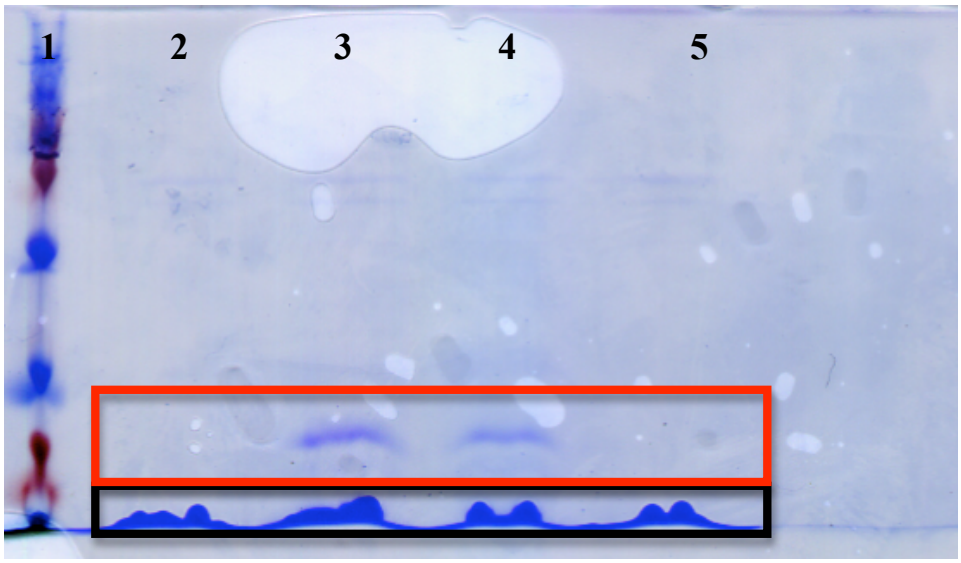

Figure 5.24. 15% SDS-PAGE of the coiled-coil/chromodomain conjugation reaction after one day and visualized with Coomassie blue. (1) Protein ladder, (2) HP1α chromodomain R74C, (3) reaction one (1:3 coiled-coil: chromodomain), (4) reaction two (1:4 coiled-coil: chromodomain), (5) reaction three (1:3 coiled-coil: chromodomain, 10 eq TCEP). The red box indicates bands that appear to correspond to fully reacted coiled-coil with chromodomain and the black box indicates unreacted chromodomain.

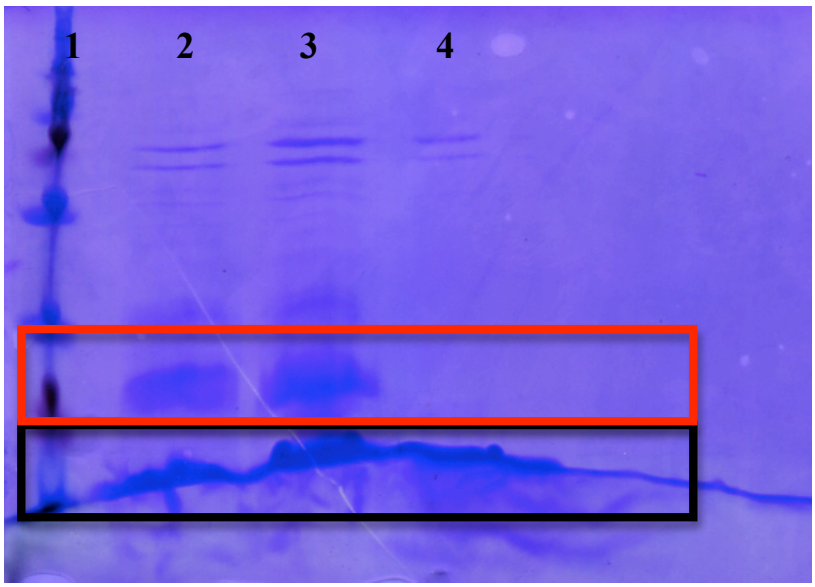

Figure 5.25. 15% SDS-PAGE of the coiled-coil/chromodomain conjugation reaction after four days (same volume of reaction was loaded on the gel). (1) Protein ladder, (2) reaction one (1:3 coiled-coil: chromodomain), (3) reaction two (1:4 coiled-coil: chromodomain), (3) reaction three (1:3 coiled-coil: chromodomain, 10 eq TCEP). The red box indicates bands that appear to corresponds for fully reaction coiled-coil with chromodomain and the black box indicates unreacted chromodomain.

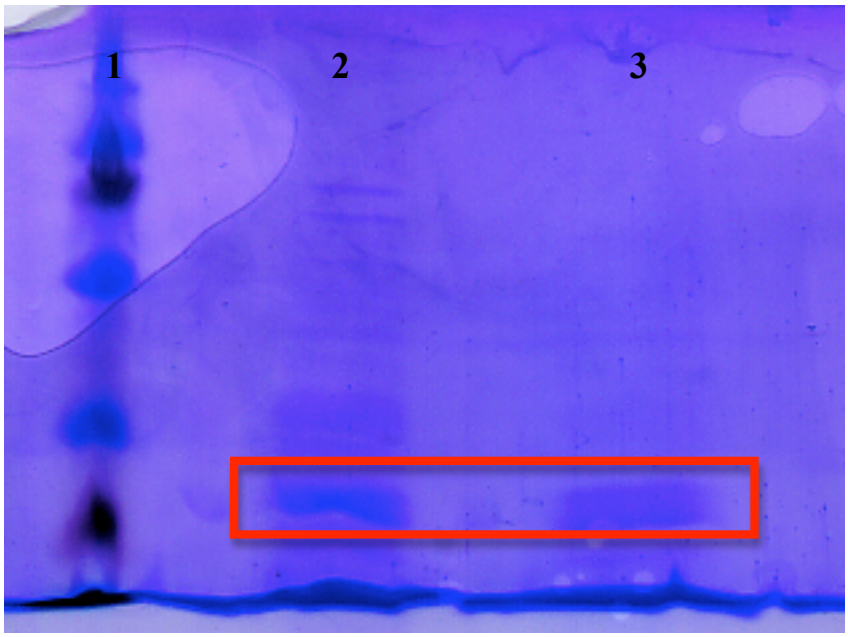

Figure 5.26. 15% SDS-PAGE of the coiled-coil/chromodomain conjugation reaction before and after purification. (1) Protein ladder, (2) conjugation before purification, (3) conjugation after purification by size exclusion. The band corresponding to the conjugate is indicated in the red box.

vi. Binding Studies with the Conjugate

Fluorescence anisotropy studies were performed using a peptide containing a two-H3 K9Me$_2$ repeat sequence ((H3 K9Me$_2$)$_2$) and the conjugate is shown in Fig. 5.23. The trimethyllated version was not used because the synthesis proved to be difficult with low yields. The data shows a significant increase in anisotropy when 5 μM conjugate is added to 1 μM peptide and immediately the signal plateaus (Fig. 5.27). If accurate, the curve fit yields a K_D of 1.5 ± 1 μM, which is nearly a 20-fold improvement over binding compared to HP1α chromodomain bound to H3 K9Me$_2$.

Ideally the concentration of the fluorophore-labelled peptide should be 10-fold lower than the dissociation constant when performing anisotropy studies. Therefore the experiments were repeated using 200 nM peptide rather than 1 μM. The conjugate was also filtered to remove any potential aggregates that can affect the anisotropy

measurements. The dissociation constant between the conjugated and H3 $K9Me_2$ was measured in addition to the repeat sequence, $(H3\ K9Me_2)_2$ (Fig. 5.28). No binding is detected in the case of the H3 $K9Me_2$ sequence. However, a dissociation constant of 3.7 ± 1 μM is measured in the case of the repeat sequence, which is 10-fold more favorable than the native chromodomain bound to the native peptide. For this data to be reliable more conjugate will be synthesized and the experiments will be repeated. Additionally, the measurements between the native chromodomain and H3 $K9Me_2$ to verify that no or minimal binding is detected at the lower peptide concentration. Other binding experiments will also include repeat sequences with only one dimethyllysine rather than two. The system can also be optimized by varying the distances between the coiled-coils and receptors and the distances between the sites of modification on the histone tail peptide. By altering these distances, we hope to enhance cooperative binding of the bivalent receptor.

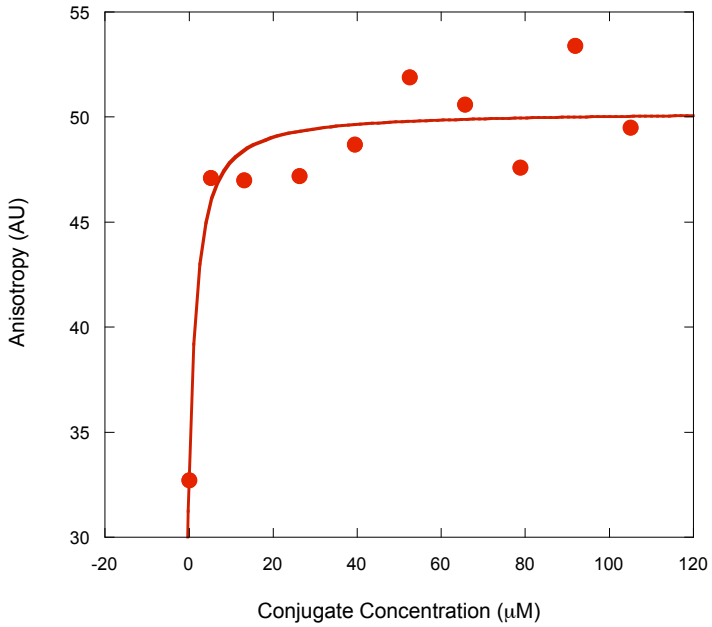

Figure 5.27. Fluorescence anisotropy binding experiments of 1 μM 5(6)-FAM (H3 $K9Me_2)_2$ with conjugate. The experiments were performed in 50 mM potassium buffer pH 8.0, 25 mM NaCl, and 4 mM DTT at 25 °C. This curve represents one run.

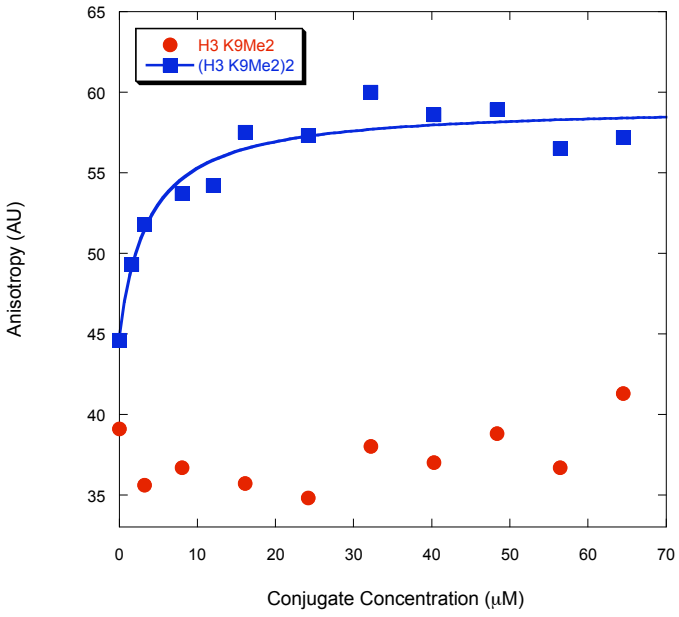

Figure 5.28. Fluorescence anisotropy binding experiments of 200 nM 5(6)-FAM (H3 $K9Me_2)_2$ and H3 $K9Me_2$ with conjugate. The experiments were performed in 50 mM potassium buffer pH 8.0, 25 mM NaCl, and 4 mM DTT at 25 °C. This curve represents one run.

D. Experimental

i. Protein Expression and Purification

The DNA plasmid containing the cloning region of *Drosophila* HP1α chromodomain was supplied by the Khorasanizadeh lab. The cysteine mutants were generated using the same conditions as described in Chapter III.[18] The primers used for the cysteine mutants are shown in Table 5.6.

An N-terminal myc tag was inserted into HP1α chromodomain using primers containing the myc sequence. The total reaction volumes were 50 μL with 1 μL DNA plasmid (~30 ng/μL), 1 μL dimethyl sulfoxide (DMSO), 1 μL of forward and reverse primers (0.01 mmol), 2.5 μL dNTP mix (10 mM), 5 μL 5X PFU buffer, 36.5 μL dH_2O, and 2 μL PfuUltra hotstart DNA polymerase (Strategene) was added last. The thermocycler settings are given in Table 5.6. Once isolated, DNA and protein expression and purification was carried out as described in Chapter III. The primers for the insert are shown in Table 5.7.

Table 5.6. Thermocycler conditions for generating HP1α chromodomain with the myc-tag.

Temperature (^oC)	Time	Cycles
Hot start: 95	30 sec	1
Melt: 95	1 min	20
Anneal: 45	1 min	
Extend: 68	13 min	
Find extend: 72	5 min	1
Pause: 4	hold	

Table 5.7. The forward primers used for generating HP1α chromodomain cysteine mutants and for inserting the N-terminal myc-tag. The point mutations are in red.

Mutant	Primer Sequence
E23C	C GAA GAG GAG GAG GAG TGC TAC GCC GTG GAA AAG ATC
K28C	GAG GAG GAG TAC GCC GTG GAA TGC ATC ATC GAC AGG C
M38C	CGG GTG CGC AAG GGA TGT GTG GAG TAC TAT CTG AAA TGG
R74C	CAG CAG TAC GAG GCG AGC TGC AAG GAT TAA GGA TCC GGC
myc-tag[1]	T TTT GTT TAA CTT TAA GAA GGA GAT ATA CAT ATG GAG CAG AAG CTG ATA TCC GAG GAG GAC CTG AAA AAA CAC CAC CAC CAC CAC CAC GCC GAA GAG GAG G

[1]The sequence containing the myc-tag is highlighted in green with the start codon in blue and an EcoRV site underlined. The N-terminal His6-tag is orange.

ii. Circular Dichroism characterization of HP1α Chromodomain

CD measurements were performed on an Aviv 62DS Circular Dichroism Spectrometer. All CD experiments were performed as described in Chapter III.

iii. Synthesis of Histone Tail Peptides

The H3 K9Me$_{2/3}$ peptides were synthesized, purified, and characterized as described in Chapter III.

iv. Fluorescence Anisotropy

Fluorescence anisotropy experiments were carried out as described in Chapters III and IV.

v. Microarray of myc-HP1α Chromodomain[7]

The peptide microarrays were prepared and analyzed by the Strahl lab. The slides were washed overnight with 20 μM chromodomain in PBS, 1% BSA, 0.3% Tween-20 followed by detection with anti-myc antibody and Alexafluor 647 labeled anti-mouse secondary antibody (Fig. 5.24).

vi. Imidazole-1-sulfonyl azide hydrochloride

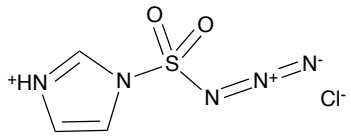

The reagent for the azotransfer reaction was synthesized as previously described. **^{1}H NMR** (400 MHz, CD_3OD): δ 7.69 (d, *J* = 7.6, 2H).[19]

vii. α-N-Fmoc-ε-azidolysine

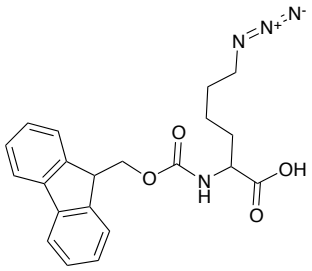

A 2.2744 g (6.173 mmol) amount of α-N-Fmoc-L-lysine was added to a 100 mL round bottom flask with imidazole-1-sulfonyl azide (1.5526 g, 7.407 mmol, 1.2 equivalents), and potassium carbonate (1.7068 g, 12.35 mmol, 2.00 equivalents). The mixture was stirred in 30 mL methanol and purged with nitrogen gas for 20 mins and 15.6 g $Cu(II)SO_4•5H_2O$ was slowly added. The reaction was allowed to continue overnight under nitrogen gas.

The reaction was concentrated under vacuum, diluted with 400 mL water and acidified with 6N HCl. The product was extracted once with 200 mL ethyl acetate and twice with 150 mL ethyl acetate. The extracts were combined and washed with 500 mL water and dried with anhydrous Na_2SO_4. The ethyl acetate was removed under vacuum. The product was isolated as a white solid by chromatography using silica gel 5% (v/v) MeOH in CH_2Cl_2. **^{1}H NMR** (400 MHz, CD_3OD): δ 7.69 (d, *J* = 7.6, 2H), δ 7.60 (t, *J* =

8.0, 2H), δ 7.31 (t, *J* = 7.2, 2H), δ 7.24 (t, *J* = 7.2, 2H), δ 4.30 (d, *J* = 6.8, 2H), δ 4.19 (m, 1H), δ 4.13 (t, *J* = 6.8, 1H), δ 3.17 (m, 2H), δ 1.90-1.35 (m, 6H);

viii. Tris-triazole ligand

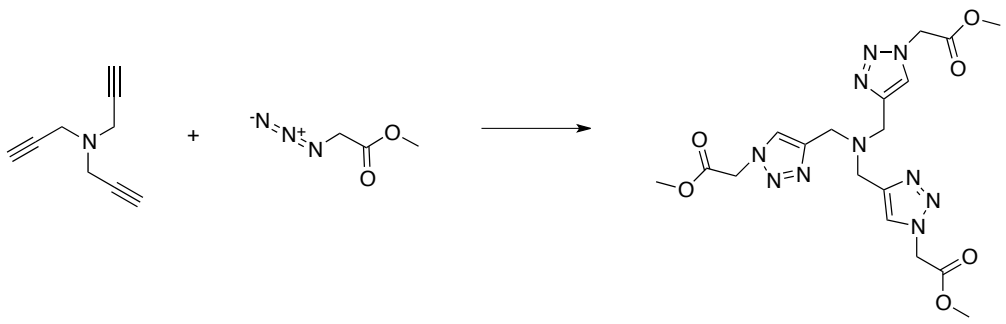

Methyl azido acetate (0.9278 g, 8.06 mmol) was added to a solution of tripropargyl amine (0.2656 g, 2.015 mmol) in 4 mL acetonitrile using a 25 mL round bottom flask in an ice bath. $[Cu(CH_3CN)_4]PF_6$ (0.246 g, 0.066 mmol) was added to the solution. Slowly, 1.2 mL DIPEA was added and purged with nitrogen for 10 mins. The reaction proceded overnight while capped with a septum. The reaction was concentrated by vacuum and dissolved in 1 mL 5% MeOH in CH_2Cl_2 and isolated by chromatography using silica gel with 5% MeOH in CH_2Cl_2 as the mobile phase. $\mathbf{H^1}$ (400 MHz, CD_2Cl_2): δ 7.842 (s, 1H), δ 5.185 (s, 2H), δ 3.815 (s, 2H), δ 3.803 (s, 3H).

ix. Synthesis of Coiled-coil and (H3 K9Me$_2$)$_2$ Peptide

Coiled-coil peptides were synthesized using automated solid phase peptide synthesis with a Thuramed tetras synthesizer on a 0.06 mmol scale. Fmoc protected amino acids were used with a Clear amide resin from Peptides International, Inc. Amino acid residues were activated with HBTU (O-benzotriazole-N,N,N',N',-tetramethyluronium hexafluorophosphate) and HOBT (N-hydroxybenzotriazole) with DIPEA (diisopropylethylamine) in DMF (N,N-dimethylformamide). Amino acids were deprotected twice with 2% DBU (1,8-diazabicyclo[5.4.0]undec-7-ene) and 2% piperidine

in DMF for 15 mins each step. Each amino acid was coupled on double cycles of 60 mins each to improve coupling. Peptides were capped on the N-terminus with an acetyl cap using a 5 mL solution of 5% acetic anhydride and 6%2,6-lutidine in DMF and allowed to mix for 30 mins. Peptides capped with bromoacetic acid were done so as follows. Four equivalents of HOBt, 4 equivalents of HBTU, and 4 equivalents of bromoacetic acid to peptide were dissolved in 5 mL DMF and added to the resin. Four equivalents of DIPEA were added last and the reaction was allowed to bubble with nitrogen for 20 mins. This sequence of steps was repeated twice. Cleavage of the peptides from the resin was performed in 95% trifluoroacetic acid (TFA), 2.5% H_2O, 2.5% triisopropylsilane (TIPS) for three hours. If cysteine was included in the sequence then 200 μL of ethane dithiol (EDT) was added to the cleavage cocktail. The TFA was evaporated off by blowing the reaction with nitrogen. Cold diethyl ether was used to precipitate the product. The product was extracted with deionized water and subsequently lyophilized to a powder for HPLC.

The (H3 $K9Me_2)_2$ peptide was synthesized as described in Chapter III only using Clear amide resin as opposed to Wang resin to improve yields. The N-terminus was capped with 5(6)-carboxyfluorescein as previously described.

Peptides were purified by reversed-phase HPLC. A Waters semi-preparative HPLC system with an Atlantis Prep OBD dC-18 semi-preparative column was used for separation with a gradient of 0% to 100% solvent B over 60 mins with solvent A (95:5 water:acetonitrile, 0.1% TFA) and solvent B (95:5 acetonitrile:water, 0.1% TFA). Peptides containing a variation of the ISAL E3 sequence eluted after 50% B so they were purified using a modified method. First gradient of 0% to 30% solvent B was reached in

2 mins and the column equilibrated at 30% for 5 mins. The gradient then proceeded to 100% solvent B in 42 mins. Peptides were then lyophilized and the molecular weight of the peptide was confirmed by ESI-TOF mass spectrometry (Table 5.8).

Peptide sequences:

I(N)SAL E3: Ac-EISALEKENSALEKEISALEKGGGY-NH_2

I(N)SAL K3: Ac-KISALKEKNSALKEKISALKEGGGY-NH_2

I(N)SAL E4: Ac-EISALEKENSALEKEISALEYEISALEK-NH_2

I(N)SAL K4: Ac-KISALKEKNSALKEKISALEYEISALEK-NH_2

G-ISAL E3-GGC: Ac-GEISALEKEISALEYEISALEKGGC-NH_2

ISAL K4-GGC: Ac-KISALKEKISALKYKISALKEGGC-NH_2

AcBr-ISAL E3-propargylG: AcBr-GGEISALEKEISALEYEISALEKGG(pG)-NH_2

AcBr-ISAL K3-azidoK: AcBr-GGKISALKEKISALKYKISALKEGG(azidoK)-NH_2

(H3 K9Me_2)$_2$: FAM-ARTKQTAR(KMe_2)STGGKAARTKQTAR(KMe_2)STKKA-NH_2

Table 5.8. Mass spectrometry data for the peptides synthesized and linked by disulfide exchange or by Huisgen cycloaddition for this study.

Peptide	Expected Mass (Da)	Experimental Mass (Da)
I(N)SAL E3	2705.4	2705.1
I(N)SAL K3	2702.5	2702.4
I(N)SAL E4	3475.8	3476.0
I(N)SAL K4	3472.0	3472.0
G-ISAL E3-GGC	2680.3	2679.5
ISAL K3-GGC	2619.5	2618.4
ISAL E3/K3-disulfide linked	5297.8	5298.3
AcBr-ISAL E3-propargylG	2806.3	2806.2
AcBr-ISAL K3-azidoK	2861.6	2861.3
ISAL E3/K3-click	5667.8	5668.1
(H3 K9Me$_2$)$_2$	3514.9	3514.8

x. Copper catalyzed Huisgen Cycloaddition

The ISAL E3-propargylG peptide and ISAL K3-azidoK peptides were each dissolved in a small volume of 10 mM potassium phosphate pH 8.0 buffer and the concentrations were determined by absorbance at 280 nm (λ_{280}=1490 $cm^{-1}M^{-1}$). The two peptides were combined in a 10 mL round bottom flask (12.63 μmol ISAL E3 propargylG, 12.484 μmol ISAL K3 azido K). The solution was degassed with nitrogen gas for 20 mins. To the solution, 1 equivalent (12.484 μmol, 5.9 mg) of tris-triazole ligand and 2 equivalents of $Cu(ACN_4)PF_6$ (24.968 μmol, 9.3 mg) were added to give a total reaction volume of 3.9 mL. After 45 hours the reaction was diluted with 10 mL of dH_2O and stored at -20^o C. The following day the reaction was filtered and purified by HPLC as described above using a gradient of 0% to 100% B over 60 mins. The product was confirmed by mass spectrometry (Table 5.5).

xi. Disulfide Exchange of Coiled-coils

A 4 mL solution with 50 μM ISAL K3-GGC and 50 μM G-ISAL E3-GGC in 10 mM sodium phosphate pH 7.4 buffer was prepared in a 20 mL glass scintillation vial. Solutions with 100 μM of either peptide were also prepared as controls. The reactions were monitored using reverse-phase HPLC with a Waters Alliance HPLC system and an Atlantis dC18 4 μm, 4.6x150 mm analytical column. The gradient used was 0%-65% solvent B over 130 mins with 50 μL of each of the three solutions. The HPLC trace was monitored at both 280 nm and 214 nm. Each peak from the ISAL K3/E3 mixture was collected on the third day because all three species were visible. The samples were lyophilized, dissolved in methanol, and analyzed by mass spectrometry (Table 5.5).

The equilibrium constant was calculated using the integration of the peaks (μV/sec) monitored at 280 nm after four days using Eq. 5.1 (Fig. 5.17) where $A_{E3/K3}$ refers to area under the ISAL E3/K3 peak, A_{E3} refers to area under the ISAL E3 peak, and A_{K3} refers to area under the ISAL K3 peak.

$$K_{eq} = \frac{\left(A_{E3/K3}\right)^2}{A_{E3} \cdot A_{K3}} \qquad \text{Eq. 5.1}$$

The free energy of binding can be calculated using Eq. 5.2.

$$\Delta G = -(1.987 \cdot 10^{-3} \frac{Kcal}{mol})(298K)\ln\left(\frac{K_{eq}}{4}\right) \qquad \text{Eq. 5.2}$$

xii. Circular Dichroism Characterization of Coiled-coils

CD measurements were performed on an Aviv 62DS Circular Dichroism Spectrometer. CD data was obtained for the chromodomain at 100 μM total peptide concentration (100 μM for homogenous solutions or 50 μM of each peptide in heterogeneous mixtures) in 10 mM Na_2HPO_4, pH 7.4. Wavelength scans were performed in triplicate and averaged. Scans were performed at 25° C from 260-185 nm. All scans were corrected by subtracting the spectrum of the buffer used in the experiment and the signal was converted to Mean Residue Ellipticity (MRE) using Eq. 5.3. Where signal refers to circular dichroism signal, ℓ is path length in cm, c is conentration in M, and r is the number of amino acid residues.

$$\Theta = \frac{signal}{10 \cdot \ell \cdot c} \cdot \frac{1}{r} \qquad \text{Eq. 5.3}$$

Guanidine denaturation experiments were carried out for I(N)SAL E4/K4 coiled-coils and monitored using circular dichroism at 222 nm. Solutions with 50 μM of each peptide and guanidine hydrochloride (0 M to 5 M) in 50 mM potassium phosphate pH7.0, 100 mM NaCl buffer were equilibrated at room temperature for 20 mins prior to analysis. Each measurement was taken with a buffer with the corresponding guanidine concentration as a blank. The signal was converted to MRE using Eq. 5.3 (Fig. 5.15).

The free energy in the presence of denaturant (ΔG_D) was calculated using Eq. 5.4 where F_F is fraction folded, θ_D is MRE when fully denatured, θ_F is MRE when fully folded, and F_u is fraction unfolded.

$$\Delta G_D = -RT\ln\left(\frac{2P_T F_U{}^2}{F_F}\right)$$
$$P_T = total\ peptide$$
$$F_F = \frac{[\theta]-[\theta]_D}{[\theta]_F-[\theta]_D}$$
$$F_U = 1 - F_F$$

Eq 5.4

From this calculation the energy of folding for the linear portion of the graph is Fig. 5.15 can be plotted against guanidine concentration (Fig. 5.16). The energy of binding without denaturant (ΔG^{H2O}) is equivalent to the Y-intercept in Fig. 5.16 and the dissociation constant can be calculated using Eq. 5.5.

$$\Delta G^{H_2O} = RT\ln(K_D) \qquad \text{Eq. 5.5}$$

xiii. Conjugation of Coiled-coils and Chromodomain

The linked BrAc-capped coiled-coils were dissolved in 50 mM potassium phosphate pH 8.0, 25 mM NaCl and the concentration was determined using a NanoDrop spectrophotometer (ε_{280} = 2980 $cm^{-1}M^{-1}$). The coiled-coil peptide was added to the appropriate amount of HP1α chromodomain R74C (3 or 4 equivalents) and TCEP (10 equivalents if applicable). The reaction was stirred for the time indicated at 4°C while covered with aluminum foil. For the large scale reaction 0.336 μmol coiled-coil was added to 1.009 μmol chromodomain R74C in a total volume of 5 mL. After four days the reaction was filtered and loaded on to an Akta Express FPLC from GE Healthcare and purified on HiLoad 16/60 Superdex 200 Gel Filtration column with a 50 mM potassium

phosphate pH7.0, 25 mM NaCl buffer as the mobile phase. The protein was concentrated using an Amicon Ultracentrifugation filter by Millipore (3000 MWCO) to 131.4 μM as determined by UV/VIS (e_{280}=40005 $cm^{-1}M^{-1}$).

xiv. Fluorescence Anisotropy with the Conjugate

The anisotropy measurements shown in Fig. 5.24 were performed using the various volumes of 131.4 μM conjugate stock with 1 μM (H3 $K9Me_2)_2$ peptide in 50 mM potassium phosphate, pH 8.0, 25 mM NaCl, 2 mM DTT (50 μL total volume). The peptide, and appropriate volumes of conjugate and additional buffer were mixed by pipetting in a Corning 385 well plate (Corning 3573) and centrifuged for 1 min at 4000 rpm and allowed to equilibrate at room temperature for 30 mins. Measurements were taken and analyzed as described in Chapter III.

The measurements shown in Fig. 5.25 were performed using the 131.4 μM conjugate stock, which was re-filtered with a 0.22 micron filter. The new concentration was determined to be 80.6 μM. Appropriate volumes of conjugate and buffer were added directly to the peptide in the Corning 385 well plate to obtain a peptide concentration of 200 nM and the samples were mixed by pipetting ten times. The plate was centrifuged, equilibrated, and analyzed as previously described.

References

1. Fischle, W.; Tseng, B. S.; Dormann, H. L.; Ueberheide, B. M.; Garcia, B. A.; Shabanowitz, J.; Hunt, D. F.; Funabiki, H.; Allis, C. D., Regulation of HP1-Chromatin Binding by Histone H3 Methylation and Phosphorylation. *Nature* **2005,** *438*, 1116-1122.

2. Ruthenburg, A. J.; Li, H.; Patel, D. J.; Allis, C. D., Multivalent Engagement of Chromatin Modifications by Linked Binding Modules. *Nat Rev Mol Cell BIol* **2007,** *8*, 984-994.

3. Peña, P. V.; Davrazou, F.; Shi, X.; Walter, K. L.; Verkhusha, V. V.; Gozani, O.; Zhao, R.; Kutateladze, T. G., Molecular Mechanism of Hisotne H3K4Me3 Recognition of Plant Homeodomain of ING2. *Nature* **2006,** *442*, 100-103.

4. Taverna, S. D.; Ueberheide, B. M.; Liu, Y.; Tackett, A. J.; Diaz, R. L.; Shabanowites, J.; Chait, T. B.; Hunt, D. F.; Allis, C. D., Long-Distance Combinatorial Linkage Between Methylation and acetylation on Histone H3 N-Termini. *Proc Natl Acad Sci* **2007,** *104*, 2086-2091.

5. Jensen, O. N.; Mann, M., Proteomic Analysis of Post-Translation Modifications. *Nature* **2003,** *21*, 255-261.

6. Chait, B. T., Mass Spectrometry: Bottom-Up or Top-Down? *Science* **2006,** *2006* (314), 65-66.

7. Fuchs, S. M.; Krajewski, K.; Baker, R. W.; Miller, V. L.; Strahl, B. D., Influence of Combinatorial Histone Modifications of Antibody and Effector Protein Recognition. *Curr Biol* **2010,** *21*, 53-58.

8. Melkko, S.; Dumelin, C. E.; Scheuermann, J.; Neri, D., On the magnitude of the Chelate Effect for the Recognition of Proteins by Pharmacophores Scaffolded by Self-Assembling Oligonucleotides. *Chem Biol* **2006,** *13*, 225-231.

9. William, B. A. R.; Ciehnelt, C. W.; Belcher, P.; Greving, M.; Woodbury, N. W.; Johnston, S. A.; Chaput, J. C., Creating Protein Affinity Reagents by Combining Peptide Ligands on Synthetic DNA Scaffolds. *J Am Chem Soc* **2009,** *131*, 17233-17241.

10. Burkhard, P.; Stetefeld, J.; Strelkov, S. V., Coiled-coils: A Highly Versatile Protein Folding Motif. *Trends Cell Biol* **2001,** *11*, 82-88.

11. Woolfson, D. N.; Alber, T., Predicting Oligomerization States of Coiled-coils. *Protein Sci* **1995,** *4*, 1596-1607.

12. Kohn, W. D.; Kay, C. M.; Hodges, R. S., Orientation, Positional, Additivity, and Oligomerization-State Effects of Interhelical Ion Pairs in α-Helical Coiled-Coils. *J Mol Biol* **1998,** *283*, 993-1012.

13. Litowski, J. R.; Hodges, R. S., Designing Heterodimeric Two-Stranded α-Helical Coiled-coils. *J Biol Chem* **2002,** *277*, 37272-37279.

14. Crick, F. H. C., The Packing of α-Helices: Simple Coiled-Coils. *Acta Crystallogr* **1953,** *6*, 689-697.

15. Graddis, T. J.; Myszka, D. G.; Chaiken, I. M., Controlled Formation of Model Homo- and Heterodimer Coiled-coil Polypeptides. *Biochemistry* **1993,** *32*, 12664-12671.

16. Gonzalez, L.; Woolfson, D. N.; Alber, T., Buried Polar Residues and Structural Specificity in the GCN4 Leucine Zipper. *Nat Struct Biol* **1996,** *3*, 1011-1018.

17. O'shea, E. K.; Lumb, K. J.; Kim, P. s., Peptide 'Velcro': Design of a Heterodimeric Coiled-coil. *Curr Biol* **1993,** *3*, 658-667.

18. Jacobs, S. A.; Taverna, S. D.; Zhang, Y.; Briggs, S. D.; Li, J.; Eissenberg, J. C.; Allis, C. D.; Khorasanizadeh, S., Specificity of the HP1 Chromo Domain for the Methylated N-Terminus of Histone H3. *EMBO J* **2001,** *20*, 5232-5241.

19. Goddard-Borger, E. D.; Stick, R. V., An Efficient, Inexpensive, and Shelf-Stable Diazotransfer Reagent: Imidazole-1-sulfonyl Azide Hydrochloride. *Org Lett* **2007,** *9*, 3797-3800.

BIBLIOGRAPHY

Allfrey, V. G.; Faulkner, R.; Mirsky, A. E., Acetylation and Methylation of Histones and Their Possible Role in the Regulation of RNA Synthesis. *Biochemistry* **1964,** 51, 786-794.

Amato, I., To Save Space, Genomic DNA is Packaged Into Chromatin. *Chem Eng News* **2006,** 84,18.

Bannister, A. J.; Zegerman, P.; Partidge, J. F.; Miska, E. A.; Thomas, J. O.; Allshire, R. C.; Kouzarides, T., Selective Recognition of Methylated Lysine 9 on Histone H3 by the HP1 Chromo Domain. *Nature* **2001,** 410, 120-124.

Bedford, M. T., Clarke, S. G., Protein Arginine Methylation in Mammals: Who, What, and Why. *Mol Cell* **2009,** 33, 1-13.

Berger, S. L., The Complex Language of Chromatin Regulation During Transcription. *Nature* **2007,** 447, 407-412.
Bernard, P.; Maur, J.-F.; Partidge, J. F.; Genier, S.; Javerzat, J.-P.; Allshire, R. C., Requirement of Heterochromatin for Cohesion at Centromeres. *Science* **2001,** 294, 2539-2542.

Botuyan, M. V.; Lee, J.; Ward, I. M.; Kim, J. E.; Thompson, J. R.; Chem, J.; Mer, G., Structural Basis for the Methylation Sate-Specific Recognition of Histone H4-K20 by 53BP1 and Crb2 in DNA Repair. *Cell* **2006,** 127,

Branscombe, T. L.; Frankel, A.; Lee, J.-H.; Cook, J. R.; Yang, Z.-H.; Pestka, S.; Clarke, S., PRMT5 (Janus Kinase-binding Protein 1) Catalyzes the Formation of Symmetric Dimethylarginine Residues in Proteins. *J Biol Chem* **2001,** 276, 32971-32976.

Briggs, S. D.; Bryk, M.; Strahl, B. D.; Cheung, W. L.; Davie, J. R.; Dent, S. Y. R.; Winston, F.; Allis, C. D., Histone H3 Lysine 4 Methylation is Mediated by Set1 and Required for Cell Growth and rDNA Silencing in *Saccharomyces cerevisiae*. *Genes Dev* **2001,** 15, 3286-3295.

Burkhard, P.; Stetefeld, J.; Strelkov, S. V., Coiled-coils: A Highly Versatile Protein Folding Motif. *Trends Cell Biol* **2001,** 11, 82-88.

Canzio, D.; Chang, E.; Shankar, S.; Kuchenbecker, K. M.; Simon, M. D.; Madhani, H. D.; Narlikar, G. J.; Al-Sady, B., Chromodomain-Mediated Oligomerization of HP1 Suggests a Nucleosome-Bridging Mechanism for Heterochromatin Assembly. *Mol Cell* **2011,** 41, 67-81.

Cao, R.; Wang, L.; Wang, H.; Xia, L.; Erdjument-Bromage, H.; Tempst, P.; Jones, R. S.; Zhang, Y., Role of Histone H3 Lysine 27 Methylation in Polycomb-Group Silencing. *Science* **2002,** 298, 1039-1043.

Chait, B. T., Mass Spectrometry: Bottom-Up or Top-Down? *Science* **2006,** 2006, 65-66.

Chang, X.; Yamada, R.; Suzuki, A.; Sawada, T.; Yoshino, S.; Tokuhiro, S.; Yamamoto, K., Localization of Peptidylarginine Deiminase 4 (PADI4) and Citrullinated Protein in Synovial Tissue of Rheumatoid Arthritis. *Rheumatology* **2004,** 44, 40-50.

Chen, D.; Ma, H.; Hong, H.; Koh, S. S.; Huang, S. M.; Schurter, B. T.; Aswad, D. W.; Stallcup, M. R., Regulation of Transcription by a Protein Methyltransferase. *Science* **1999,** 240, 2174-2177.

Cheng, X.; Zhang, Y., Structural Dynamics of Protein Lysine Methylation and Demethylation. *Mutat Res* **2007,** 618, 102-115.

Cheung, P.; Tanner, K. G.; Cheung, W. L.; Sassone-Cori, P.; Denu, J. M.; Allis, C. D., Synergistic Coupling of Histone H3 Phosphorylation and Acetylation in Response to Epidermal Growth Factor Stimulation. *Mol Cell* **2000,** 5, 905-915.

Chin, H. G.; Patnaik, D.; Estève, P.-O.; Jacobsen, S. E.; Pradhan, S., Catalytic Properties and Kinetic Mechanism of Human Recombinant Lys-9 Histone H3 Methyltransferase SUV39H1: Participation of the Chromodomain in Enzymatic Catalysis. *BIochemistry* **2006,** 45, 3272-3284.

Chochran, A. G.; Tong, R. T.; Starovasnik, M. A.; Park, E. J.; McDowell, R. S.; Theaker, J. E.; Skelton, N. J., A Minimal Peptide Scaffold for β-Turn Display: Optimizing a Strand Position in Disulfide-Cyclized β-Hairpins. *J Am Chem Soc* **2001,** 123, 625-632.

Couture, J.-F.; Collazo, E.; Trievel, R. C., Molecular Recognition of Histone H3 by the WD40 Protein WDR5. *Nat Struct Mol Biol* **2006,** 13, 698-703.

Crick, F. H. C., The Packing of α-Helices: Simple Coiled-Coils. *Acta Crystallogr* **1953,** 6, 689-697.

Daujat, S.; Zeissler, U.; Waldmann, T.; Happel, N.; Schneider, R., HP1 Bind Specifically to Lys^{26} Methylated Histone 1.4, Whereas Simultaneous Ser^{27} Phosphorylation Blocks HP1 Binding. *J Biol Chem* **2005,** 280, 28090-28095.

Dou, Y.; Gorovsky, M. A., Phosphorylation of Linker Histone H1 Regulates Gene Expression In Vivo by Creating a Charge Patch. *Mol Cell* **2000,** 6, 225-231.

Egger, G.; Liang, G.; Aparicio, A.; Jones, P. A., Epigenetics in Human Disease and Prospects for Epigenetic Therapy. *Nature* **2004,** 429, 457-463.

Fabbrizio, E.; Messaoudi, S. E.; Polanowka, J.; Paul, C.; Cook, J. R.; Lee, J.-H.; Nègre, V.; Rousset, M.; Pestka, S.; Cam, A. L.; Sardet, C., Negative Regulation of Transcription by the Type II Arginine Methyltransferase PRMT5. *EMBO Rep* **2002,** 3, 641-645.

Fischle, W.; Tseng, B. S.; Dormann, H. L.; Ueberheide, B. M.; Garcia, B. A.; Shabanowitz, J.; Hunt, D. F.; Funabiki, H.; Allis, C. D., Regulation of HP1-Chromatin Binding by Histone H3 Methylation and Phosphorylation. *Nature* **2005,** 438, 1116-1122.

Fischle, W.; Wang, Y.; Jacobs, S. A.; Kim, Y.; Allis, C. D.; Khorasanizadeh, S., Molecular Basis for the Discrimination of Repressive Methyl-Lysine Marks in Histone H3 by Polycomb and HP1 Chromodomains. *Genes Dev* **2003,** 17, 1870-1881.

Flanagan, J. F.; Mi, L. Z.; Chruszcz, M.; Cymborowski, M.; Clines, K. L.; Kim, Y.; Minor, W.; Rastinejad, F.; Khorasanizadeh, S., Double Chromodomains Cooperate to Recognize the Methylated Histone H3 Tail. *Nature* **2005,** 438, 1181-1185.

Frenster, J. H.; Allfrey, V. G.; Mirsky, A. E., Repressed and Active Chromatin Isolated from Interphase Lymphocytes. *Biochemistry* **1963,** 50, 1026-1032.

Fuchs, S. M.; Krajewski, K.; Baker, R. W.; Miller, V. L.; Strahl, B. D., Influence of Combinatorial Histone Modifications of Antibody and Effector Protein Recognition. *Curr Biol* **2010,** 21, 53-58.

Fuks, F.; Hurd, P. J.; Wolf, D.; Nan, X.; Bird, A. P.; Kouzarides, T., The Methyl-CpG-binding Protein MeCP2 Links DNA Methylation to Histone Methylation. *J Biol Chem* **2003,** 278, 4035-4040.

Gallivan, J. P.; Dougherty, D. A., Cation-π Interactions in Structural Biology. *Proc Natl Acad Sci* **1999,** 96, 9459-9464.

Goddard-Borger, E. D.; Stick, R. V., An Efficient, Inexpensive, and Shelf-Stable Diazotransfer Reagent: Imidazole-1-sulfonyl Azide Hydrochloride. *Org Lett* **2007,** 9, 3797-3800.

Gonzalez, L.; Woolfson, D. N.; Alber, T., Buried Polar Residues and Structural Specificity in the GCN4 Leucine Zipper. *Nat Struct Biol* **1996,** 3, 1011-1018.

Graddis, T. J.; Myszka, D. G.; Chaiken, I. M., Controlled Formation of Model Homo- and Heterodimer Coiled-coil Polypeptides. *Biochemistry* **1993,** 32, 12664-12671.

Greenfield, N. J., Methods to Estimate the Conformation of Proteins and Polypeptides from Circular Dichroism Data. *Anal Biochem* **1996,** 235, 1-10.

Guo, Y.; Nady, N.; Qi, C.; Allali-Hassani, A.; Zhu, H.; Pan, P.; Adams-Cioaba, M. A.; Amaya, M. F.; Dong, A.; Vedadi, M.; Schapira, M.; Read, R. J.; Arrowsmith, C. H.; Min, J., Methylation-State-Specific Recognition of Histones by the MBT Repeat Protein L3MBTL2. *Nucl Acids Res* **2009,** 37, 2204-2210.

György, B.; Tóth, E.; Tarcsa, E.; Falus, A.; Buzás, E., Citrullination: A Posttranslational Modification in Health and Disease. *Int J Biochem Cell Biol* **2006,** 38, 1662-1677.

Hagiwara, T.; Nakashima, K.; Hirano, H.; Senshu, T.; Yamada, M., Demination of Arginine Residues in Neucleophosmin/B23 and Histones in HL-60 Granulocytes. *Biochem Biophys Res Commun* **2002,** 290, 979-983.

Hansen, J. C.; Tse, C.; Wolffe, A. P., Structure and Function of the Core Histone N-Termini: More Than Meets the Eye. *Biochemistry* **1998,** 37, 17637-17641.

Hirota, T.; Lipp, J. J.; Toh, B.-H.; Peters, J.-M., Histone H3 Serine 10 Phosphorylation by Aurora B Causes HP1 Dissociation from Heterochromatin. *Nature* **2005,** 438, 1176-1180.

Hughes, R. M.; Waters, M. L., Arginine Methylation in a β-Hairpin Peptide: Implications for Arg-π Interactions, ΔC_p^o, and the Cold Denatured State. *J Am Chem Soc* **2006,** 128, 12735-12742.

Hughes, R. M.; Wiggins, K. R.; Khorasanizadeh, S.; Waters, M. L., Recognition of Trimethyllysine by a Chromodomain is not Driven by the Hydrophobic Effect. *Proc Natl Acad Sci* **2007,** 104, 11184-11188.

Hunter, C. A.; Lawson, K. R.; Perkins, J.; Urch, C. J., Aromatic Interactions. *J Chem Soc-Prkin Trans* **2001,** 2, 651-669.

Hutchinson, E. G.; Sessions, R. B.; Thornton, J. M.; Woolfson, D. N., Determinants of Strand Register in Antiparallel β-sheets of Proteins. *Protein Sci* **1998,** 7, 2287-2300.

Iberg, A. N.; Espejo, A.; Cheng, D.; Kim, D.; Michaud-Levesque, J.; Richard, S.; Bedford, M. T., Arginine Methylation of the Histone H3 Tail Impedes Effector Binding. *J Biol Chem* **2008,** 283, 3006-3010.

Iwase, S.; Lan, F.; Bayliss, P.; Torr-Ubieta, L.; Huarte, M.; Qi, H. H.; Whetstine, J. R.; Bonni, A.; Roberts, T. M.; Shi, Y., The X-Linked Mental Retardation Gene SMCX/JARID1C Defines a Family of HIstone H3 Lysine 4 Demethylases. *Cell* **2007,** 128, 1077-1088.

Jackrel, M. E.; Valverde, R.; Regan, L., Redesign of a Protein-Peptide Interaction Characterization and Applications. *Protein Sci* **2009,** 18, 762-774.

Jacobs, S. A.; Fischle, W.; Khorasanizadeh, S., Assays for the Determination of Structure and Dynamics of the Interaction of the Chromodomain with Histone Peptides. *Methods Enzymol* **2004,** 376, 131-148.

Jacobs, S. A.; Khorasanizadeh, S., Structure of HP1 Chromodomain Bound to a Lysine 9-Methylated Histone H3 Tail. *Science* **2002,** 295, 2080-2083.

Jacobs, S. A.; Taverna, S. D.; Zhang, Y.; Briggs, S. D.; Li, J.; Eissenberg, J. C.; Allis, C. D.; Khorasanizadeh, S., Specificity of the HP1 Chromo Domain for the Methylated N-Terminus of Histone H3 *EMBO J* **2001,** 20, 5232-5241.

Jacobson, R. H.; Ladurner, A. G.; King, D. S.; Tjian, R., Structure and Funciton of Human $TAF_{II}250$ Double Bromodomain Module. *Science* **2000,** 288, 1422-1425.

Jensen, O. N.; Mann, M., Proteomic Analysis of Post-Translation Modifications. *Nature* **2003,** 21, 255-261.

Johnson, L.; Mollah, S.; Garcia, B. A.; Muratore, T. L.; Shabanowites, J.; Hunt, D. F.; Jacobsen, S. E., Mass Spectrometry Analysis of *Arabidopsis* Histone H3 Reveals Distinct Combinations of Post-Translational Modifications. *Nucl Acids Res* **2004,** 32, 6511-6518.

Kearney, P. L.; Bhatia, M.; Jones, N. G.; Yuan, L.; Glascock, M. C.; Catchings, K. L.; Yamada, M.; Thompson, P. R., Kinetics Characterization of Protein Arginine Deiminase 4: A Transcriptional Corepressor Implicated in the Onset and Progression of Rheumatoid Arthritis. *Biochemistry* **2005,** 44, 10570-10582.

Kelly, S. M.; Price, N. C., The Use of Circular Dichroism in the Investigation of Protein Structure and Function. *Curr Protein Pept Sci* **2000,** 1, 349-384.

Keogh, M.-C.; Kurdistani, S. K.; Morris, S. A.; Ahn, S. H.; Podolny, V.; Collins, S. R.; Schuldiner, M.; Chin, K.; Punna, T.; Thompson, N. J.; Boone, C.; Emili, A.; Weissman, J. S.; Hughes, T. R.; Strahl, B. D.; Grunstein, M.; Greenblatt, J. F.; Buratowski, S.; Krogan, N. J., Cotranscriptional Set2 Methylation of Histone H3 Lysine 36 Recruits a Repressive Rpd3 Complex. *Cell* **2005,** 123, 593-605.

Kohn, W. D.; Kay, C. M.; Hodges, R. S., Orientation, Positional, Additivity, and Oligomerization-State Effects of Interhelical Ion Pairs in α-Helical Coiled-Coils. *J Mol Biol* **1998,** 283, 993-1012.

Kouzarides, T., Chromatin Modifications and Their Function. *Cell* **2007,** 128, 693-705.
Lachner, M.; O'Carroll, D.; Rea, S.; Mechtler, K.; Jenuwein, T., Methylation of Histone H3 Lysine 9 Creates a Binding Site for HP1 Proteins. *Nature* **2001,** 410, 116-120.

Lan, F.; Collins, R. E.; Cegli, R. D.; Alpatov, R.; Horton, J. R.; Shi, X.; Gozani, O.; Cheng, X.; Shi, Y., Recognition of Unmethylated Histone H3 Lysine 4 Links BHC80 to LSD1-Mediated Gene Repression. *Nature* **2007,** 448, 718-722.

Langan, T. A., Histone Phosphorylation: Stimulation by Adenosine 3',5'-Monophosphate. *Science* **1968,** 162, 579-580.

Langan, T. A., Cyclic AMP and Histone Phosphorylation. *Ann NY Acad Sci* **1971,** 185, 166-180.

Latham, J. A.; Dent, S. Y. R., Cross-Regulation of Histone Modifications. *Nat Struct Mol Biol* **2007,** 14, 1017-1024.

Lee, D. Y.; Teyssier, C.; Strahl, B. D.; Stallcup, M. R., Role of Protein Methylation in Regulatio of Transcription. *Endocr Rev* **2005,** 26, 147-170.

Lee, J.-H.; Cook, J. R.; Yang, Z.-H.; Mirochnitchenko, O.; I., G. S.; Felix, A. M.; Herth, N.; Hoffman, R.; Peska, S., PRMT7, a New Protein Arginine Methyltransferase that Synthesizes Symmetric Dimethylarginine. *J Biol Chem* **2005,** 280, 3656-3664.

Li, H.; Fischle, W.; Wang, W.; Duncan, E. M.; Liang, L.; Murakami-Ishibe, S.; Allis, C. D.; Patel, D. J., Structural Basis for Lower Lysine Methylation Sate-Specific Readout by MBT Repeats of L3MBTL1 and an Engineered PHD Finger. *Mol Cell* **2007,** 28, 677-691.

Li, H.; Llin, S.; Wang, W.; Duncan, E. M.; Wysocka, J.; Allis, C. D.; Patel, D. J., Molecular Basis for Site-Specific Read-Out of Histone H3K4me3 by the BPTF PHD Finger of NURF. *Nature* **2006,** 442, 91-95.

Liang, G.; Lin, J. C. Y.; Wei, V.; Yoo, C.; Cheng, J. C.; Nguyen, C. T.; Weisenberger, D. J.; Egger, G.; Takai, D.; Gonzales, F. A.; Jones, P. A., Distinct Localization of Hisotne H3 Acetylation and H3-K4 Methylation to the Transcriptional Start Sites in the Human Genome. *Proc Natl Acad Sci* **2004,** 101, 7357-7362.

Lindroth, A. M.; Shultis, D.; Jasencakova, Z.; Fuchs, J.; Johnson, L.; Schubert, D.; Patnaik, D.; Pradhan, S.; Goodrich, J.; Schubert, I.; Jenuwein, T.; Khorasanizadeh, S.; Jacobson, S. E., Dual Histone H3 Methylation Marks at Lysines 9 and 27 Required for Interaction with Chromomethylase3. *EMBO J* **004,** 23, 4286-4296.

Litowski, J. R.; Hodges, R. S., Designing Heterodimeric Two-Stranded α-Helical Coiled-coils. *J Biol Chem* **2002,** 277, 37272-37279.

Lo, W.-S.; Trievel, R. C.; Rojas, J. R.; Duggan, L.; Hsu, J.-Y.; Allis, C. D.; Marmorstein, R.; Berger, S. L., Phosphorylation of Serine 10 in Histone H3 Is Functionally Linked In Vitro and In Vivo to Gcn5-Mediated Acetylation at Lysine 14 *Mol Cell* **2000,** 5, 917-926.

Lorenzo, A. D.; Bedford, M. T., Histone Arginine Methylation. *FEBS Lett* **2011,**
Lu, Q.; Qiu, X.; Hu, N.; Wen, H.; Su, Y.; Richardson, B. C., Epigenetics, Disease, and Therapeutic Interventions. *Ageing Res Rev* **2006,** 5, 449-467.

Luger, K.; Mäder, A. W.; Richmond, R. K.; Sargent, D. F.; Richmond, T. R., Crystal Structure of the Nucleosome Core Particle at 2.8Å Resolution. *Nature* **1997,** 389, 251-160.

Ma, J. C.; Dougherty, D. A., The Cation-π Interaction. *Chem Rev* **1997,** 97, 1303.
Mahadevan, L. C.; Willis, A. C.; Barratt, M. J., Rapid Hisonte H3 Phosphorylation in Response to Growth Factors, Phorbol Ester, Okadaic Acid, and Protein Synthesis Inhibitors. *Cell* **1991,** 65, 775-783.

Maison, C.; Bailly, D.; Peters, H. E. M.; Quivy, J. P.; Roche, D.; Taddei, A.; Jenuwein, T.; Almousni, G., Higher-Order Structure in Pericentric Heterochromatin Involves a Distinct Pattern of HIstone Modification and an RNA Component. *Nat Genet* **2002,** 30, 329-334.

Martin, C.; Zhang, Y., The Diverse Functions of HIstone Lysine Methylation. *Nat Rev Mol Cell BIol* **2005,** 6, 838-849.

Marvin, K. W.; Yau, P.; Bradbury, E. M., Isolation and Characterization of Acetylated Histones H3 and H4 and Their Assembly into Nucleosomes. *J Biol Chem* **1990,** 265, 19839-19847.

Melkko, S.; Dumelin, C. E.; Scheuermann, J.; Neri, D., On the magnitude of the Chelate Effect for the Recognition of Proteins by Pharmacophores Scaffolded by Self-Assembling Oligonucleotides. *Chem BIol* **2006,** 13, 225-231.
Mello, C. C.; Conte, D., Revealing the World of RNA Interference. *Nature* **2004,** 431, 338-342.

Meyer, E. A.; Catellano, R. K.; Diederich, F., Interactions with Aromatic Rings in Chemical and Biological Recognition. *Angew Chem Int Ed* **2003,** 42, 1210-1250.

Minor, D. L.; Kim, P. S., Context is a Major Determinant of β-Sheet Propensity. *Nature* **1994,** 371, 264-267.

Moscarello, M. A.; Mastronardi, F. G.; Wood, D. D., The Role of Citrullinated Proteins Suggests a Novel Mechanism in the Pathogenesis of Multiple Sclerosis. *Neurochem Res* **2007,** 32, 251-256.

Nakayama, J.-I.; Rice, J. C.; Strahl, B. D.; Allis, C. D.; Grewal, S. I. S., Role of Histone H3 Lysine 9 Methylation in Epigenetic Control of Heterochromatin Assembly. *Science* **2001,** 292, 110-113.

Ng, H. H.; Ciccone, D. N.; Morshead, K. B.; Oettinger, M. A.; Struhl, K., Lysine-79 of Histone H3 is Hypomethylated at Silenced Loci in Yeast and Mammalian Cells: A Potential Mechanism for Position-Effect Variegation. *Proc Natl Acad Sci* **2003,** 100, 1820-1825.

Nielson, R. R.; Nietlispach, D.; Mott, H. R.; Callaghan, J.; Bannister, A.; Kousarides, T.; Murzin, A. G.; Murzina, N. V.; Laue, E. D., Stucture of the HP1 Chromodomain Bound to Histone H3 Methylated at Lysine9. *Nature* **2002,** 416, 103-107.

Noma, K.-i.; Allis, C. D.; Grewal, S. I. S., Transitions in Distinct Histone H3 Methylation Patterns at the Heterochromatin Domain Boundaries. *Science* **2001,** 293, 1150-1155.
O'shea, E. K.; Lumb, K. J.; Kim, P. s., Peptide 'Velcro': Design of a Heterodimeric Coiled-coil. *Curr Biol* **1993,** 3, 658-667.

Pace, C. N.; Scholtz, J. M., A Helix Propensity Scale Based on Experimental Studies of Peptides and Proteins. *Biophys J* **1998,** 75, 422-427.

Pal, S.; Vishwanath, S. N.; Erdjument-Bromage, H.; Tempst, P.; Sif, S., Human SWI/SNF-Associated PRMT5 Methylates Histone H3 Arginine 8 and Negatively Regulates Expression of ST7 and NM23 Tumor Suppressor Genes. *Mol Cell BIol* **2004,** 24, 9630-9645.

Pardon, J. F.; WIlkins, M. H. F.; Richards, B. M., Super-Helical Model for Nucleohistone. *Nature* **1967,** 215, 508-509.

Peña, P. V.; Davrazou, F.; Shi, X.; Walter, K. L.; Verkhusha, V. V.; Gozani, O.; Zhao, R.; Kutateladze, T. G., Molecular Mechanism of Hisotne H3K4Me3 Recognition of Plant Homeodomain of ING2. *Nature* **2006,** 442, 100-103.

Peters, A. H.; Mermoud, J. E.; O'Carroll, D.; Pagani, M.; Schweizer, D.; Brockdorff, N.; Jenuwein, T., Histone H3 Lysine 9 Methylation is an Epigenetic Imprint of Facultative Heterochromatin. *Nat Genet* **2001,** 30, 77-80.

Peters, A. H.; O'Carroll, D.; Scherthan, H.; Mechtler, K.; Sauer, S.; Schöfer, C.; Weipoltshammer, K.; Pagani, M.; Lachner, M.; Kohlmaier, A.; Opravil, S.; Doyle, M.; Sibilia, M.; Jenuwein, T., Loss of the Suv39h Histone Methyltransferases Impairs Mammalian Heterochromatin and Genome Stability. *Cell* **2001,** 107, 323-337.

Platero, J. S.; Hartnett, T.; Eissenberg, J. C., Functional Analysis of the Chromo Domain of HP1. *EMBO J* **1999,** 14, 3977-3986.

Pray-Grant, M. G.; Daniul, J. A.; Schieltz, D.; Yates, J. F.; Grant, P. A., Chd1 Chromodomain Links Histone H3 Methylation with SAGA-and SLIK-Dependent Acetylation. *Nature* **2005,** 433, 434-438.

Ren, Q.; Gorovsky, M. A., Histone H2A.Z Acetylation Modulates and Essential Charge Patch. *Mol Cell* **2001,** 7, 1329-1335.

Riemen, A. J.; Waters, M. L., Controlling Peptide Folding with Repulsive Interactions Between Phosphorylated Amino Acids and Tryptophan. *J Am Chem Soc* **2009,** 131, 14081-14087.

Russell, S. J.; Blandl, T.; Skelton, N. J.; Cochran, A. G., Stability of Cyclic β-Hairpins: Asymmetric Contributions from Side Chains of a Hydrogen-Bonded Cross-Strand Residue Pair. *J Am Chem Soc* **2002,** 124, 388-395.

Russell, S. J.; Cochran, A. G., Designing Stable β-Hairpins: Energetic Contributions from Cross-Strand Residues. *J Am Chem Soc* **2000,** 122, 12600-12601.

Ruthenburg, A. J.; Li, H.; Milne, T. A.; Dewell, S.; McHinty, R. K.; Yuen, M.; Ueberheide, B. M.; Dou, Y.; Muir, T. W.; Patel, D. J.; Allis, C. D., Recognition of a Mononucleosomal Histone Modification Pattern by BPTF via Multivalent Interactions. *Cell* **2011,** 145, 692-706.

Ruthenburg, A. J.; Li, H.; Patel, D. J.; Allis, C. D., Multivalent Engagement of Chromatin Modifications by Linked Binding Modules. *Nat Rev Mol Cell BIol* **2007,** 8, 984-994.

Santon-Rosa, H.; Schneider, R.; Bannister, A. J.; Sherriff, J.; Berstein, B. E.; Tolga Emre, N. C.; Schreiber, S. L.; Mellow, J.; Kouzarides, T., Active Genes are Tri-methylated at K4 of Histone H3. *Nature* **2002,** 419, 407-411.

Schalch, T.; Job, G.; Noffsinger, V. J.; Shanker, S.; Kuscu, C.; Joshua-Tor, L.; Partridge, J. F., High-Affinity Binding of Chp1 Chromodomaini to K9 Methylated Histone H3 Is Required to Establish Centromeric Heterochromatin. *Mol Cell* **2009,** 34, 36-46.

Schotta, G.; Ebbert, A.; Krauss, V.; Fischer, A.; Hoffmann, J.; Rea, S.; Jenuwein, T.; Dorn, R.; Reuter, G., Central Role of *Drosophila* SU(VAR)3-9 in Histone H3-K9 Methylation and Heterochromatic Gene Silencing. *EMBO J* **2002,** 21, 1121-1131.

Schreiber, G.; Fersht, A. R., Energetics of Protein-Protein Interactions: Analysis of the Barnase-Barstar Interface by Single Mutations and Double Mutant Cycles. *J Mol Biol* **1995,** 248, 478-486.

Schurter, B. T.; Koh, S. S.; Chen, D.; Bunick, G. J.; Harp, J. M.; Hanson, B. L.; Henschen-Edman, A.; Mackay, D. R.; Stallcup, M. R.; Aswad, D. W., Methylation of Histone H3 by Coactivator-Associated Arginine Methyltransferase 1. *Biochemistry* **2001,** 40, 5747-5756.

Shahbazian, M. D.; Grunstein, M., Functions of Site-Specific Histone Acetylation and Deacetylation. *Annu Rev Biochem* **2007,** 76, 75-100.

Shi, X.; *al, e.*, ING2 PHD Domain Links Histone H3 Lysine 4 Methylation to Active Gene Repression. *Nature* **2006,** 442, 96-99.

Shi, Y.; Lan, F.; Matson, C.; Mulligan, P.; Whetstine, J. R.; Cole, P. A.; Casero, R. A.; Shi, Y., Histone Demethylation Mediated by the Nuclear Amine Oxidase Homolog LSD1. *Cell* **2004,** 119, 941-953.

Shogren-Knaak, M.; Ishii, H.; Sun, J.-M.; Pazin, M. J.; Davie, J. R.; Peterson, C. L., Histone H4-K16 Acetylation Controls Chromatin Structure and Protein Interactions. *Science* **2006,** 311, 844-847.

Sims, R. J.; F., C. C.; Santos-Rosa, H.; Kouzarides, T.; Patel, S. S.; Reinberg, D., Human but Not Yeast CHD1 Binds Directly and Selectively to Histone H3 Methylated at Lysine 4 via Its Tandem Chromodomains. *J Biol Chem* **2005,** 280, 41789-41792.

Smith, C. K.; Regan, L., Guidelines for Protein Design: The Energetics of β--Sheet Side Chain Interactions. *Science* **1995,** 270, 980-982.

Smith, C. K.; Regan, L., Construction and Design of β-Sheets. *Acc Chem Res* **1997,** 30, 153-161.

Smith, C. K.; Withka, J. M.; Regan, L., A Thermodynamic Sale for the β-Sheet Forming Tendencies of the Amino Acids. *Biochemistry* **1994,** 33, 5510-5517.

Smothers, J. F.; Henikoff, S., The HP1 Chromo Shadow Domain Binds a Consensus Peptide Pentamer. *Curr Biol* **2000,** 10, 27-30.

Stokes, D. G.; Perry, R. P., DNA-Binding and Chromatin Localization Properties of CHD1. *Mol Cell Biol* **1995,** 15, 2745-2753.

Strahl, B. D.; Allis, C. D., The Language of Covalent Histone Modifications. *Nature* **2000,** 403, 41-45.

Strahl, B. D.; Briggs, S. D.; Brame, C. J.; Caldwell, J. A.; Koh, S. S.; Ma, H.; Cook, R. G.; Shabanowites, J.; Hunt, D. F.; Stallcup, M. R.; Allis, C. D., Methylation of Histone H4 at Arginine 3 Occurs In Vivo and is Mediated by the Nuclear Receptor Coactivator PRMT1. *Curr Biol* **2001,** 11, 996-1000.

Stravropoulos, P.; Blobel, G.; Hoelz, A., Crystal Structure and Mechanism of Human Lysine-Specific Demethylase-1. *Nat Struct Mol Biol* **2006,** 13, 626-632.

Strelkov, S. V.; Davie, J. R., Ser-10 Phosphorylation of Histone H3 and Immediate Early Gene Expression in Oncogene-Transformed Mouse Fibroblasts. *Cancer Res* **2002,** 62, 75-78.

Syud, F. A.; Stanger, H. E.; Gellman, S. H., Interstrand Side Chain-Side Chain Interactions in a Designed β-Hairpin: Significance of Both Lateral and Diagonal Pairings. *J Am Chem Soc* **2001,** 123, 8667-8677.

Tate, P. H.; Bird, A. P., Effects of DNA Methylation on DNA-BOnding Proteins and Gene Expression. *Curr Opin Genet Dev* **1993,** 226-231.

Tatko, C. D.; Waters, M. L., Selective Aromatic Interactions in β-Hairpin Peptides. *J Am Chem Soc* **2002,** 124, 9372-9373.

Tatko, C. D.; Waters, M. L., The Geometry and Efficacy of Cation-π Interactions in a Diagonal Position of a Desgined β-Hairpin. *Protein Sci* **2003,** 12, 2443-2452.

Taverna, S. D.; Li, H.; Ruthenburg, A. J.; Allis, C. D.; Patel, D. J., How Chromatin-Binding Modules Interpret Histone Modifications: Lessons from Professional Pocket Pickers. *Nat Struct Mol Biol* **2007,** 14, 1025-1040.

Taverna, S. D.; Ueberheide, B. M.; Liu, Y.; Tackett, A. J.; Diaz, R. L.; Shabanowites, J.; Chait, T. B.; Hunt, D. F.; Allis, C. D., Long-Distance Combinatorial Linkage Between Methylation and acetylation on Histone H3 N-Termini. *Proc Natl Acad Sci* **2007,** 104, 2086-2091.

Thoma, F.; Koller, T. H.; Klug, A., Involvement of Histone H1 in the Organization of the Nucleosome and of the salt-Dependent Superstructures of Chromatin. *J Cell Biol* **1979,** 83, 403-427.

Tran, H. G.; Steger, D. J.; Lyer, V. R.; Johnson, A. D., The Chromo Domain Protein Chd1p from Budding Yeast is an ATP-Dependent Chromatin-Modifying Factor. *EMBO J* **2000,** 19, 2323-2331.

Tsukada, Y.-i.; Fang, J.; Erdjument-Bromage, H.; Warren, M. E.; Borchers, C. H.; Tempst, P.; Zhang, Y., Histone Demethylation by a Family of JmjC Domain-Containing Proteins. *Nature* **2006,** 439, 811-816.

vanHolde, K. E., (ed. Rich, A.) 111-148 (Springer, NewYork, 1988). **1988,**

Venter, J. C.; *al, e.*, The Sequence of the Human Genome. *Science* **2001,** 291, 1304-1351.

Waddington, C. H., The Epigenotype. *Endeavour* **1942,** 1, 18-20.

Waddington, C. H. (1957). The Strategy of the Genes. London, Allen and Unwin.

Wang, H.; Huang, Z.-Q.; Xia, L.; Feng, Q.; Erdjument-Bromage, H.; Strahl, B. D.; Briggs, S. D.; Allis, C. D.; Wong, J.; Tempst, P.; Zhang, Y., Methylation of Hisotne H4 at Arginine 3 Facilitating Transcriptional Activation by Nuclear Hormone Recptor. *Science* **2001,** 293, 853-857.

Wang, Y.; Wysocka, J.; Syegh, J.; Lee, Y. H.; Perlin, J. R.; Leonelli, L.; Sonbuchner, L. S.; McDonald, C. H.; Cook, R. G.; Dou, Y.; Roeder, R. G.; Clarke, S.; Stallcup, M. R.; Allis, C. D.; Coonrod, S. A., Human PAD4 Regulates Histone Arginine Methylation Levels via Demethylimination. *Science* **2004,** 306, 279-283.

Wei, Y.; Yu, L.; Bowen, J.; Gorovsky, M. A.; Allis, C. D., Phosphorylation of Hisonte H3 is Required for Proper Chromosome Condensation and Segregation. *Cell* **1999,** 91, 99-109.

Whetstine, J. R.; Nottke, A.; Lan, F.; Smolikov, S.; Chen, Z.; Spooner, E.; Li, E.; Zhang, G.; Colaiacovo, M.; Shi, Y., Reversal of Histone Lysine Trimethylation by the JMJD2 Family of Histone Demethylases. *Cell* **2006,** 125, 467-481.

Widom, J., Toward a Unified Model of Chromatin Folding. *Annu Rev Biophys Bio* **1989,** 18, 365-395.

William, B. A. R.; Ciehnelt, C. W.; Belcher, P.; Greving, M.; Woodbury, N. W.; Johnston, S. A.; Chaput, J. C., Creating Protein Affinity Reagents by Combining Peptide Ligands on Synthetic DNA Scaffolds. *J Am Chem Soc* **2009,** 131, 17233-17241.

Williams, R. W.; Chang, A.; Juretić, D.; Loughran, S., Secondary Structure Predictions and Medium Range Interactions. *Biochim Biophys Acta* **1987,** 916, 200-204.
Wolffe, A. P.; Hayes, J. J., Chromatin Disruption and Modification. *Nucl Acids Res* **1999,** 27, 711-720.

Woolfson, D. N.; Alber, T., Predicting Oligomerization States of Coiled-coils. *Protein Sci* **1995,** 4, 1596-1607.

Wouters, M. A.; Curmi, P. M. G., An Analysis of Side Chain Interactions and Pair Correlations Within Antiparallel β-Sheets: The Differences Between Backbone Hydrogen-Bonded and Non-Hydrogen-Bonded Residue Pairs. *Proteins* **1995,** 22, 119-131.

Wysocka, J.; Allis, C. D.; Coonrod, S., Histone Arginine Methylation and its Dynamic Regulation. *Font Biosci* **2006,** 11, 344-355.

Xiao, B.; Jing, C.; Wilson, J. R.; Walker, P. A.; Vasisht, N.; Kelly, G.; Howell, S.; Taylor, I. A.; Blackburn, M.; Gamblin, S. J., Structure and Catalytic Mechanism of the Human Histone Methyltransferase SET7/9. *Nature* **2003,** 421, 652-656.

Yang, Y.; Lu, Y.; Espejo, A.; Wu, J.; Xu, W.; Liang, S.; Bedford, M. T., TDRD3 is an Effector Molecule for Arginine-Methylated Histone Marks. *Mol Cell* **2010,** 40, 1016-1023.

Zhang, Y.; Reinberg, D., Transcription Regulation by Histone Methylation: Interplay Between Different Covalent Modifications of the Core Histone Tails. *Genes Dev* **2001,** 15, 2343-2360.

Zhao, Q.; Rank, G.; Tan, Y. T.; Li, H.; Moritz, R. L.; Simpson, R. J.; Cerruti, L.; Curtis, D. J.; Patel, D. J.; Allis, C. D.; Cunningham, J. M.; Jane, S. M., PRMT5-Mediated Methylation of Histone H4R3 Recruits DNMT3A, Coupling Histone and DNA Methylation in Gene Silencing. *Nat Struct Mol Biol* **2009,** 16, 304-311.

Zhao, X. D.; Han, X.; Chew, J. L.; Liu, J.; Chiu, K. P.; Choo, A.; Orlov, Y. L.; Sung, W.-K.; Shahab, A.; Kuznetsov, V. A.; Bourque, G.; Oh, S.; Ruan, Y.; JNg, H.-H.; Wei, C.-L., Whole-Genome Mapping of Histone H3 Lys4 and 27 Trimethylations Reveals Distinct Genomic Compartments in Human Embryonic Stem Cells. *Cell Stem Cell* **2007,** 1, 286-298.